Title
Snapshot Spectroscopic Studies of the In Vivo Regulation of Photosynthetic Light Harvesting and Photoprotection

Author
Steen, Collin J

Publication Date
2022

Peer reviewed|Thesis/dissertation

Snapshot Spectroscopic Studies of the *In Vivo* Regulation of Photosynthetic Light Harvesting and Photoprotection

By

Collin J. Steen

A dissertation submitted in partial satisfaction of the

requirements for the degree of

Doctor of Philosophy

in

Chemistry

in the

Graduate Division

of the

University of California, Berkeley

Committee in charge:

Professor Graham R. Fleming, Chair
Professor Naomi S. Ginsberg
Professor Krishna N. Niyogi

Spring 2022

Abstract

Snapshot Spectroscopic Studies of the *In Vivo* Regulation
of Photosynthetic Light Harvesting and Photoprotection

by

Collin Joseph Steen

Doctor of Philosophy in Chemistry

University of California, Berkeley

Professor Graham R. Fleming, Chair

As the global population continues to grow, optimizing photosynthetic light harvesting has emerged as an important route for increasing the production of food and bioenergy. Under periods of excess illumination, photosynthetic organisms initiate a suite of photoprotective mechanisms, collectively referred to as nonphotochemical quenching (NPQ), which thermally dissipate chlorophyll excited states. However, the molecular basis for NPQ is still unclear, partly due to overlapping dissipation mechanisms, shared molecular players, significant variation across species, and the difficulty of experimentally measuring dissipation *in vivo* and under physiologically relevant conditions. Additionally, while NPQ is thought to protect against downstream oxidative damage, there has been little direct investigation of the temporal and spatial connections between NPQ and reactive oxygen species, such as singlet oxygen, which is thought to be a toxic byproduct of photosynthesis though it may also play essential roles in intra-cellular signaling.

In this dissertation, I employ a suite of "snapshot" spectroscopic methods – including transient absorption, fluorescence lifetime, and electron paramagnetic resonance techniques – in order to better understand the complex operation of NPQ in intact photosynthetic systems. By applying these snapshot methods to a range of genetically altered plants and algae under dynamically changing illumination conditions, a more complete understanding of the complex *in vivo* operation of excitation energy dissipation is obtained, with particular emphasis on the roles of carotenoids, pH-sensing proteins, and oxidative species. These fundamental findings hold great promise for ongoing efforts to boost the biomass yields of natural photosynthesis as well as improve the sustainable production of bioenergy.

To my family and the many teachers who helped me get to where I am today.

Table of Contents

List of Figures

List of Tables

List of Symbols and Abbreviations

Ant	antheraxanthin
BBY	Berthold–Babcock–Yocum PSII-enriched particles
Car	carotenoid
^{1}Car*	singlet excited state of carotenoid
CCM	carbon concentrating mechanism
Chl	chlorophyll
^{1}Chl*	singlet excited state of chlorophyll
^{3}Chl*	triplet excited state of chlorophyll
$Chl^{\bullet-}$	chlorophyll radical anion
CT	charge transfer
DCBQ	2,6-dichloro-1,4-benzoquinone
DCMU	2-(3,4-dichlorophenyl)-1,1-dimethylurea
DES	de-epoxidation state
DTSSP	3,3′-dithiobis(sulfosuccinimidyl propionate)
DTT	1,4-Dithiothreitol
EET	excitation energy transfer
EPR	electron paramagnetic resonance spectroscopy
ESA	excited state absorption
FWHM	full width at half-maximum
HL	high light
HPLC	high-performance liquid chromatography
ISC	intersystem crossing
LHC	light-harvesting complex
$^1O_2$*	singlet excited state of molecular oxygen
$^3O_2$	triplet ground state of molecular oxygen
LHCSR	light-harvesting complex stress-related protein
LHCX	light-harvesting complex stress-related protein
Lut	lutein
MV	methyl viologen
NIR	near-infrared range
NPQ	nonphotochemical quenching
OD	optical density
OEC	oxygen evolving complex of PSII
PAM	pulse-amplitude modulation fluorimetry
PPFD	photosynthetic photon flux density
PSI	photosystem I
PSII	photosystem II
PsbS	PSII subunit S protein
PQ	plastoquinone
P680	primary donor in the RC of PSII
ΔpH	proton gradient across thylakoid membrane
qE	energy-dependent quenching
qH	sustained quenching

qI	photoinhibitory quenching
qT	state-transition quenching
qZ	zeaxanthin-dependent quenching
Q_y	Chl excited state
RB	rose bengal
RC	reaction center
ROS	reactive oxygen species
S_1	singlet excited state
SOSG	singlet oxygen sensor green
STT	serine/threonine-protein kinase
T_1	triplet excited state
TA	transient absorption spectroscopy
TB	toluidine blue
VAZ	violaxanthin-antheraxanthin-zeaxanthin (xanthophyll) cycle
TCSPC	time-correlated single photon counting
TEMP	2,2,6,6-tetramethylpiperidine (spin trap)
TEMPD	2,2,6,6-tetramethyl-4-piperidone (spin trap)
TEMP-OH	4-hydroxy-2,2,6,6-tetramethylpiperidine (spin trap)
TEMPO	2,2,6,6-tetramethyl-1-piperidinyloxyl (spin label)
TTET	triplet-triplet energy transfer
VDE	violaxanthin de-epoxidase enzyme
Vio	violaxanthin
Zea	zeaxanthin
$Zea^{\bullet+}$	zeaxanthin radical cation
Φ_{ISC}	quantum yield for intersystem crossing
Φ_{Δ}	quantum yield of singlet oxygen

Acknowledgements

I have been fortunate to have a strong network of people supporting me throughout graduate school.

First and foremost, I am grateful for an excellent research advisor in Graham Fleming, who played a major role in crafting me into the scientist that I am today. Graham has consistently believed in me, even when I didn't always believe in myself, and provided numerous opportunities and resources for the exploration of scientific questions that interested me. He also has consistently demonstrated that he valued my input and always encouraged me to play a major role in shaping the overall direction of the project. I have benefitted from Graham's wealth of knowledge about the physical chemistry of photosynthesis, and from his many scientific connections. Graham has taught me how to become a collaborative scientist, an important skill I that have come to cherish and will continue to hone in the future.

It has been a privilege to interact with so many brilliant scientists at UC Berkeley and elsewhere. From the Fleming group, I am forever grateful to Soomin Park and Ali Fischer, who mentored me during my first year in the lab and were willing to patiently answer any question that I had. The opportunity to work alongside Soomin and Ali was one of the major reasons I joined the Fleming group and that first year was filled with exciting science, teamwork, and lot of learning. Sabine Oldemeyer was a great collaborator who kept me going even when things weren't going our way in lab. Jonathan Morris spearheaded the first iteration of the periodic illumination experiments and modeling efforts that now occupy a large fraction of this dissertation. Pallavi Bhattacharyya was very kind to provide advice about the multi-timescale mathematical model of NPQ presented in Chapter 4. Thanks to my current co-workers – especially Lam Lam, Tsung-Yen Lee, and Audrey Short – for their many contributions. It has been a pleasure to work alongside them during the last several years of my Ph.D. My gratitude also goes to Sara Ricks, whose numerous efforts ensure the Fleming group remains able to function. Finally, special thanks to my fellow P-chem cohort members, Eric Arsenault and Kaydren Orcutt, who have been there for me at every step of the way, both scientifically and personally. I cannot imagine grad school without either of them. I will always remember our daily coffee breaks and lab lunch/dinner outings. Thanks for being willing to talk through weird data or help brainstorm what might be going wrong with a laser setup. Your friendship has been a highlight of my graduate school experience.

My research would not have been possible without exceptional collaborators in the Niyogi group at UC Berkeley. I have greatly enjoyed the opportunity to learn from so many experts in plant and algal biology, a field that I initially knew very little about. Among them, Adrien Burlacot has been an exceptional colleague and a constant source of enthusiasm about science, especially new experimental approaches. Thien Crisanto has been incredibly generous with her time and energy and has grown numerous cultures of *Nannochloropsis* to support a range of experiments. Setsuko Wakao has taught me how to think critically about oxidative stress from a biological perspective and has been very patient as we worked through many experimental difficulties related to the detection of singlet oxygen in *Chlamydomonas*. Thanks to Dhruv Patel and Cindy Amstutz for assistance with growing plants and valuable advice on numerous occasions. A collaboration with Alizée Malnoë on the molecular mechanisms of qH, not described in this dissertation, has been

especially rewarding. My deep appreciation goes to Masa Iwai, my go-to person for any time questions came up, whether they were about specific details in experimental protocols or much more general in scope. Neary all of the projects I worked on during my Ph.D. have benefited from Masa's informed input and thoughtful suggestions. He is an endless source of knowledge and enthusiasm about photosynthesis. Thanks to Marilyn Kobayashi for help in securing access to the instrumentation and resources necessary to conduct photosynthesis research. Finally, thank you to Prof. Kris Niyogi for the opportunity to work so closely with him and his team. Kris is a phenomenal scientist and a model of humility for the younger generation of scientists.

Thank you to the members of my qualifying exam and dissertation committees at UC Berkeley, especially Naomi Ginsberg for many insightful suggestions/comments and Ron Cohen for his early advice that success in science comes from identifying one's own areas of strength and then cultivating them.

During my final year of graduate school, I had the opportunity to perform a portion of my dissertation research at Argonne National Laboratory through funding from the Department of Energy (DOE) Office of Science Graduate Student Research (SCGSR) program. Dave Tiede and the rest of the Solar Energy Conversion Group enthusiastically welcomed me and provided the resources and connections necessary to perform my work, in the middle of the COVID-19 pandemic nonetheless! Thanks in particular to Lisa Utschig for sharing her expertise with membrane biochemistry and her enthusiasm for photosynthesis, Oleg Poluektov for his patience and wisdom regarding all things EPR, and Jens Niklas for his careful approach to science and impressive attention to details. Lisa, Oleg, and Jens were fantastic mentors and I feel lucky to have had the chance to work with them. Their encouragement and advice – at nearly every stage of this project – was invaluable. Important conversations and resources in the SECG were also provided by Karen Mulfort, Lin Chen, Emily Sprague-Klein, and Nina Ponomarenko. Thanks to Rich Schaller for providing access to a time-correlated single-photon counting setup at the Center for Nanoscale Materials. Just as importantly, I want to acknowledge my Aunt Velvet, Uncle Stuart, and Grandma Barb who welcomed me into their home and family for a six-month stay while working at Argonne. They gracefully tolerated many intangible conversations about graduate school and scientific research. The time we spent together, especially our regular Euchre matches, is something that I will always cherish.

To all my friends in Berkeley, thank you for many wonderful memories. Whether it was post-ChemKeg shenanigans, late nights spent working on quantum mechanics problem sets, or hikes in the Berkeley Fire Trails, I have truly relied on your friendship throughout graduate school. In particular, thanks to Kaydren Orcutt, Eric Arsenault, Isabel Bogacz, Bryan Place, Dipti Jasrasaria, Jenna Tan, Zach Heim, Valerie McGraw, Stephen Bierschenk, Abdul Aldossary, Avishek Das, Joey DeGrandchamp, Elliot Rossomme, Chin Lee, and Elliot Martin. Special appreciation to my partner Paul Wrona. Paul is one of the most selfless people I know and has been a never-ending source of love and encouragement for me when I needed it the most. I cannot imagine the last five years without him.

Finally, thank you to all members of my family, especially my parents, for their unwavering support of all of my endeavors and for providing me with the resources to succeed.

Funding Statement: Most of the work presented in this dissertation was supported by the U.S. Department of Energy, Office of Science, Basic Energy Sciences, Chemical Sciences, Geosciences, and Biosciences Division under the field work proposal 449B. The EPR-based work described in Chapter 6 was supported by a Department of Energy (DOE) Office of Science Graduate Student Research (SCGSR) award, providing funding to perform research in the Solar Energy Conversion Group (SECG) at Argonne National Lab and by the U.S. Department of Energy, Office of Science, Office of Basic Energy Sciences, Division of Chemical Sciences, Geosciences, and Biosciences, under Contract No. DE-AC02-06CH11357.

Chapter 1

Introduction to Nonphotochemical Quenching and Snapshot Spectroscopy

Natural photosynthesis is central to life on Earth. Over billions of years of evolution, photosynthetic organisms have refined the ability to harness energy from the sun and convert it to usable forms of chemical energy. Starting from water, carbon dioxide, and light as the primary inputs, plants and algae are able to synthesize sugars and other energy-rich complex organic molecules while also producing oxygen as a byproduct. Photosynthesis thus powers virtually all life on Earth by contributing to the vast majority of the planet's food, energy, and oxygen supplies.[1]

Studying natural photosynthesis is of global importance as it may enable new solutions to many ongoing challenges related to food, energy, and climate.[2–4] Photosynthesis, which is required for production of all of humanity's food supplies, is key to improving crop yields.[5] It is also a source for biofuels and many other energy resources.[5] Finally, photosynthesis creates all of the oxygen on the planet[6] – approximately half of it originating from phytoplankton in the ocean[7] – and provides a blueprint for possible mitigation of carbon dioxide levels in the atmosphere, currently sequestering ~100 gigatons of carbon annually.[1]

The amount of energy contained in the sunlight that reaches the Earth's surface far exceeds current and future worldwide energy consumption,[8] making solar energy an under-utilized resource.[9] One way the harvesting of solar energy could be improved is by translating the design principles of natural photosynthesis into various artificial systems, leading to advanced technologies in artificial photosynthesis,[10,11] solar light harvesting and catalysis,[12,13] or sustainable energy production.[14,15] Furthermore, as the effects of climate change increase in coming years,[16,17] understanding the fundamental mechanisms of biological solar energy conversion is of utmost importance for future agricultural productivity.[18–20] The ability to make targeted improvements to photosynthesis may also help to alleviate humanity's increasing demand for food and energy in the face of population growth.[2,5]

In this chapter, I provide a brief introduction to the process of oxygenic photosynthesis and the regulation of photosynthetic light harvesting. I then outline the approach of snapshot spectroscopy and comment on the useful insights that can be gained about the underlying molecular mechanisms, kinetics, and steady-state operation of photoprotection. I hope that this knowledge may one day help to improve the performance of natural photosynthesis in years to come.

1.1 Photosynthetic Light Harvesting

In eukaryotic algae and plants, the process of oxygenic photosynthesis occurs in an organelle known as the chloroplast. The so-called "light reactions" of photosynthesis are housed in and around the chloroplast thylakoid membrane, a complex structure that is densely packed with various pigment-protein complexes, which can constitute up to 80% of the total membrane area.[21] The thylakoid membrane is heterogeneous; in higher plants, it is composed of distinct grana and stroma lamellae, corresponding to disc-like stacked and tube-like unstacked regions, respectively.[22] The grana thylakoid membrane encloses a continuous interior aqueous region (the lumen), separating it from an exterior aqueous region (the stroma) that is enclosed within the chloroplast. Many of the initial events of light absorption, performed by photosystem (PS) II and its associated light-harvesting antenna system,[23] are housed in the grana. However, PSI predominantly resides in the stroma lamellae and is an important determinant of the rate of electron transfer through the photosynthetic membrane. The combined action of the two photosystems, mediated by the cytochrome b_6f complex, results in the shuttling of electrons originating from water molecules in the lumen through an intricate chain of membrane co-factors to generate reducing equivalents in the stroma.[24]

For energetic input into the system, both photosystem complexes possess an array of peripheral antenna proteins that harvest sunlight, primarily through the absorption of photons by chlorophyll (Chl) pigments.[25] Following the initial absorption event, a network of several hundred antenna Chl pigments efficiently transfers the excitation energy to the reaction center (RC) where charge separation can occur.[26] The RC is optimized for rapid spatial separation of electrons and holes, minimizing wasteful recombination of photogenerated charge carriers. Upon receiving excitation energy from the antenna, two strongly coupled RC Chl pigments – referred to as P680 in the case of PSII – undergo charge separation. The photogenerated electron is transferred from P680 to a pheophytin pigment, and then to plastoquinone (PQ),[27] a small lipophilic charge carrier that shuttles the electron away from the PSII complex through the thylakoid membrane towards downstream portions of the electron transport chain. The final products, the energy-rich molecules ATP and NADPH, are utilized in the Calvin-Benson cycle to convert CO_2 to carbohydrates including sugars and starch.[1] The export of an electron to the electron transport chain leaves behind a hole, which is replaced by electrons obtained from the splitting of water by the Oxygen Evolving Complex and supplied to the RC via a tyrosine residue located near P680.[28] In the process of water oxidation, molecular oxygen and protons are also released in the interior lumenal region, which, along with the action of cytochrome b_6f, contributes to the formation of a proton gradient (ΔpH) across the thylakoid membrane.

The photosynthetic apparatus is exquisitely designed for light harvesting under normal, light-limited conditions, such as those commonly found in the environment, *i.e.* the dim sunlight experienced at dawn, dusk, or during a cloudy day. The photochemistry of PSII is highly efficient under these low light conditions, with more than 80% of absorbed photosynthetically-active quanta being utilized for productive charge separation.[29] The overall quantum yield of photochemistry in the RC is near unity with one charge separation event occurring per photon absorbed.[30] This feat is primarily due to the architecture of the light-harvesting antenna,[31,32] characterized by densely packed pigments held in precise configurations by a protein scaffold. The antenna enables efficient excitation energy transfer[33] while also avoiding the concentration quenching of excitation energy

that occurs for Chl pigments in solution at similar densities as those found in photosynthetic pigment-protein complexes.[34]

Light-harvesting complex II (LHCII) is the primary antenna for PSII and the most abundant protein in the thylakoid membrane. Each LHCII monomer binds a maximum of 14 Chl molecules (8 Chl *a*, 6 Chl *b*), each separated by an average distance of ~10 Å, as well as 4 Car molecules (1 neoxanthin, 2 lutein, 1 violaxanthin).[35] Both Chl and Car pigments possess delocalized conjugated π-electron systems, with absorption spectra that cover much of the visible region of the solar radiation spectrum (see Figure 1-1).[36,37] The PSII supercomplex is composed of a variable number of LHCII trimers per core, depending on the photosynthetic species and the environmental conditions. The most common arrangement, referred to as $C_2S_2M_2$, is composed of a dimeric core with two strongly-bound and two moderately-bound LHCII trimers, and is commonly found in plants under low light conditions.[38] Overall, the PSII supercomplex is essential to the efficient operation of photosynthesis, both in terms of light harvesting function and the ability to protect against photodamage.

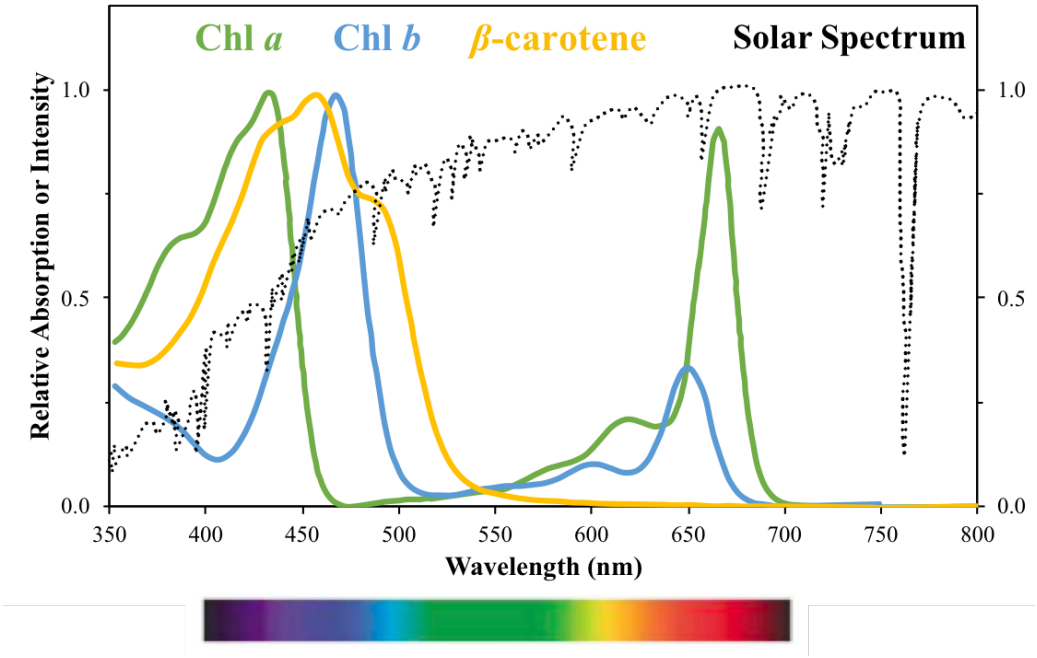

Figure 1-1. Absorption spectra of the pigments (Chl *a*, green; Chl *b*, blue; *β*-carotene, yellow) involved in photosynthetic light harvesting in plants. Chlorophyll pigments, including Chl *a* and *b*, are abundant in photosynthetic systems and absorb primarily in the blue and red regions of the solar spectrum. Carotenoids, such as *β*-carotene, are secondary pigments that also function in absorption of light energy and play critical roles in photoprotection. The pigment spectra are from Johnson *Essays in Biochemistry* 2016, *60*, 255-273 (reference [6]). Also shown is the solar spectrum at ground level, from Wolf and Blankenship *Photosynthesis Research* 2019, *142*, 349-359 (reference [124]). Light with wavelengths between 400-700 nm, corresponding to the visible region of the electromagnetic spectrum, is referred to as photosynthetically active radiation.

While the strong absorption of sunlight enabled by an extensive light-harvesting antenna system helps to drive photosynthesis under low light intensities, it necessarily results in excessive absorption under the high light (HL) intensities regularly encountered in the natural environment. Under such conditions, PSII becomes quickly saturated due to depletion of electron acceptor

molecules following the reduction of the quinones Q_A, Q_B, and the PQ pool,[39] leading to decreased photosynthetic efficiency.[29] Consequently, additional excitation energy is unable to be trapped by the reaction center, leading to accumulation of longer-lived excitations in the light-harvesting antenna. As the average lifetime of excitations becomes longer, alternative deactivation pathways of chlorophyll pigments become relevant (Figure 1-2). For example, the singlet excited state of chlorophyll (^{1}Chl*) can undergo intersystem crossing (ISC) leading to the triplet state (^{3}Chl*), which can then react with triplet molecular oxygen ($^3O_2$) to generate singlet oxygen ($^1\Delta_g$ or $^1O_2$*)[40] and other reactive oxygen species (ROS).[41,42] $^1O_2$* is the highly-reactive excited state of molecular oxygen and is capable of causing damage to proteins and other components of the photosynthetic apparatus.

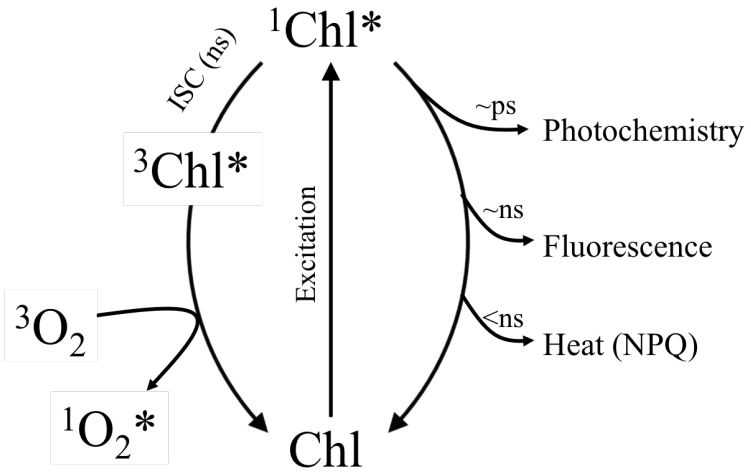

Figure 1-2. Photophysical processes involved in de-excitation of the chlorophyll singlet excited state in photosynthetic systems. The approximate timescale of each process is indicated. Adapted from Müller et al. *Plant Physiol.* 2001, *125,* 1558-1566 (reference [125]).

In the environment, photosynthetic organisms are regularly exposed to dynamic conditions, especially in terms of the light intensity reaching the photosynthetic apparatus in any given cell. In fact, light levels in nature are highly irregular with abrupt variations in intensity (~10 orders of magnitude) occurring within very short periods of time (as short as seconds) due to changes in the environmental surroundings.[43] Some examples on land include sunflecks occurring in a plant canopy and shading by clouds or vegetration.[44,45] In aquatic environments, rapid mixing of the water column or subsurface focusing by waves can also create highly dynamic light patterns, both in terms of the intensity and spectral characteristics.[46,47] As such, efficient operation of photosynthesis demands not only a delicate balancing act between energy harvesting and photoprotection, but also the ability to quickly transition between these two modes at the level of individual cells, or even individual chloroplasts, in response to environmental circumstances. Survival under natural environmental conditions requires continuous regulation of ROS,[48] and photosynthetic organisms employ a multipronged approach involving both short-term prevention and long-term mitigation of photo-oxidative stress. One such photoprotective strategy found in virtually all photosynthetic organisms is nonphotochemical quenching,[49] the ability to remove excitation energy in excess of what can be utilized by the RCs for photochemistry at any given time.

1.2 Regulation of Light-Harvesting by Nonphotochemical Quenching

Under HL conditions, photosynthetic organisms initiate a variety of photoprotective strategies to mitigate the consequences of photo-oxidative stress, one of which is nonphotochemical quenching (NPQ). NPQ is a broad set of processes that results in harmless dissipation of excitation energy as heat. Upon increasing light intensities and the accompanying saturation of RCs, the activation of NPQ provides the organism with an additional de-excitation pathway for the Chl excited state (Figure 1-2), minimizing the production of ROS.

The underlying photophysical dissipation mechanisms of NPQ must occur on ultrafast timescales in order to outcompete the nanosecond timescales of ISC leading to ^{3}Chl*. Several mechanisms have been proposed, including charge transfer (CT) and excitation energy transfer (EET) quenching (Figure 1-3). CT quenching involves a dimer consisting of coupled Chl and Car pigments, which is able to accept excitation energy from a nearby Chl pigment, then undergo charge separation and recombination to dissipate the energy as heat.[50,51] In contrast, EET quenching involves energy transfer from the excited state of Chl (Q_y) to the S_1 state of a Car, which subsequently undergoes rapid internal conversion to the ground state.[52,53] Beyond carotenoid-based CT and EET, both of which have been observed using transient absorption spectroscopy, quenching arising from Chl-Chl interactions has also been proposed. For example, a Chl-Chl charge transfer scheme may be involved in the dissipation.[54–56] However, this remains difficult to probe spectroscopically in intact photosynthetic systems.

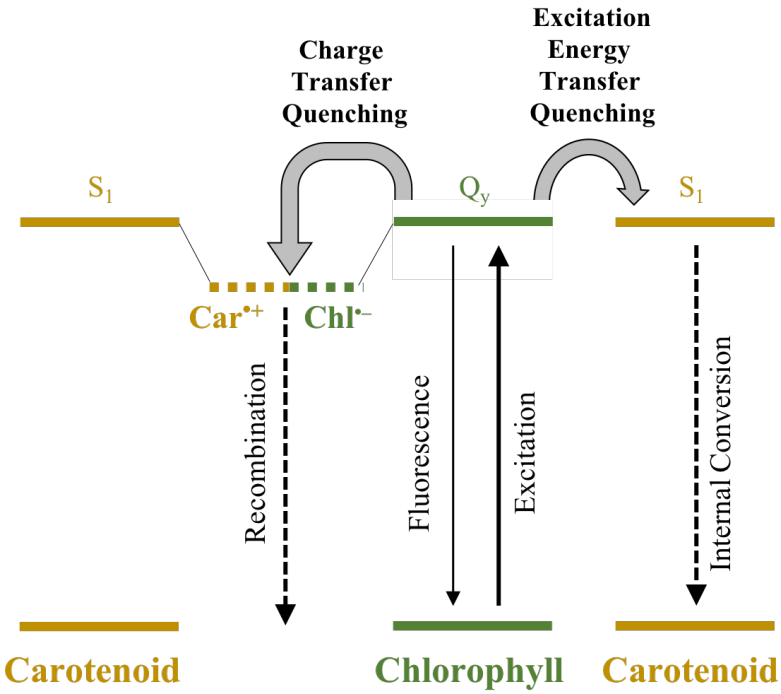

Figure 1-3. Ultrafast photophysical dissipation mechanisms proposed to underlie NPQ, resulting in removal of excess energy from the Q_y excited state of Chl pigments. Charge Transfer (CT) involves a dimer involving a Car and Chl charge-separated pair, which rapidly recombines to dissipate energy. Excitation Energy Transfer (EET) is based on energy transfer to the short-lived dark Car S_1 state. Adapted from Park, Steen, Fischer, and Fleming, *Photosynthesis Research* 2019, *141*, 367-376 (reference [120]).

The various photophysical mechanisms are not mutually exclusive; multiple dissipative pathways could be occurring simultaneously in different regions of the thylakoid membrane, the combination of which would dictate the overall level of quenching in the cell. In recent work, both CT and EET mechanisms have been observed to be active in the same photosynthetic system at the level of an individual LHCSR protein,[57] within spinach thylakoid membranes,[58,59] or even in fully intact algal cells.[60] It is also worth noting that the mechanisms of NPQ may differ in samples of various degrees of complexity; the intactness of the membrane, composition of lipids, and presence of protein-protein interactions are all important determinants of function. *In vivo* investigations are thus critical to understanding the regulation of photosynthesis by NPQ in fully intact systems.

While the ultrafast photophysical mechanisms enable photoprotection during periods of excess illumination, they can be challenging to study because they are switched on and off within seconds to minutes of HL exposure in response to biochemical and/or structural changes in the thylakoid membrane system. The phenomenon of NPQ is traditionally monitored by the quenching of Chl *a* fluorescence that occurs under HL conditions that saturate photosynthesis.[61] Typically, the NPQ components have been characterized based on the rate of activation and deactivation upon transitions to HL or dark conditions, respectively. However, this can be a challenging distinction due to the overlapping timescales associated with each process (see Figure 1-4). Alternatively, the NPQ components can be distinguished according to the underlying biochemical regulators (pigments and/or proteins) that are involved in the dissipation, however this also leads to some overlapping categorizations. For example, the *in vivo* photoprotective response initially arises from the acidification of the thylakoid lumen, occurring within seconds of HL exposure. Following this ΔpH trigger, the onset of the various phases of NPQ is highly complex, with both shared and unique biochemical regulators and feedback cues, as discussed below.

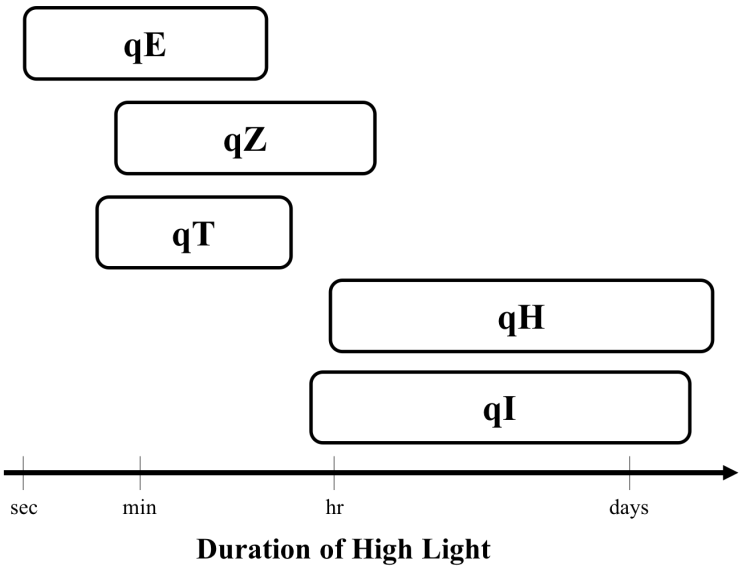

Figure 1-4. Approximate timescales of activation and deactivation for each NPQ component in response to excess light exposure. Many of the NPQ processes overlap in time and molecular players. Adapted from Erickson et al. *Plant Journal* 2015, *82*, 449-465 (reference [106]).

The rapidly-reversible component of NPQ, the so-called energy-dependent quenching (qE), is triggered by the rapid decrease in the pH of the thylakoid lumen upon HL exposure.[62,63] In all species, qE requires a pH-sensing protein that is thought to undergo a structural change in response to the formation of the ΔpH.[64] qE also involves de-epoxidized xanthophyll pigments,[65,66] either zeaxanthin (Zea) and/or lutein (Lut),[67,68] and likely occurs in the light-harvesting antenna of PSII.[69–71] The next fastest NPQ process, zeaxanthin-dependent quenching (termed qZ), operates on a timescale of 10 minutes following exposure to HL. qZ correlates with the de-epoxidation of violaxanthin (Vio) to Zea by the enzyme violaxanthin de-epoxidase (VDE).[72] Other than the indirect requirement of low lumenal pH for the activation of VDE, qZ is thought to be independent of ΔpH.[73] A third possible contributor to overall NPQ is quenching via state transitions (qT), or the redistribution of light-harvesting antenna proteins in response to imbalanced rates of electron transport between the two photosystems,[74] each of which absorb slightly different wavelengths of light. qT is triggered by the redox state of the electron transport chain between PSII and PSI. Overreduction of the PQ pool activates a kinase that phosphorylates LHCII,[75] resulting in detachment from PSII and increased mobility in the thylakoid membrane.

Given that qE, qZ, and qT are the fastest components of NPQ, they are the primary focus of this dissertation. However, additional components of NPQ become active on the timescale of hours in response to environmental stress conditions. Photoinhibition (qI) is the light-dependent decrease in the quantum yield of photosynthesis occurring due to irreversible damage to the D1 protein of PSII caused by intense illumination.[76,77] More recently, a sustained form of photoprotection (termed qH) has been identified.[78] qH is activated by HL and cold stress, involves strong dissipation within LHCII trimers, and is regulated by the activity of the SOQ1, ROQH1, and LCNP proteins.[79–81]

There is significant interest in improving photosynthetic efficiency given its implications for boosting crop and biomass yields.[82,83] NPQ is known to be critical to plant fitness under fluctuating light conditions and in the field.[84] At the same time, it has been estimated that the delayed recovery from a photoprotective (NPQ active) state (Figure 1-5), which can last for several minutes upon transition from HL to dark conditions, imposes a penalty of up to 30% on total carbon uptake by photosynthesis.[85] In recent years it has been demonstrated that accelerating the relaxation of NPQ during the dark by overexpressing key NPQ players (PsbS and the VAZ cycle enzymes) can result in 15-20% higher biomass accumulation in tobacco plants grown under field conditions.[86] Additionally, optimization of photoprotection can enhance water use efficiency and canopy radiation use efficiency.[87,88]

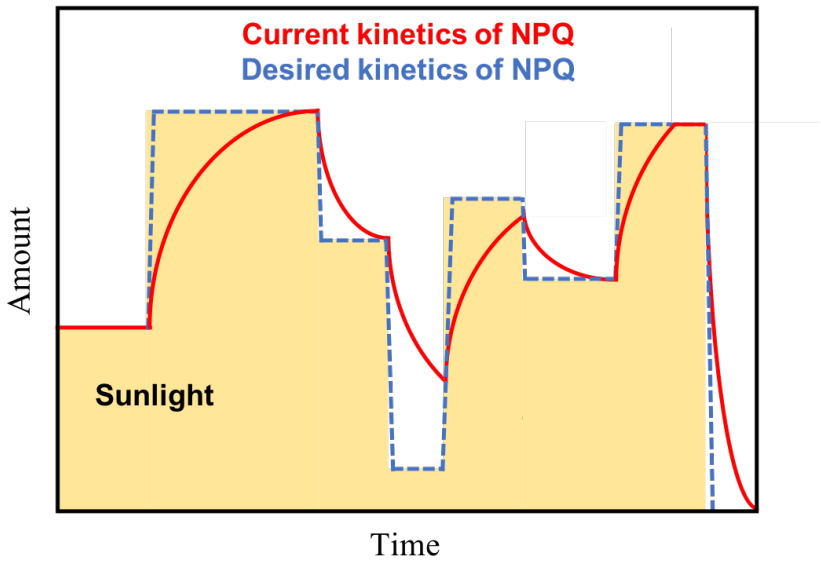

Figure 1-5. The goal of optimizing photosynthetic light harvesting by accelerating the kinetics of NPQ. Currently, the activation and relaxation of NPQ lags behind the rapid changes in sunlight intensity that occur in the environment. The current operation of NPQ (depicted by solid red curves) therefore leads to periods of under-protection (those when HL intensities lead to the absorption of more energy than can be used for productive photosynthesis) as well as periods of wasteful energy dissipation (those when the amount of energy dissipation by NPQ exceeds what is needed for a given light intensity). Accelerating the kinetics of NPQ could help to protect the organism against rapid increases in light intensity, as well as enable efficient light-harvesting upon a return to low light levels. Schematic adapted from Ruban *Nature* 2017, *541*, 36-37.

Despite these initial successes, future improvements in the biomass and biofuel productivity of photosynthesis could be assisted by detailed knowledge of the molecular, biochemical and biophysical mechanisms underlying photoprotection. This includes the ultrafast photophysical mechanisms that enable the dissipation, the kinetics associated with the activation and deactivation of individual NPQ components under variations in solar illumination, and the regulation of ROS by the photosynthetic apparatus. Importantly, these features should be studied in intact photosynthetic systems that contain the complex feedback loops necessary for the activation and deactivation of NPQ. It is also advantageous to consider the operation of NPQ under controlled laboratory conditions that resemble those found in the natural environment, such as repetitive exposure to HL and dark.

1.3 The Cast of NPQ: Photosynthetic Species, Pigments, and Proteins

Photosynthesis is abundant in the world, capable of functioning efficiently in diverse terrestrial and aquatic habitats characterized by very different light environments. Despite widespread differences in environmental context, nearly all photosynthetic organisms employ some form of NPQ-based photoprotection, although the specific mechanisms and molecular players differ significantly.[89,90] Therefore, to understand the principles underlying efficient photoprotection in nature, it is highly advantageous to consider the operation of NPQ across a diverse range of species, including plants and algae, as well as in response to a range of high-light intensities.

Much of the foundational work on NPQ was conducted using the model angiosperm *Arabidopsis thaliana* due to its fast growth time and the availability of mutants affected in many of the pigments and proteins involved in NPQ. Among these biochemical players include the xanthophylls zeaxanthin (Zea)[91] and lutein (Lut),[92] two key carotenoid pigments suspected to play roles in qE and/or qZ. Whereas Lut is typically present in leaves at constant levels over the course of a day, Zea is well-known to rapidly accumulate upon HL exposure[93] via the activation of the violaxanthin de-epoxidase (VDE) enzyme[94] which converts Vio to Zea.[95] The transmembrane PsbS protein, an atypical member of the light-harvesting complex (LHC) superfamily, is required for qE.[96,97] PsbS is likely involved in sensing the ΔpH via protonation of two lumen-facing acidic glutamate residues.[98] Although PsbS does not stably bind pigments,[97,99] it is currently believed that a pH-induced conformational change in PsbS[100] activates the NPQ response by altering the pigment (Chl-Car) interactions within another LHC protein[99] and/or by modifying the organization of proteins in the thylakoid membrane.[101,102] Finally, the STN7 and STN8 kinases are necessary for activation of qT in response to reduction of the PQ pool.[103] Phosphorylation of LHCII results in its dissociation from PSII and association with PSI, forming a PSI-LHCI-LHCII supercomplex.[104]

It has been quite challenging to study NPQ mechanisms in isolated thylakoid membranes from *A. thaliana*, likely due to partial loss of molecular interactions necessary for activating NPQ in the intact system. Many recent studies of the photophysical mechanisms of NPQ in plants have instead relied on thylakoid membranes isolated from spinach, which are amenable to ultrafast transient absorption spectroscopy,[58,59] in combination with chemical treatments to alter the xanthophyll composition or to disrupt protein interactions.

In contrast to plants, the green alga *Chlamydomonas reinhardtii* relies predominantly on light-harvesting complex stress-related (LHCSR) proteins for NPQ.[105,106] Unlike PsbS, LHCSRs are pigment-binding proteins that contain exposed residues that undergo protonation upon lumen acidification.[107] This indicates that LHCSRs could be a site of quenching *in vivo*. Evidence from single-molecule techniques suggests that LHCSRs may undergo a conformational change in response to quenching conditions.[108] Analysis of NPQ mutants in *Chlamydomonas* indicates that much of the quenching relies on the xanthophyll Lut, though Zea may play a minor role.[65,109] Additionally, state transitions appear to be quite prominent in *C. reinhardtii*[110] where they rely on the activity of the STT7 kinase.[111,112] Therefore, *C. reinhardtii* represents an ideal platform for dissecting the operation of qT in the presence and absence of qE. Finally, *C. reinhardtii* possesses a carbon concentrating mechanism (CCM) which assists in the relative enrichment of CO_2 relative to O_2 in the vicinity of the carbon-fixing enzyme Rubisco,[113] and is linked to the energetic budget of the cell.[114]

Unfortunately, transient absorption spectroscopy is not possible for *C. reinhardtii* due to intense scattering arising from its relatively large cell size (~10 μm in diameter). Recently, *Nannochloropsis oceanica*, a heterokont microalga that is closely related to diatoms and brown algae, has emerged as an excellent system for *in vivo* spectroscopic investigations due to its small size (2-3 μm), high quenching capacity, and amenability to genetic modification.[115,116] Compared to other plant and algal species, *N. oceanica* is relatively simple in its pigment and protein composition; it contains LHCX stress-related proteins[117] and the carotenoid Zea, but lacks Lut and is not thought to possess a kinase involved in qT.[118] This makes *Nannochloropsis* an ideal system for dissecting the operation of NPQ, especially the mechanistic contributions of Zea and LHCX1 in qE,[60] or the organism's ability to rapidly activate and deactivate NPQ in response to fluctuating light conditions.[119]

Overall, the significant differences between photosynthetic lineages emphasizes the importance of systematic *in vivo* assessments of NPQ in a range of different species, while avoiding generalizations regarding the underlying mechanisms. Each species likely possesses unique characteristics of NPQ that enable survival under vastly different environmental contexts. Understanding these various design principles could assist future efforts to optimize photosynthetic light harvesting in a range of environmental conditions.

1.4 The Approach of Snapshot Spectroscopy

In this dissertation, I present three forms of snapshot spectroscopy designed to probe the molecular and biophysical basis of nonphotochemical quenching in a range of intact photosynthetic samples. The successful operation of photosynthesis, and its necessary regulation, requires an array of processes operating on vastly different length and time scales. Therefore, the experimental techniques must cover disparate timescales so as to monitor chemical and/or photophysical processes ranging from the femtoseconds to microseconds. Under conditions found in nature, these processes are also actively regulated on timescales ranging from seconds to hours in response to variations in the incident solar flux. The goal of snapshot spectroscopy is to repetitively accumulate "snapshot" measurements, each of which provides insight into the operation of any given process, and more importantly, to track each process in real time as the overall machinery of NPQ turns on or off during changes in illumination conditions. Thus, snapshot spectroscopy allows for the monitoring of fast photophysical processes (ranging from fs to μs) on the much slower (sec-hours) timescales associated with dynamical photosynthetic acclimation to environmental changes.

Each snapshot technique presented in this dissertation provides a different glimpse into the real-time operation of the photoprotective regulation of light harvesting, ranging from molecular mechanisms to reactive chemical species (Figure 1-6). The integration of these various spectroscopic methods, especially when all applied to identical (or similar) samples, enables new insights to be gained and different questions to be asked. For example, on the ultrafast timescale, snapshot transient absorption (TA) spectroscopy provides insights into the underlying picosecond timescale photophysical energy dissipation mechanisms – charge transfer and excitation energy transfer – as well as their rates of activation and deactivation under light to dark transitions.[120] On the nanosecond timescale, fluorescence lifetime snapshot measurements probe both the kinetics and magnitude of energy quenching by NPQ[121] and are capable of monitoring this in real time during exposure to fluctuating light conditions. Finally, spin-trapping electron paramagnetic resonance (EPR) snapshot spectroscopy measurements provide a picture of the steady-state accumulation of singlet oxygen excited states in the photosynthetic membrane.

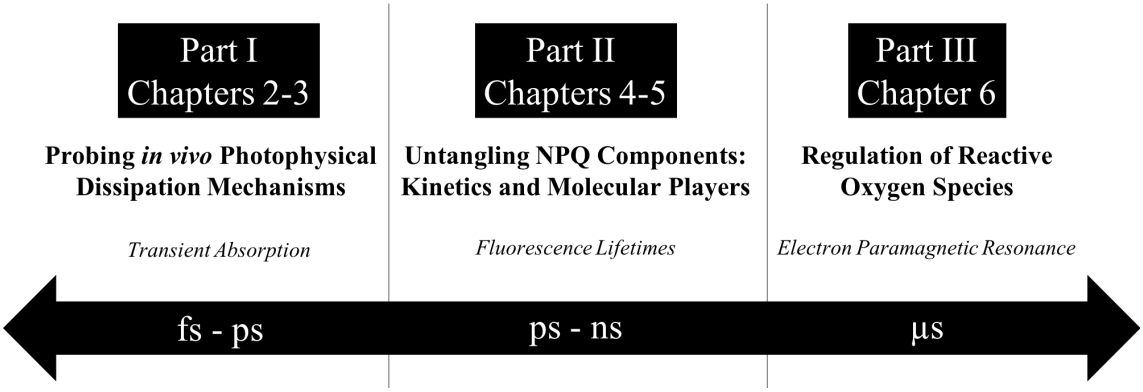

Figure 1-6. Summary of the three main forms of "snapshot" spectroscopy techniques employed in this dissertation, along with the NPQ topics of interest and the relevant photophysical timescales. Transient absorption spectroscopy probes the Chl and Car excited states involved in NPQ dissipation mechanisms on the fs-ps timescale. Fluorescence lifetime measurements report on the average lifetime of Chl excited state and can provide insight into the kinetics of NPQ under changing light conditions. Electron paramagnetic resonance can provide insights into the concentration of singlet oxygen, a transient excited state of molecular oxygen with a lifetime in the range of μs, in the photosynthetic membrane in response to illumination conditions.

Part I of the dissertation (Chapters 2 and 3) presents the results from ultrafast TA spectroscopy measurements of Chl-Car EET and CT quenching processes occurring in intact photosynthetic systems. The snapshot TA technique provides the ability to monitor the dynamics of ultrafast processes that evolve over time, such as probing the timescale and activation dynamics of NPQ quenching mechanisms with a time resolution of 30 seconds in response to HL exposure. In Chapter 2, the approach of snapshot TA is presented[120] along with its application to spinach thylakoid membranes.[59] In Chapter 3, the technique is extended to intact cells of the microalgal species *Nannochloropsis oceanica*, along with mutants lacking the xanthophyll Zea or the LHCX1 protein.[60]

In Part II (Chapters 4 and 5), I explore the dynamics of NPQ and NPQ-related processes in intact photosynthetic organisms via the nanosecond photophysics associated with the Chl excited states as monitored by fluorescence lifetime snapshots under fluctuating HL/dark conditions. In Chapter 4, the technique is applied to leaves of *Arabidopsis thaliana*, as well as to mutants affected in PsbS, Zea, and/or Lut.[122] Multi-timescale kinetic modeling is employed to understand the plant's response to periodic illumination, and provides a basis for future optimization of the NPQ response under dynamic light conditions. In Chapter 5, the approach is extended to intact cells of the model green alga *Chlamydomonas reinhardtii* during exposure to light fluctuations occurring at various frequencies. By utilizing multiple mutants of the LHCSR proteins and/or state transitions, the contributions of qE and qT are disentangled during periods of illumination and darkness.[123]

Finally, in Part III (Chapter 6), I turn to steady-state measurements of singlet oxygen production, primarily by chemical trapping and subsequent detection by EPR spectroscopy, in order to ascertain the suspected implications of NPQ for the management of reactive oxygen species during prolonged light stress. The results are consistent with the conventional model of NPQ in modulating the concentration of singlet oxygen in the thylakoid membrane.

Although the overall importance of NPQ for photosynthetic biomass production and crop yields is well established, the *in vivo* operation of the individual mechanisms remains controversial. Continued integration of the aforementioned snapshot spectroscopies and their application to emerging model organisms and new NPQ mutants is poised to unravel the many molecular and photophysical intricacies of photoprotection. The techniques are well-suited for studying photoprotection in a range of plant and algal species and should be capable of monitoring the real-time response of a plant or algal cell to a wide range of environmental perturbations, not just high light. Therefore, snapshot spectroscopy approaches can be used to inform ongoing efforts to optimize photoprotection under realistic conditions such as those found in the natural environment.

1.5 References

(1) Shevela, D.; Bjorn, L. O.; Govindjee. *Photosynthesis: Solar Energy for Life*; World Scientific, 2019.

(2) Godfray, H. C. J.; Beddington, J. R.; Crute, I. R.; Haddad, L.; Lawrence, D.; Muir, J. F.; Pretty, J.; Robinson, S.; Thomas, S. M.; Toulmin, C. Food security: The challenge of feeding 9 billion people. *Science* **2010**, *327* (5967), 812–818.

(3) Food and Agriculture Organization of the United Nations. *The Future of Food and Agriculture – Alternative Pathways to 2050*; 2018.

(4) Canadell, J. G.; Schulze, E. D. Global potential of biospheric carbon management for climate mitigation. *Nat. Commun.* **2014**, *5* (1), 1–12.

(5) Ort, D. R.; Merchant, S. S.; Alric, J.; Barkan, A.; Blankenship, R. E.; Bock, R.; Croce, R.; Hanson, M. R.; Hibberd, J. M.; Long, S. P.; Moore, T. A.; Moroney, J.; Niyogi, K. K.; Parry, M. A. J.; Peralta-Yahya, P. P.; Prince, R. C.; Redding, K. E.; Spalding, M. H.; van Wijk, K. J.; Vermaas, W. F. J.; von Caemmerer, S.; Weber, A. P. M.; Yeates, T. O.; Yuan, J. S.; Zhu, X.-G. Redesigning photosynthesis to sustainably meet global food and bioenergy demand. *Proc. Natl. Acad. Sci. U. S. A.* **2015**, *112* (28), 8529–8536.

(6) Johnson, M. P. Photosynthesis. *Essays Biochem.* **2016**, *60* (3), 255–273.

(7) Field, C. B.; Behrenfeld, M. J.; Randerson, J. T.; Falkowski, P. Primary production of the biosphere: integrating terrestrial and oceanic components. *Science* **1998**, *281* (5374), 237–240.

(8) Blankenship, R. E.; Tiede, D. M.; Barber, J.; Brudvig, G. W.; Fleming, G. R.; Ghirardi, M.; Gunner, M. R.; Junge, W.; Kramer, D. M.; Melis, A.; Moore, T. A.; Moser, C. C.; Nocera, D. G.; Nozik, A. J.; Ort, D. R.; Parson, W. W.; Prince, R. C.; Sayre, R. T. Comparing photosynthetic and photovoltaic efficiencies and recognizing the potential for improvement. *Science* **2011**, *332* (6031), 805–809.

(9) Lewis, N. S.; Nocera, D. G. Powering the planet: chemical challenges in solar energy utilization. *Proc. Natl. Acad. Sci. U. S. A.* **2006**, *103* (43), 15729–15735.

(10) Gust, D.; Moore, T. A.; Moore, A. L. Solar fuels via artificial photosynthesis. *Acc. Chem. Res.* **2009**, *42* (12), 1890–1898.

(11) Wang, C.; Zhou, Z.; Ouyang, Y.; Wang, J.; Neumann, E.; Nechushtai, R.; Willner, I. Gated Dissipative Dynamic Artificial Photosynthetic Model Systems. *J. Am. Chem. Soc.* **2021**, *143* (31), 12120–12128.

(12) Proppe, A. H.; Li, Y. C.; Aspuru-Guzik, A.; Berlinguette, C. P.; Chang, C. J.; Cogdell, R.; Doyle, A. G.; Flick, J.; Gabor, N. M.; van Grondelle, R.; Hammes-Schiffer, S.; Jaffer, S. A.; Kelley, S. O.; Leclerc, M.; Leo, K.; Mallouk, T. E.; Narang, P.; Schlau-Cohen, G. S.; Scholes, G. D.; Vojvodic, A.; Yam, V. W.-W.; Yang, J. Y.; Sargent, E. H. Bioinspiration in light harvesting and catalysis. *Nat. Rev. Mater.* **2020**, *5*, 828–846.

(13) Utschig, L. M.; Soltau, S. R.; Tiede, D. M. Light-driven hydrogen production from Photosystem I-catalyst hybrids. *Curr. Opin. Chem. Biol.* **2015**, *25*, 1–8.

(14) Scholes, G. D.; Fleming, G. R.; Olaya-Castro, A.; van Grondelle, R. Lessons from nature about solar light harvesting. *Nat. Chem.* **2011**, *3* (10), 763–774.

(15) Hambourger, M.; Moore, G. F.; Kramer, D. M.; Gust, D.; Moore, A. L.; Moore, T. A. Biology and technology for photochemical fuel production. *Chem. Soc. Rev.* **2009**, *38* (1), 25–35.

(16) Searchinger, T.; Hanson, C.; Ranganathan, J.; Lipinski, B.; Waite, R.; Winterbottom, R.;

Dinshaw, A.; Heimlich, R. *The Great Balancing Act. Working Paper, Installment 1 of Creating a Sustainable Food Future, Washington, DC: World Resources Institute*; 2013.
(17) Flavelle, C. Climate Change Threatens the World's Food Supply, United Nations Warns. *The New York Times*. August 8, 2019.
(18) Hussain, S.; Ulhassan, Z.; Brestic, M.; Zivcak, M.; Zhou, W.; Allakhverdiev, S. I.; Yang, X.; Safdar, M. E.; Yang, W.; Liu, W. Photosynthesis research under climate change. *Photosynth. Res.* **2021**, *1*, 1–15.
(19) Walter, J.; Kromdijk, J. Here comes the sun: How optimization of photosynthetic light reactions can boost crop yields. *J. Integr. Plant Biol.* **2022**, *64* (2), 564–591.
(20) Kromdijk, J.; Long, S. P. One crop breeding cycle from starvation? How engineering crop photosynthesis for rising CO2 and temperature could be one important route to alleviation. *Proc. R. Soc. B* **2016**, *283* (1826), 20152578.
(21) Kirchhoff, H.; Tremmel, I.; Haase, W.; Kubitscheck, U. Supramolecular Photosystem II Organization in Grana Thylakoid Membranes: Evidence for a Structured Arrangement. *Biochemistry* **2004**, *43* (28), 9204–9213.
(22) Dekker, J. P.; Boekema, E. J. Supramolecular organization of thylakoid membrane proteins in green plants. *Biochim. Biophys. Acta - Bioenerg.* **2005**, *1706* (1–2), 12–39.
(23) Umena, Y.; Kawakami, K.; Shen, J.-R.; Kamiya, N. Crystal structure of oxygen-evolving photosystem II at a resolution of 1.9 Å. *Nature* **2011**, *473* (7345), 55–60.
(24) Nelson, N.; Ben-Shem, A. The complex architecture of oxygenic photosynthesis. *Nat. Rev. Mol. Cell Biol.* **2004**, *5* (12), 971–982.
(25) Croce, R.; van Amerongen, H. Natural strategies for photosynthetic light harvesting. *Nat. Chem. Biol.* **2014**, *10* (7), 492–501.
(26) Blankenship, R. E. *Molecular Mechanisms of Photosynthesis*, 2nd ed.; Blackwell Science, 2014.
(27) Kirchhoff, H.; Mukherjee, U.; Galla, H. J. Molecular architecture of the thylakoid membrane: Lipid diffusion space for plastoquinone. *Biochemistry* **2002**, *41* (15), 4872–4882.
(28) Shen, J.-R. The Structure of Photosystem II and the Mechanism of Water Oxidation in Photosynthesis. *Annu. Rev. Plant Biol.* **2015**, *66* (1), 23–48.
(29) Björkman, O.; Demmig, B. Photon yield of O2 evolution and chlorophyll fluorescence characteristics at 77 K among vascular plants of diverse origins. *Planta* **1987**, *170* (4), 489–504.
(30) Wraight, C. A.; Clayton, R. K. The absolute quantum efficiency of bacteriochlorophyll photooxidation in reaction centres of Rhodopseudomonas spheroides. *Biochim. Biophys. Acta - Bioenerg.* **1974**, *333* (2), 246–260.
(31) Liu, H.; Blankenship, R. E. On the interface of light-harvesting antenna complexes and reaction centers in oxygenic photosynthesis. *Biochim. Biophys. Acta - Bioenerg.* **2019**, *1860* (11), 148079.
(32) Arshad, R.; Saccon, F.; Bag, P.; Biswas, A.; Calvaruso, C.; Bhatti, A. F.; Grebe, S.; Mascoli, V.; Mahbub, M.; Muzzopappa, F.; Polyzois, A.; Schiphorst, C.; Sorrentino, M.; Streckaité, S.; van Amerongen, H.; Aro, E.-M.; Bassi, R.; Boekema, E. J.; Croce, R.; Dekker, J.; van Grondelle, R.; Jansson, S.; Kirilovsky, D.; Kouřil, R.; Michel, S.; Mullineaux, C. W.; Panzarová, K.; Robert, B.; Ruban, A. V; van Stokkum, I.; Wientjes, E.; Büchel, C. A kaleidoscope of photosynthetic antenna proteins and their emerging roles. *Plant Physiol.* **2022**.

(33) Mirkovic, T.; Ostroumov, E. E.; Anna, J. M.; van Grondelle, R.; Govindjee; Scholes, G. D. Light Absorption and Energy Transfer in the Antenna Complexes of Photosynthetic Organisms. *Chem. Rev.* **2017**, *117* (2), 249–293.
(34) Beddard, G. S.; Porter, G. Concentration quenching in chlorophyll. *Nature* **1976**, *260* (5549), 366–367.
(35) Liu, Z.; Yan, H.; Wang, K.; Kuang, T.; Zhang, J.; Gui, L.; An, X.; Chang, W. Crystal structure of spinach major light-harvesting complex at 2.72 Å resolution. *Nature* **2004**, *428* (6980), 287–292.
(36) Lichtenthaler, H. K. Chlorophylls and carotenoids: pigments of photosynthetic biomembranes. In *Methods in Enzymology*; Packer, L., Douce, R., Eds.; Academic Press, 1987; pp 350–382.
(37) Polívka, T.; Frank, H. A. Molecular Factors Controlling Photosynthetic Light Harvesting by Carotenoids. *Acc. Chem. Res.* **2010**, *43* (8), 1125–1134.
(38) Su, X.; Ma, J.; Wei, X.; Cao, P.; Zhu, D.; Chang, W.; Liu, Z.; Zhang, X.; Li, M. Structure and assembly mechanism of plant C2S2M2-type PSII-LHCII supercomplex. *Science* **2017**, *357* (6353), 815–820.
(39) Krause, G. H.; Weis, E. Chlorophyll Fluorescence and Photosynthesis: The Basics. *Annu. Rev. Plant Physiol. Plant Mol. Biol.* **1991**, *42* (1), 313–349.
(40) Krieger-Liszkay, A. Singlet oxygen production in photosynthesis. *J. Exp. Bot.* **2004**, *56* (411), 337–346.
(41) Khorobrykh, S.; Havurinne, V.; Mattila, H.; Tyystjärvi, E. Oxygen and ROS in Photosynthesis. *Plants* **2020**, *9* (1), 91.
(42) Krieger-Liszkay, A.; Shimakawa, G. Regulation of the generation of reactive oxygen species during photosynthetic electron transport. *Biochem. Soc. Trans.* **2022**.
(43) Demmig-Adams, B.; Cohu, C. M.; Muller, O.; Adams, W. W. Modulation of photosynthetic energy conversion efficiency in nature: from seconds to seasons. *Photosynth. Res.* **2012**, *113* (1–3), 75–88.
(44) Gjindali, A.; Herrmann, H. A.; Schwartz, J.-M.; Johnson, G. N.; Calzadilla, P. I. A Holistic Approach to Study Photosynthetic Acclimation Responses of Plants to Fluctuating Light. *Front. Plant Sci.* **2021**, *12*, 1–20.
(45) Slattery, R. A.; Walker, B. J.; Weber, A. P. M.; Ort, D. R. The Impacts of Fluctuating Light on Crop Performance. *Plant Physiol.* **2018**, *176* (2), 990–1003.
(46) MacIntyre, H. L.; Kana, T. M.; Geider, R. J. The effect of water motion on short-term rates of photosynthesis by marine phytoplankton. *Trends Plant Sci.* **2000**, *5* (1), 12–17.
(47) Schenck, H. On the Focusing of Sunlight by Ocean Waves. *J. Opt. Soc. Am.* **1957**, *47* (7), 653.
(48) Roach, T.; Krieger-Liszkay, A. Photosynthetic Regulatory Mechanisms for Efficiency and Prevention of Photo-Oxidative Stress. In *Annual Plant Reviews online*; Wiley, 2019; pp 1–34.
(49) Niyogi, K. K. Photoprotection Revisited: Genetic and Molecular Approaches. *Annu. Rev. Plant Physiol. Plant Mol. Biol.* **1999**, *50* (1), 333–359.
(50) Holt, N. E.; Zigmantas, D.; Valkūnas, L.; Li, X.-P.; Niyogi, K. K.; Fleming, G. R. Carotenoid cation formation and the regulation of photosynthetic light harvesting. *Science* **2005**, *307* (5708), 433–436.
(51) Ahn, T. K.; Avenson, T. J.; Ballottari, M.; Cheng, Y.-C.; Niyogi, K. K.; Bassi, R.; Fleming, G. R. Architecture of a charge-transfer state regulating light harvesting in a plant antenna

protein. *Science* **2008**, *320* (5877), 794–797.
(52) Ma, Y.-Z.; Holt, N. E.; Li, X.-P.; Niyogi, K. K.; Fleming, G. R. Evidence for direct carotenoid involvement in the regulation of photosynthetic light harvesting. *Proc. Natl. Acad. Sci.* **2003**, *100* (3), 4377–4382.
(53) Ruban, A. V.; Berera, R.; Ilioaia, C.; van Stokkum, I. H. M.; Kennis, J. T. M.; Pascal, A. A.; van Amerongen, H.; Robert, B.; Horton, P.; van Grondelle, R. Identification of a mechanism of photoprotective energy dissipation in higher plants. *Nature* **2007**, *450* (7169), 575–578.
(54) Miloslavina, Y.; Wehner, A.; Lambrev, P. H.; Wientjes, E.; Reus, M.; Garab, G.; Croce, R.; Holzwarth, A. R. Far-red fluorescence: A direct spectroscopic marker for LHCII oligomer formation in non-photochemical quenching. *FEBS Lett.* **2008**, *582* (25–26), 3625–3631.
(55) Müller, M. G.; Lambrev, P.; Reus, M.; Wientjes, E.; Croce, R.; Holzwarth, A. R. Singlet Energy Dissipation in the Photosystem II Light-Harvesting Complex Does Not Involve Energy Transfer to Carotenoids. *ChemPhysChem* **2010**, *11* (6), 1289–1296.
(56) Wahadoszamen, M.; Margalit, I.; Ara, A. M.; van Grondelle, R.; Noy, D. The role of charge-transfer states in energy transfer and dissipation within natural and artificial bacteriochlorophyll proteins. *Nat. Commun.* **2014**, *5* (1), 5287.
(57) Pinnola, A.; Staleva-Musto, H.; Capaldi, S.; Ballottari, M.; Bassi, R.; Polívka, T. Electron transfer between carotenoid and chlorophyll contributes to quenching in the LHCSR1 protein from Physcomitrella patens. *Biochim. Biophys. Acta - Bioenerg.* **2016**, *1857* (12), 1870–1878.
(58) Park, S.; Fischer, A. L.; Li, Z.; Bassi, R.; Niyogi, K. K.; Fleming, G. R. Snapshot Transient Absorption Spectroscopy of Carotenoid Radical Cations in High-Light-Acclimating Thylakoid Membranes. *J. Phys. Chem. Lett.* **2017**, *8* (22), 5548–5554.
(59) Park, S.; Fischer, A. L.; Steen, C. J.; Iwai, M.; Morris, J. M.; Walla, P. J.; Niyogi, K. K.; Fleming, G. R. Chlorophyll-Carotenoid Excitation Energy Transfer in High-Light-Exposed Thylakoid Membranes Investigated by Snapshot Transient Absorption Spectroscopy. *J. Am. Chem. Soc.* **2018**, *140* (38), 11965–11973.
(60) Park, S.; Steen, C. J.; Lyska, D.; Fischer, A. L.; Endelman, B.; Iwai, M.; Niyogi, K. K.; Fleming, G. R. Chlorophyll–carotenoid excitation energy transfer and charge transfer in Nannochloropsis oceanica for the regulation of photosynthesis. *Proc. Natl. Acad. Sci.* **2019**, *116* (9), 3385–3390.
(61) Baker, N. R. Chlorophyll Fluorescence: A Probe of Photosynthesis In Vivo. *Annu. Rev. Plant Biol.* **2008**, *59* (1), 89–113.
(62) Wraight, C. A.; Crofts, A. R. Energy-Dependent Quenching of Chlorophyll a Fluorescence in Isolated Chloroplasts. *Eur. J. Biochem.* **1970**, *17* (2), 319–327.
(63) Briantais, J.-M.; Vernotte, C.; Picaud, M.; Krause, G. H. A quantitative study of the slow decline of chlorophyll a fluorescence in isolated chloroplasts. *Biochim. Biophys. Acta - Bioenerg.* **1979**, *548* (1), 128–138.
(64) Giovagnetti, V.; Ruban, A. V. The evolution of the photoprotective antenna proteins in oxygenic photosynthetic eukaryotes. *Biochem. Soc. Trans.* **2018**, *46* (5), 1263–1277.
(65) Niyogi, K. K.; Björkman, O.; Grossman, A. R. The roles of specific xanthophylls in photoprotection. *Proc. Natl. Acad. Sci. U. S. A.* **1997**, *94* (25), 14162–14167.
(66) Demmig-Adams, B.; Adams, W. W. The role of xanthophyll cycle carotenoids in the protection of photosynthesis. *Trends Plant Sci.* **1996**, *1* (1), 21–26.
(67) Jahns, P.; Holzwarth, A. R. The role of the xanthophyll cycle and of lutein in

photoprotection of photosystem II. *Biochim. Biophys. Acta - Bioenerg.* **2012**, *1817* (1), 182–193.
(68) Demmig-Adams, B.; Polutchko, S. K.; Adams III, W. W. Structure-Function-Environment Relationship of the Isomers Zeaxanthin and Lutein. *Photochem* **2022**, *2* (2), 308–325.
(69) Dall'Osto, L.; Cazzaniga, S.; Bressan, M.; Paleček, D.; Židek, K.; Niyogi, K. K.; Fleming, G. R.; Zigmantas, D.; Bassi, R. Two mechanisms for dissipation of excess light in monomeric and trimeric light-harvesting complexes. *Nat. Plants* **2017**, *3* (5), 17033.
(70) Nicol, L.; Nawrocki, W. J.; Croce, R. Disentangling the sites of non-photochemical quenching in vascular plants. *Nat. Plants* **2019**, *5*, 1177–1183.
(71) Guardini, Z.; Bressan, M.; Caferri, R.; Bassi, R.; Dall'Osto, L. Identification of a pigment cluster catalysing fast photoprotective quenching response in CP29. *Nat. Plants* **2020**, *6* (3), 303–313.
(72) Nilkens, M.; Kress, E.; Lambrev, P.; Miloslavina, Y.; Müller, M.; Holzwarth, A. R.; Jahns, P. Identification of a slowly inducible zeaxanthin-dependent component of non-photochemical quenching of chlorophyll fluorescence generated under steady-state conditions in Arabidopsis. *Biochim. Biophys. Acta - Bioenerg.* **2010**, *1797* (4), 466–475.
(73) Dall'Osto, L.; Caffarri, S.; Bassi, R. A Mechanism of Nonphotochemical Energy Dissipation, Independent from PsbS, Revealed by a Conformational Change in the Antenna Protein CP26. *Plant Cell* **2005**, *17* (4), 1217–1232.
(74) Minagawa, J. State transitions—The molecular remodeling of photosynthetic supercomplexes that controls energy flow in the chloroplast. *Biochim. Biophys. Acta - Bioenerg.* **2011**, *1807* (8), 897–905.
(75) Rochaix, J. D.; Lemeille, S.; Shapiguzov, A.; Samol, I.; Fucile, G.; Willig, A.; Goldschmidt-Clermont, M. Protein kinases and phosphatases involved in the acclimation of the photosynthetic apparatus to a changing light environment. *Philos. Trans. R. Soc. B Biol. Sci.* **2012**, *367* (1608), 3466–3474.
(76) Long, S. P.; Humphries, S.; Falkowski, P. G. Photoinhibition of Photosynthesis in Nature. *Annu. Rev. Plant Physiol. Plant Mol. Biol.* **1994**, *45* (1), 633–662.
(77) Aro, E.-M.; Virgin, I.; Andersson, B. Photoinhibition of Photosystem II. Inactivation, protein damage and turnover. *Biochim. Biophys. Acta - Bioenerg.* **1993**, *1143* (2), 113–134.
(78) Malnoë, A. Photoinhibition or photoprotection of photosynthesis? Update on the (newly termed) sustained quenching component qH. *Environ. Exp. Bot.* **2018**, *154* (1), 123–133.
(79) Brooks, M. D.; Sylak-Glassman, E. J.; Fleming, G. R.; Niyogi, K. K. A thioredoxin-like/β-propeller protein maintains the efficiency of light harvesting in Arabidopsis. *Proc. Natl. Acad. Sci. U. S. A.* **2013**, *110* (29), E2733-40.
(80) Amstutz, C. L.; Fristedt, R.; Schultink, A.; Merchant, S. S.; Niyogi, K. K.; Malnoë, A. An atypical short-chain dehydrogenase–reductase functions in the relaxation of photoprotective qH in Arabidopsis. *Nat. Plants* **2020**, 1–13.
(81) Bru, P.; Steen, C. J.; Park, S.; Amstutz, C. L.; Sylak-Glassman, E. J.; Lam, L.; Fekete, A.; Mueller, M. J.; Longoni, F.; Fleming, G. R.; Niyogi, K. K.; Malnoë, A. An energy-dissipative state of the major antenna complex of plants. *bioRxiv* **2022**, 2021.07.09.450705.
(82) Zhu, X.-G.; Long, S. P.; Ort, D. R. Improving Photosynthetic Efficiency for Greater Yield. *Annu. Rev. Plant Biol.* **2010**, *61* (1), 235–261.
(83) Zhu, X.-G.; Long, S. P.; Ort, D. R. What is the maximum efficiency with which photosynthesis can convert solar energy into biomass? *Curr. Opin. Biotechnol.* **2008**, *19* (2), 153–159.

(84) Külheim, C.; Agren, J.; Jansson, S. Rapid regulation of light harvesting and plant fitness in the field. *Science* **2002**, *297* (5578), 91–93.
(85) Zhu, X.-G.; Ort, D. R.; Whitmarsh, J.; Long, S. P. The slow reversibility of photosystem II thermal energy dissipation on transfer from high to low light may cause large losses in carbon gain by crop canopies: a theoretical analysis. *J. Exp. Bot.* **2004**, *55* (400), 1167–1175.
(86) Kromdijk, J.; Głowacka, K.; Leonelli, L.; Gabilly, S. T.; Iwai, M.; Niyogi, K. K.; Long, S. P. Improving photosynthesis and crop productivity by accelerating recovery from photoprotection. *Science* **2016**, *354* (6314), 857–861.
(87) Hubbart, S.; Smillie, I. R. A.; Heatley, M.; Swarup, R.; Foo, C. C.; Zhao, L.; Murchie, E. H. Enhanced thylakoid photoprotection can increase yield and canopy radiation use efficiency in rice. *Commun. Biol.* **2018**, *1* (1), 22.
(88) Głowacka, K.; Kromdijk, J.; Kucera, K.; Xie, J.; Cavanagh, A. P.; Leonelli, L.; Leakey, A. D. B.; Ort, D. R.; Niyogi, K. K.; Long, S. P. Photosystem II Subunit S overexpression increases the efficiency of water use in a field-grown crop. *Nat. Commun.* **2018**, *9* (1), 868.
(89) Niyogi, K. K.; Truong, T. B. Evolution of flexible non-photochemical quenching mechanisms that regulate light harvesting in oxygenic photosynthesis. *Curr. Opin. Plant Biol.* **2013**, *16* (3), 307–314.
(90) Magdaong, N. C. M.; Blankenship, R. E. Photoprotective, excited-state quenching mechanisms in diverse photosynthetic organisms. *J. Biol. Chem.* **2018**, *293* (14), 5018–5025.
(91) Niyogi, K. K.; Grossman, A. R.; Björkman, O. Arabidopsis mutants define a central role for the xanthophyll cycle in the regulation of photosynthetic energy conversion. *Plant Cell* **1998**, *10* (7), 1121–1134.
(92) Li, Z.; Ahn, T. K.; Avenson, T. J.; Ballottari, M.; Cruz, J. A.; Kramer, D. M.; Bassi, R.; Fleming, G. R.; Keasling, J. D.; Niyogi, K. K. Lutein accumulation in the absence of zeaxanthin restores nonphotochemical quenching in the Arabidopsis thaliana npq1 mutant. *Plant Cell* **2009**, *21* (6), 1798–1812.
(93) Adams, W. W.; Demmig-Adams, B. Operation of the xanthophyll cycle in higher plants in response to diurnal changes in incident sunlight. *Planta* **1992**, *186* (3), 390–398.
(94) Arnoux, P.; Morosinotto, T.; Saga, G.; Bassi, R.; Pignol, D. A structural basis for the pH-dependent xanthophyll cycle in Arabidopsis thaliana. *Plant Cell* **2009**, *21* (7), 2036–2044.
(95) Jahns, P.; Latowski, D.; Strzalka, K. Mechanism and regulation of the violaxanthin cycle: The role of antenna proteins and membrane lipids. *Biochim. Biophys. Acta - Bioenerg.* **2009**, *1787* (1), 3–14.
(96) Li, X.-P.; Björkman, O.; Shih, C.; Grossman, A. R.; Rosenquist, M.; Jansson, S.; Niyogi, K. K. A pigment-binding protein essential for regulation of photosynthetic light harvesting. *Nature* **2000**, *403* (6768), 391–395.
(97) Fan, M.; Li, M.; Liu, Z.; Cao, P.; Pan, X.; Zhang, H.; Zhao, X.; Zhang, J.; Chang, W. Crystal structures of the PsbS protein essential for photoprotection in plants. *Nat. Struct. Mol. Biol.* **2015**, *22* (9), 729–735.
(98) Li, X.-P.; Gilmore, A. M.; Caffarri, S.; Bassi, R.; Golan, T.; Kramer, D. M.; Niyogi, K. K. Regulation of photosynthetic light harvesting involves intrathylakoid lumen pH sensing by the PsbS protein. *J. Biol. Chem.* **2004**, *279* (22), 22866–22874.
(99) Dominici, P.; Caffarri, S.; Armenante, F.; Ceoldo, S.; Crimi, M.; Bassi, R. Biochemical properties of the PsbS subunit of photosystem II either purified from chloroplast or

recombinant. *J. Biol. Chem.* **2002**, *277* (25), 22750–22758.
(100) Krishnan-Schmieden, M.; Konold, P. E.; Kennis, J. T. M.; Pandit, A. The molecular pH-response mechanism of the plant light-stress sensor PsbS. *Nat. Commun.* **2021**, *12* (1), 2291.
(101) Correa-Galvis, V.; Poschmann, G.; Melzer, M.; Stühler, K.; Jahns, P. PsbS interactions involved in the activation of energy dissipation in Arabidopsis. *Nat. Plants* **2016**, *2* (2), 15225.
(102) Kiss, A. Z.; Ruban, A. V; Horton, P. The PsbS protein controls the organization of the photosystem II antenna in higher plant thylakoid membranes. *J. Biol. Chem.* **2008**, *283* (7), 3972–3978.
(103) Bellafiore, S.; Barneche, F.; Peltier, G.; Rochaix, J.-D. State transitions and light adaptation require chloroplast thylakoid protein kinase STN7. *Nature* **2005**, *433* (7028), 892–895.
(104) Rantala, M.; Rantala, S.; Aro, E. M. Composition, phosphorylation and dynamic organization of photosynthetic protein complexes in plant thylakoid membrane. *Photochem. Photobiol. Sci.* **2020**, *19* (5), 604–619.
(105) Peers, G.; Truong, T. B.; Ostendorf, E.; Busch, A.; Elrad, D.; Grossman, A. R.; Hippler, M.; Niyogi, K. K. An ancient light-harvesting protein is critical for the regulation of algal photosynthesis. *Nature* **2009**, *462* (7272), 518–521.
(106) Erickson, E.; Wakao, S.; Niyogi, K. K. Light stress and photoprotection in Chlamydomonas reinhardtii. *Plant J.* **2015**, *82* (3), 449–465.
(107) Bonente, G.; Ballottari, M.; Truong, T. B.; Morosinotto, T.; Ahn, T. K.; Fleming, G. R.; Niyogi, K. K.; Bassi, R. Analysis of LhcSR3, a Protein Essential for Feedback De-Excitation in the Green Alga Chlamydomonas reinhardtii. *PLoS Biol.* **2011**, *9* (1), e1000577.
(108) Manna, P.; Schlau-Cohen, G. S. Photoprotective conformational dynamics of photosynthetic light-harvesting proteins. *Biochim. Biophys. Acta - Bioenerg.* **2022**, *1863* (4), 148543.
(109) Niyogi, K. K.; Bjorkman, O.; Grossman, A. R. Chlamydomonas Xanthophyll Cycle Mutants Identified by Video Imaging of Chlorophyll Fluorescence Quenching. *Plant Cell* **1997**, *9* (8), 1369–1380.
(110) Delosme, R.; Olive, J.; Wollman, F. A. Changes in light energy distribution upon state transitions: an in vivo photoacoustic study of the wild type and photosynthesis mutants from Chlamydomonas reinhardtii. *Biochim. Biophys. Acta - Bioenerg.* **1996**, *1273* (2), 150–158.
(111) Allorent, G.; Tokutsu, R.; Roach, T.; Peers, G.; Cardol, P.; Girard-Bascou, J.; Seigneurin-Berny, D.; Petroutsos, D.; Kuntz, M.; Breyton, C.; Franck, F.; Wollman, F.-A.; Niyogi, K. K.; Krieger-Liszkay, A.; Minagawa, J.; Finazzi, G. A dual strategy to cope with high light in Chlamydomonas reinhardtii. *Plant Cell* **2013**, *25* (2), 545–557.
(112) Depège, N.; Bellafiore, S.; Rochaix, J. D. Role of chloroplast protein kinase Stt7 in LHCII phosphorylation and state transition in Chlamydomonas. *Science* **2003**, *299* (5612), 1572–1575.
(113) Giordano, M.; Beardall, J.; Raven, J. A. CO2 Concentrating Mechanisms in Algae: Mechanisms, Environmental Modulation, and Evolution. *Annu. Rev. Plant Biol.* **2005**, *56*, 99–131.
(114) Burlacot, A.; Dao, O.; Auroy, P.; Cuiné, S.; Li-Beisson, Y.; Peltier, G. Alternative photosynthesis pathways drive the algal CO2-concentrating mechanism. *Nature* **2022**, 1–6.
(115) Kilian, O.; Benemann, C. S. E.; Niyogi, K. K.; Vick, B. High-efficiency homologous recombination in the oil-producing alga Nannochloropsis sp. *Proc. Natl. Acad. Sci. U. S. A.*

2011, *108* (52), 21265–21269.
(116) Vieler, A.; Wu, G.; Tsai, C.-H.; Bullard, B.; Cornish, A. J.; Harvey, C.; Reca, I.-B.; Thornburg, C.; Achawanantakun, R.; Buehl, C. J.; Campbell, M. S.; Cavalier, D.; Childs, K. L.; Clark, T. J.; Deshpande, R.; Erickson, E.; Armenia Ferguson, A.; Handee, W.; Kong, Q.; Li, X.; Liu, B.; Lundback, S.; Peng, C.; Roston, R. L.; Sanjaya; Simpson, J. P.; TerBush, A.; Warakanont, J.; Zäuner, S.; Farre, E. M.; Hegg, E. L.; Jiang, N.; Kuo, M.-H.; Lu, Y.; Niyogi, K. K.; Ohlrogge, J.; Osteryoung, K. W.; Shachar-Hill, Y.; Sears, B. B.; Sun, Y.; Takahashi, H.; Yandell, M.; Shiu, S.-H.; Benning, C. Genome, Functional Gene Annotation, and Nuclear Transformation of the Heterokont Oleaginous Alga Nannochloropsis oceanica CCMP1779. *PLoS Genet.* **2012**, *8* (11), e1003064.
(117) Litvín, R.; Bína, D.; Herbstová, M.; Gardian, Z. Architecture of the light-harvesting apparatus of the eustigmatophyte alga Nannochloropsis oceanica. *Photosynth. Res.* **2016**, *130* (1–3), 137–150.
(118) Alboresi, A.; Le Quiniou, C.; Yadav, S. K. N.; Scholz, M.; Meneghesso, A.; Gerotto, C.; Simionato, D.; Hippler, M.; Boekema, E. J.; Croce, R.; Morosinotto, T. Conservation of core complex subunits shaped the structure and function of photosystem I in the secondary endosymbiont alga *Nannochloropsis gaditana*. *New Phytol.* **2017**, *213* (2), 714–726.
(119) Short, A. H.; Fay, T. P.; Crisanto, T.; Hall, J.; Steen, C. J.; Niyogi, K. K.; Limmer, D. T.; Fleming, G. R. Xanthophyll-cycle based model of the rapid photoprotection of Nannochloropsis in response to regular and irregular light/dark sequences. *J. Chem. Phys.* **2022**.
(120) Park, S.; Steen, C. J.; Fischer, A. L.; Fleming, G. R. Snapshot transient absorption spectroscopy: toward in vivo investigations of nonphotochemical quenching mechanisms. *Photosynth. Res.* **2019**, *141* (3), 367–376.
(121) Sylak-Glassman, E. J.; Zaks, J.; Amarnath, K.; Leuenberger, M.; Fleming, G. R. Characterizing non-photochemical quenching in leaves through fluorescence lifetime snapshots. *Photosynth. Res.* **2016**, *127* (1), 69–76.
(122) Steen, C. J.; Morris, J. M.; Short, A. H.; Niyogi, K. K.; Fleming, G. R. Complex Roles of PsbS and Xanthophylls in the Regulation of Nonphotochemical Quenching in Arabidopsis thaliana under Fluctuating Light. *J. Phys. Chem. B* **2020**, *124* (46), 10311–10325.
(123) Steen, C. J.; Burlacot, A.; Short, A. H.; Niyogi, K. K.; Fleming, G. R. Interplay between LHCSR proteins and state transitions governs the NPQ response in intact cells of Chlamydomonas during light fluctuations. *bioRxiv* **2022**, 2021.12.31.474662.
(124) Wolf, B. M.; Blankenship, R. E. Far-red light acclimation in diverse oxygenic photosynthetic organisms. *Photosynth. Res.* **2019**, *142*, 349–359.
(125) Müller, P.; Li, X.-P.; Niyogi, K. K. Non-photochemical quenching. A response to excess light energy. *Plant Physiol.* **2001**, *125* (4), 1558–1566.

Chapter 2

Snapshot Transient Absorption Studies of Photophysical Dissipation Mechanisms in Intact Photosynthetic Samples

Sections of this chapter are reproduced with permission from the following publications:

S. Park, A.L. Fischer, C.J. Steen, M. Iwai, J.M. Morris, P.J. Walla, K.N. Niyogi, G.R. Fleming
"Chlorophyll-Carotenoid Excitation Energy Transfer in High-Light-Exposed Thylakoid Membranes Investigated by Snapshot Transient Absorption Spectroscopy"
Journal of the American Chemical Society (2018) 140, 38, 11965–11973
DOI: 10.1021/jacs.8b04844. Copyright © 2018 American Chemical Society

S. Park, C.J. Steen, A.L. Fischer, G.R. Fleming
"Snapshot transient absorption spectroscopy:
toward *in vivo* investigations of nonphotochemical quenching mechanisms"
Photosynthesis Research (2019) 141, 367–376
DOI: 10.1007/s11120-019-00640-x. Copyright © 2019 Springer Nature

This chapter also contains unpublished snapshot TA data
collected in collaboration with Soomin Park.

2.1 Abstract

Nonphotochemical quenching (NPQ) provides an essential photoprotection in plants, assuring safe dissipation of excess energy as heat under high light. Although excitation energy transfer (EET) between chlorophyll (Chl) and carotenoid (Car) molecules plays an important role in NPQ, detailed information on the EET quenching mechanism under *in vivo* conditions, including the triggering mechanism and activation dynamics, is very limited. Here, we observed EET between the Chl Q_y state and the Car S_1 state in high-light-exposed spinach thylakoid membranes. The kinetic and spectral analyses using transient absorption (TA) spectroscopy revealed that the Car S_1 excited state absorption (ESA) signal after Chl excitation has a maximum absorption peak around 540 nm and a lifetime of ~8 ps. Snapshot TA spectroscopy at multiple time delays allowed us to track the Car S_1 ESA signal as the thylakoid membranes were exposed to various light conditions. The obtained snapshots indicate that maximum Car S_1 ESA signal quickly rose and slightly dropped during the initial high-light exposure (<3 min) and then gradually increased with a time constant of ~5 min after prolonged light exposure. This suggests the involvement of both rapidly activated and slowly activated mechanisms for EET quenching. 1,4-Dithiothreitol (DTT) and 3,3′-dithiobis(sulfosuccinimidyl propionate) (DTSSP) chemical treatments further support that the Car S_1 ESA signal (or the EET quenching mechanism) is primarily dependent on the accumulation of zeaxanthin and partially dependent on the reorganization of membrane proteins, perhaps due to the pH-sensing protein photosystem II subunit S.

2.2 Snapshot TA probes the ultrafast molecular mechanisms of NPQ

Photosynthetic organisms must consistently balance efficient light harvesting and the need to avoid the harmful effects associated with absorbing too much light.[1,2] One such way that photosynthetic organisms minimize photooxidative damage is through the dissipation of excess absorbed light energy as heat, a process referred to as nonphotochemical quenching (NPQ). Technically, NPQ encompasses a suite of different processes that differ in the molecular species involved, in the timescales of their activation and subsequent relaxation, and possibly in their specific location within the chloroplast. The activation of NPQ decreases the lifetime of excited chlorophyll (Chl*), which in turn can make the formation of reactive oxygen species less probable. Energy-dependent quenching (qE) accounts for the majority (~ 75%) of the overall NPQ[3] and is the most rapid component of the photoprotective response, becoming active within seconds to minutes of exposure to high light.[4] A deeper knowledge of the underlying molecular mechanisms associated with qE is beneficial especially since it has recently been shown that regulating proteins involved in qE can improve water use efficiency[5] as well as increase biomass productivity in algae[6] and green plants[7] under fluctuating light conditions.

Despite the importance of qE to plant fitness and survival, its underlying mechanisms remain controversial or unknown. Several different mechanisms have been proposed including excitation energy transfer (EET) quenching in which energy is transferred from a Chl molecule to a carotenoid (Car) molecule followed by energy dissipation (Figure 2-1a).[8–10] Charge transfer (CT) quenching is also possible in which electron transfer from Car to Chl results in the formation of a dimer state which can accept energy from a neighboring Chl molecule (Figure 2-1b).[11,12] This is followed by charge recombination and rapid relaxation to the ground state, dissipating energy in the process. Other proposed mechanisms include an excitonic quenching model based on bidirectional energy transfer between Chl and Car[13] and Chl–Chl CT.[14,15] We note that it is possible that multiple mechanisms may be occurring simultaneously and that the given mechanisms may differ depending upon the overall protein (and chemical) environment.

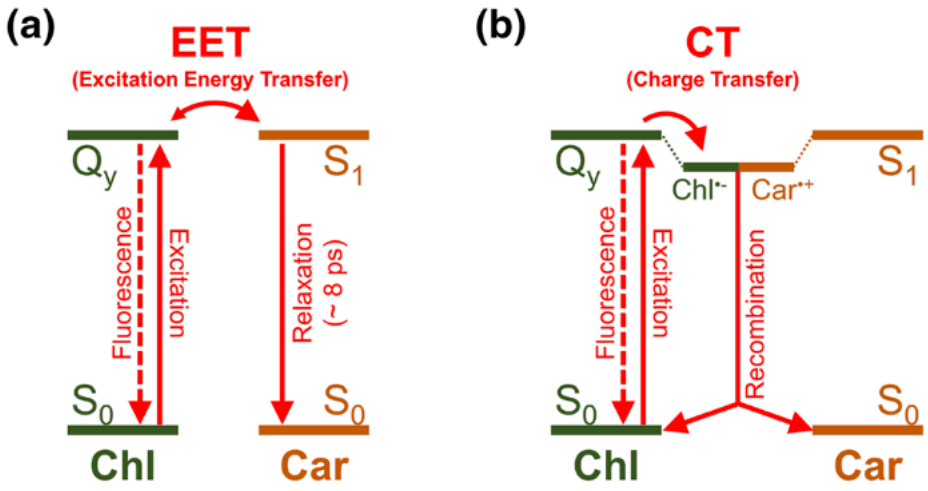

Figure 2-1. Schematic energy-level diagrams illustrating the steps involved in the proposed excitation energy transfer (EET) and charge transfer (CT) quenching mechanisms involving Chl-Car interactions.

However, these proposed mechanisms have been largely based on *in vitro* studies of isolated proteins, which cannot reflect normal physiological conditions. Recent studies have revealed that Car orientations,[10,16] as well as various Car-Chl,[17] Car-protein,[10] pigment-protein,[18–20] and protein–protein interactions[21] can control the dynamics of excitation energy in intact systems. As such, to obtain physiologically relevant information, it is necessary to perform experiments on systems that exist in a state as near native as possible. For example, previous TA spectroscopy studies of crude thylakoid membranes from spinach and *Arabidopsis thaliana* have confirmed the presence of both EET[22] and CT[23] quenching based on the observation of Car S_1 and $Car^{\bullet+}$ excited state absorptions (ESA) after Chl excitation. However, it is still very challenging to obtain information on specific mechanisms *in vivo* because conventional TA measurements of intact samples (e.g., cells, leaves, and thylakoid membranes) are accompanied by large scattering, many spectrally overlapping signals, and a poor signal-to-noise ratio. For these reasons, it has not been possible to collect quantitative and dynamic information on the specific quenching mechanisms in intact samples.

To address these issues, we have developed an ultrafast spectroscopic technique called snapshot TA spectroscopy. Using this technique, snapshots that correspond to the ESA signal can be collected from intact thylakoid membranes or whole cells in 10 s windows at intervals ranging from 30 s to 1 min, which is adequate to resolve the timescale of qE. Consequently, snapshot TA allows us to not only observe the molecular species involved in the qE mechanisms, but also to monitor their participation as photosynthetic organisms experience changes in light intensity in real time. By combining our snapshot TA data in conjunction with Chl fluorescence lifetimes, which are measured using the previously reported Chl fluorescence lifetime snapshot technique,[24] we gain important insights into the activation of the EET and CT mechanisms in the context of overall Chl* quenching.

2.3 Probing Photoprotective Dissipative Mechanisms in Spinach Thylakoids

The capacity of photosynthetic organisms to utilize the flow of excitation energy from absorbed sunlight is not unlimited. Under light-saturated conditions, the reaction center in photosystem II (PSII) closes due to lack of plastoquinones available for electron transfer.[25] As a consequence, the fluorescence lifetime (~ns) of excited chlorophyll (Chl) in the antenna increases, which in turn increases the probability of formation of the Chl triplet state and reactive oxygen species, which can damage photosynthetic proteins.[26] Nonphotochemical quenching (NPQ) is a proxy for photoprotective thermal dissipation in which absorbed light energy is safely converted into heat.[4] NPQ is a term which encapsulates many components, termed qE, qZ, qT, and qI, which were conventionally classified based on their induction and relaxation kinetics.[4,27,28] Among them, energy-dependent quenching (qE) is the fastest component, and is responsible for the largest portion of overall Chl de-excitation, providing relaxation pathways for the excited Chl on a time scale of a few seconds to minutes after excess light conditions occur.[4,29]

The carotenoid (Car) pigments in PSII serve an essential role in qE.[30] In land plants, the enzymatic production of the carotenoid zeaxanthin (Zea) increases in response to high light, and Zea appears to be essential for maximum qE.[31–33] Direct involvement of Zea in Chl quenching has been suggested based on evidence of the interactions between Zea S_1 and Chl Q_y excited states.[34,35] To explain Chl-Zea energy transfer and subsequent Chl quenching, two mechanisms have been proposed: a charge-transfer (CT) quenching and excitation energy transfer (EET) quenching.[36] In the CT quenching mechanism, Chl and Zea are in close enough proximity to form a Chl-Zea heterodimer, which accepts excitation energy from the bulk Chl pool. Then, the heterodimer becomes charge-separated and forms a Zea radical cation ($Zea^{\bullet+}$) and a Chl radical anion ($Chl^{\bullet-}$).[12,23,37,38] This is followed by charge recombination which leads to energy dissipation. In the EET quenching mechanism, the excitation energy is directly transferred from the Chl Q_y state to the Zea S_1 state.[22] The direction of energy transfer is not necessarily Chl $Q_y \rightarrow$ Zea S_1, as bidirectional energy transfer, Chl $Q_y \leftrightarrow$ Zea S_1, has been shown to occur when the two state energies are similar and there is strong electronic coupling between them.[13,36,39–41] After energy transfer, the Zea S_1 state rapidly relaxes to the ground state with a lifetime of ~9 ps.[22,42–44] Other carotenoids, such as lutein (Lut), have also been considered as direct quenchers in CT and EET quenching mechanisms.[8,30,45] Although it has been speculated that both quenching mechanisms contribute to overall qE, the specific details of the quenching sites, triggering factors, activation time courses, and relative contributions of individual mechanisms are not well understood.

Recently, we reported the use of snapshot TA spectroscopy to gather quantitative and dynamic information on the $Zea^{\bullet+}$-mediated CT quenching mechanism in high-light-exposed spinach thylakoid membranes.[38] Those experiments focused on one wavelength (1000 nm) and time delay (20 ps), and allowed us to collect the $Zea^{\bullet+}$ excited state absorption (ESA) signal within 10 s windows over the course of high-light exposure. The $Zea^{\bullet+}$ ESA signal reaches maximum intensity at the beginning (≤2 min) of high-light exposure, which suggests that $Zea^{\bullet+}$ formation is closely related to early qE. The evolution of the $Zea^{\bullet+}$ signal correlated well with the lumenal $[H^+]$ and the rate of Chl fluorescence quenching. In addition, a cross-linking assay[46] arresting rearrangement of the pH-sensing PSII subunit S (PsbS) protein completely removed $Zea^{\bullet+}$ signals, and suggested that the CT quenching mechanism was triggered by a ΔpH → messenger protein(s) pathway.[29,47]

To investigate a Chl-Car EET quenching mechanism in thylakoid membranes during exposure to high-light, we have modified our above-mentioned snapshot TA technique to probe at 540 nm where maximum Car S_1–S_N absorption is observed. Increased population of the Car S_1 state after Chl excitation (650 nm) should provide evidence for the EET quenching mechanism.[40,42,48] Combining the new data with fluorescence lifetime snapshot data and our previous $Zea^{\bullet+}$ snapshot data,[38] we provide a broader picture of the EET and CT quenching mechanisms.

2.4 Experimental Methods

2.4.1 Isolation of Thylakoid Membranes

Fresh spinach leaves were purchased the day before the measurements and stored in the dark at 4 °C overnight. The spinach leaves used in the experiment were grown in northern California and harvested in early spring (February to March). Isolation of crude thylakoid membranes was performed in a dark cold room (4 °C), following the protocol reported by Gilmore et al.[49] The final concentrations of all thylakoid samples were adjusted to 100 μg Chl/mL using reaction buffer before measurement. The reaction buffer at pH 8 contained 30 mM ascorbic acid, 0.5 mM ATP, and 50 μM methyl viologen. The working concentrations of DTSSP and DTT were 3 and 2 mM, respectively.

2.4.2 Fluorescence Lifetime Snapshots

Fluorescence decay snapshots were recorded with a home-built time-correlated single photon counting (TCSPC) apparatus described previously.[24,50,51] First, 840 nm output pulses generated by Ti:sapphire oscillator (Coherent, Mira 900f, 76 MHz) were frequency-doubled using a beta barium borate (BBO) crystal. The resultant 420 nm pulses correspond to the Soret band absorption of Chl *a*. Before the sample, the beam was split by a beam splitter, so that a portion was directed to a photodiode providing SYNC for the TCSPC card (Becker-Hickl, SPC-630 and SPC-850). The remainder of the beam was sent to excite the sample and was intermittently blocked by a shutter controlled by a LabVIEW program. The excitation laser power was set to 1.6 mW (≅1650 μmol photons·m^{-2}·s^{-1}) at the sample, which is enough to close reaction centers.[52] The sample was intermittently exposed to an actinic light (Schott, KL1500) with an intensity of 850 μmol photons·m^{-2}·s^{-1}, also controlled by a shutter and LabVIEW program. After the sample, a monochromator set to 680 nm and a MCP PMT detector (Hamamatsu, R3809U) were placed for fluorescence detection. The fluorescence decay curves were measured at intervals varying from every 10 s to every 30 s. In each measurement, the sample was exposed to the laser for one second, divided up into five steps of 0.2 s. The step with the longest fluorescence lifetime was selected in data processing to ensure that the PSII reaction centers were closed.[24] Each fluorescence decay curve was fit to a sum of three exponential decay components (Picoquant, Fluofit Pro-4.6). Following data fitting, the amplitude-weighted average lifetime (τ_{avg}) and NPQτ values were calculated using the following equations:[24,38,51]

$$\tau_{\mathrm{avg}} = \frac{\sum_{\mathrm{i}} A_{\mathrm{i}}\tau_{\mathrm{i}}}{\sum_{\mathrm{i}} A_{\mathrm{i}}} \quad (1)$$

where A_{i} and τ_{i} are the amplitudes and the fluorescence lifetime components, respectively, which are obtained from fitting the fluorescence decay with 3 exponentials. The NPQ response (NPQ_{τ}) in terms of the average florescence lifetime is defined as:

$$NPQ_{\tau} = \frac{\tau_{\mathrm{avg,dark}} - \tau_{\mathrm{avg,light}}}{\tau_{\mathrm{avg,light}}} \quad (2)$$

where $\tau_{\mathrm{avg,dark}}$ is the average of three lifetimes measured during the initial dark period.

2.4.3 Pump–Probe Spectroscopy for TA Measurements

A description of the pump–probe transient absorption spectroscopy setup used in this study can be found in previous literature.[12,23,37,38] Briefly, the experiments were performed using a Ti:sapphire regenerative amplifier (Coherent, RegA 9050) seeded by a Ti:sapphire oscillator (Coherent, MIRA Seed), generating an 800 nm pulse with a repetition rate of 250 kHz. The beam was split to generate the pump and probe beams. For the probe, the beam was focused on a 1 mm sapphire crystal to produce a visible continuum, and a 700 nm short pass filter was placed after continuum generation. For the pump, another beam pumped an optical parametric amplifier (Coherent, OPA 9450). The OPA was tuned to generate a 20 nJ/pulse centered at 650 nm for the Chl *b* Q_y transition which yielded higher signal-to-noise ratio than 680 nm. The fwhm of pump pulses was 50 fs. The pump and probe were overlapped at the sample at the magic-angle (54.7°) polarization. The diameters of the pump and probe at the sample position were 150 and 65 μm, respectively. The cross-correlation time between the pump pulse and probe pulse was found to be ∼120 fs. After the sample, a second polarization filter set to the probe polarization and a 658 ± 26 nm notch filter were placed to minimize pump scattering and ensure a clean probe signal. After passing through a monochromator (Acton Research Corp., SpectraPro 300i), the signal was detected by using a Si-biased photodiode (Thorlabs, DET10A) which was connected to a lock-in amplifier (Stanford Research, SR830). The lock-in amplifier was synchronized with a chopper positioned in the pump beam path. An actinic light with a heat absorbing filter (KG1) was set to an intensity of 850 μmol photons$\cdot m^{-2}\cdot s^{-1}$ at the sample position.

2.4.4 Development of Snapshot TA Spectroscopy

For collecting snapshot TA data at fixed time delays (1 and 40 ps) and wavelength (540 nm), a pump and probe shutter was controlled to open for 10 s at intervals ranging from 30 s to 1 min throughout the high-light-exposure sequence. The experimental setup and data acquisition sequence for snapshot TA is shown in Figure 2-2.

For snapshot TA of *Nannochloropsis oceanica* microalgae, live cell sample solutions were prepared in Ficoll 400 buffer at a concentration of 40 μg Chl *a*/mL. For all experiments, the sample cuvette had a path length of 1 mm and was continuously translocated to prevent sample damage and accumulation of long-lived triplet Chl* state. Photodegradation is primarily dependent on the stability of the sample throughout exposure to the laser and actinic light. Spinach thylakoid membranes and intact cells of *N. oceanica* were found to be stable for at least 30 min of snapshot TA. Importantly, to further prevent sample agglomeration and precipitation, the sample solution was gently mixed by bubbling air between snapshot measurements (Figure 2-2b).

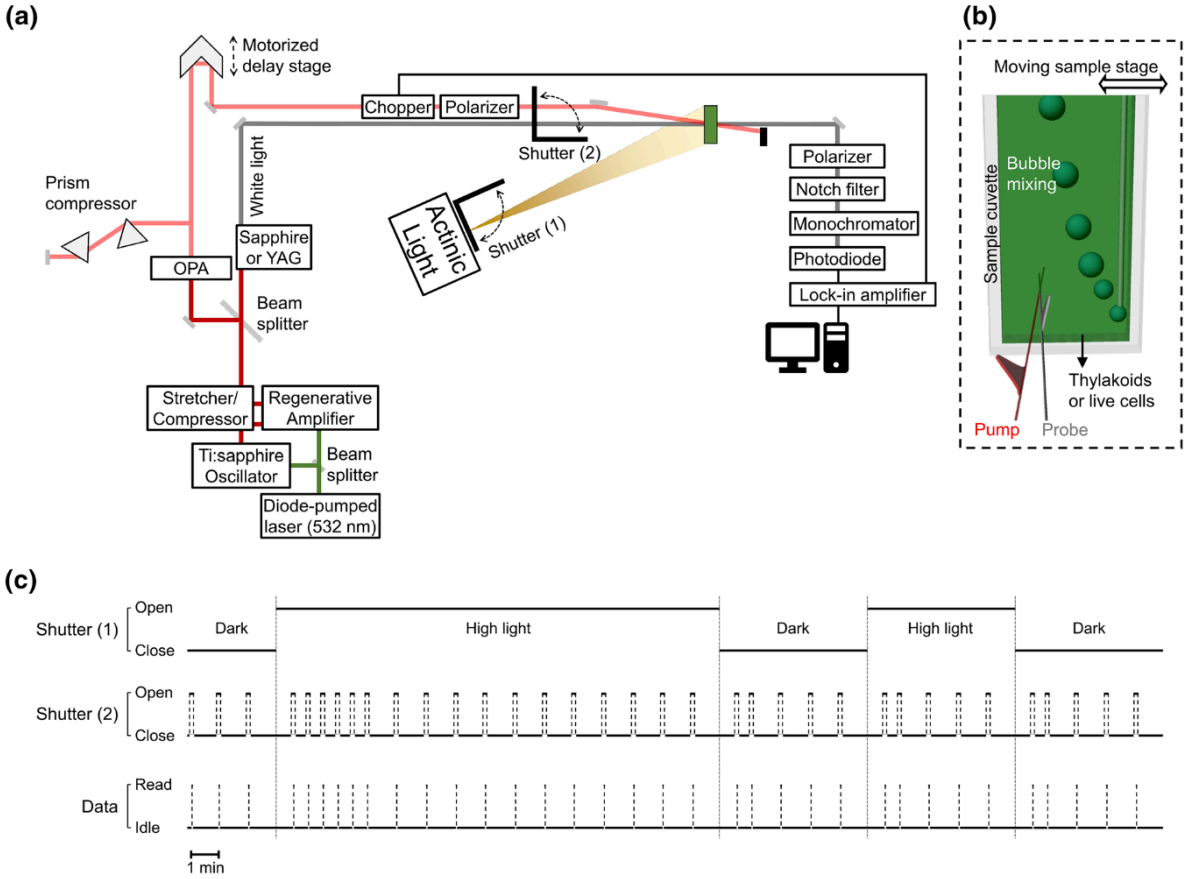

Figure 2-2. Experimental setup and data acquisition sequence for snapshot transient absorption spectroscopy. (a) Block diagram of the laser setup utilized for snapshot TA spectroscopy. (b) Pictorial representation of the sample cell containing thylakoid membranes or live *N. oceanica* cells in a cuvette. (c) Schematic of the data acquisition process. Shutter 1 controls the exposure of the sample to an actinic light, while shutter 2 controls the exposure of the laser beams to the sample for data acquisition as described in the text.

A custom LabVIEW program was used for data collection. Each snapshot measurement was controlled by a shutter programmed to open for 10 s increments at various times throughout the exposure of a sample to high light or dark conditions, while the data was continuously collected by the lock-in amplifier. Further decreases in the duration of the data acquisition (below 10 s windows) is limited by the signal-to-noise (SN) ratio. Measurements of intact samples (e.g., thylakoid membranes and live algae cells), though physiologically relevant, exhibit high scattering and consequently poor SN ratio. This required us to use a rather intense pump laser (20–40 nJ/pulse), which can generate significant Chl*–Chl* annihilation and provide an additional Chl* de-excitation pathway beyond the naturally occurring NPQ mechanisms. For samples with very little scatter, it will be possible to decrease the snapshot time windows. It is also possible that a more sensitive detector (e.g., a photodiode and data acquisition card whose sampling clock is synchronized to the repetition rate of the laser[53]) could help to minimize annihilation processes by permitting the use of reduced pump power and increasing the temporal resolution (currently 10 s) of the snapshot TA system.

The specific actinic light and snapshot sequence used in our TA experiments is depicted in Figure 2-2c. Snapshots were taken periodically throughout an initial 3 min dark period. Then, an actinic

light with intensity 850 μmol photons m^{-2} s^{-1} was used to activate qE. The actinic light remained on for 15 min and snapshots were taken throughout this period. Following light exposure, snapshots were taken for 5 min in the dark to assess recovery from qE. A second cycle of 5 min periods of light and dark exposure was incorporated in order to assess the effect of dark recovery and subsequent re-exposure to quenching-inducing conditions.

As shown in Figure 2-3, 15 data points can be collected during the 10 s time window between shutter open and close. Note that the number of data points collected within the time window can be controlled by adjusting the time constant of the lock-in amplifier. When shutter 2 opens, the signal transiently fluctuated due to the response time of the sensing system before stabilizing within a few seconds. In order to obtain reliable data and ensure that all PSII reaction centers are closed, we calculate the average of five data (dΔOD) points which were collected 5.5–8.5 s after the opening of the shutter.

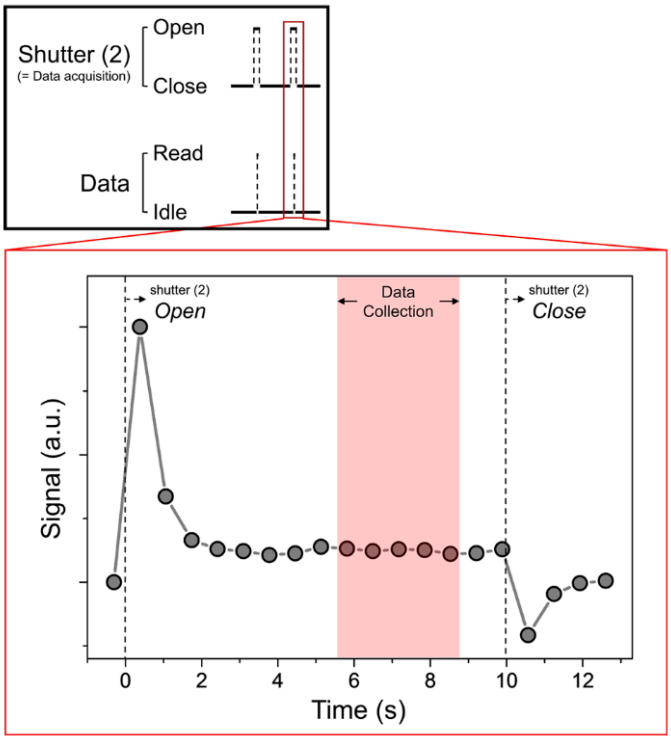

Figure 2-3. Representative snapshot TA data measurement performed on spinach thylakoid membranes. Vertical lines correspond to the time at which the laser shutter was opened or closed. The red region corresponds to reliable measurements which were averaged to provide a single "snapshot" data point.

2.5 Results: Excitation Energy Transfer Quenching in Spinach Thylakoid Membranes

2.5.1 TA Kinetic Profile and Spectrum of Car S_1 ESA

Figure 2-4a shows the TA kinetic profiles of high-light- and dark-exposed thylakoid membranes probed at 540 nm. At wavelengths longer than 520 nm, there is a considerable amount of Chl ESA signal detected in addition to Car S_1–S_N absorption.[54] As Chl Q_y excited states depopulate via quenching or another de-excitation pathway, the intensity of the ESA signal corresponding to Chl Q_y decreases significantly, which explains why high-light-exposed samples have an overall lower level of ESA signal compared to dark-adapted samples (Figure 2-4a). Correspondingly, the Car S_1–S_N transition becomes the more dominant signal at shorter time delays under high-light conditions. We found that the two TA kinetic profiles are kinetically indistinguishable at longer time delays (≥40 ps) at which the Car S_1 ESA contribution should be negligible.[22,40] To account for the significant decrease in Chl ESA and clearly compare TA kinetic profiles, we scaled the profile of the dark-exposed sample to match that of the high-light-exposed profile based on signals at around 40 ps time delay. Figure 2-4b shows that the high-light-exposed profile and scaled dark-exposed profile overlap well at time delays greater than 40 ps.

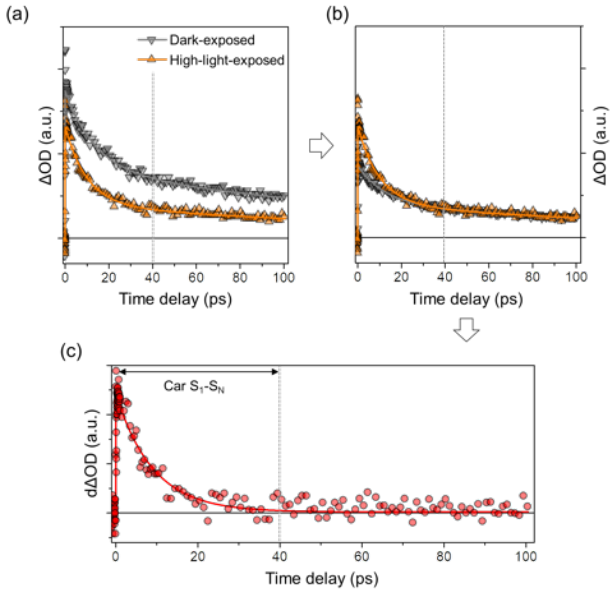

Figure 2-4. (a) TA kinetic profiles for spinach thylakoid membranes under dark (gray, down triangle) and high-light (orange, up triangle) conditions. The samples were excited and probed at 650 and 540 nm, respectively. (b) Scaled TA kinetic trace obtained by matching the dark-exposed thylakoids (gray, down triangle) to the respective trace measured under high-light conditions (orange, up triangle) at a time delay of 40 ps. (c) Difference between high-light and scaled dark-exposed kinetic profiles. For the high-light condition, thylakoids were continuously exposed to actinic light at 850 μmol photons·m^{-2}·s^{-1}.

Figure 2-4c shows the difference between the high-light- and dark-exposed (scaled) profiles. The difference profile fits well to a single exponential decay, with a lifetime of 7.81 ps (±0.83 ps). This value agrees with the literature values of the S_1 lifetime of Zea, which range from 7 to 11 ps.[22,42,43] In this fit, there was no resolvable rise time within the time resolution (~120 fs) of our TA setup.[22,40] If we consider the difference decay profile as the excitation energy population in the Car S_1 state, a lack of a resolvable rise time indicates near instantaneous excitation equilibrium near

Chl-Car EET quenching sites. One possible scenario is that the mixing of Chl Q_y and Car S_1 states is reinforced by increased electronic coupling after high-light exposure, which eventually results in instantaneous excitation equilibrium via bidirectional energy transfer between Chl-Car at EET quenching sites. Such bidirectional Chl-Car EET was observed experimentally by Kennis,[36] Walla,[13,39–41] and co-workers.

To determine the origin of the signal in Figure 2-4c, we performed a global analysis on the TA kinetic profiles of high-light-exposed thylakoid samples. Through global analysis, it was deduced that at least three lifetime components (τ_1 = 7.81 ps, τ_2 = 28.2 ps, and τ_3 = 160 ps) are required for fitting the ESA signals in the wavelength range of 530–620 nm (Figure 2-5). From the TA kinetic profile at 620 nm, the two longest lifetime components (τ_2 = 28.2 ps and τ_3 = 160 ps) mainly represent the contribution of Chl ESA. As shown in Figure 2-6, the lifetime component of 7.81 ps with maximum absorption amplitude at 540 nm strongly resembles the S_1–S_N absorption spectrum of Zea in methanol from Polívka et al., which features an asymmetric peak centered at 555 nm.[43,55] The peak in Figure 2-6 is slightly blue-shifted (~15 nm) from the spectra reported previously,[43,55] likely due to differences between solvent vs protein environments. A similar magnitude of blue-shift in the spinach thylakoid membrane environment has also been observed in previous studies.[22,40] Considering its lifetime (~8 ps) and spectrum, it seems likely that the observed ESA signal is from a Car S_1–S_N transition, and the Car is presumably Zea.

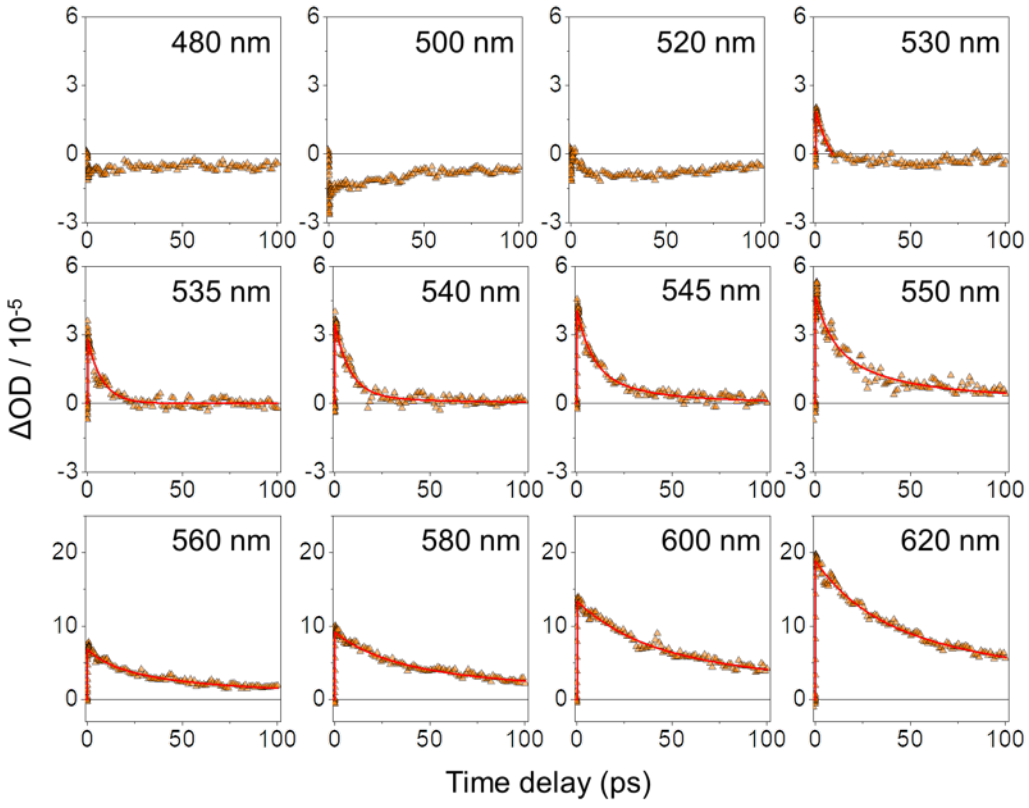

Figure 2-5. TA kinetic profiles of high-light-exposed spinach thylakoid membranes. Through global analysis, it was deduced that at least three lifetime components (τ_1=7.81 ps, τ_2=28.2 ps, and τ_3=160 ps) are required for fitting the ESA signal of the samples in the wavelength range of 530-620 nm. From the TA kinetic profile at 620 nm, the two longest lifetime components (τ_2=28.2 ps and τ_3=160 ps) mainly represent the contribution of Chl ESA. The probe wavelength is denoted in each panel.

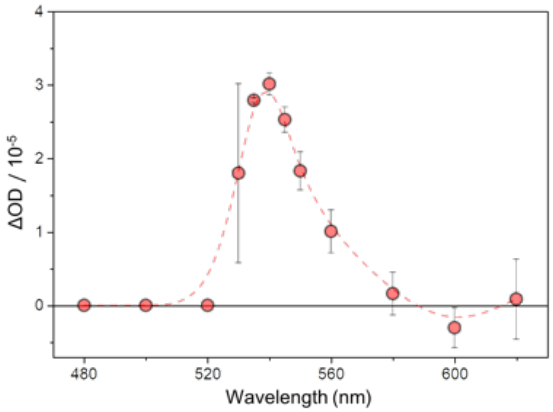

Figure 2-6. The 7.81 ps decay component-associated spectrum obtained by global analysis of the decay profiles of excited state absorption signals measured on high-light-exposed thylakoids. The decay profile at each wavelength is presented in Figure 2-5. Data are presented as the fit parameters ± SE. Dashed line represents a b-spline interpolation among the data points.

2.5.2 Kinetic Analysis

To further confirm the origin of the observed signal, we explored possible kinetic pathways that would lead to the dynamics observed in Figure 2-4c. Considering that the Chl fluorescence lifetime of the thylakoid membrane is in the range of 0.35–1.47 ns (see Figure 2-12a), it is probable that Chl*–Chl* annihilation is the dominant factor in determining the rate of Chl* de-excitation and the excitation diffusion length, which results in a shortened Chl ESA signal lifetime ($\tau_{avg} < 0.1$ ns) in our TA measurement. The signal decay difference between dark- and high-light-exposed samples was negligible at 620 and 680 nm where Chl ESA and ground state bleaching signals dominate, respectively (Figure 2-7). If the high-light exposure were to cause variations in Chl excitation energy dynamics beyond turning on quenching mechanisms (e.g., Chl*–Chl* annihilation), a significant change should appear at 620 and 680 nm. Therefore, it is reasonable to assume that Chl*–Chl* annihilation is consistent during the transition from dark to high light.

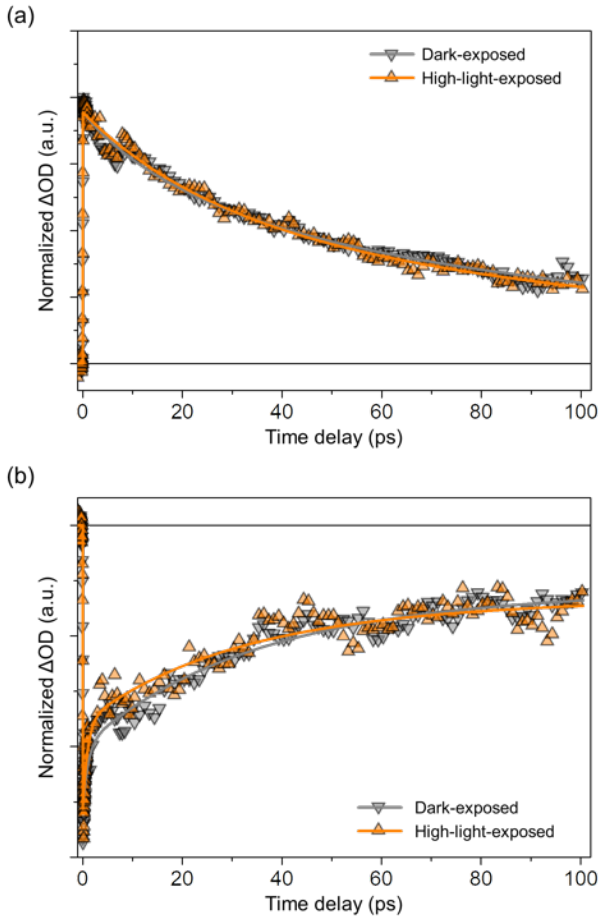

Figure 2-7. Transient absorption kinetics of Chl ESA and GSB in spinach thylakoid membranes under dark-exposed (gray, down triangle) and high-light-exposed (orange, up triangle) conditions. Samples were excited at 650 nm and probed at (a) 620 nm and (b) 680 nm.

Before continuing our analysis, we note that the relative time scales of excitation transport and/or trapping in the photosystem II antenna system would suggest that observing states with lifetimes as short as 8 ps would be very difficult, if not impossible, due to the extremely low steady-state concentration of the short-lived species if the formation time is several hundred picoseconds. However, the presence of Chl*–Chl* annihilation in the TA measurement restricts the diffusion length of excitations in the antenna and enables the direct observation of short-lived intermediates. Valkunas and co-workers estimated a rapid annihilation rate of $(16\ \text{ps})^{-1}$ per light-harvesting complex II (LHCII) trimer for extended aggregates.[56] If we assume that annihilation in thylakoid membranes occurs on a much faster time scale than the excitation migration time through LHCII to an immobilized trap, the presence of the annihilation process will reduce the excitation diffusion length. A key feature in our data is the lack of an observable rise time in the excited signal at 540 nm, in contrast to our data at 1000 nm.[23,38] Below we show that this difference arises from the differing lifetimes of the two quenching species.

The dynamics of the Car S_1 state population was investigated using a linear chain model in which instantaneous excitation equilibrium between a subset of Chl and Car was assumed (Figure 2-8a). To model how Chl*–Chl* annihilation influences the Car S_1 population after Chl excitation, we divided the total Chl population into two groups. The ***Y*** group contains Chl molecules that are close enough to a Car molecule in a configuration consistent with downhill energy transfer such that EET would be very rapid, while the ***X*** group contains all other Chl molecules that are far enough away from a Car molecule in a quenching configuration such that EET would be significantly slower. By varying the initial populations of the ***X*** and ***Y*** groups that are excited, which are depicted as the relative percentages of Chl excitations in Figure 2-8b, we can observe changes in the dynamics of the excited Car S_1 state. Figure 2-8b suggests that only Chl that are excited very close to Car molecules will populate the Car S_1 state we observe. Increasing the proportion of Chl excited near a Car (***Y*** group) to just 10% of the excited population in the bulk Chl pool (***X*** group) removes the rise component and results in a decay profile of the Car S_1 population that is well overlapped with the experimentally observed difference decay profile (Figure 2-8b). The absence of a rise component in the Car S_1 kinetic profile differs from the previously observed $Zea^{\bullet+}$ kinetic profiles, which are fitted with rise and decay components.[12,23,37] This difference can be attributed to the fact that a slower de-excitation rate ($\leq 2.5 \times 10^{10}$ s^{-1}) of the CT state allows for the observation of an increase in the $Zea^{\bullet+}$ population after Chl excitation (Figure 2-9).

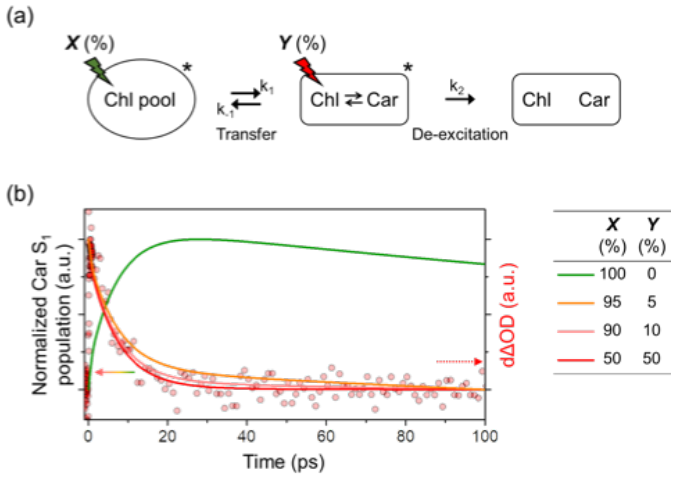

Figure 2-8. (a) Kinetic scheme for excitation equilibration among pigments involved in the EET quenching mechanism in high-light-exposed thylakoid membranes. The coupled Chl Q_y-Car S_1 state is regarded as an individual state which signifies a near instantaneous excitation equilibrium via bidirectional Chl↔Car energy transfer or a very rapid (≤120 fs) buildup of population in Car S_1 state at quenching sites. Relative percentages of Chl excitations between Chl pool and a Chl adjacent to Car are denoted as X and Y, respectively. The rate constants k_1 and k_{-1} were assumed to be $(350\ ps)^{-1}$ based on our bulk Chl fluorescence lifetime in the quenched state (Figure 2-12a). k_2 is $(8\ ps)^{-1}$ based on the lifetime of the Zea S_1 state.[12,40,41] (b) Dynamics of the Car S_1 state population calculated with various initial excitation populations of the bulk Chl pool vs Chl close to Car. The solid curves represent the simulated dynamics. The difference TA kinetic data points (red dots) from Figure 2-4c are also displayed.

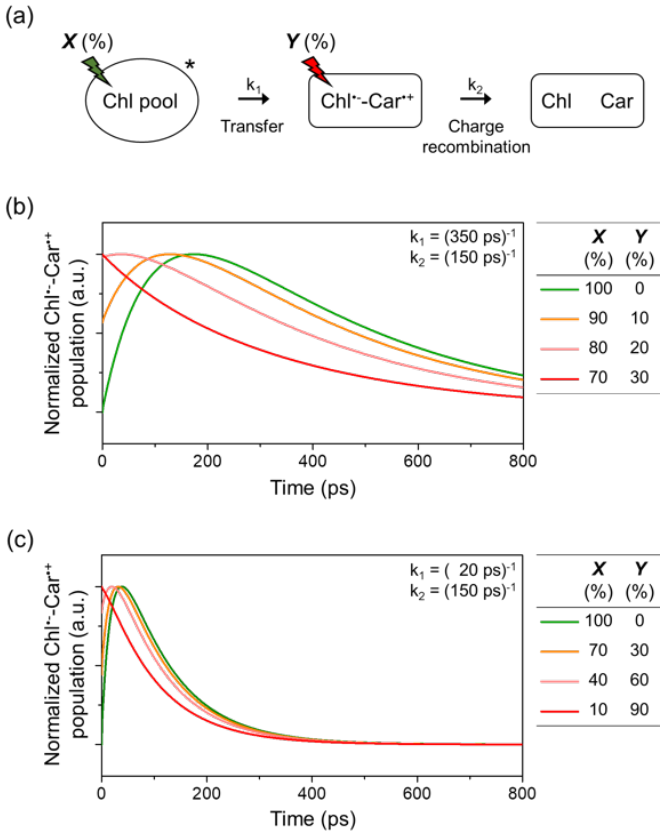

Figure 2-9. (a) Kinetic scheme for excitation equilibration among pigments involved in the CT quenching mechanism in light-exposed thylakoid membranes. Relative percentages of Chl excitations between Chl pool and a Chl adjacent to Car are denoted as ***X*** and ***Y***, respectively. (b, c) Dynamics of the charge-transfer (CT) state population calculated with various initial excitation populations at the bulk Chl pool vs. Chl close to Car. The scheme uses a slower de-excitation (charge recombination) rate ($k_2 \cong (150\ ps)^{-1}$) at quenching sites. The rate constant k_1 can vary as the PSII antenna structure changes during light exposure, so calculation was performed with two different values. (b) The k_1 was assumed to be $(350\ ps)^{-1}$ based on the bulk Chl fluorescence lifetime in quenched state (Figure 2-12a). (c) The k_1 was assumed to be $(20\ ps)^{-1}$ based on previous literature.[79] In both cases, due to the slower charge recombination (k_2), rise components exist in the simulated dynamics even after significant initial population (~20% and ~60% for (b) and (c), respectively) is placed on the ***Y*** group (a).

We also considered a second possibility: that rapid membrane restructuring occurs in high-light conditions, producing small isolated clusters of LHCIIs each containing a quenching site. This, rather implausible, scenario would explain the lack of rise time for the Car S_1 signal, though not the existence of a rise time for the $Zea^{\bullet+}$ signal.[12,23,37] It is also difficult to see how this would provide effective protection to the reaction center in the presence of excess light. Nor does it seem likely that such a mechanism would be rapidly reversible or provide such clear correspondence between the absorption and fluorescence data which will be presented in the following text. Accordingly, we did not pursue this model further.

2.5.3 Snapshot TA Spectroscopy

Using the previously described method for extracting the Car S_1 ESA signal from Chl ESA at 540 nm, we performed snapshot TA measurements at two different time delays after the excitation pulse. The Car S_1 ESA signal has a decay constant of less than 10 ps, while the Chl ESA signal decays on a much longer time scale.[22] Therefore, the TA signal was measured at 40 ps to account for the overall decrease in Chl ESA as thylakoids were exposed to high light. The Car S_1 ESA signal has disappeared by this time delay (Figure 2-4c). Therefore, to measure Car S_1 ESA at 540 nm, the signal is measured at a delay time of 1 ps, then scaled using the 40 ps signal to account for the underlying decrease in Chl *a* ESA signal:

$$\mathrm{d\Delta OD_{Car\,S_1}}(t) = \Delta\mathrm{OD_{at\,1\,ps}}(t) - \Delta\mathrm{OD_{at\,1\,ps}}(\mathrm{dark}) \times \left(\frac{\Delta\mathrm{OD_{at\,40\,ps}}(t)}{\Delta\mathrm{OD_{at\,40\,ps}}(\mathrm{dark})}\right) \quad (3)$$

where $\Delta\mathrm{OD_{at\,1\,ps}}(t)$ and $\Delta\,\Delta\mathrm{OD_{at\,40\,ps}}(t)$ represent the snapshot TA signal measured at time delays of 1 and 40 ps, respectively. ΔOD (dark) is the average of TA signals measured during the initial dark period. The dΔOD spectrum presented in Figure 2-10, reconstructed by the same scaling and subtraction at various wavelengths, shows a distinct peak centered at 540 nm, which proves the validity of the above-mentioned method (Equation 3) for extracting dΔOD values corresponding to Car S_1 ESA.

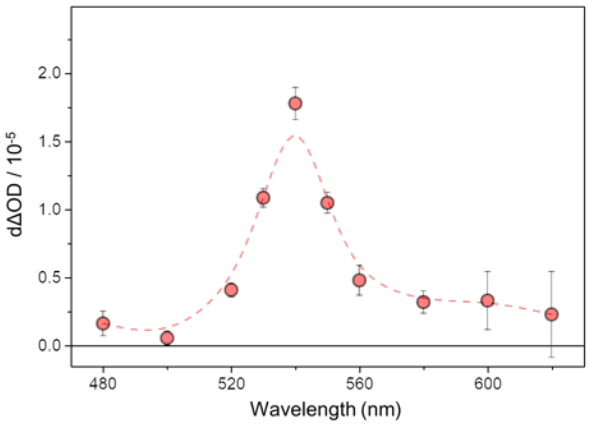

Figure 2-10. Difference TA spectrum reconstructed by subtracting the dark-exposed signal from the high-light-exposed signal. The dΔOD spectrum was reconstructed using the following equation:

$$d\Delta OD_{\mathrm{Car\,S_1}}(\lambda) = \Delta OD_{\mathrm{at\,1\,ps}}(\lambda, \mathrm{light}) - \Delta OD_{\mathrm{at\,1\,ps}}(\lambda, \mathrm{dark}) \times \left(\frac{\Delta OD_{\mathrm{at\,40\,ps}}(\lambda, \mathrm{light})}{\Delta OD_{\mathrm{at\,40\,ps}}(\lambda, \mathrm{dark})}\right)$$

where λ is the probe wavelength. Data are presented as the mean ±SE (n=5). The dashed line represents a b-spline interpolation among the experimental data points.

Figure 2-11a shows individual snapshot TA results measured at 1 and 40 ps during a time sequence of the actinic light turning on and off. Each data point in the 1 ps trace is then scaled using the data point of the corresponding light exposure time in the 40 ps trace, which gives the result shown in Figure 2-11b, overlaid with data from the $Zea^{\bullet+}$ snapshot TA data of Park et al.[38] Much like the $Zea^{\bullet+}$ signal, the Car S_1 ESA signal appears very rapidly (<3 min) after the actinic light is turned

on, well within the time scale of the qE response. Considering the fact that Zea accumulates exponentially with a rise time of 2–3 min,[38] it seems surprising that the amount of Car S_1 ESA signal indicative of Chl-Zea EET quenching is substantial in the early stages (≤3 min) of qE. This difference in time scale may result from ΔpH or ΔpH-triggered mechanisms,[47] such as a structural change in LHC proteins, which may enhance the appearance of the Car S_1 ESA signal in early qE. If this is so, during the first few minutes of high-light exposure, the amount of EET quenching may not be significantly limited by the concentration of Zea. In this context, we note that in the coarse-grained model of qE in the grana membrane developed by Bennett et al.,[57] wild-type levels of qE can be achieved with only 12–15% of potential LHCII quenching sites active as quenchers. Notably, both Car S_1 and $Zea^{\bullet+}$ ESA signals are well-correlated with ΔpH calculated from the model developed by Zaks et al. at early qE (Figure 2-11c), suggesting the important role of ΔpH or ΔpH-triggered mechanisms.

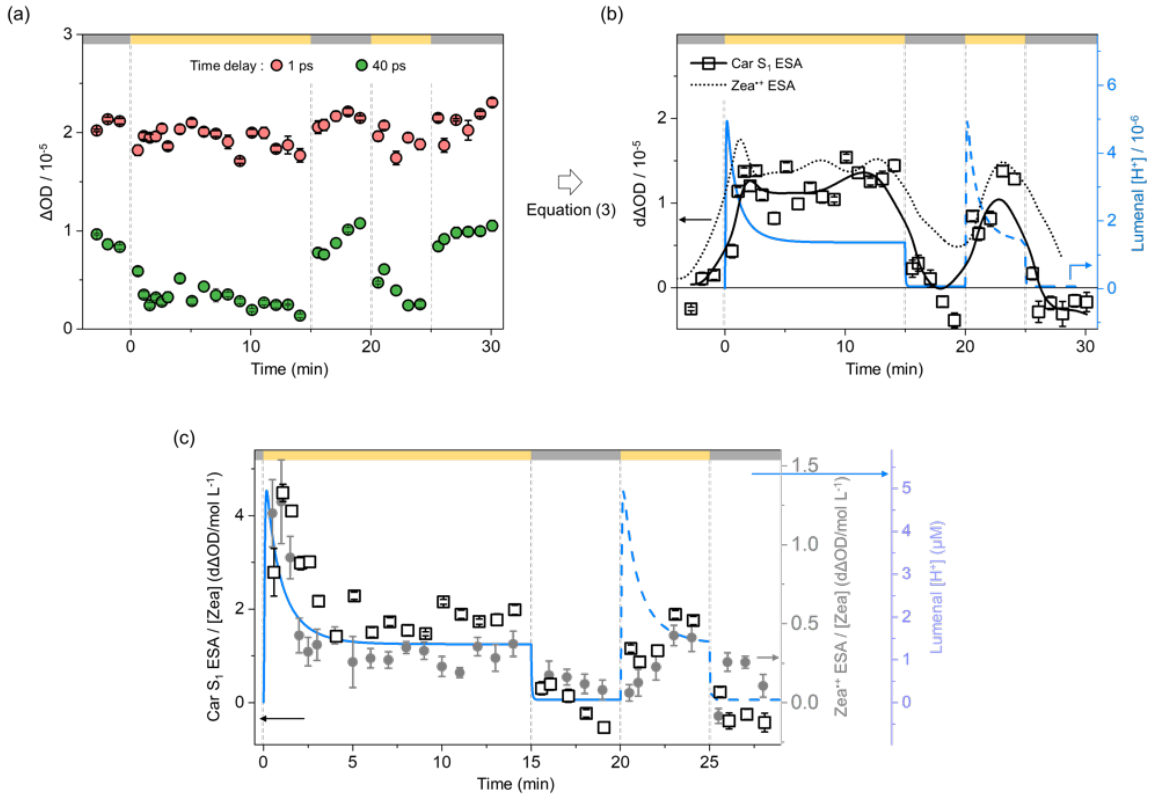

Figure 2-11. (a) Snapshot TA data obtained at 1 ps (red) and 40 ps (green) after Chl excitation. The vertical lines (gray, dashed) and bars at the top of the figures indicate the time sequence of actinic light on (yellow) and off (dark gray). (b) Difference (high-light-exposed minus dark-exposed) snapshot TA data at 1 ps (black, squares) with the zero line representing the average signal during the initial dark period. See Equation 3 in the text for the calculation of the difference snapshot TA data (dΔOD). The solid black line is a smoothed line from the data points corresponding to Car S_1 ESA. The smoothed line for $Zea^{\bullet+}$ absorption (dotted line) from high-light-exposed spinach thylakoids is also displayed.[38] The calculated lumenal $[H^+]$ (blue line) in response to high-light/dark exposures is based on the kinetic model described by Zaks et al.[29,47] Note that there is considerable uncertainty in the lumenal $[H^+]$ during the second high-light exposure period as the model was devised for completely dark-adapted systems. (c) Evolution of normalized Car S_1 absorption (Car S_1 ESA/[Zea]) (black squares) and normalized $Zea^{\bullet+}$ absorption ($Zea^{\bullet+}$ ESA/[Zea]) (gray circles). [Zea] was determined by time-resolved HPLC measurements (Figure 2-13). All data are presented as the mean ± SE (n = 5).

After the initial rapid response, the Car S_1 ESA signal appears to drop, then increases more slowly, perhaps implying the existence of both rapidly activated and slowly activated mechanisms. Two quenching time scales were previously observed by Dall'Osto et al. in *Arabidposis thaliana* plants lacking minor complexes.[58] Interestingly, the Car S_1 ESA signal disappears very rapidly (≤1 min) after turning the actinic light off, much faster than the $Zea^{\bullet+}$ signal, which does not fully disappear even after the actinic light has been turned off for 5 min.[38] The rapid disappearance of Car S_1 ESA signal in response to dark exposure suggests that the EET quenching mechanism plays a central role in rapidly reversible qE quenching, which is known to improve plant fitness under fluctuating light conditions.[7,59] In addition, it is conceivable that the CT and EET mechanisms involve different protein/carotenoid conformations with one able to relax more quickly than the other.[16]

Under *in vivo* conditions, for sufficiently strong Chl–Car coupling, the average lifetime of overall excited Chl could significantly decrease as coupled Chl–Car molecules form in grana membranes during high-light exposure.[35,54] In order to compare the Car S_1 ESA data with data on the overall Chl fluorescence quenching, changes in the Chl fluorescence lifetime of the same thylakoid samples used for snapshot TA were monitored during high-light exposure using fluorescence lifetime snapshot spectroscopy.[24,50,51] Examining the Chl fluorescence decay and corresponding lifetime value (τ_{avg}) at each time point allows for the assessment of Chl* quenching independent of Chl concentration, Chl*-Chl* annihilation, or photobleaching. Figure 2-12a and b present τ_{avg} and calculated NPQ parameters (NPQτ), respectively. NPQτ values are closely related to the conventional NPQ parameter (see Experimental Methods).[38,51] Notably, the appearance time of the Car S_1 ESA presented in Figure 2-11b coincides with the Chl* quenching indicated by NPQτ (Figure 2-12b).

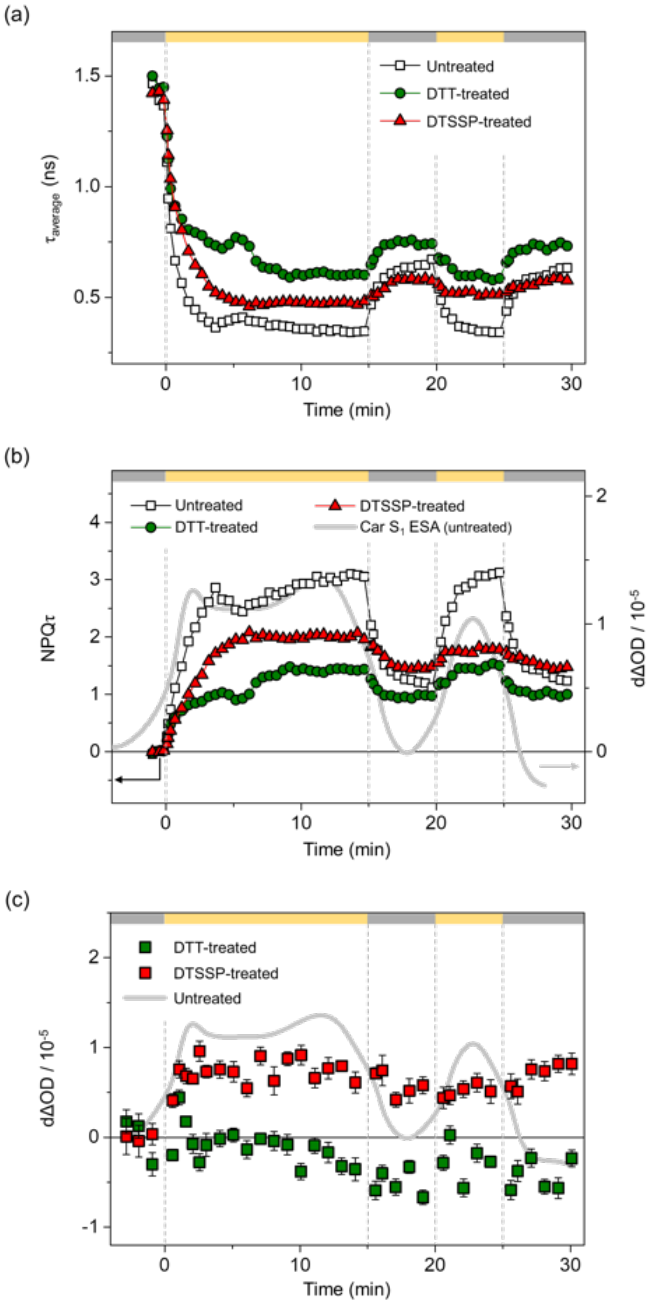

Figure 2-12. Fluorescence lifetime snapshot results presented as (a) average chlorophyll fluorescence lifetimes ($\tau_{average}$) and (b) calculated NPQτ values of untreated (white squares), DTT (green circles)- and DTSSP (red triangles)-treated thylakoids in response to high-light/dark exposure. The vertical lines (gray, dashed) and bars at the top of the figures indicate the time sequence of actinic light on (yellow) and off (dark gray). See Experimental Methods for further discussion of $\tau_{average}$ and NPQτ values. The Car S_1 ESA signal of the untreated sample is displayed as a smoothed trajectory (gray curve). (c) Difference (high-light-exposed minus dark-exposed) TA snapshot results of DTSSP (red)- and DTT (green)-treated thylakoid membranes at 540 nm and 1 ps delay time. The zero line represents the averaged signal from the initial dark period. See Equation 3 in the text for the calculation of the difference snapshot TA data (dΔOD). Data are presented as the mean ± SE (n = 5).

2.5.4 Chemical Treatments

To examine Car S_1 ESA in thylakoids without accumulated Zea, samples were treated with 1,4-dithiothreitol (DTT) to inhibit violaxanthin de-epoxidase (VDE) activity.[60,61] VDE is a thylakoid lumen protein responsible for the accumulation of Zea by de-epoxidizing violaxanthin in response to lumen acidification.[31,32] Time-resolved high-performance liquid chromatography revealed that the accumulation of Zea is not noticeable under DTT-treated conditions (Figure 2-13). The DTT-treated thylakoid showed a substantially lowered NPQτ value compared to the untreated sample (Figure 2-12b). As shown in Figure 2-12c, the snapshot TA data of the DTT-treated thylakoid showed a transient spike in the Car S_1 ESA signal in the first 2 min of high-light exposure. However, after the spike, there was no signal higher than that of the initial dark-exposed state, suggesting that Zea accumulation is necessary to sustain a Chl–Car EET quenching process. This observation, together with its lifetime of ~8 ps, strongly suggests that the Zea S_1 state is directly involved in EET quenching of excited Chl.

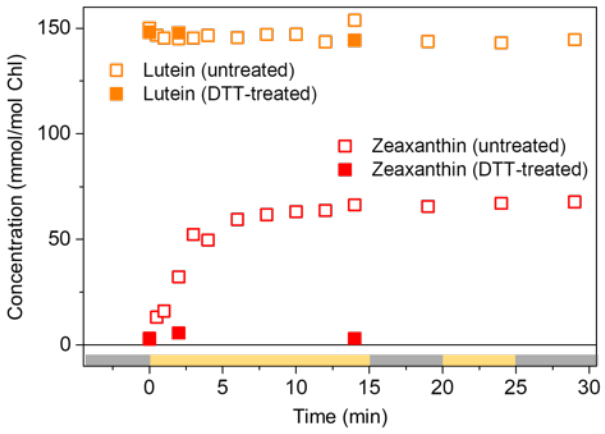

Figure 2-13. Concentrations of zeaxanthin and lutein in untreated and DTT-treated thylakoid membranes determined by time-resolved high-performance liquid chromatography measurements. The accumulation of zeaxanthin in this figure originally published in S. Park et al., *J. Phys. Chem. Lett.* 2017, 8 (22), 5548–5554 (ref [38]).

Slightly negative signals were observed with DTT after 10 min of high-light exposure. We speculate that the process of high-light exposure under the condition that few quenchers are available can slightly alter Chl ESA dynamics or Chl*–Chl* annihilation (Figure 2-14) which likely originates from a structural difference in dark- and light-exposed grana membranes and/or the early onset of other quenching processes. The DTT treatment may also alter the way the membrane responds to high light and returns to low light.

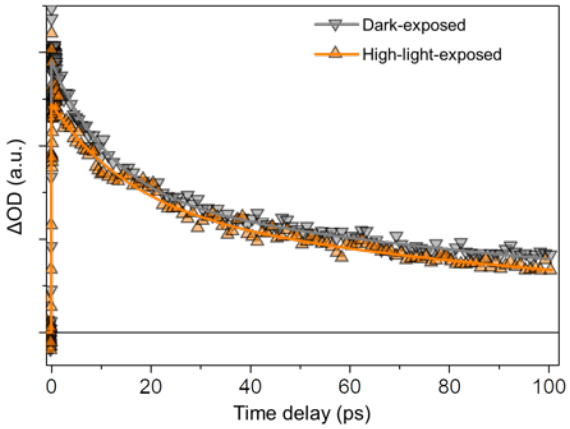

Figure 2-14. Transient absorption kinetics of DTT-treated spinach thylakoid membranes under dark-exposed (gray, down triangle) and high-light-exposed (orange, up triangle) conditions. Samples were excited and probed at 650 nm and 540 nm, respectively.

Cross-linking using 3,3′-dithiobis(sulfosuccinimidyl propionate) (DTSSP) is suggested to stop PsbS-controlled conformational changes of the thylakoid membrane, resulting in behavior similar to the *npq4 Arabidposis thaliana* mutant.[38,46,62] As reported previously, DTSSP-treated and *npq4* thylakoids do not show any $Zea^{\bullet+}$ TA signal, consistent with the idea that the interactions of active PsbS are essential for $Zea^{\bullet+}$ formation that is indicative of CT quenching.[23,38] Interestingly, DTSSP-treated thylakoids showed a 50% lower amount of Car S_1 ESA signal compared to the untreated sample (Figure 2-12c). In addition, the signal was largely unchanged during subsequent changes in actinic light intensity. This result suggests that deactivated PsbS does not completely remove EET quenching induction, and its activation allows for a larger quantity of EET quenching and improves the reversibility.[51,63]

2.6 Discussion: EET Quenching in Spinach Thylakoid Membranes

Recently, Croce and co-workers reported that intense Chl*–Chl* annihilation and a higher excited state of Chl *a* within isolated LHCII produced a (Chl *a*-Lut)* byproduct (referred to as ***Q***) which has a ESA peak at around 535 nm.[64] We closely examined the reported ***Q*** ESA and compared it to our Car S_1 ESA data in case the high-light exposure significantly increases the extent of Chl*–Chl* annihilation, which would seem unlikely. The Car S_1 ESA signals observed in our study have decay time constants of ∼8 ps and are very small by 20 ps after Chl excitation (650 nm). Our Car S_1 ESA kinetics remained unchanged when measured under various pump intensities. In contrast, the majority of the ***Q*** ESA signal remains after 20 ps as the species appears to be relatively long-lived or slow-formed. According to the species-associated difference spectrum of ***Q***, the measured ***Q*** state is populated with a time constant of several picoseconds. However, the rise time component of Car S_1 ESA signal was not resolvable with the time resolution (≅120 fs) of our TA setup. Consequently, the kinetics of the Car S_1 ESA signals appear quite distinct from that of ***Q*** and exhibit a fast decay time constant very similar to the values for xanthophyll S_1 lifetimes obtained in annihilation-free conditions in dilute solution.[42–44] The signals in both this work and our previous study of CT quenching are observable because of the restricted diffusion length of excitation through moderate excitation annihilation. It is important to ask, then, if the intrinsic rate of CT or EET quenching is accurately obtained from the data reported here and in previous literature.[12,22,23,37,38,40] As the simple model calculation in Figure 2-8 shows, for quite small (∼10%) and either direct or very rapid (≤120 fs) population of the quencher state, within our experimental error, the same decay time (≅8 ps) is observed for Zea S_1.[42–44] The CT ($Chl^{\bullet-}$–$Zea^{\bullet+}$) states in thylakoid membranes have been observed to have longer decay times (40–150 ps)[23,38] which could be influenced by Chl-Zea separation and the surrounding protein environment. We therefore consider that the time scales of the decay of the two trap states are the ones that should be used in quantitative models of qE such as that of Bennett et al.[57] Incorporation of Chl*–Chl* annihilation into such a model should enable a quantitative estimate of the relative importance of EET and CT mechanisms.

The thylakoid membrane contains several carotenoids in addition to the violaxanthin–antheraxanthin–zeaxanthin set. Of these, Lut is a key component of LHCII and has also been proposed as a quencher of excited Chl.[30] Spectroscopic studies on isolated LHCs[8] and calculations of excitation quenching in LHCII focused on Lut coupled to Chla_{610}– Chla_{611}– Chla_{612} domain[65,66] have argued that Chl → Lut excitation energy transfer is a possible quenching pathway. In our view, several lines of evidence suggest that Zea is the major quencher in our study reported here. The lifetime of the Car S_1 ESA signal observed is ∼8 ps. As discussed above, this value coincides with literature values for the S_1 lifetime of Zea, which range from 7 to 11 ps.[22,42,43] On the other hand, Lut has a S_1 lifetime of ∼14 ps,[43] which is significantly different from our experimental observation. More importantly, DTT-treated thylakoids showed no Car S_1 ESA signal, strongly suggesting that the Zea S_1 state is predominantly responsible for EET quenching in high-light-exposed spinach thylakoids. The extent to which isolated pigment–protein complexes provide an accurate guide for the natural system is not clear. There may well be structural and conformational differences between pigment–protein complexes within isolated LHCII and intact thylakoid membranes. Indeed, significant differences are seen in Chl fluorescence lifetimes of detergent-solubilized LHCII (>3 ns),[67] aggregated LHCII crystals (0.2–1.5 ns),[68] and thylakoids (0.35–1.47 ns; this study). It has been reported that the presence of Lut can recover the wild type phenotype

in the absence of Zea, indicating that Lut can replace Zea as a quencher.[45,50] However, on a per-molecule basis, Zea in intact leaves is estimated to be 10 times more effective in overall Chl* quenching than Lut,[50] consistent with the snapshot TA data in this study. Nonetheless, we cannot completely rule out the possibility that accumulated Zea indirectly facilitates Lut S_1-mediated EET quenching and that both Zea S_1 and Lut S_1 states are involved in such quenching.[8] Future snapshot TA studies of various mutants containing different levels of Zea and Lut (e.g., *npq1*, *szl1npq1*, and *lut2*) should greatly aid in the investigation of Zea S_1- and Lut S_1-mediated EET quenching in the native state.

In our previous work,[38] we found that inhibiting the activity of PsbS by DTSSP removed the $Zea^{\bullet+}$ signal, and an increased $Zea^{\bullet+}$ signal was observed when a higher concentration of Zea was available for excited Chl quenching as a result of the VDE action. Somewhat similarly, Zea accumulation is necessary for the Car S_1 ESA signal, though activated PsbS further increases the Car S_1 ESA signal. This suggests that both Zea and PsbS are required to achieve maximum EET and CT quenching. However, the degree to which each signal relies on each component differs significantly, as evidenced by their differing responses to chemical treatments (Figure 2-12c). For example, the $Zea^{\bullet+}$ ESA signal was eliminated with the addition of PsbS-inhibiting DTSSP.[38] Meanwhile, the Car S_1 ESA signal was considerably less affected by the DTSSP treatment, indicating that activation of EET quenching via a PsbS-triggered pathway is not the only activation mechanism. It is also noteworthy that the $Zea^{\bullet+}$ ESA signal appeared very quickly after high-light exposure ($\leq$30 s),[38] while the Car S_1 ESA signal appears more slowly after high-light exposure ($\leq$1 min), suggesting differing dependences on a fast-acting PsbS pathway.

The apparently biphasic activation of EET quenching further implies the existence of two different triggering pathways, which are activated on different time scales (Figure 2-15). In this scenario, the fast pathway seems to be mainly directed by activated PsbS in response to ΔpH. The activation of this pathway is not significantly limited by the concentration of Zea, which is supported by the snapshots of DTT-treated samples showing a positive Car S_1 ESA signal during the early period of high-light exposure ($\leq$2 min) (Figure 2-12c). In contrast, the slower activation pathway seems to be primarily dependent on the accumulation of Zea. Although active PsbS/membrane reorganization may be less influential in the activation of EET quenching, PsbS likely still plays an important role in dark recovery, as shown in Figure 2-12c where the addition of DTSSP removed much of the reversibility of the Car S_1 ESA signal. Overall, we speculate that the operation of these two triggering pathways enables the rapid establishment and sustained operation of the EET quenching mechanism, emphasizing its importance in qE (Figure 2-16).

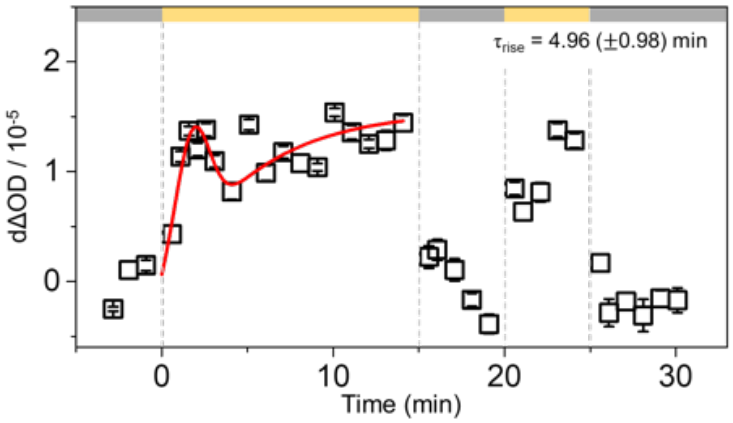

Figure 2-15. Snapshot TA data of untreated thylakoid samples with curve fit (red) in the first high-light-exposure period. Curve fittings use a combined single exponential rise and Gaussian peak function. The Gaussian peak function with a center at 1.9 min was included to account for the sharp rise and fall of the data which is likely a result of the sharp spike in ΔpH following high-light exposure. The time constants of the single exponential rise component are denoted.

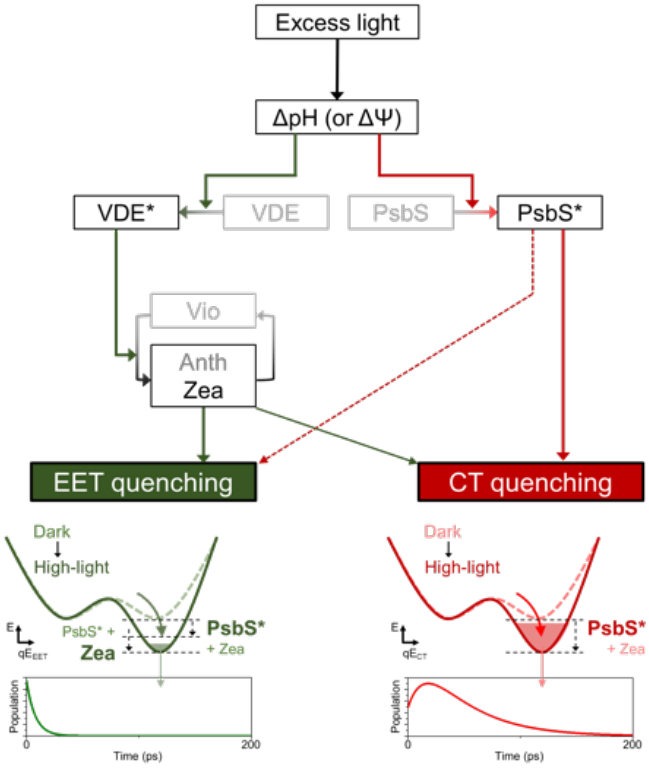

Figure 2-16. Proposed triggering system for the EET and CT quenching mechanisms underlying qE. Regarding the involvement of PsbS and Zea, essential steps are denoted by solid arrows, and nonessential but influential steps are denoted by the dashed arrow. VDE* and PsbS* represent activated proteins by ΔpH and protonation, respectively. In the very initial stages of high-light exposure, CT quenching appears to depend on the small pool of Zea (or Anth) that is present in the dark.[38]

A study on a cyanobacterial LHC protein showed that switching into the quenched state can be achieved by very subtle changes in pigment–protein or pigment–pigment interactions.[16] In this context, it is probable that these different states include different Chl–Car distances, excited state couplings, and relative site energies, which could make certain quenching pathways viable in the intact system but not in isolated complexes, or vice versa. The picture that emerges from these and other recent studies is of a highly flexible control system capable of being switched by small structural changes between at least two quenching pathways: EET and CT. By biasing the inherent structural fluctuations of light harvesting pigment–protein complexes through pigment exchange, protein–protein interactions, and gradients of protons or ions, a system capable of rapid (seconds to minutes) responses to light level changes protects green plants from photo-oxidative damage.

2.7 Real-time Detection of Car S_1 and $Car^{\bullet+}$ ESA via Snapshot TA

Snapshot TA is a variation of conventional TA spectroscopy that utilizes a fixed time delay and wavelength in order to monitor slow changes (s to min timescale) in the dynamics of ultrafast processes (fs to ps timescale). Here, we focus on the detection of Car S_1 and $Car^{\bullet+}$ ESA signals via snapshot TA spectroscopy, thereby demonstrating its utility to monitor the EET and CT mechanisms in spinach thylakoid membranes and live cells of *Nannochloropsis oceanica*. First, the time delay and probe wavelength for snapshot TA experiments must be selected to correspond to the time delay and wavelength associated with the absorption maximum in the TA kinetic profile and spectrum, respectively.

Figure 2-17 shows conventional TA kinetic profiles and reconstructed spectra of Car S_1 and $Car^{\bullet+}$ ESA measured in spinach thylakoid membranes after Chl excitation at 650 nm. The ESA signals at 540 nm in dark and high light were measured to evaluate the Car S_1 ESA. In high light, there is a decrease in the overall contribution of Chl *a* ESA in the visible region due to the activation of de-excitation pathways (NPQ, etc.) for the Chl Q_y excited state. However, the dark and high-light TA kinetic profiles exhibit nearly identical kinetics for time delays greater than 40 ps. In order to extract the contribution of only the Car S_1–S_N ESA from the overall profile, it is necessary to scale the dark profile to match the high-light profile at a time delay of 40 ps in order to remove the contribution of Chl *a* ESA. The scaling factor is simply the ratio between the OD at 40 ps in the light ($\Delta OD_{at\ 40\ ps}(t)$) and dark ($\Delta OD_{at\ 40\ ps}(dark)$). It should also be noted that the decrease in Chl *a* ESA upon high-light exposure is rather insignificant in the near IR; thus, no re-scaling is necessary for the Car radical cation signal (Figure 2-17c). This scaling process is described in Figure 2-17a and Table 2-1. Therefore, for accurate kinetic analyses, precise determination of the background signal (dark signal) is important in order to assess the effect induced by high-light exposure. Our previous publications[38,69] include similar snapshot TA data for spinach thylakoid membranes and above-mentioned data analyses.

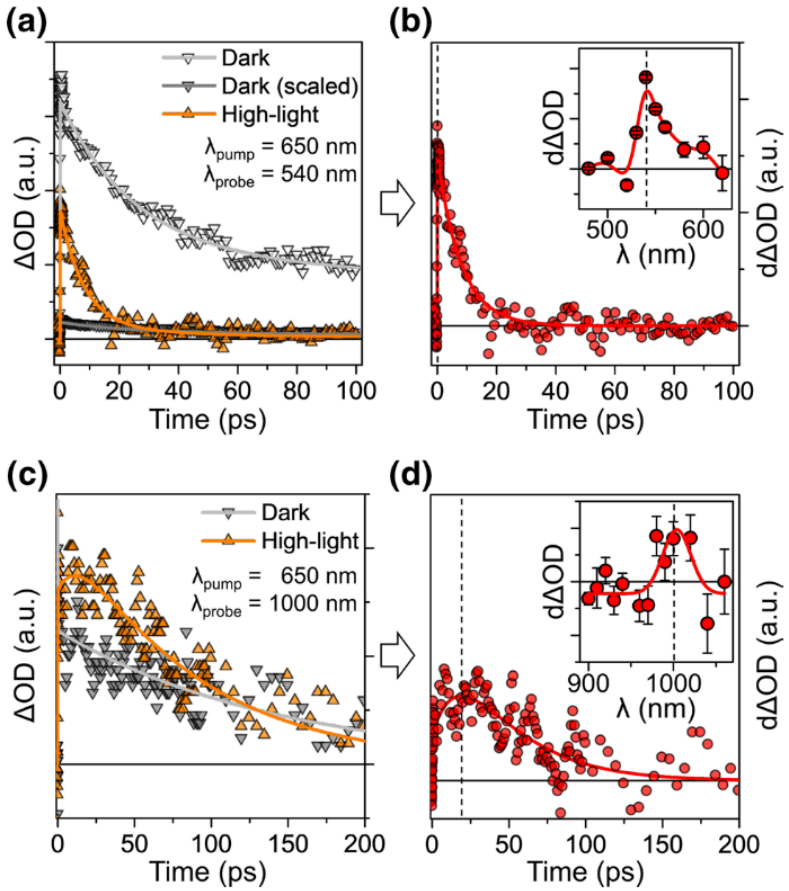

Figure 2-17. TA kinetic profiles for spinach thylakoid membranes probed at 540 nm (a) and 1000 nm (c) under dark and high-light conditions, respectively. Note that the dark profile at 540 nm was re-scaled to account for the decrease in overall Chl ESA that occurs in the visible region upon high-light exposure. Difference TA kinetic profiles obtained by subtracting the dark kinetic profile from the high-light profile, which corresponds to Car S_1 ESA signal (b) and $Car^{\bullet+}$ ESA signal (d). The inset graph shows the difference TA spectra measured in the visible and near-IR regions. Dashed vertical lines indicate the specific time delay and wavelength selected for each snapshot TA measurements. Each data point is presented as the mean ± SE (n = 5).

Table 2-1. Equations used to calculate Car S_1 and $Car^{\bullet+}$ ESA signals

excited state		equation
Car S_1		$d\Delta OD_{\mathrm{Car\ S_1}}(T) = \Delta OD_{\mathrm{at\ 1\ ps}}(T) - \Delta OD_{\mathrm{at\ 1\ ps}}(\mathrm{dark}) \times \left(\frac{\Delta OD_{\mathrm{at\ 40\ ps}}(T)}{\Delta OD_{\mathrm{at\ 40\ ps}}(\mathrm{dark})}\right)$
	Conditions	• Selected wavelength / time delay: 540 nm / 1 ps • Car S_1 ESA at 40 ps ≅ 0 [22] • $\Delta OD_{at\ 40\ ps}$ (high light) < ΔOD_{at40ps} (dark) [69]
$Car^{\bullet+}$		$d\Delta OD_{\mathrm{Car^{\bullet+}}}(T) = \Delta OD_{\mathrm{at\ 20\ ps}}(T) - \Delta OD_{\mathrm{at\ 20\ ps}}(\mathrm{dark})$
	Conditions	• Selected wavelength / time delay: 1000 nm / 20 ps • Chl $ESA_{at\ 20\ ps}$ (high light) ≅ Chl $ESA_{at\ 20\ ps}$ (dark) [23,38]

Note that $\Delta OD_{at\ 1\ ps}(T)$, $\Delta OD_{at\ 20\ ps}(T)$, and $\Delta OD_{at\ 40\ ps}(T)$ represent the snapshot TA signal measured at time delays of 1 ps, 20 ps, and 40 ps, respectively, over the course of light exposure. ΔOD(dark) is the average of TA signals measured during the

The general form of equation for extracting snapshot TA signal (dΔOD) can be written as

$$dOD_x(T) = dOD_{\mathrm{at}\ t,\lambda}(T) - C \cdot dOD_{\mathrm{at}\ t,\lambda}(T = 0)$$

where *x* is the excited-state species of interest (i.e., Car S_1), *t* and λ are the time delay and wavelength where the maximum signal was observed from conventional TA spectroscopy, respectively. *T* is the real time (time after high-light exposure) and *C* is the scaling factor, the ratio of amplitudes of background signals at $T = 0$ compared to *T*, which is used to remove the contribution of Chl *a* ESA as mentioned above.

Figure 2-17b shows difference (dΔOD) TA profiles, which were fitted well to a single exponential decay with a lifetime of 8.03 ± 0.40 ps, which is consistent with the characteristic decay time for the S_1 state of the carotenoid zeaxanthin (Zea). The spectrum of this difference TA signal (Figure 2-17b, inset) closely resembles those reported in the literature for a Car S_1–S_N transition.[43] Additionally, this difference TA spectrum exhibits a peak at 540 nm which is slightly blue-shifted (~ 15 nm) from the Zea S_1–S_N absorption peak measured in methanol, likely due to differences attributed to the environment (protein vs. solvent).[43] Finally, we have previously observed that treatment with DTT, an inhibitor of violaxanthin de-epoxidase (VDE), resulted in negligible accumulation of Zea and elimination of the Car S_1 ESA signal,[69] further suggesting that the specific carotenoid involved is zeaxanthin. Detailed information on the kinetics of this Car S_1 ESA signal will be discussed later. Based on these observations, snapshot measurements of the Car S_1 ESA signals were collected at a selected time delay of 1 ps and a wavelength of 540 nm.

Using a similar subtraction of dark and high-light kinetic profiles, the $Car^{\bullet+}$ ESA shows a characteristic rise ($\tau_{rise} = 19.2 \pm 13.7$ ps) and decay ($\tau_{decay} = 34.4 \pm 18.7$ ps) (Figure 2-17c and d). For snapshot TA, we selected a time delay of 20 ps and a wavelength of 1000 nm because this is where the $Car^{\bullet+}$ ESA signal shows maximum absorption. Using these fixed time delays and wavelengths, the ESA signals were collected during the time sequence of actinic light on and off. The specific equations used to calculate Car S_1 and $Car^{\bullet+}$ ESA (dΔOD) and related assumptions are presented in Table 2-1.

Figure 2-18a shows the results of snapshot TA measurements on isolated spinach thylakoid membranes. The signals for both Car S_1 and $Car^{\bullet+}$ ESA clearly increase and decrease in response to high-light and dark exposure, suggesting that the EET (Chl $Q_y \rightarrow$ Car S_1) and CT ($Chl^{\bullet-}$–$Car^{\bullet+}$) mechanisms become active in the high-light-adapted state of spinach thylakoid membranes. Both signals rapidly increase and reach a maximum within 2 to 3 min of high-light exposure and quickly disappear within 5 min of subsequent dark exposure.

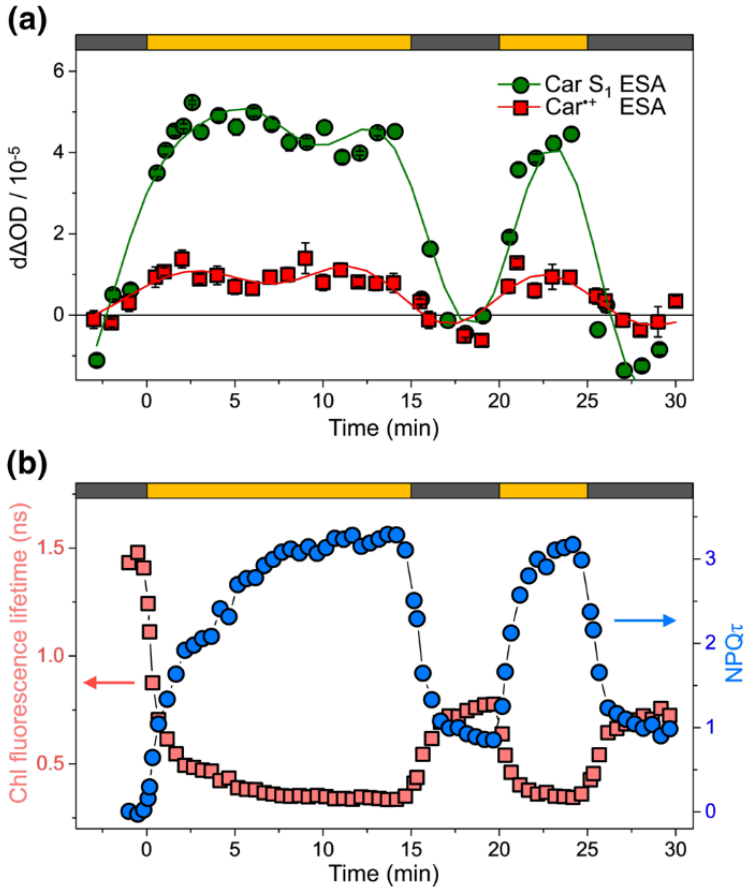

Figure 2-18. TA and fluorescence lifetime snapshot results for spinach thylakoid membranes. (a) TA snapshots corresponding to the Car S_1 ESA and $Car^{\bullet+}$ ESA are shown in green circles and red squares, respectively. The probe wavelength was set to 540 and 1000 nm for the EET (Car S_1 ESA) and CT ($Car^{\bullet+}$ ESA) mechanisms, respectively. (b) Fluorescence lifetime snapshots (pink squares) and the corresponding NPQτ parameter (blue circles). The bars at the top of the panels indicate the time sequence of actinic light on (yellow) and off (dark gray).

These snapshot TA results are well complemented by fluorescence lifetime snapshot measurements.[24] Fluorescence lifetime snapshots provide direct information on the quenching of Chl* by monitoring the evolution of the fluorescence lifetime as intact samples adapt to high light. Fluorescence lifetimes are also independent of photobleaching and chloroplast movement, making them preferable to conventional PAM fluorescence. Figure 2-18b shows the results of fluorescence lifetime snapshots of spinach thylakoid membranes. Upon illumination, the average Chl fluorescence lifetime rapidly decreases from ~ 1.5 ns to ~ 0.3 ns, which is indicative of the activation of qE. Following 15 min of high light, the actinic light was turned off and the fluorescence lifetime increased to ~ 0.8 ns, reflecting recovery of qE. Subsequent light exposure results in another decrease in the fluorescence lifetime. All of these changes in the fluorescence lifetime are contained in NPQτ (blue data points in Figure 2-18b, see Methods section for the calculation), a lifetime-based parameter analogous to the conventional NPQ value ($NPQ=(F_m-F'_m)/F'_m$).

Fundamentally, fluorescence tells us that "energy goes away" from a specific excited state, but it provides no indication as to "where it goes". In this regard, snapshot TA is a valuable complement to the fluorescence lifetime snapshot technique. The combination of snapshot TA results and fluorescence lifetime snapshots (Figure 2-18) can simultaneously show the appearance of the quenching species (i.e., Car S_1 and $Car^{\bullet+}$) in the overall context of Chl* quenching (i.e., Chl fluorescence lifetime). In spinach thylakoids, while the Car S_1 and $Car^{\bullet+}$ signals were at their maximum after 5 min of light exposure, 82% of the overall NPQτ was achieved. In the subsequent 5 min of dark exposure, both ESA signals rapidly disappeared while a 75% loss in the NPQτ level was observed. Moreover, the second period of high light generated a similar amplitude of both ESA signals. These observations suggest that the Chl-Car EET and CT mechanisms play a central role in rapidly reversible qE and photoprotection under fluctuating light conditions. Note that both Car S_1 and $Car^{\bullet+}$ signals are zero in the second dark period, but the fluorescence lifetime is not fully recovered to the original dark-adapted value, suggesting a longer-lasting mechanism not signaled by absorptions at 540 nm or 1000 nm.

In the quantitative analysis of Car S_1 and $Car^{\bullet+}$ ESA snapshots and their correlation with Chl* quenching as determined by fluorescence, we face two main issues. First, precise molar extinction coefficients (ε) for the Car S_1–S_N and $Car^{\bullet+}$ D_0–D_2 transitions in the photosystem II (PSII) protein environment are unavailable. If the values for ε become available, the density of quenching traps could then be calculated and incorporated in quantitative models of qE.[57,70] The second issue is related to the process of annihilation, which is more prevalent within photosynthetic complexes at high pulse powers.[56,71] Our snapshot TA measurements are taken at pump intensities ranging from 20 to 40 nJ/pulse. Given that the lifetime of the Chl ESA signal observed in the TA measurement is less than 0.1 ns (Figure 2-17a), which is significantly lower than the Chl fluorescence lifetime (0.3–1.5 ns, Figure 2-18b) measured under annihilation-free condition (21 pJ/pulse), it seems obvious that annihilation significantly affects the dynamics of excitation energy transfer. As discussed below, this difference makes it difficult to directly correlate the appearance of quenching species observed from snapshot TA with the degree of Chl* quenching quantified by Chl fluorescence lifetime snapshot measurements.

For example, under annihilation-free (natural) conditions, the rate of excitation energy transfer via diffusion ($k_{\text{diffusion}} \cong (350\ \text{ps})^{-1}$; see details in Table 2-2) is significantly slower than that of de-

excitation by EET quenching ($k_{EETquenching} \cong (8\ ps)^{-1}$; see details in Table 2-2). This fast quenching rate results in negligible population of the Car S_1 excited states (Figure 2-19a).[43] However, in our TA measurement, the diffusion length for excitation energy becomes significantly restricted due to the presence of annihilation, which apparently acts as a strong Chl* quenching pathway.[56] Consequently, only energy residing on Chl pigments that are very close to a Car molecule can populate the Car excited states. In other words, we can only observe the populated Car S_1 state and corresponding ESA signal presented in Figure 2-17b under conditions where annihilation is active. The lack of rise time for the Car S_1 ESA signal in Figure 2-17b indicates that the Car S_1 state is instantaneously (≤ 120 fs) populated after Chl excitation, which is possible only if $k_{diffusion} > k_{EETquenching}$ (Figure 2-19b). Interestingly, in the case of the Chl-Car CT state ($Car^{\bullet+}$ ESA) we were able to observe an increasing population of the CT state with a rise time of ~ 20 ps. This difference is likely attributed to the slower $Chl^{\bullet-}$–$Car^{\bullet+}$ charge recombination process ($\leq (40\ ps)^{-1}$; see details in Table 2-2) relative to Car S_1 relaxation. Therefore, to draw more quantitative information (e.g., the densities of EET and CT quenching sites) from our snapshot TA data, the relative speeds of excitation diffusion and quenching in addition to the effect of annihilation on Chl* dynamics need to be considered when developing a quantitative qE model such as Bennett et al.[57] Once annihilation is incorporated into the model, we will be able to accurately simulate the natural dynamics of excitation energy transport in intact grana membranes based on the appearance and disappearance of EET and CT quenching sites as determined from TA spectroscopy.

Table 2-2. Estimated rate constants of excitation diffusion and de-excitation by quenching.

Process	Rate constant	Experimental basis	Reference
Excitation diffusion	$k_{diffusion} \cong (350\ ps)^{-1}$	Chl fluorescence lifetime (τ~350 ps) of quenched thylakoids under annihilation-free condition	- This study (Fig. 2-18b) - Park et al. 2017, 2018
EET quenching	$k_{EETquenching} \cong (8\ ps)^{-1}$	S_1 lifetime of carotenoid Zea (τ_{decay}~8 ps)	- This study (Fig. 2-17b) - Ma et al. 2003 - Park et al. 2018
CT quenching	$k_{CTquenching} = (40\ ps)^{-1} \sim (150\ ps)^{-1}$	Lifetime of Car radical cation (τ_{decay}= 40~150 ps)	- This study (Fig. 2-17d) - Holt et al. 2005 - Park et al. 2017

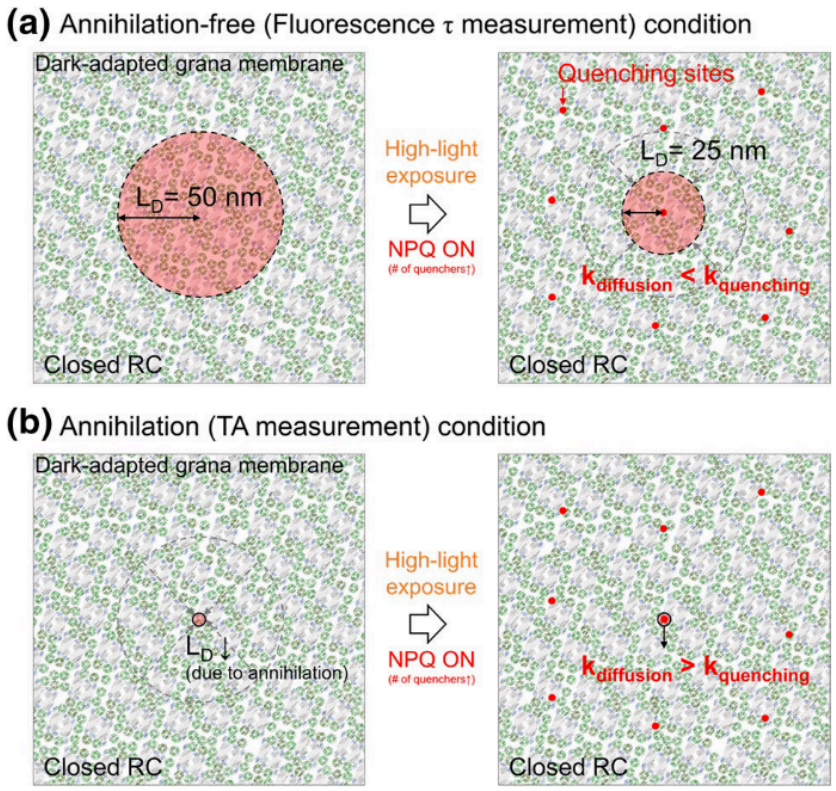

Figure 2-19. Proposed scheme showing the excitation diffusion length (LD, red circles) in dark and high-light-exposed grana membranes when all reaction centers (RCs) are closed. (a) Under annihilation-free conditions, such as the pulse powers used in fluorescence lifetime snapshots, the diffusion lengths were estimated based on the recently developed multiscale model (Bennett et al. 2018)[57] and our Chl fluorescence lifetime snapshot data (Figure 2-18b). In response to high-light exposure, the appearance of quenching sites (red dots) decreases the diffusion length to 25 nm which corresponds to NPQ ≅ 3, according to the empirical relationship between the NPQ parameter and LD shown in Bennett et al.[57] Under this condition, the rate of excitation diffusion is less than that of quenching, resulting in the case where excited states of the quencher are hardly populated. (b) Intense pump powers, such as those used in the snapshot TA measurements, can result in significant annihilation. This results in a dramatic decrease in the excitation diffusion length regardless of the presence of quenchers. If the reduced diffusion length is small enough, the rate of diffusion becomes faster than the rate of quenching. In this case, we can observe both the rapid population of the excited states of the quenching species as well as the subsequent relaxation process.

While we have thus far focused on snapshot TA investigations of isolated thylakoid membranes, the technique can also be applied to completely *in vivo* systems. As an *in vivo* proof-of-concept study, we performed preliminary snapshot TA measurements to monitor the $Car^{\bullet+}$ ESA and Car S_1 ESA signals in live cells of an alga, *Nannochloropis oceanica*. *N. oceanica* appears to be an ideal sample for snapshot TA given that is smaller (2–3 μm) than other model algae[72] and it possesses a simple pigment composition.[73] These factors result in suppressed pump scattering and less spectrally overlapping signals, respectively.

Figure 2-20 shows the results of *in vivo* snapshot TA spectroscopy and the corresponding Chl fluorescence lifetime snapshots for WT cells. Since *N. oceanica* does not contain the carotenoid lutein, zeaxanthin is the most probable Chl* quencher. In fact, a knock-out mutant of violaxanthin de-epoxidase (VDE), an enzyme that is responsible for the accumulation of Zea in response to high light, lacks most of the qE capabilities of wild-type *N. oceanica*.[74] The Car (Zea) S_1 ESA signal extracted by subtracting the dark signal from the high-light signal was fitted well with a

single exponential decay (τ_{decay} = 7.71 ± 1.34 ps), which is almost identical to the decay of the Car S_1 ESA observed in spinach thylakoid membranes.

It appears that both the $Car^{\bullet+}$ and Car (Zea) S_1 snapshots in *N. oceanica* correlate well with the onset of overall quenching as evidenced by the NPQτ values calculated from fluorescence lifetime snapshots (Figure 2-20). Both mechanisms are activated and seem to saturate within 10 min of high light exposure. This suggests that both CT and EET mechanisms may underlie the activation of NPQ during high light. Interestingly, while no positive CT signal was observed during the first 3 min of illumination, the signal corresponding to the EET mechanism showed some activation. In contrast, upon transition to the dark, the CT signal began to show a decrease, while the EET signal remained constant. This could suggest that CT and EET have slightly different *in vivo* regulatory functions, with EET representing the fastest initial response to illumination while CT underlies the rapid relaxation of quenching upon a transition from high light to dark conditions.

We recently discovered that this EET mechanism as well as the CT mechanism is controlled by two important proteins,[74] as described in Chapter 3 of this Dissertation. Future snapshot TA studies of WT cells under variable actinic light conditions, as well as site-directed protonation mutants of the pH-sensing LHCX1 protein, may enable further dissection of the molecular basis for CT and EET quenching in *N. oceanica*.

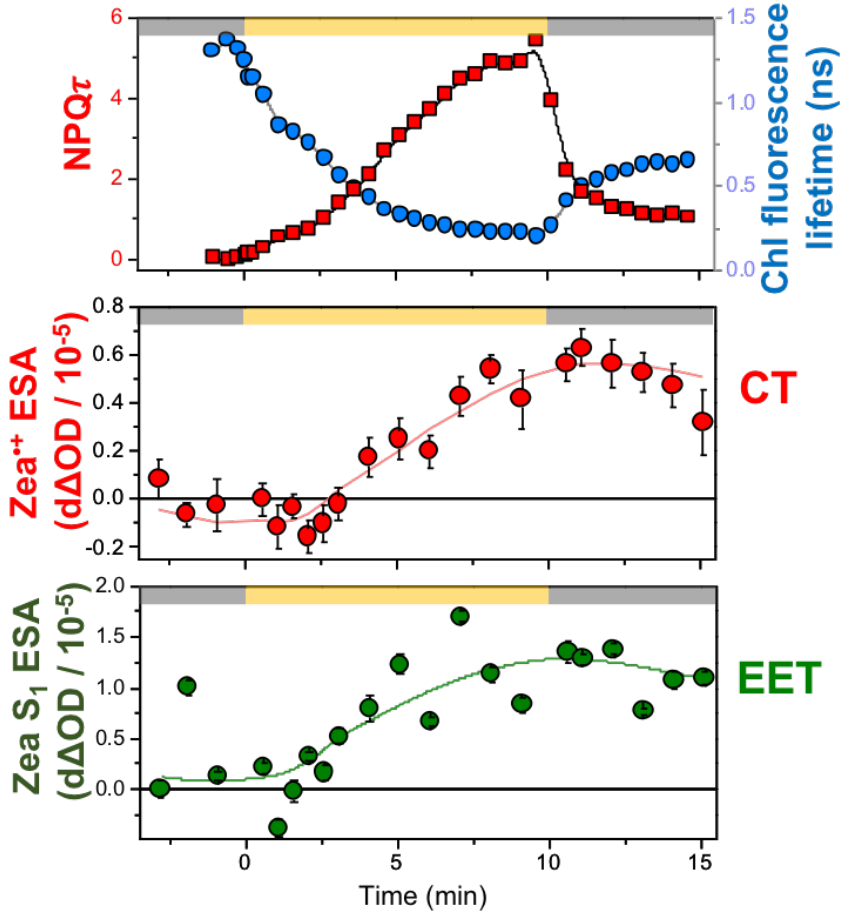

Figure 2-20. Snapshot fluorescence lifetimes and snapshot TA measurements of live cells of *Nannochloropsis oceanica*. For snapshot TA, the probe wavelength was set to 1000 nm for the CT ($Car^{\bullet+}$ ESA) or 540 nm for the EET (Car S_1 ESA) quenching mechanism. The TA snapshots corresponding to the $Car^{\bullet+}$ ESA and Car S_1 ESA are depicted by red and circles, respectively. Each data point is presented as the mean ± SE (n = 5). The NPQτ values (blue circles) were calculated from Chl fluorescence lifetime snapshots using Eq. 2. The bars at the top of the panels indicate the time sequence of actinic light on (yellow) and off (dark gray).

2.8 Concluding Remarks

Although NPQ processes are routinely assessed by measuring the reduced amount or lifetime of Chl fluorescence, which is a downstream effect of quenching, the complexity of NPQ mechanisms and their ensemble effect make it infeasible to characterize individual quenching mechanisms and understand the design principles of such mechanisms under *in vivo* conditions. By monitoring the Car S_1 and $Car^{\bullet+}$ ESA in real time as intact samples adapt to high light, it is possible to observe the timescale and activation dynamics of the Chl-Car EET and CT mechanisms. Using the snapshot TA method in conjunction with known chemical inhibitors of important qE players (e.g., PsbS, VDE), we were able to observe the EET and CT quenching mechanisms in spinach thylakoid membranes, each of which is triggered by different processes.[38,69] By recording quantitative and dynamic signals of the individual quenching mechanisms and combining the data with fluorescence lifetime snapshots[24] performed on the same intact samples, we are able to provide a broader picture of the overall excitation quenching mechanisms that are so essential to plant fitness and crop yields.

Our studies have focused exclusively on the temporal response of the photosynthetic apparatus to high-light exposure, but the snapshot TA technique is potentially valuable for tracking the excited state population and dynamics within any sample that changes over time. Some examples of this include tracking processes such as in situ thin-film formation for photovoltaic applications[75,76] and degradation of perovskites by moisture/O_2.[77,78]

2.9 References

(1) Barber, J.; Andersson, B. Too much of a good thing: light can be bad for photosynthesis. *Trends Biochem. Sci.* **1992**, *17* (2), 61–66.

(2) Li, Z.; Wakao, S.; Fischer, B. B.; Niyogi, K. K. Sensing and Responding to Excess Light. *Annu. Rev. Plant Biol.* **2009**, *60* (1), 239–260.

(3) Demmig-Adams, B.; Adams III, W. W.; Barker, D. H.; Logan, B. A.; Bowling, D. R.; Verhoeven, A. S. Using chlorophyll fluorescence to assess the fraction of absorbed light allocated to thermal dissipation of excess excitation. *Physiol. Plant.* **1996**, *98* (2), 253–264.

(4) Müller, P.; Li, X.-P.; Niyogi, K. K. Non-photochemical quenching. A response to excess light energy. *Plant Physiol.* **2001**, *125* (4), 1558–1566.

(5) Głowacka, K.; Kromdijk, J.; Kucera, K.; Xie, J.; Cavanagh, A. P.; Leonelli, L.; Leakey, A. D. B.; Ort, D. R.; Niyogi, K. K.; Long, S. P. Photosystem II Subunit S overexpression increases the efficiency of water use in a field-grown crop. *Nat. Commun.* **2018**, *9* (1), 868.

(6) Berteotti, S.; Ballottari, M.; Bassi, R. Increased biomass productivity in green algae by tuning non-photochemical quenching. *Sci. Rep.* **2016**, *6* (1), 21339.

(7) Kromdijk, J.; Głowacka, K.; Leonelli, L.; Gabilly, S. T.; Iwai, M.; Niyogi, K. K.; Long, S. P. Improving photosynthesis and crop productivity by accelerating recovery from photoprotection. *Science* **2016**, *354* (6314), 857–861.

(8) Ruban, A. V.; Berera, R.; Ilioaia, C.; van Stokkum, I. H. M.; Kennis, J. T. M.; Pascal, A. A.; van Amerongen, H.; Robert, B.; Horton, P.; van Grondelle, R. Identification of a mechanism of photoprotective energy dissipation in higher plants. *Nature* **2007**, *450* (7169), 575–578.

(9) Staleva, H.; Komenda, J.; Shukla, M. K.; Šlouf, V.; Kaňa, R.; Polívka, T.; Sobotka, R. Mechanism of photoprotection in the cyanobacterial ancestor of plant antenna proteins. *Nat. Chem. Biol.* **2015**, *11* (4), 287–291.

(10) Liguori, N.; Xu, P.; van Stokkum, I. H. M.; van Oort, B.; Lu, Y.; Karcher, D.; Bock, R.; Croce, R. Different carotenoid conformations have distinct functions in light-harvesting regulation in plants. *Nat. Commun.* **2017**, *8* (1), 1994.

(11) Dreuw, A.; Fleming, G. R.; Head-Gordon, M. Charge-Transfer State as a Possible Signature of a Zeaxanthin−Chlorophyll Dimer in the Non-photochemical Quenching Process in Green Plants. *J. Phys. Chem. B* **2003**, *107* (27), 6500–6503.

(12) Ahn, T. K.; Avenson, T. J.; Ballottari, M.; Cheng, Y.-C.; Niyogi, K. K.; Bassi, R.; Fleming, G. R. Architecture of a charge-transfer state regulating light harvesting in a plant antenna protein. *Science* **2008**, *320* (5877), 794–797.

(13) Bode, S.; Quentmeier, C. C.; Liao, P.-N.; Hafi, N.; Barros, T.; Wilk, L.; Bittner, F.; Walla, P. J. On the regulation of photosynthesis by excitonic interactions between carotenoids and chlorophylls. *Proc. Natl. Acad. Sci. U. S. A.* **2009**, *106* (30), 12311–12316.

(14) Miloslavina, Y.; Wehner, A.; Lambrev, P. H.; Wientjes, E.; Reus, M.; Garab, G.; Croce, R.; Holzwarth, A. R. Far-red fluorescence: A direct spectroscopic marker for LHCII oligomer formation in non-photochemical quenching. *FEBS Lett.* **2008**, *582* (25–26), 3625–3631.

(15) Müller, M. G.; Lambrev, P.; Reus, M.; Wientjes, E.; Croce, R.; Holzwarth, A. R. Singlet Energy Dissipation in the Photosystem II Light-Harvesting Complex Does Not Involve Energy Transfer to Carotenoids. *ChemPhysChem* **2010**, *11* (6), 1289–1296.

(16) Hontani, Y.; Kloz, M.; Polívka, T.; Shukla, M. K.; Sobotka, R.; Kennis, J. T. M. Molecular Origin of Photoprotection in Cyanobacteria Probed by Watermarked Femtosecond

Stimulated Raman Spectroscopy. *J. Phys. Chem. Lett.* **2018**, *9* (7), 1788–1792.
(17) Balevičius, V.; Fox, K. F.; Bricker, W. P.; Jurinovich, S.; Prandi, I. G.; Mennucci, B.; Duffy, C. D. P. Fine control of chlorophyll-carotenoid interactions defines the functionality of light-harvesting proteins in plants. *Sci. Rep.* **2017**, *7* (1), 13956.
(18) Pascal, A. A.; Liu, Z.; Broess, K.; van Oort, B.; van Amerongen, H.; Wang, C.; Horton, P.; Robert, B.; Chang, W.; Ruban, A. Molecular basis of photoprotection and control of photosynthetic light-harvesting. *Nature* **2005**, *436* (7047), 134–137.
(19) Wahadoszamen, M.; Margalit, I.; Ara, A. M.; van Grondelle, R.; Noy, D. The role of charge-transfer states in energy transfer and dissipation within natural and artificial bacteriochlorophyll proteins. *Nat. Commun.* **2014**, *5* (1), 5287.
(20) Sacharz, J.; Giovagnetti, V.; Ungerer, P.; Mastroianni, G.; Ruban, A. V. The xanthophyll cycle affects reversible interactions between PsbS and light-harvesting complex II to control non-photochemical quenching. *Nat. Plants* **2017**, *3* (2), 16225.
(21) Liguori, N.; Periole, X.; Marrink, S. J.; Croce, R. From light-harvesting to photoprotection: structural basis of the dynamic switch of the major antenna complex of plants (LHCII). *Sci. Rep.* **2015**, *5* (1), 15661.
(22) Ma, Y.-Z.; Holt, N. E.; Li, X.-P.; Niyogi, K. K.; Fleming, G. R. Evidence for direct carotenoid involvement in the regulation of photosynthetic light harvesting. *Proc. Natl. Acad. Sci.* **2003**, *100* (3), 4377–4382.
(23) Holt, N. E.; Zigmantas, D.; Valkūnas, L.; Li, X.-P.; Niyogi, K. K.; Fleming, G. R. Carotenoid cation formation and the regulation of photosynthetic light harvesting. *Science* **2005**, *307* (5708), 433–436.
(24) Sylak-Glassman, E. J.; Zaks, J.; Amarnath, K.; Leuenberger, M.; Fleming, G. R. Characterizing non-photochemical quenching in leaves through fluorescence lifetime snapshots. *Photosynth. Res.* **2016**, *127* (1), 69–76.
(25) Krause, G. H.; Weis, E. Chlorophyll fluorescence as a tool in plant physiology - II. Interpretation of fluorescence signals. *Photosynth. Res.* **1984**, *5* (2), 139–157.
(26) Tripathy, B. C.; Oelmüller, R. Reactive oxygen species generation and signaling in plants. *Plant Signal. Behav.* **2012**, *7* (12), 1621–1633.
(27) Pinnola, A.; Bassi, R. Molecular mechanisms involved in plant photoprotection. *Biochem. Soc. Trans.* **2018**, *46*, 467–482.
(28) Demmig-Adams, B.; Cohu, C. M.; Muller, O.; Adams, W. W. Modulation of photosynthetic energy conversion efficiency in nature: from seconds to seasons. *Photosynth. Res.* **2012**, *113* (1–3), 75–88.
(29) Zaks, J.; Amarnath, K.; Sylak-Glassman, E. J.; Fleming, G. R. Models and measurements of energy-dependent quenching. *Photosynth. Res.* **2013**, *116* (2–3), 389–409.
(30) Jahns, P.; Holzwarth, A. R. The role of the xanthophyll cycle and of lutein in photoprotection of photosystem II. *Biochim. Biophys. Acta - Bioenerg.* **2012**, *1817* (1), 182–193.
(31) Demmig-Adams, B. Carotenoids and photoprotection in plants: A role for the xanthophyll zeaxanthin. *Biochim. Biophys. Acta - Bioenerg.* **1990**, *1020* (1), 1–24.
(32) Niyogi, K. K.; Grossman, A. R.; Björkman, O. Arabidopsis mutants define a central role for the xanthophyll cycle in the regulation of photosynthetic energy conversion. *Plant Cell* **1998**, *10* (7), 1121–1134.
(33) Demmig-Adams, B.; Adams, W. W. An integrative approach to photoinhibition and photoprotection of photosynthesis. *Environ. Exp. Bot.* **2018**, *154*, 1–3.

(34) Young, A. J.; Frank, H. A. Energy transfer reactions involving carotenoids: quenching of chlorophyll fluorescence. *J. Photochem. Photobiol. B Biol.* **1996**, *36* (1), 3–15.
(35) van Amerongen, H.; van Grondelle, R. Understanding the Energy Transfer Function of LHCII, the Major Light-Harvesting Complex of Green Plants. *J. Phys. Chem. B* **2001**, *105* (3), 604–617.
(36) Kloz, M.; Pillai, S.; Kodis, G.; Gust, D.; Moore, T. A.; Moore, A. L.; van Grondelle, R.; Kennis, J. T. M. Carotenoid Photoprotection in Artificial Photosynthetic Antennas. *J. Am. Chem. Soc.* **2011**, *133* (18), 7007–7015.
(37) Avenson, T. J.; Ahn, T. K.; Zigmantas, D.; Niyogi, K. K.; Li, Z.; Ballottari, M.; Bassi, R.; Fleming, G. R. Zeaxanthin radical cation formation in minor light-harvesting complexes of higher plant antenna. *J. Biol. Chem.* **2008**, *283* (6), 3550–3558.
(38) Park, S.; Fischer, A. L.; Li, Z.; Bassi, R.; Niyogi, K. K.; Fleming, G. R. Snapshot Transient Absorption Spectroscopy of Carotenoid Radical Cations in High-Light-Acclimating Thylakoid Membranes. *J. Phys. Chem. Lett.* **2017**, *8* (22), 5548–5554.
(39) Holleboom, C.-P.; Walla, P. J. The back and forth of energy transfer between carotenoids and chlorophylls and its role in the regulation of light harvesting. *Photosynth. Res.* **2014**, *119* (1–2), 215–221.
(40) Liao, P.-N.; Holleboom, C.-P.; Wilk, L.; Kühlbrandt, W.; Walla, P. J. Correlation of Car S 1 → Chl with Chl → Car S 1 Energy Transfer Supports the Excitonic Model in Quenched Light Harvesting Complex II. *J. Phys. Chem. B* **2010**, *114* (47), 15650–15655.
(41) Liao, P. N.; Pillai, S.; Gust, D.; Moore, T. A.; Moore, A. L.; Walla, P. J. Two-photon study on the electronic interactions between the first excited singlet states in carotenoid-tetrapyrrole dyads. *J. Phys. Chem. A* **2011**, *115* (16), 4082–4091.
(42) Billsten, H. H.; Pan, J.; Sinha, S.; Pascher, T.; Sundström, V.; Polívka, T. Excited-State Processes in the Carotenoid Zeaxanthin after Excess Energy Excitation. *J. Phys. Chem. A* **2005**, *109* (31), 6852–6859.
(43) Polívka, T.; Sundström, V. Ultrafast Dynamics of Carotenoid Excited States−From Solution to Natural and Artificial Systems. *Chem. Rev.* **2004**, *104* (4), 2021–2072.
(44) Polívka, T.; Herek, J. L.; Zigmantas, D.; Akerlund, H. E.; Sundström, V. Direct observation of the (forbidden) S1 state in carotenoids. *Proc. Natl. Acad. Sci. U. S. A.* **1999**, *96* (9), 4914–4917.
(45) Li, Z.; Ahn, T. K.; Avenson, T. J.; Ballottari, M.; Cruz, J. A.; Kramer, D. M.; Bassi, R.; Fleming, G. R.; Keasling, J. D.; Niyogi, K. K. Lutein accumulation in the absence of zeaxanthin restores nonphotochemical quenching in the Arabidopsis thaliana npq1 mutant. *Plant Cell* **2009**, *21* (6), 1798–1812.
(46) Correa-Galvis, V.; Poschmann, G.; Melzer, M.; Stühler, K.; Jahns, P. PsbS interactions involved in the activation of energy dissipation in Arabidopsis. *Nat. Plants* **2016**, *2* (2), 15225.
(47) Zaks, J.; Amarnath, K.; Kramer, D. M.; Niyogi, K. K.; Fleming, G. R. A kinetic model of rapidly reversible nonphotochemical quenching. *Proc. Natl. Acad. Sci. U. S. A.* **2012**, *109* (39), 15757–15762.
(48) Walla, P. J.; Linden, P. A.; Ohta, K.; Fleming, G. R. Excited-State Kinetics of the Carotenoid S1 State in LHC II and Two-Photon Excitation Spectra of Lutein and β-Carotene in Solution: Efficient Car S1→Chl Electronic Energy Transfer via Hot S1 States? *J. Phys. Chem. A* **2002**, *106* (10), 1909–1916.
(49) Gilmore, A. M.; Shinkarev, V. P.; Hazlett, T. L.; Govindjee. Quantitative Analysis of the

Effects of Intrathylakoid pH and Xanthophyll Cycle Pigments on Chlorophyll a Fluorescence Lifetime Distributions and Intensity in Thylakoids. *Biochemistry* **1998**, *37* (39), 13582–13593.

(50) Leuenberger, M.; Morris, J. M.; Chan, A. M.; Leonelli, L.; Niyogi, K. K.; Fleming, G. R. Dissecting and modeling zeaxanthin- and lutein-dependent nonphotochemical quenching in Arabidopsis thaliana. *Proc. Natl. Acad. Sci. U. S. A.* **2017**, *114* (33), E7009–E7017.

(51) Sylak-Glassman, E. J.; Malnoë, A.; De Re, E.; Brooks, M. D.; Fischer, A. L.; Niyogi, K. K.; Fleming, G. R. Distinct roles of the photosystem II protein PsbS and zeaxanthin in the regulation of light harvesting in plants revealed by fluorescence lifetime snapshots. *Proc. Natl. Acad. Sci. U. S. A.* **2014**, *111* (49), 17498–17503.

(52) Schansker, G.; Tóth, S. Z.; Strasser, R. J. Dark recovery of the Chl a fluorescence transient (OJIP) after light adaptation: The qT-component of non-photochemical quenching is related to an activated photosystem I acceptor side. *Biochim. Biophys. Acta - Bioenerg.* **2006**, *1757* (7), 787–797.

(53) Werley, C. A.; Teo, S. M.; Nelson, K. A. Pulsed laser noise analysis and pump-probe signal detection with a data acquisition card. *Rev. Sci. Instrum.* **2011**, *82* (12), 123108.

(54) Gradinaru, C. C.; Stokkum, I. H. M. van; Pascal, A. A.; Grondelle, R. van; Amerongen, H. van. Identifying the Pathways of Energy Transfer between Carotenoids and Chlorophylls in LHCII and CP29. A Multicolor, Femtosecond Pump−Probe Study. *J. Phys. Chem. B* **2000**, *104* (39), 9330–9342.

(55) Polívka, T.; Zigmantas, D.; Herek, J. L.; He, Z.; Pascher, T.; Pullerits, T.; Cogdell, R. J.; Frank, H. A.; Sundström, V. The Carotenoid S1 State in LH2 Complexes from Purple Bacteria Rhodobacter sphaeroides and Rhodopseudomonas acidophila: S1 Energies, Dynamics, and Carotenoid Radical Formation. *J. Phys. Chem. B* **2002**, *106* (42), 11016–11025.

(56) Barzda, V.; Gulbinas, V.; Kananavicius, R.; Cervinskas, V.; van Amerongen, H.; van Grondelle, R.; Valkunas, L. Singlet-singlet annihilation kinetics in aggregates and trimers of LHCII. *Biophys. J.* **2001**, *80* (5), 2409–2421.

(57) Bennett, D. I. G.; Fleming, G. R.; Amarnath, K. Energy-dependent quenching adjusts the excitation diffusion length to regulate photosynthetic light harvesting. *Proc. Natl. Acad. Sci.* **2018**, *114* (41), E9523–E9531.

(58) Dall'Osto, L.; Cazzaniga, S.; Bressan, M.; Paleček, D.; Žídek, K.; Niyogi, K. K.; Fleming, G. R.; Zigmantas, D.; Bassi, R. Two mechanisms for dissipation of excess light in monomeric and trimeric light-harvesting complexes. *Nat. Plants* **2017**, *3* (5), 17033.

(59) Külheim, C.; Agren, J.; Jansson, S. Rapid regulation of light harvesting and plant fitness in the field. *Science* **2002**, *297* (5578), 91–93.

(60) Adams, W. W.; Demmig-Adams, B.; Winter, K. Relative Contributions of Zeaxanthin-Related and Zeaxanthin-Unrelated Types of "High-Energy-State" Quenching of Chlorophyll Fluorescence in Spinach Leaves Exposed to Various Environmental Conditions. *Plant Physiol.* **1990**, *92* (2), 302–309.

(61) Bilger, W.; Björkman, O. Role of the xanthophyll cycle in photoprotection elucidated by measurements of light-induced absorbance changes, fluorescence and photosynthesis in leaves of Hedera canariensis. *Photosynth. Res.* **1990**, *25* (3), 173–185.

(62) Li, X.-P.; Björkman, O.; Shih, C.; Grossman, A. R.; Rosenquist, M.; Jansson, S.; Niyogi, K. K. A pigment-binding protein essential for regulation of photosynthetic light harvesting. *Nature* **2000**, *403* (6768), 391–395.

(63) Li, X.-P.; Muller-Moule, P.; Gilmore, A. M.; Niyogi, K. K. PsbS-dependent enhancement of feedback de-excitation protects photosystem II from photoinhibition. *Proc. Natl. Acad. Sci. U. S. A.* **2002**, *99* (23), 15222–15227.
(64) van Oort, B.; Roy, L. M.; Xu, P.; Lu, Y.; Karcher, D.; Bock, R.; Croce, R. Revisiting the Role of Xanthophylls in Nonphotochemical Quenching. *J. Phys. Chem. Lett.* **2018**, *9* (2), 346–352.
(65) Chmeliov, J.; Bricker, W. P.; Lo, C.; Jouin, E.; Valkunas, L.; Ruban, A. V.; Duffy, C. D. P. An 'all pigment' model of excitation quenching in LHCII. *Phys. Chem. Chem. Phys.* **2015**, *17* (24), 15857–15867.
(66) Duffy, C. D. P.; Chmeliov, J.; Macernis, M.; Sulskus, J.; Valkunas, L.; Ruban, A. V. Modeling of Fluorescence Quenching by Lutein in the Plant Light-Harvesting Complex LHCII. *J. Phys. Chem. B* **2013**, *117* (38), 10974–10986.
(67) Moya, I.; Silvestri, M.; Vallon, O.; Cinque, G.; Bassi, R. Time-Resolved Fluorescence Analysis of the Photosystem II Antenna Proteins in Detergent Micelles and Liposomes. *Biochemistry* **2001**, *40* (42), 12552–12561.
(68) Fox, K. F.; Ünlü, C.; Balevičius, V.; Ramdour, B. N.; Kern, C.; Pan, X.; Li, M.; van Amerongen, H.; Duffy, C. D. P. A possible molecular basis for photoprotection in the minor antenna proteins of plants. *Biochim. Biophys. Acta - Bioenerg.* **2018**, *1859* (7), 471–481.
(69) Park, S.; Fischer, A. L.; Steen, C. J.; Iwai, M.; Morris, J. M.; Walla, P. J.; Niyogi, K. K.; Fleming, G. R. Chlorophyll-Carotenoid Excitation Energy Transfer in High-Light-Exposed Thylakoid Membranes Investigated by Snapshot Transient Absorption Spectroscopy. *J. Am. Chem. Soc.* **2018**, *140* (38), 11965–11973.
(70) Amarnath, K.; Bennett, D. I. G.; Schneider, A. R.; Fleming, G. R. Multiscale model of light harvesting by photosystem II in plants. *Proc. Natl. Acad. Sci. U. S. A.* **2016**, *113* (5), 1156–1161.
(71) Gulbinas, V.; Valkunas, L.; Kuciauskas, D.; Katilius, E.; Liuolia, V.; Zhou, W.; Blankenship, R. E. Singlet−Singlet Annihilation and Local Heating in FMO Complexes. *J. Phys. Chem.* **1996**, *100* (45), 17950–17956.
(72) Vieler, A.; Wu, G.; Tsai, C.-H.; Bullard, B.; Cornish, A. J.; Harvey, C.; Reca, I.-B.; Thornburg, C.; Achawanantakun, R.; Buehl, C. J.; Campbell, M. S.; Cavalier, D.; Childs, K. L.; Clark, T. J.; Deshpande, R.; Erickson, E.; Armenia Ferguson, A.; Handee, W.; Kong, Q.; Li, X.; Liu, B.; Lundback, S.; Peng, C.; Roston, R. L.; Sanjaya; Simpson, J. P.; TerBush, A.; Warakanont, J.; Zäuner, S.; Farre, E. M.; Hegg, E. L.; Jiang, N.; Kuo, M.-H.; Lu, Y.; Niyogi, K. K.; Ohlrogge, J.; Osteryoung, K. W.; Shachar-Hill, Y.; Sears, B. B.; Sun, Y.; Takahashi, H.; Yandell, M.; Shiu, S.-H.; Benning, C. Genome, Functional Gene Annotation, and Nuclear Transformation of the Heterokont Oleaginous Alga Nannochloropsis oceanica CCMP1779. *PLoS Genet.* **2012**, *8* (11), e1003064.
(73) Llansola-Portoles, M. J.; Litvin, R.; Ilioaia, C.; Pascal, A. A.; Bina, D.; Robert, B. Pigment structure in the violaxanthin–chlorophyll-a-binding protein VCP. *Photosynth. Res.* **2017**, *134* (1), 51–58.
(74) Park, S.; Steen, C. J.; Lyska, D.; Fischer, A. L.; Endelman, B.; Iwai, M.; Niyogi, K. K.; Fleming, G. R. Chlorophyll–carotenoid excitation energy transfer and charge transfer in Nannochloropsis oceanica for the regulation of photosynthesis. *Proc. Natl. Acad. Sci.* **2019**, *116* (9), 3385–3390.
(75) Hernandez, J. L.; Reichmanis, E.; Reynolds, J. R. Probing film solidification dynamics in polymer photovoltaics. *Org. Electron.* **2015**, *25*, 57–65.

(76) Wilson, K. S.; Wong, C. Y. In Situ Measurement of Exciton Dynamics During Thin-Film Formation Using Single-Shot Transient Absorption. *J. Phys. Chem. A* **2018**, *122* (31), 6438–6444.
(77) Wang, H.; Whittaker-Brooks, L.; Fleming, G. R. Exciton and Free Charge Dynamics of Methylammonium Lead Iodide Perovskites Are Different in the Tetragonal and Orthorhombic Phases. *J. Phys. Chem. C* **2015**, *119* (34), 19590–19595.
(78) Ginting, R. T.; Jeon, M.-K.; Lee, K.-J.; Jin, W.-Y.; Kim, T.-W.; Kang, J.-W. Degradation mechanism of planar-perovskite solar cells: correlating evolution of iodine distribution and photocurrent hysteresis. *J. Mater. Chem. A* **2017**, *5* (9), 4527–4534.
(79) Cheng, Y.-C.; Ahn, T. K.; Avenson, T. J.; Zigmantas, D.; Niyogi, K. K.; Ballottari, M.; Bassi, R.; Fleming, G. R. Kinetic Modeling of Charge-Transfer Quenching in the CP29 Minor Complex. *J. Phys. Chem. B* **2008**, *112* (42), 13418–13423.

Chapter 3

In vivo Transient Absorption Spectroscopy of the Microalga *Nannochloropsis oceanica*

This chapter is reproduced with permission from

S. Park, C.J. Steen, D. Lyska, A.L. Fischer, B. Endelman, M. Iwai, K.N. Niyogi, G.R. Fleming
"Chlorophyll–carotenoid excitation energy transfer and charge transfer
in *Nannochloropsis oceanica* for the regulation of photosynthesis"
Proc. Natl. Acad. Sci. U.S.A. (2019) 116, 9, 3385-3390
DOI: 10.1073/pnas.1819011116.

3.1 Abstract

Nonphotochemical quenching (NPQ) is a proxy for photoprotective thermal dissipation processes that regulate photosynthetic light harvesting. The identification of NPQ mechanisms and their molecular or physiological triggering factors under *in vivo* conditions is a matter of controversy. Here, to investigate chlorophyll (Chl)–zeaxanthin (Zea) excitation energy transfer (EET) and charge transfer (CT) as possible NPQ mechanisms, we performed transient absorption (TA) spectroscopy on live cells of the microalga *Nannochloropsis oceanica*. We obtained evidence for the operation of both EET and CT quenching by observing spectral features associated with the Zea S_1 and $Zea^{\bullet+}$ excited-state absorption (ESA) signals, respectively, after Chl excitation. Knockout mutants for genes encoding either violaxanthin de-epoxidase or LHCX1 proteins exhibited strongly inhibited NPQ capabilities and lacked detectable Zea S_1 and $Zea^{\bullet+}$ ESA signals *in vivo*, which strongly suggests that the accumulation of Zea and active LHCX1 is essential for both EET and CT quenching in *N. oceanica*.

3.2 Significance

Manipulating the nonphotochemical quenching (NPQ) capabilities of photosynthetic organisms is known to result in increased crop productivity. However, optimization of yields also requires a detailed molecular understanding of the mechanism of NPQ *in vivo* with specific attention to the roles of the carotenoid zeaxanthin and various ΔpH-sensing proteins, such as photosystem II subunit S and stress-related antenna proteins (e.g., LHCX). Here, to investigate such *in vivo* NPQ mechanisms, we report transient absorption spectroscopy measurements on live cells of *Nannochloropsis oceanica*. We show that two fundamental processes proposed as NPQ mechanisms are active in *N. oceanica* and specifically require violaxanthin de-epoxidase as well as the LHCX1 protein. These findings have implications for optimizing the yields of algal biofuels.

3.3 Introduction

Photosynthetic organisms must balance the needs for efficient light harvesting and photoprotection depending on environmental conditions. As such, they have evolved important regulatory processes (frequently assessed from nonphotochemical quenching, NPQ) that allow for the harmless dissipation of excessively excited chlorophyll (Chl*) during periods of high-light exposure, thereby minimizing the formation of reactive oxygen species and avoiding photooxidative stress.[1,2] Energy-dependent quenching (qE) is the fastest component of NPQ, becoming active on a timescale of a few seconds to minutes after high-light exposure.[2] Due to its rapid response to light, qE plays a central role in photosynthetic organisms' ability to cope with fluctuating light conditions. Recent studies have shown that genetic manipulation of qE-related proteins in higher plants and green algae could be a promising way to increase biomass productivity and water use efficiency.[3–5]

Extensive studies have aimed to uncover the molecular mechanisms involved in qE. The majority of these investigations utilize measurements of Chl fluorescence yield quenching, which are unable to provide information about the identity of the quenching species.[6–8] Ultrafast transient absorption (TA) spectroscopy enables the detection of key species (e.g., carotenoid excited states) associated with specific mechanisms and can provide insight into the operation and timescales of the associated quenching. However, most TA experiments have used light-harvesting complex II (LHCII) or photosystem II (PSII) supercomplexes isolated from intact systems.[9–15] Under *in vivo* conditions, transmembrane proton gradients (ΔpH), along with various interactions between pigment–protein complexes, control the induction and relaxation of qE.[16,17] Rapid relaxation of such gradients[18] and subtle changes in pigment–pigment and pigment–protein orientations and distances can alter the operation of qE-related processes.[19–21] This suggests that observations from isolated proteins may not capture a full picture of the behavior of natural systems. Unfortunately, strong scattering makes fully intact systems (e.g., leaves, live cells) difficult to study using TA. However, isolated crude thylakoid membranes, which exhibit moderate quenching capabilities and less scattering, have been a useful sample for studying NPQ in the near-native state.[22,23] Nevertheless, there are significant differences between thylakoid membranes and fully intact systems in terms of the kinetics of qE induction/relaxation and the overall extent of quenching. These differences stem from regulatory loops, including feedback from the plant's sugar-consuming sink tissues. This makes it highly desirable to observe the operation of qE mechanisms in the fully native state.

The heterokont alga *Nannochloropsis oceanica* is a promising candidate for live-cell TA spectroscopy due to its small size (2–3 μm compared with ∼10 μm for the reference green alga *Chlamydomonas reinhardtii*) and high quenching capacity (NPQ ≅ 6). Recently, *N. oceanica* has attracted growing scientific and industrial interest due to its ability to accumulate high levels of polyunsaturated fatty acids and its high growth rate.[24–26] Unlike land plants and green algae, its LHCs bind only Chl *a* and the carotenoids violaxanthin, antheraxanthin, and zeaxanthin (Vio-Ant-Zea) and vaucheriaxanthin.[27,28] This relatively simple pigment composition allows us to study qE mechanisms in a less complex system. *N. oceanica* also lacks the photosystem II subunit S (PsbS) protein,[29] which is necessary for qE in plants,[30] but it has LHCX proteins[6,31,32] that are homologs of the stress-related LHCSR proteins that function in qE in green algae,[33] mosses,[34] and diatoms.[35] *N. oceanica* also has a plant-type violaxanthin de-epoxidase

(VDE),[29] which is a thylakoid lumen protein responsible for the accumulation of Zea in response to lumen acidification under high-light conditions. Although both LHCX1 and VDE are hypothesized to be NPQ components in *Nannochloropsis* species,[6] it is still unclear which qE mechanisms are controlled by these two proteins under *in vivo* conditions.

Although the mechanisms of NPQ in *N. oceanica* remain to be determined, it is well known that electronic interactions between carotenoids (Car) and Chl play a major role in NPQ, and that coupled Chl–Car pairs can provide quenching sites.[36–38] As shown in Figure 3-1, two possible mechanisms of Chl–Car energy transfer and subsequent de-excitation have been reported to explain the role of Car as a direct quencher.[23,39] In the first, excitation energy transfer (EET) quenching can be achieved by energy transfer from the Chl Q_y state to the Car S_1 state.[9,10,23,40] Excitation energy that reaches a coupled Chl–Car pair undergoes rapid de-excitation because the lifetime of the Car S_1 state is much shorter (~10 ps) than that of Chl Q_y (>1 ns). Bidirectional energy transfer, Chl $Q_y \leftrightarrow$ Car S_1, has also been proposed under the condition that strong electronic coupling exists between the two states.[41–43] Another possible mechanism, charge transfer (CT) quenching, involves the transient formation of a CT state composed of $Car^{\bullet+}$ and $Chl^{\bullet-}$.[12–15,22,44,45] The excitation energy in the CT state is then de-excited through a charge recombination process (≥40 ps), followed by relaxation to the ground states. Ultrafast TA spectroscopy of plant thylakoid membranes has demonstrated that both the Car S_1 and $Car^{\bullet+}$ excited states are transiently populated following an initial Chl excitation, providing evidence for active EET and CT mechanisms, respectively.[22,23,40,45]

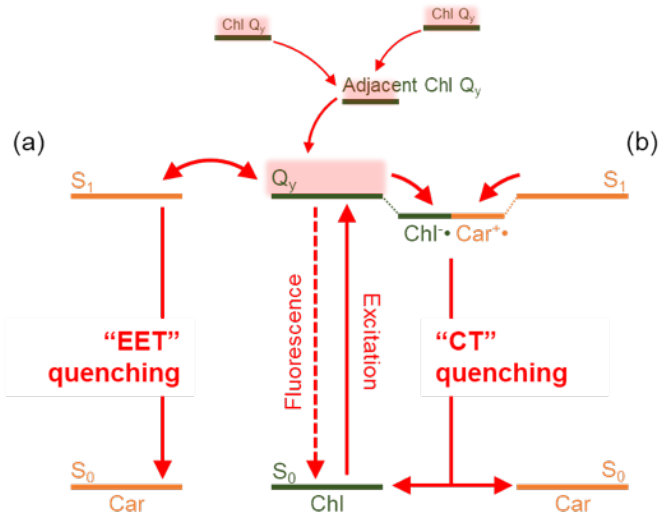

Figure 3-1. Schematic illustration for the Chl–Car EET (a) and Chl–Car CT (b) quenching processes.

Here, to obtain insight into the possible roles of EET and CT mechanisms in the qE of *N. oceanica*, we performed live-cell TA spectroscopy in conjunction with Chl fluorescence lifetime snapshots and time-resolved HPLC measurements. We utilized *lhcx1* and *vde* mutants of *N. oceanica* that lack LHCX1 and VDE, respectively, to specifically investigate the involvement of these proteins. We show that both EET and CT mechanisms are active in wild type and that LHCX1 and VDE are essential for both mechanisms in *N. oceanica*.

3.4 Materials and Methods

3.4.1 Strains, Growth Conditions, and Sample Preparation

N. oceanica CCMP1779 wild type and *vde* and *lhcx1* mutant strains were grown in F2N medium under low-light conditions (30 μmol of photons per $m^{-2} \cdot s^{-1}$) until late-exponential phase (~5 × 10^7 cells per milliliter). The Chl *a* concentration was determined based on the calculation described by Porra et al.[46] The cell suspension for TA measurements was adjusted to 80 μg Chl *a* per milliliter by centrifuging the culture at 3220 × *g* for 5 min and resuspending the pellet in 20% (wt/vol) Ficoll in 20 mM Hepes-KOH (pH 7.2). The samples were dark-acclimated for 30 min and transferred to a cuvette for spectroscopic measurements.

3.4.2 Live-Cell TA Spectroscopy

The pump-probe TA spectroscopy setup was similar to those described in previous works by Park et al.[22,23] Briefly, the pump beam, generated by optical parametric amplification of the 800-nm fundamental of an amplified Ti/sapphire laser at a repetition rate of 250 kHz, was centered at 665 nm for the Chl Q_y transition. The pump pulses had an energy of 40 nJ per pulse, and the FWHM of the autocorrelation trace was 42 fs. The probe beam was a white-light continuum, created by focusing the 800-nm laser on either a 1-mm-thick sapphire or 1-mm-thick yttrium aluminum garnet crystal, which exhibits greater conversion efficiencies in the visible and near-infrared (NIR) ranges, respectively. A 700-nm short-pass filter or 850-nm long-pass filter was placed after the crystal for visible and NIR continuum generation, respectively. The polarizations of the pump and probe were set to the magic angle (54.7°). The diameters of the pump and probe at the sample position were 140 μm and 65 μm, respectively. After the sample, a second polarization filter set to the probe polarization and a 658 ± 26-nm notch filter were placed to minimize pump scattering and ensure a clean probe signal. After a monochromator (SpectraPro 300i; Acton Research Corp.), Si (DET10A; Thorlabs), and InGaAs (DET410; Thorlabs) photodiodes were used to monitor the changes in absorption signal in the visible and NIR ranges, respectively. The cross-correlation between pump and probe was around 120 fs. The actinic light was set to an intensity of 850 μmol of photons per $m^{-2} \cdot s^{-1}$ at the sample position after a heat-absorbing filter (KG1). The sample solution was gently stirred between measurements, and the sample cuvette was translocated continuously during measurements to prevent sample damage. The path length of the cuvette was 1 mm.

3.4.3 Fluorescence Lifetime Snapshots

Our home-built fluorescence lifetime snapshot apparatus has been described in detail previously.[22,23,47] The excitation laser power was 1.6 mW (21 pJ per pulse), and an actinic light (Schott KL1500) was set to an intensity of 850 μmol of photons per $m^{-2} \cdot s^{-1}$ at the sample. After fitting the fluorescence decays collected upon excitation at 680 nm with two exponential decay components, the $\tau_{average}$ and NPQ_τ values were calculated by the following equations:[22,23,48]

$$\tau_{\mathrm{average}} = \frac{\sum_{\mathrm{i}} A_{\mathrm{i}} \tau_{\mathrm{i}}}{\sum_{\mathrm{i}} A_{\mathrm{i}}}$$

where A_{i} and τ_{i} are the amplitudes and the fluorescence lifetime components, respectively, and

$$NPQ_\tau = \frac{\tau_{\text{avg,dark}} - \tau_{\text{avg,light}}}{\tau_{\text{avg,light}}}$$

where $\tau_{\text{avg,dark}}$ is the average of three lifetimes measured at the initial dark period.

3.4.4 HPLC Analysis of Pigments

Cells were prepared as described above. Five hundred microliters of the cell suspension was dark-acclimated in the cuvette for 30 min, followed by a 10-min light exposure (850 μmol of photons per $m^{-2} \cdot s^{-1}$) and a 5-min dark recovery phase. Aliquots of 100 μL for HPLC analysis were frozen in liquid nitrogen after dark acclimation, 5 and 10 min of illumination, and 5 min of dark recovery. For pigment extraction, the cells were thawed at room temperature and pelleted at 10,000 × *g* for 5 min. The supernatant was removed, and the pellet was frozen again in liquid nitrogen. Cells were broken (6.5 $m \cdot s^{-1}$ for 60 s) using the cryorotor of a Fastprep-24 (MP Bio) and extracted with 100 μL of acetone by vortexing. Cell debris was pelleted at 21,000 × *g* for 5 min. The pellet was extracted a second time with 100 μL of acetone, and the supernatants were pooled. Extracted pigments were analyzed with a Spherisorb 5-μm ODS1 column (Waters Corp) as described by Müller-Moulé et al.[49]

3.5 Results

Figure 3-2a and b shows the results of Chl fluorescence lifetime snapshots of *N. oceanica* live cells. The data are presented as amplitude-weighted average lifetime ($\tau_{average}$) and NPQτ values, respectively (calculations of $\tau_{average}$ and NPQτ are provided in Materials and Methods).[22,23] The Chl fluorescence lifetime of wild-type *N. oceanica* decreased substantially from 1.25 to 0.22 ns during 10 min of high-light exposure (Figure 3-2a), which is equivalent to an NPQτ value of 6.2. However, the *vde* and *lhcx1* mutants showed very low quenching (NPQτ ≅ 0.4), which was not rapidly reversible. It is apparent that active VDE and LHCX1 proteins in *N. oceanica* are necessary for qE induction.

Figure 3-2c presents time-resolved HPLC data for the concentration of the Zea pigment in response to dark/light exposure. The data confirm that the *vde* mutant lacks the ability to accumulate Zea due to the absence of the VDE enzyme. In contrast, wild type and the *lhcx1* mutant actively accumulate Zea in response to high-light exposure, although the accumulation of Zea in the *lhcx1* mutant was lower than in the wild type. The reverse reaction of epoxidation (Zea → Ant → Vio) during the dark recovery period was clearly slower than that of de-epoxidation. Given that the NPQτ value of the wild type was significantly lowered (6.2 → 0.8) following dark recovery despite only a small change in Zea concentration (−8.7%), the level of NPQ was not strictly correlated with the concentration of Zea. These observations suggest the existence of other qE feedback processes beyond the Vio-Ant-Zea cycle, such as sensing of the transthylakoid ΔpH, in which the LHCX1 protein is presumably involved.

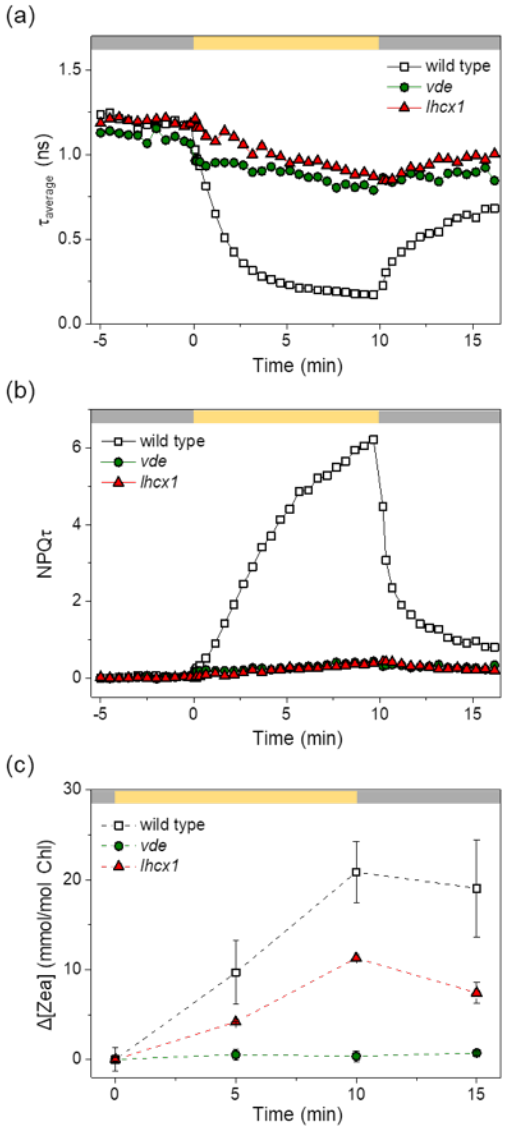

Figure 3-2. Fluorescence lifetime snapshot results presented as average Chl fluorescence lifetime ($\tau_{average}$) (a) and calculated NPQτ values for wild type (white squares), *vde* mutant (green circles), and *lhcx1* mutant (red triangles) (b) in response to dark/high-light exposure. Bars at the top of the figures indicate the time sequence of actinic light on (yellow, 850 µmol of photons per $m^{-2} \cdot s^{-1}$) and off (dark gray). A detailed discussion of $\tau_{average}$ and calculated NPQτ values is provided in Materials and Methods. (c) Kinetics of Zea concentration determined by time-resolved HPLC measurements. Data are presented as the mean ± SD ($n = 3$).

To investigate the activation of the EET mechanism upon high-light exposure, we measured the Zea S_1 excited-state absorption (ESA) signal in *N. oceanica* cells before and after high-light exposure (Figure 3-3a). As shown in Figure 3-1a, an active EET quenching pathway results in transient population of the Zea S_1 state after Chl *a* excitation (665 nm), which can be probed at 540 nm (Zea S_1–S_N transition).[23,40] Because a significant amount of Chl *a* ESA signal is also detected at this wavelength, the signals measured at 540 nm after high-light exposure are a combination of Zea S_1 ESA and Chl ESA. Because high light activates a variety of de-excitation pathways, the Chl excited-state population should be lower in high-light–exposed cells, and, indeed, the amplitude of the Chl ESA significantly decreases. This accounts for the overall lower amplitude of the ESA signal at 540 nm after high-light exposure despite the rapid contribution of the Zea S_1 ESA at early time delays (Figure 3-3a). When we compared the kinetics of the ESA signals measured in the dark and in high light, the two profiles were kinetically equivalent at time delays ≥40 ps. This ESA signal at longer time delays can mainly be attributed to the Chl ESA since the Zea S_1 states are almost entirely de-populated by this time delay. We therefore scaled the kinetic profile measured in the dark (mostly Chl ESA) to match that in high light based on signals at about 40 ps. Subtraction of the scaled dark signal from the high-light signal allows us to extract the contribution of Zea S_1 ESA from the overall Chl ESA. The Zea S_1 ESA profiles (Figure 3-3b) showed a single exponential decay with a lifetime of 7.71 ps and no resolvable rise time within the time resolution (~120 fs) of our TA setup. The lifetime of this difference signal coincides with literature values for the S_1 lifetime of Zea, which range from 7 to 11 ps.[23,40,50,51] Additionally, the difference spectrum (Figure 3-3a, *Inset*) clearly resembles the Car S_1 ESA spectrum observed in both methanol[51] and isolated thylakoid membranes. [23,40] We considered whether the well-known transient electrochromic shift of the Car S_0–S_2 absorption resulting from the light-induced transmembrane electric field ($\Delta\Psi$) could give rise to the signal at 540 nm. Typical electrochromic shift spectra show peaks between 515 and 520 nm in various plants and green algae,[52] while the difference spectrum (Figure 3-3a, *Inset*) has peak absorption at 540 nm and no absorption at 520 nm. This, along with the lifetime of this feature, suggests that the difference signal most likely comes from Car S_1–S_N absorption. The lack of positive difference signals from *vde* and *lhcx1* mutants (Figure 3-4a and c) further supports this conclusion.

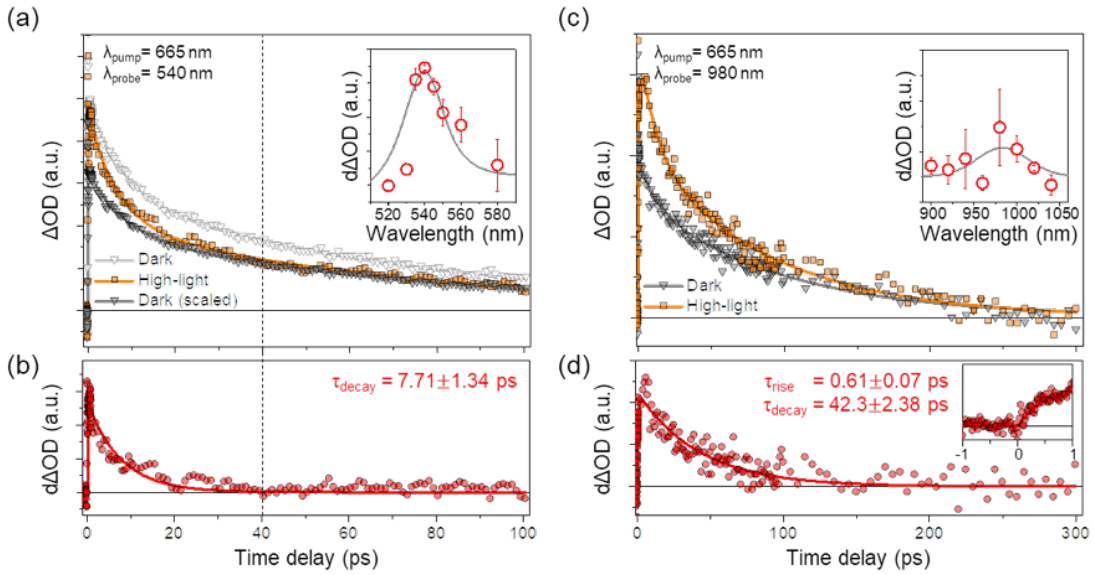

Figure 3-3. TA kinetic profiles for *N. oceanica* cells after Chl *a* excitation at 665 nm. (a) Profiles for wild-type *N. oceanica* probed at 540 nm under dark (light gray, inverted triangles) and high-light (orange squares) conditions. The samples were exposed to an actinic light (850 µmol of photons per $m^{-2}{\cdot}s^{-1}$) for 15 min of high-light exposure. The scaled dark profile (dark gray, inverted triangles) is also displayed. (*Inset*) Graph shows the difference TA spectrum reconstructed by subtracting the scaled dark signal from the high-light signal at 1 ps. Each data point is presented as the mean ± SE (n = 5). The spectrum of the Car S_1 ESA (gray line) from spinach thylakoid membranes is also shown in the *Inset* as a reference.[23] (b) Difference between high-light and scaled dark kinetic profiles measured at 540 nm. The lifetime obtained from fitting with a single exponential decay is 7.71 ± 1.34 ps. (c) Profiles probed at 980 nm under dark (dark gray, inverted triangles) and high-light (orange squares) conditions. These profiles are not normalized. (*Inset*) Graph shows the difference TA spectrum reconstructed by subtracting the dark signal from the high-light signal at 20 ps. Each data point is presented as the mean ± SE (n = 5). The gray curve represents the Gaussian fit to the difference data. (d) Difference between high-light and dark kinetic profiles measured at 980 nm. The lifetimes of the rise (τ_{rise}) and decay (τ_{decay}) components are 0.61 ± 0.07 ps and 42.3 ± 2.38 ps, respectively. ΔOD, changes in optical density; dΔOD, changes in ΔOD.

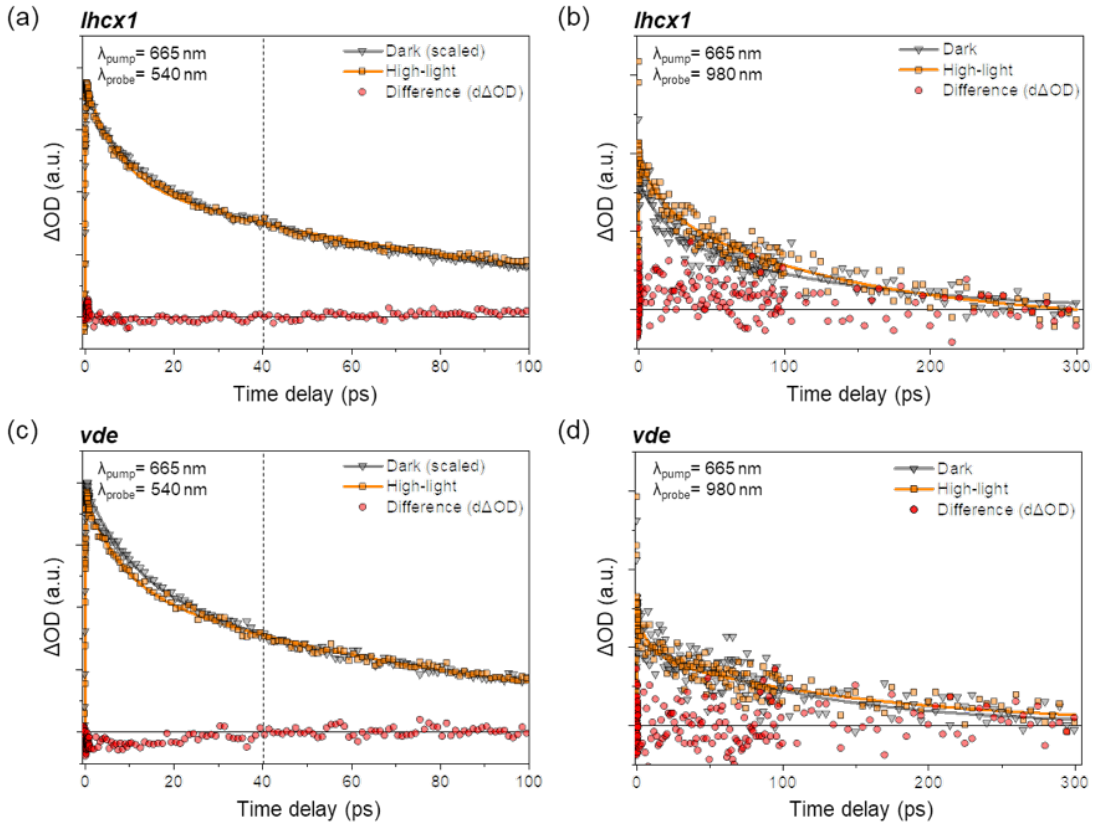

Figure 3-4. TA kinetic profiles of *lhcx1* (a) and *vde* (c) mutants probed at 540 nm under dark (gray inverted triangles) and high-light (orange squares) conditions, as well as the difference (dΔOD, red circles) between high light and dark. The samples were exposed to an actinic light (850 µmol of photons per $m^{-2} \cdot s^{-1}$) for 15 min of high-light exposure. Note that the dark profiles in a and c are scaled to match the high-light profiles at 40 ps. Profiles of *lhcx1* (b) and *vde* (d) mutants probed at 980 nm under dark (gray inverted triangles) and high-light conditions (orange squares), as well as the difference (dΔOD, red circles) between high light and dark. The dark and high-light kinetic profiles in b and d were not normalized. ΔOD, changes in optical density.

Chl*–Chl* annihilation is present at the intensities necessary for our TA measurements. This additional loss mechanism for excited Chl results in a decrease of the excitation diffusion length. The presence of annihilation is signaled by the decrease in the Chl fluorescence lifetime, which ranged from 0.22 to 1.25 ns (Figure 3-2a) under annihilation-free conditions, significantly longer than the Chl ESA signal lifetime ($\tau_{average} \leq 0.1$ ns) observed in our TA measurement (Figure 3-3a). In this condition, the Chl*–Chl* annihilation dominantly affects the Chl ESA decay kinetics. Given that the annihilation rate is constant during the transition from dark to high light, Chl ESA in dark and high light should have kinetically equivalent decays, which allows us to extract the Car S_1 ESA signal as the difference between dark and high-light TA profiles.[23] In addition, the presence of significant annihilation suggests that only those Chls that are excited in close proximity to Car molecules will populate the Car S_1 state we observe via TA. In this regard, the key observation in our Zea S_1 ESA kinetic profile (Figure 3-3b) is the lack of a resolvable rise time, which suggests near-instantaneous excitation energy equilibrium between the excited states of Zea and Chls nearby to Zea. The results of a kinetic simulation of the Zea S_1 state population with specific consideration of annihilation processes were described in our recent study.[23]

Figure 3-3c shows the ESA signals measured at 980 nm, where $Zea^{\bullet+}$ peak absorption appears[14,22,45] before and after high-light exposure of *N. oceanica* cells. Multiple species (e.g., ^{1}Chl*, ^{3}Chl*, ^{1}Car*) have ESA at 980 nm, making it difficult to deconvolute the individual species and corresponding ESA in the intact system. However, in the absence of $Zea^{\bullet+}$ ESA, we observed no noticeable change in the amplitude of the 980-nm ESA signal upon high-light exposure (Figure 3-4), which is consistent with our previous observations in thylakoid membranes.[22,45] Therefore, the dark and high-light kinetic profiles in Figure 3-3c do not need to be normalized in any way. The difference ESA signal between the high-light and dark conditions (Figure 3-3d) corresponds to the kinetic profile of $Zea^{\bullet+}$ and exhibits both rise (0.61 ps) and decay (40 ps) components. Unlike the Zea S_1 ESA, the $Zea^{\bullet+}$ ESA profile has a resolvable rise component (τ_{rise} = 0.61 ps). We believe this is due to the slower (~40 ps) charge recombination process for CT states ($Zea^{\bullet+} – Chl^{\bullet-}$), which allows excitation energy to be transferred to and populate the Chl–Zea pair before dissipation.[23] Interestingly, the same $Zea^{\bullet+}$ decay time (40 ps) was observed from high-light–exposed spinach thylakoid membranes in our recent study.[22] However, the rise time constant (0.61 ps) from *N. oceanica* was significantly smaller than that from spinach thylakoid membranes (15.4 ps).[22] This difference may be due to different antenna sizes and structures, which could influence the extent of annihilation and the kinetics of excitation transfer and trapping within PSII.

We took advantage of *lhcx1* and *vde* knockout mutants to investigate the specific roles of the LHCX1 and VDE proteins in the EET and CT mechanisms. In the *lhcx1* mutant, no noticeably positive ESA signal was observed (Figure 3-4a and b); thus, neither the Zea S_1 nor $Zea^{\bullet+}$ state appears to be present. This observation strongly suggests that the LHCX1 protein is necessary for activation of both EET and CT quenching. We were also unable to observe either Zea S_1 or $Zea^{\bullet+}$ ESA in the *vde* mutant (Figure 3-4c and d), indicating that accumulated Zea is also necessary for the EET and CT mechanisms in *N. oceanica*. In addition to lacking active EET and CT mechanisms, both the *lhcx1* and *vde* mutants exhibited negligible overall Chl* quenching in response to high-light exposure (Figure 3-2a and b), further supporting the idea that both EET quenching and CT quenching play a central role in Chl* de-excitation in high light.

3.6 Discussion

Our data clearly provide evidence that both Chl–Zea EET and CT mechanisms are active in intact live cells of *N. oceanica*. Our data do not specifically identify the quenching site(s) in *N. oceanica*, but the data in Figure 3-2 and Figure 3-4 strongly suggest that LHCX1 may be both the sensor of ΔpH and the actual site of quenching. The finding that Zea accumulation alone produces little qE and no detectable Zea S_1 or $Zea^{\bullet+}$ makes it highly likely that Zea binding to LHCX1 is essential for qE in *N. oceanica*, and that Zea binding to other light-harvesting proteins does not produce significant qE under the conditions of our experiments. Given that the propensity for either Chl–Zea energy transfer or change transfer is very sensitive to the spatial separation of the pair,[44] it is possible that a natural (or controlled) distribution of Chl–Zea separations and energy gaps within Zea–LHCX1* results in some quenching of excited Chl by EET and some by CT.

Both mechanisms require the VDE and LHCX1 proteins, which are activated by the formation of high-light–induced ΔpH across the thylakoid membrane (Figure 3-5).[53] In this picture, Zea produced by VDE binds to LHCX1* to generate a Zea–LHCX1* pigment–protein complex similar to that observed in green algae and moss.[12,54] The quenching sites associated with this Zea–LHCX1* pigment complex are switched on and off by at least two *in vivo* control systems, one based on the concentration of Zea pigment and one based on activated LHCX1. An NPQ value (NPQτ) of 6 suggests that the Zea–LHCX1* combination is a remarkably effective quencher. If the model for green plant thylakoid membranes developed by Bennett et al.[55] applies to *N. oceanica*, an NPQ value of 6 implies an excitation diffusion length of less than 20 nm (Figure 4 of Ref. [55]).

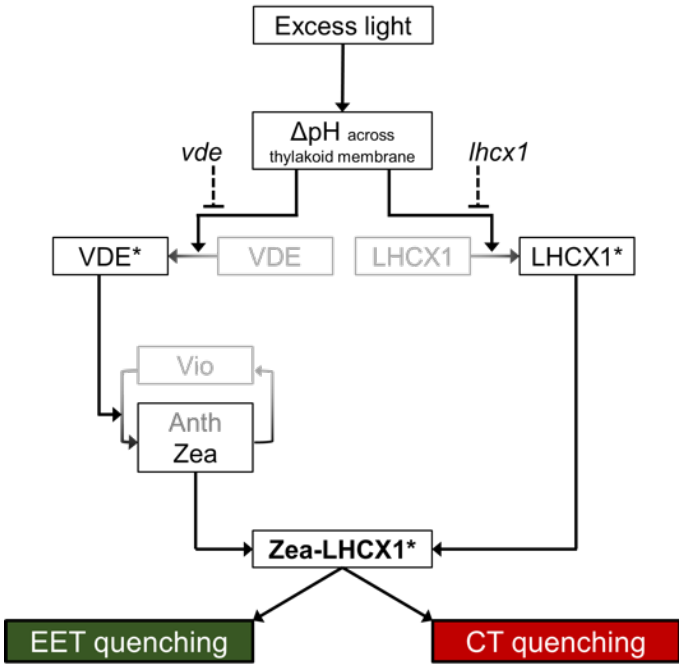

Figure 3-5. Proposed scheme for the triggering system of the EET and CT quenching mechanisms for qE in *N. oceanica*. VDE* and LHCX1* indicate activated VDE and LHCX1 proteins, respectively. We hypothesize that Zea produced by VDE binds to LHCX1* to generate a pigment–protein complex that is necessary for both EET and CT quenching mechanisms.

3.7 Conclusions

It has been shown that it is possible to improve crop yield by modification of the NPQ response through overexpression of three genes,[3] one specifically encoding for the ΔpH-sensing protein (PsbS) and the other two encoding the enzymes responsible for interconversion between Zea and Vio via the xanthophyll cycle. To explore how large an increase in yield is possible, a mechanism for the role of Zea is needed. Measurements on isolated complexes lacking the full complexity of the intact system with its various feedback loops, sensing/activating proteins (e.g., PsbS or LHCSR/LHCX), and protein–protein interactions, along with pH and ionic gradients, do not capture the behavior of the *in vivo* system. Although subject to much speculation, no demonstration of the direct involvement of Zea in intact systems (e.g., live cells, leaves) had been made before this work. Specifically, the application of TA spectroscopy to live cells of *N. oceanica* enabled us to observe the operation of the Chl–Zea EET and CT mechanisms and their control systems *in vivo*. Building upon our previous observations from spinach thylakoid membranes, which showed that both the EET and CT mechanisms are involved in qE and are controlled by PsbS,[22,23] the present evidence further supports that the presence of de-epoxidized xanthophylls (e.g., Zea) and a ΔpH-sensing protein (e.g., LHCX, LHCSR, PsbS) is essential for the operation of both EET and CT mechanisms of qE in a variety of photosynthetic organisms. Developing a fundamental understanding of the qE mechanisms operating *in vivo* should provide a basis for increasing the yield of *N. oceanica*, which is a promising source for renewable biodiesel.[24–26]

3.8 References

(1) Tripathy, B. C.; Oelmüller, R. Reactive oxygen species generation and signaling in plants. *Plant Signal. Behav.* **2012**, *7* (12), 1621–1633.

(2) Müller, P.; Li, X.-P.; Niyogi, K. K. Non-photochemical quenching. A response to excess light energy. *Plant Physiol.* **2001**, *125* (4), 1558–1566.

(3) Kromdijk, J.; Głowacka, K.; Leonelli, L.; Gabilly, S. T.; Iwai, M.; Niyogi, K. K.; Long, S. P. Improving photosynthesis and crop productivity by accelerating recovery from photoprotection. *Science* **2016**, *354* (6314), 857–861.

(4) Głowacka, K.; Kromdijk, J.; Kucera, K.; Xie, J.; Cavanagh, A. P.; Leonelli, L.; Leakey, A. D. B.; Ort, D. R.; Niyogi, K. K.; Long, S. P. Photosystem II Subunit S overexpression increases the efficiency of water use in a field-grown crop. *Nat. Commun.* **2018**, *9* (1), 868.

(5) Berteotti, S.; Ballottari, M.; Bassi, R. Increased biomass productivity in green algae by tuning non-photochemical quenching. *Sci. Rep.* **2016**, *6* (1), 21339.

(6) Chukhutsina, V. U.; Fristedt, R.; Morosinotto, T.; Croce, R. Photoprotection strategies of the alga Nannochloropsis gaditana. *Biochim. Biophys. Acta - Bioenerg.* **2017**, *1858* (7), 544–552.

(7) Amarnath, K.; Zaks, J.; Park, S. D.; Niyogi, K. K.; Fleming, G. R. Fluorescence lifetime snapshots reveal two rapidly reversible mechanisms of photoprotection in live cells of Chlamydomonas reinhardtii. *Proc. Natl. Acad. Sci. U. S. A.* **2012**, *109* (22), 8405–8410.

(8) Nilkens, M.; Kress, E.; Lambrev, P.; Miloslavina, Y.; Müller, M.; Holzwarth, A. R.; Jahns, P. Identification of a slowly inducible zeaxanthin-dependent component of non-photochemical quenching of chlorophyll fluorescence generated under steady-state conditions in Arabidopsis. *Biochim. Biophys. Acta - Bioenerg.* **2010**, *1797* (4), 466–475.

(9) Staleva, H.; Komenda, J.; Shukla, M. K.; Šlouf, V.; Kaňa, R.; Polívka, T.; Sobotka, R. Mechanism of photoprotection in the cyanobacterial ancestor of plant antenna proteins. *Nat. Chem. Biol.* **2015**, *11* (4), 287–291.

(10) Ruban, A. V.; Berera, R.; Ilioaia, C.; van Stokkum, I. H. M.; Kennis, J. T. M.; Pascal, A. A.; van Amerongen, H.; Robert, B.; Horton, P.; van Grondelle, R. Identification of a mechanism of photoprotective energy dissipation in higher plants. *Nature* **2007**, *450* (7169), 575–578.

(11) Walla, P. J.; Linden, P. A.; Ohta, K.; Fleming, G. R. Excited-State Kinetics of the Carotenoid S1 State in LHC II and Two-Photon Excitation Spectra of Lutein and β-Carotene in Solution: Efficient Car S1→Chl Electronic Energy Transfer via Hot S1 States? *J. Phys. Chem. A* **2002**, *106* (10), 1909–1916.

(12) Bonente, G.; Ballottari, M.; Truong, T. B.; Morosinotto, T.; Ahn, T. K.; Fleming, G. R.; Niyogi, K. K.; Bassi, R. Analysis of LhcSR3, a Protein Essential for Feedback De-Excitation in the Green Alga Chlamydomonas reinhardtii. *PLoS Biol.* **2011**, *9* (1), e1000577.

(13) Avenson, T. J.; Ahn, T. K.; Niyogi, K. K.; Ballottari, M.; Bassi, R.; Fleming, G. R. Lutein can act as a switchable charge transfer quencher in the CP26 light-harvesting complex. *J. Biol. Chem.* **2009**, *284* (5), 2830–2835.

(14) Ahn, T. K.; Avenson, T. J.; Ballottari, M.; Cheng, Y.-C.; Niyogi, K. K.; Bassi, R.; Fleming, G. R. Architecture of a charge-transfer state regulating light harvesting in a plant antenna protein. *Science* **2008**, *320* (5877), 794–797.

(15) Avenson, T. J.; Ahn, T. K.; Zigmantas, D.; Niyogi, K. K.; Li, Z.; Ballottari, M.; Bassi, R.;

Fleming, G. R. Zeaxanthin radical cation formation in minor light-harvesting complexes of higher plant antenna. *J. Biol. Chem.* **2008**, *283* (6), 3550–3558.
(16) Correa-Galvis, V.; Poschmann, G.; Melzer, M.; Stühler, K.; Jahns, P. PsbS interactions involved in the activation of energy dissipation in Arabidopsis. *Nat. Plants* **2016**, *2* (2), 15225.
(17) Sacharz, J.; Giovagnetti, V.; Ungerer, P.; Mastroianni, G.; Ruban, A. V. The xanthophyll cycle affects reversible interactions between PsbS and light-harvesting complex II to control non-photochemical quenching. *Nat. Plants* **2017**, *3* (2), 16225.
(18) Zaks, J.; Amarnath, K.; Kramer, D. M.; Niyogi, K. K.; Fleming, G. R. A kinetic model of rapidly reversible nonphotochemical quenching. *Proc. Natl. Acad. Sci. U. S. A.* **2012**, *109* (39), 15757–15762.
(19) Balevičius, V.; Fox, K. F.; Bricker, W. P.; Jurinovich, S.; Prandi, I. G.; Mennucci, B.; Duffy, C. D. P. Fine control of chlorophyll-carotenoid interactions defines the functionality of light-harvesting proteins in plants. *Sci. Rep.* **2017**, *7* (1), 13956.
(20) Hontani, Y.; Kloz, M.; Polívka, T.; Shukla, M. K.; Sobotka, R.; Kennis, J. T. M. Molecular Origin of Photoprotection in Cyanobacteria Probed by Watermarked Femtosecond Stimulated Raman Spectroscopy. *J. Phys. Chem. Lett.* **2018**, *9* (7), 1788–1792.
(21) Liguori, N.; Xu, P.; van Stokkum, I. H. M.; van Oort, B.; Lu, Y.; Karcher, D.; Bock, R.; Croce, R. Different carotenoid conformations have distinct functions in light-harvesting regulation in plants. *Nat. Commun.* **2017**, *8* (1), 1994.
(22) Park, S.; Fischer, A. L.; Li, Z.; Bassi, R.; Niyogi, K. K.; Fleming, G. R. Snapshot Transient Absorption Spectroscopy of Carotenoid Radical Cations in High-Light-Acclimating Thylakoid Membranes. *J. Phys. Chem. Lett.* **2017**, *8* (22), 5548–5554.
(23) Park, S.; Fischer, A. L.; Steen, C. J.; Iwai, M.; Morris, J. M.; Walla, P. J.; Niyogi, K. K.; Fleming, G. R. Chlorophyll-Carotenoid Excitation Energy Transfer in High-Light-Exposed Thylakoid Membranes Investigated by Snapshot Transient Absorption Spectroscopy. *J. Am. Chem. Soc.* **2018**, *140* (38), 11965–11973.
(24) Adarme-Vega, T.; Lim, D. K. Y.; Timmins, M.; Vernen, F.; Li, Y.; Schenk, P. M. Microalgal biofactories: a promising approach towards sustainable omega-3 fatty acid production. *Microb. Cell Fact.* **2012**, *11* (1), 96.
(25) Simionato, D.; Sforza, E.; Corteggiani Carpinelli, E.; Bertucco, A.; Giacometti, G. M.; Morosinotto, T. Acclimation of Nannochloropsis gaditana to different illumination regimes: Effects on lipids accumulation. *Bioresour. Technol.* **2011**, *102* (10), 6026–6032.
(26) Chisti, Y. Biodiesel from microalgae. *Biotechnol. Adv.* **2007**, *25* (3), 294–306.
(27) Keşan, G.; Litvín, R.; Bína, D.; Durchan, M.; Šlouf, V.; Polívka, T. Efficient light-harvesting using non-carbonyl carotenoids: Energy transfer dynamics in the VCP complex from Nannochloropsis oceanica. *Biochim. Biophys. Acta - Bioenerg.* **2016**, *1857* (4), 370–379.
(28) Carbonera, D.; Agostini, A.; Di Valentin, M.; Gerotto, C.; Basso, S.; Giacometti, G. M.; Morosinotto, T. Photoprotective sites in the violaxanthin–chlorophyll a binding Protein (VCP) from Nannochloropsis gaditana. *Biochim. Biophys. Acta - Bioenerg.* **2014**, *1837* (8), 1235–1246.
(29) Vieler, A.; Wu, G.; Tsai, C.-H.; Bullard, B.; Cornish, A. J.; Harvey, C.; Reca, I.-B.; Thornburg, C.; Achawanantakun, R.; Buehl, C. J.; Campbell, M. S.; Cavalier, D.; Childs, K. L.; Clark, T. J.; Deshpande, R.; Erickson, E.; Armenia Ferguson, A.; Handee, W.; Kong, Q.; Li, X.; Liu, B.; Lundback, S.; Peng, C.; Roston, R. L.; Sanjaya; Simpson, J. P.; TerBush,

A.; Warakanont, J.; Zäuner, S.; Farre, E. M.; Hegg, E. L.; Jiang, N.; Kuo, M.-H.; Lu, Y.; Niyogi, K. K.; Ohlrogge, J.; Osteryoung, K. W.; Shachar-Hill, Y.; Sears, B. B.; Sun, Y.; Takahashi, H.; Yandell, M.; Shiu, S.-H.; Benning, C. Genome, Functional Gene Annotation, and Nuclear Transformation of the Heterokont Oleaginous Alga Nannochloropsis oceanica CCMP1779. *PLoS Genet.* **2012**, *8* (11), e1003064.

(30) Li, X.-P.; Björkman, O.; Shih, C.; Grossman, A. R.; Rosenquist, M.; Jansson, S.; Niyogi, K. K. A pigment-binding protein essential for regulation of photosynthetic light harvesting. *Nature* **2000**, *403* (6768), 391–395.

(31) Umetani, I.; Kunugi, M.; Yokono, M.; Takabayashi, A.; Tanaka, A. Evidence of the supercomplex organization of photosystem II and light-harvesting complexes in Nannochloropsis granulata. *Photosynth. Res.* **2018**, *136* (1), 49–61.

(32) Litvín, R.; Bína, D.; Herbstová, M.; Gardian, Z. Architecture of the light-harvesting apparatus of the eustigmatophyte alga Nannochloropsis oceanica. *Photosynth. Res.* **2016**, *130* (1–3), 137–150.

(33) Peers, G.; Truong, T. B.; Ostendorf, E.; Busch, A.; Elrad, D.; Grossman, A. R.; Hippler, M.; Niyogi, K. K. An ancient light-harvesting protein is critical for the regulation of algal photosynthesis. *Nature* **2009**, *462* (7272), 518–521.

(34) Alboresi, A.; Gerotto, C.; Giacometti, G. M.; Bassi, R.; Morosinotto, T. Physcomitrella patens mutants affected on heat dissipation clarify the evolution of photoprotection mechanisms upon land colonization. *Proc. Natl. Acad. Sci. U. S. A.* **2010**, *107* (24), 11128–11133.

(35) Bailleul, B.; Rogato, A.; de Martino, A.; Coesel, S.; Cardol, P.; Bowler, C.; Falciatore, A.; Finazzi, G. An atypical member of the light-harvesting complex stress-related protein family modulates diatom responses to light. *Proc. Natl. Acad. Sci. U. S. A.* **2010**, *107* (42), 18214–18219.

(36) Demmig-Adams, B.; Garab, G.; Adams Iii, W. *Non-Photochemical Quenching and Energy Dissipation in Plants, Algae and Cyanobacteria*; 2014.

(37) Young, A. J.; Frank, H. A. Energy transfer reactions involving carotenoids: quenching of chlorophyll fluorescence. *J. Photochem. Photobiol. B Biol.* **1996**, *36* (1), 3–15.

(38) van Amerongen, H.; van Grondelle, R. Understanding the Energy Transfer Function of LHCII, the Major Light-Harvesting Complex of Green Plants. *J. Phys. Chem. B* **2001**, *105* (3), 604–617.

(39) Kloz, M.; Pillai, S.; Kodis, G.; Gust, D.; Moore, T. A.; Moore, A. L.; van Grondelle, R.; Kennis, J. T. M. Carotenoid Photoprotection in Artificial Photosynthetic Antennas. *J. Am. Chem. Soc.* **2011**, *133* (18), 7007–7015.

(40) Ma, Y.-Z.; Holt, N. E.; Li, X.-P.; Niyogi, K. K.; Fleming, G. R. Evidence for direct carotenoid involvement in the regulation of photosynthetic light harvesting. *Proc. Natl. Acad. Sci.* **2003**, *100* (3), 4377–4382.

(41) Liao, P.-N.; Holleboom, C.-P.; Wilk, L.; Kühlbrandt, W.; Walla, P. J. Correlation of Car S 1 → Chl with Chl → Car S 1 Energy Transfer Supports the Excitonic Model in Quenched Light Harvesting Complex II. *J. Phys. Chem. B* **2010**, *114* (47), 15650–15655.

(42) Holleboom, C.-P.; Walla, P. J. The back and forth of energy transfer between carotenoids and chlorophylls and its role in the regulation of light harvesting. *Photosynth. Res.* **2014**, *119* (1–2), 215–221.

(43) Bode, S.; Quentmeier, C. C.; Liao, P.-N.; Hafi, N.; Barros, T.; Wilk, L.; Bittner, F.; Walla, P. J. On the regulation of photosynthesis by excitonic interactions between carotenoids and

chlorophylls. *Proc. Natl. Acad. Sci. U. S. A.* **2009**, *106* (30), 12311–12316.
(44) Dreuw, A.; Fleming, G. R.; Head-Gordon, M. Charge-Transfer State as a Possible Signature of a Zeaxanthin−Chlorophyll Dimer in the Non-photochemical Quenching Process in Green Plants. *J. Phys. Chem. B* **2003**, *107* (27), 6500–6503.
(45) Holt, N. E.; Zigmantas, D.; Valkūnas, L.; Li, X.-P.; Niyogi, K. K.; Fleming, G. R. Carotenoid cation formation and the regulation of photosynthetic light harvesting. *Science* **2005**, *307* (5708), 433–436.
(46) Porra, R. J.; Thompson, W. A.; Kriedemann, P. E. Determination of accurate extinction coefficients and simultaneous equations for assaying chlorophylls a and b extracted with four different solvents: verification of the concentration of chlorophyll standards by atomic absorption spectroscopy. *Biochim. Biophys. Acta - Bioenerg.* **1989**, *975* (3), 384–394.
(47) Leuenberger, M.; Morris, J. M.; Chan, A. M.; Leonelli, L.; Niyogi, K. K.; Fleming, G. R. Dissecting and modeling zeaxanthin- and lutein-dependent nonphotochemical quenching in Arabidopsis thaliana. *Proc. Natl. Acad. Sci. U. S. A.* **2017**, *114* (33), E7009–E7017.
(48) Sylak-Glassman, E. J.; Malnoë, A.; De Re, E.; Brooks, M. D.; Fischer, A. L.; Niyogi, K. K.; Fleming, G. R. Distinct roles of the photosystem II protein PsbS and zeaxanthin in the regulation of light harvesting in plants revealed by fluorescence lifetime snapshots. *Proc. Natl. Acad. Sci. U. S. A.* **2014**, *111* (49), 17498–17503.
(49) Müller-Moulé, P.; Conklin, P. L.; Niyogi, K. K. Ascorbate deficiency can limit violaxanthin de-epoxidase activity in vivo. *Plant Physiol.* **2002**, *128* (3), 970–977.
(50) Billsten, H. H.; Pan, J.; Sinha, S.; Pascher, T.; Sundström, V.; Polívka, T. Excited-State Processes in the Carotenoid Zeaxanthin after Excess Energy Excitation. *J. Phys. Chem. A* **2005**, *109* (31), 6852–6859.
(51) Polívka, T.; Sundström, V. Ultrafast Dynamics of Carotenoid Excited States−From Solution to Natural and Artificial Systems. *Chem. Rev.* **2004**, *104* (4), 2021–2072.
(52) Bailleul, B.; Cardol, P.; Breyton, C.; Finazzi, G. Electrochromism: a useful probe to study algal photosynthesis. *Photosynth. Res.* **2010**, *106* (1–2), 179–189.
(53) Cao, S.; Zhang, X.; Xu, D.; Fan, X.; Mou, S.; Wang, Y.; Ye, N.; Wang, W. A transthylakoid proton gradient and inhibitors induce a non-photochemical fluorescence quenching in unicellular algae Nannochloropsis sp. *FEBS Lett.* **2013**, *587* (9), 1310–1315.
(54) Kondo, T.; Pinnola, A.; Chen, W. J.; Dall'Osto, L.; Bassi, R.; Schlau-Cohen, G. S. Single-molecule spectroscopy of LHCSR1 protein dynamics identifies two distinct states responsible for multi-timescale photosynthetic photoprotection. *Nat. Chem.* **2017**, *9* (8), 772–778.
(55) Bennett, D. I. G.; Fleming, G. R.; Amarnath, K. Energy-dependent quenching adjusts the excitation diffusion length to regulate photosynthetic light harvesting. *Proc. Natl. Acad. Sci.* **2018**, *114* (41), E9523–E9531.

Chapter 4

Photoprotection in *A. thaliana* under Fluctuating Light

This chapter is reproduced with permission from
C.J. Steen, J.M. Morris, A.H. Short, K.N. Niyogi, G.R. Fleming
"Complex Roles of PsbS and Xanthophylls in the Regulation of Nonphotochemical Quenching in *Arabidopsis thaliana* under Fluctuating Light"
J. Phys. Chem. B (2020) *124, 46, 10311–10325*
DOI: 10.1021/acs.jpcb.0c06265.

The chapter also contains unpublished HPLC data collected in collaboration with Audrey Short.

4.1 Abstract

Protection of photosystem II against damage from excess light by nonphotochemical quenching (NPQ) includes responses on a wide range of timescales. The onset of the various phases of NPQ overlap in time making it difficult to discern if they influence each other or involve different photophysical mechanisms. To unravel the complex relationship of the known actors in NPQ, we perform fluorescence lifetime snapshot measurements throughout multiple cycles of alternating 2 min periods of high light and darkness. By comparing the data with an empirically based mathematical model that describes both fast and slow quenching responses, we suggest that the rapidly reversible quenching response depends on the state of the slower response. By studying a series of *Arabidopsis thaliana* mutants, we find that removing zeaxanthin (Zea) or enhancing PsbS concentration, for example, influences the amplitudes of the slow quenching induction and recovery, but not the timescales. The plants' immediate response to high light appears independent of the illumination history, while PsbS and Zea have distinct roles in both quenching and recovery. We further identify two parameters in our model that predominately influence the recovery amplitude and propose that our approach may prove useful for screening new mutants or overexpressors with enhanced biomass yields under field conditions.

4.2 Introduction

The initial step of photosynthesis requires absorption of light to drive charge separation via photochemistry[1]. However, fluctuating sunlight can transiently exceed the capacity of photosynthetic organisms to use the absorbed energy for productive charge separation. To avoid damage to the photosynthetic apparatus, photosynthetic organisms regulate photoprotective processes in response to light conditions, ensuring that excess energy is dissipated safely.[2] Recent work has shown that increasing photosynthetic organisms' ability to rapidly match the level of photoprotection to incident light conditions can improve crop yields.[3,4] Nonetheless, the individual contributions of the various biochemical actors are still under debate, especially under natural light conditions.

When light absorption outpaces charge separation, photosystem II (PSII) experiences longer-lived excitation kinetics[2,5] and is more susceptible to damage than photosystem I.[2,6–8] The suite of photoprotective mechanisms that protect PSII by dissipating excess excitation – referred to collectively as nonphotochemical quenching (NPQ), the reduction in the observed chlorophyll *a* (Chl *a*) fluorescence by mechanisms other than photochemistry[9–11] – have been the subject of intense study.

The contributions to overall NPQ are often separated into components, including (but not limited to) qE[12–17] (rapidly reversible phase), qZ[18–21] (dependent on zeaxanthin (Zea)), and qI[22–25] (associated with photoinhibition). More recently, a slowly reversible component called qH (which is induced by a combination of high light (HL) and low temperature) has been added.[26] However, many of the NPQ components overlap in time and it is not clear if they involve the same underlying photophysical dissipation mechanism(s) controlled by different kinetic regulatory processes or utilize differing dissipation mechanisms. To unravel the complex relationships of the known actors in NPQ, rather than measuring the response of leaves over a single light–dark cycle, we employ multiple cycles of short (2 min) periods of high light (HL) alternating with dark periods of the same duration.

Rapidly alternating HL and dark periods over a series of 10 cycles allows us to measure how the rapid response evolves as the slow responses simultaneously move toward their steady-state behavior. This periodic illumination sequence is also more representative of the fluctuating light exposure patterns that plants experience in nature.[4,27–30] By combining these data with a mathematical model that incorporates both fast and slow responses, but which is agnostic as to the specific molecular mechanisms underlying the components, we demonstrate that the rapidly reversible response depends on the slower response.

Here, time-correlated single photon counting (TCSPC) measurements of the fluorescence lifetime are performed on whole *Arabidopsis thaliana* leaves under exposure to periodic actinic light. As discussed elsewhere,[31] directly measuring the fluorescence lifetimes in snapshots enables us to focus only on processes that quench chlorophyll excitations. As opposed to fluorescence yields, fluorescence lifetimes are not influenced by processes that reduce the fluorescence quantum yield but do not result in quenching of chlorophyll excitation,[32,33] such as enhanced light scattering, chloroplast movement,[34] or chromophore bleaching.

To disentangle how the various known biochemical actors influence the timescales and amplitudes of the quenching response, we utilized a range of mutants for comparison to wild type (WT, Col-0 ecotype; see Table 4-1 for a summary of all genotypes). As the involvement of the pH-sensing protein PsbS in qE is well established,[35,36] we selected a PsbS-deficient mutant, *npq4*, and a PsbS-overexpressing mutant, *L17*.[37] Similarly, low lumen pH activates the enzyme violaxanthin de-epoxidase (VDE) which converts violaxanthin via antheraxanthin to zeaxanthin (Zea) in the HL-dependent half of the VAZ cycle.[2,9,10,38] There has been extensive discussion in the literature concerning the role(s) of Zea[39–43] and another de-epoxidized xanthophyll — lutein (Lut)[44–47] — in the dissipation mechanism underlying NPQ. Accordingly, we utilized the mutant *npq1*, which lacks VDE and is unable to generate Zea,[48,49] and the *szl1* mutant, which does not accumulate Zea but possesses increased levels of lutein.[45,50]

Table 4-1. *A. thaliana* genotypes investigated in this study.
The color of each genotype matches those used throughout the chapter.

Abbreviation	Phenotype	Reference
WT	wild type	
L17	overexpresses PsbS	37
szl1	minimal [Zea], increased [Lut]	45, 50
npq4	lacks PsbS function	35
npq1	no VDE activity	48, 49

By considering these various mutants in the context of our model, we discuss the molecular species and identify specific model parameters controlling the extent of recovery from maximum quenching. We propose that determination of these parameters could provide a rapid method for selecting new mutants and overexpressors with enhanced recovery amplitudes for field trials aimed at increasing biomass yields.

4.3 Methods and Data Analysis

4.3.1 Plant Genotypes and Growth Conditions

Five *A. thaliana* genetic lines were selected for a comparison of the effects of both PsbS and xanthophylls (Zea and Lut) in rapid and moderate-to-long timescale quenching dynamics usually classified as qE, qZ, or qI. The specific genotypes studied are summarized in Table 4-1. Plants were germinated on MS plates, transplanted to pots after 2 weeks, and grown in growth chambers under 110 μmol photons m^{-2} s^{-1} on a 10-h day and 14-h night cycle at 23 °C. All plants were between 5 and 8 weeks of age at the time of experiments.

4.3.2 TCSPC Measurements and Exponential Fitting

Chlorophyll fluorescence lifetime snapshot measurements of whole leaves of *A. thaliana* were collected via time-correlated single photon counting (TCSPC) to measure changes in the fluorescence lifetimes (picoseconds to nanoseconds) of chlorophyll *a* (Chl *a*) in PSII in response to high-light exposure (seconds to minutes). TCSPC fluorescence lifetime measurements are less sensitive to changes in absorbance, due to e.g., chloroplast avoidance, than traditional yield measurements,[31] allowing lengthier actinic light exposure patterns to be studied.

After an hour of initial dark acclimation, leaves were removed from the plant and placed in a custom-built sample holder. A 532 nm Coherent Verdi G10 diode laser pumped an ultrafast Ti:sapphire Coherent Mira 900f oscillator with a center wavelength of 840 nm and full width at half-maximum (FWHM) of approximately 9 nm. The 840 nm output pulses from the Mira were then frequency doubled to 420 nm using a β-barium borate crystal to excite the Soret band of Chl *a*. The beam was split, with a portion directed to a sync photodiode providing a reference for TCSPC measurements and the remainder directed to the sample. The portion of the beam that reached the sample was incident on the leaf at a ∼70° angle to the adaxial side of the leaf. The average power of the laser at the sample was 1.75 mW, saturating reaction centers.[51] Fluorescence was collected through a monochromator (HORIBA Jobin-Yvon; H-20) set to transmit 680 ± 8 nm placed before a microchannel plate (MCP)-photomultiplier tube (PMT) detector (Hamamatsu R3809U MCP-PMT) to selectively observe fluorescence from the Q_y band of Chl *a* in PSII. The detector was cooled to −30 °C and the gain was set to 94% yielding an instrument response function with a FWHM of 36–38 ps. Data were acquired using a Becker & Hickl SPC-850 data acquisition card combined with a sequence of trigger and shutter operations executed with LabView. The actinic light source was a Leica KL1500 LCD with a peak intensity of 648 nm and FWHM of 220 nm. TCSPC snapshots were collected at 30 s intervals over 10 4 min cycles consisting of 2 min of high light (700 μmol photons m^{-2} s^{-1} actinic white light) and 2 min of darkness. Fluorescence decays were collected for each of the 0.2 s steps during the 1 s snapshot measurement and fit to biexponential functions using reconvolution fitting with the measured instrument response function. The amplitude-weighted average lifetime for each decay was calculated, and the step with the longest lifetime was chosen as the step with the reaction centers closed to saturation, as described in the previous work.[52,53]

4.3.3 Data and Error Analysis

High snapshot time resolution is required to resolve the timescale of the rapid induction and relaxation of quenching upon transitions between darkness and high light. Measurements at 30 s snapshot resolution were collected for two "time offsets" describing the initial timepoint: one starting at 0 s (resulting in measurements at 0, 30, 60 s, and so on) and another at 15 s (resulting in measurements at 15, 45, 75 s, and so on). To achieve a final data set with 15 s snapshot resolution, pairwise permutations of 0 and 15 s leaf samples were combined and a first-order Butterworth filter with a critical frequency of 15 s^{-1} was applied to remove high-frequency oscillations due to leaf-to-leaf variability. The resulting filtered traces were averaged at each timepoint to obtain fluorescence lifetime snapshot traces and uncertainty was estimated as the standard error, where the number of independent samples was the number of filtered, pairwise permutations for each genotype. For example, three independent leaves measured using both the 0 and 15 s sequences yields nine possible pairwise permutations.

To quantify quenching, NPQ_τ values were calculated from the mean snapshot lifetime traces, as previously described.[31,42,43] The formula for NPQ_τ is analogous to the traditional NPQ parameter[1,48,54] ($NPQ = (F_m - F_m')/F_m'$). The error in NPQ_τ was again estimated as the standard error. To quantify the interperiod behavior, upper and lower envelope traces were obtained by selecting the NPQτ values at the light-to-dark transitions (maximum quenching) and dark-to-light transitions (maximum recovery) and these data points were fit to an exponential function of the form $a\,e^{-t/\tau} + c$, where a was negative. To quantify the intraperiod behavior at steady state, the data from the penultimate (ninth) HL and dark periods were fit to an exponential function of the form $a\,e^{-t/\tau} + c$, where a was negative.

All data analysis and modeling was performed using MATLAB. In all cases, the model's differential equation (see Equation 1 in the Appendix) was integrated over the duration of the experiment (0–40 min) in steps of 0.005 min using the fourth order Runge–Kutta (RK4) method. The structure of the model and the necessary equations are described extensively in a section titled "Mathematical Model of Multi-timescale Regulatory Processes" (Section 4.4.3) and the equations are also presented in the Appendix (Section 4.7).

4.3.4 Analysis of Fluorescence Lifetime Snapshot Traces

Figure 4-1 shows scatter plots of average fluorescence lifetime snapshot values collected from intact *A. thaliana* leaves at 15 s resolution for the various genotypes studied. The mean and uncertainty values were obtained by combining ("interleaving") all possible combinations of data sets collected with two different time offsets, each with 30 s resolution between snapshot measurements. Although individual traces of snapshots obtained from a single leaf are consistent from snapshot to snapshot, there is noticeable leaf-to-leaf variability that introduces high frequency measurement error when combining the two phases that is eliminated by application of a first-order Butterworth filter.

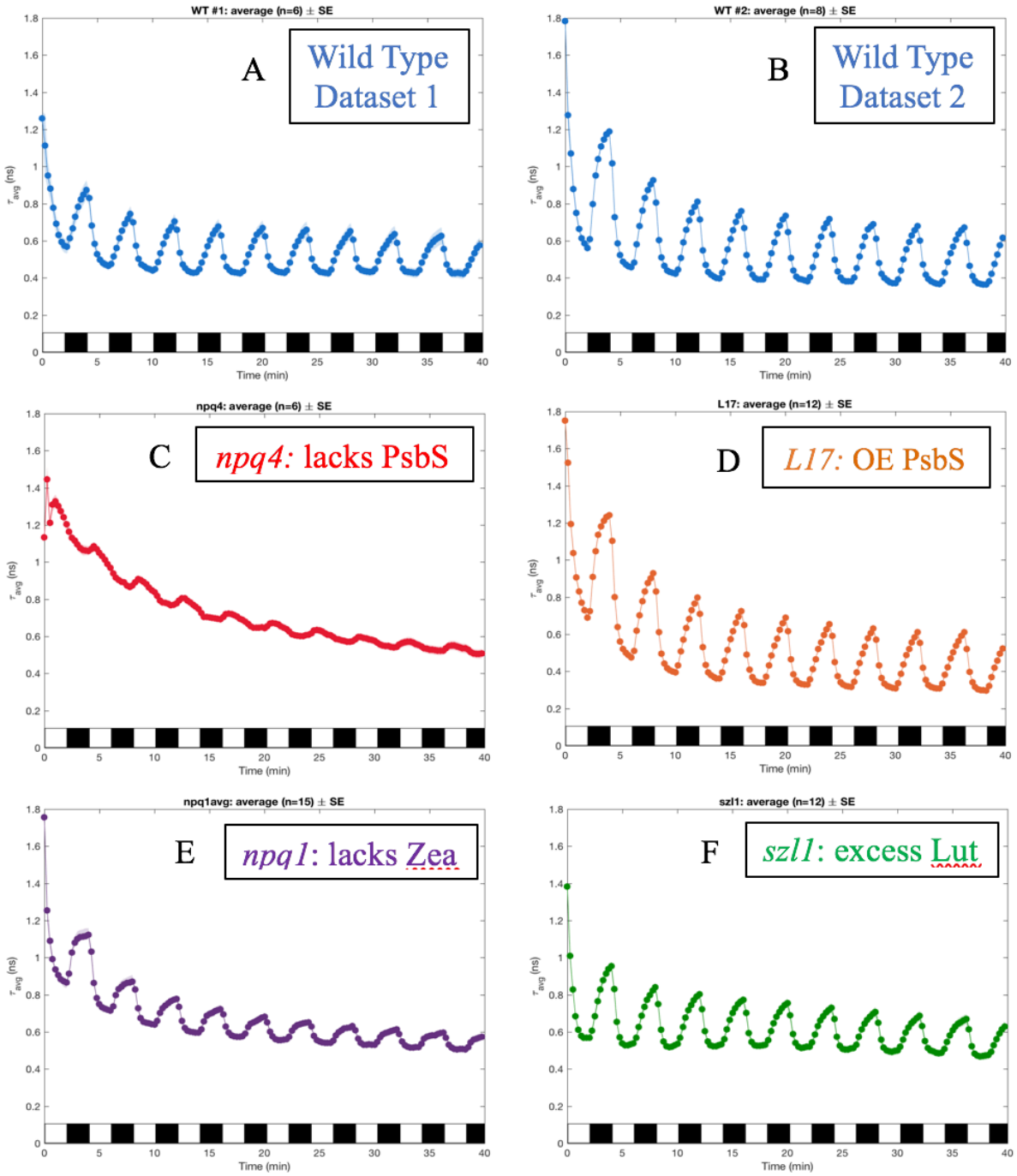

Figure 4-1. Snapshot fluorescence lifetime values collected from *A. thaliana* leaves for (A) and (B) two representative WT datasets, (C) *npq4*, (D) *L17*, (E) *npq1*, and (F) *szl1*. For each individual leaf, measurements were taken with 30 s resolution. A 1st order Butterworth filter was applied to smooth data sets collected with 0 s and 15 s phase offsets. Data are presented as average with SE represented by shaded regions (for most genotypes, SE was less than the symbol size). The number of independent leaf samples measured for each genotype is the same as presented in Figure 4-2. WT dataset #2 was used for all analysis presented in the main text.

The mean snapshot traces for each mutant (Figure 4-1) show the expected response pattern to the repeated cycles of high light (HL) and dark exposure. During HL exposure, the lifetime rapidly decreases due to nonphotochemical quenching of the Chl singlet excited state. During subsequent dark exposure, the fluorescence lifetime recovers partially, but does not fully return the original dark-adapted lifetime. After a few HL-dark cycles, the lifetimes during HL saturate due to maximum quenching, followed a few periods later by the saturation of the maximum recovery lifetimes during dark relaxation. By the end of the ten cycles, dynamics reach a quasi-periodic steady state, with only small variations between periods. This type of oscillatory behavior is common in electronic circuits and in signal processing, where the smooth curves that describe time dependent extrema or amplitudes of an oscillatory signal are referred to as "envelopes."

Different mutants exhibit different average fluorescence lifetimes in the dark (Figure 4-1), making it difficult to directly compare the genotypes. However, calculating NPQ_τ, an observable defined analogously to the conventional NPQ parameter[1,10,48,53,54] (see Results section for NPQ_τ equation) enables direct comparison of the dynamics of photoprotection in WT and the various mutants (Figure 4-2).

At the time of initial data collection WT plants were measured alongside the *L17*, *szl1*, and *npq4* mutants. Several months later, a second set of WT plants were measured alongside the *npq1* mutant. This second set of WT yielded greater oscillations in the average Chl fluorescence lifetime as a function of HL and dark (Figure 4-1B). In order to directly compare all mutants on the same NPQ_τ scale (Figure 4-2), we normalized the NPQ_τ values of the second set of WT plants to match the NPQ data for the first set of WT plants. Based on this scaling factor we also normalized the NPQ_τ values for *npq1*. This approach of scaling NPQ_τ values is reasonable because it does not impact the kinetics/dynamics (i.e., the τ value in the exponential fit) which is the main focus of the present study. Additionally, by scaling the second set of WT plants we obtained reasonable agreement with literature values for the magnitude of NPQ.

4.3.5 HPLC Sample Preparation and Analysis

Plants were grown as specified above. At 6 weeks of age, leaves were detached from dark-adapted plants, placed on wet paper towels and immediately exposed to the ten cycles of 2 min high light followed by 2 min dark. The high-light illumination at 740 µE or 1500 µE was provided by a JBeamBio LED panel with cool white LEDs (BXRA-56C1100-B-00). For each specified time point (every minute for 0-8 min and every other minute from 8-40 min), a leaf was removed, a 50 mm^2 leaf disc was cut and immediately flash-frozen with liquid nitrogen and stored at 77 K until analysis. Frozen leaf discs were broken using a MP Bio-sciences MP-24 bead beater (6.5 m/s, 30 s). 250 µL of 80% (v/v) acetone was added to the leaf debris before centrifugation at 14,000 rpm (Eppendorf 5430 R) for 5 min at 4 °C. The supernatant was filtered through a Durapore PVDF 0.22 µm filter. Pigments were determined by high performance liquid chromatography (HPLC; 100 HPLC, Agilent) as previously described[55] and reported as mmol pigment/mol Chl.

4.4 Results and Empirical Fitting

4.4.1 Overview of the NPQ response during fluctuating light

Fluorescence lifetime snapshot measurements were collected at 15 s resolution on intact leaves from the five *A. thaliana* strains listed in Table 4-1. Detailed descriptions of the fluorescence lifetime data accumulation, combination of different time offsets, and filtering to eliminate the leaf-to-leaf variability within a single strain are given in Section 4.3.4 (see "Analysis of Fluorescence Lifetime Snapshot Traces"). Fluorescence lifetime determinations of NPQ have a number of advantages over the more standard pulse amplitude modulated (PAM) fluorescence method,[31] as discussed in the Introduction. To convert the measured average fluorescence decay lifetimes to a unitless form similar to the NPQ value obtained from PAM measurements, we define $NPQ_\tau(t) = \frac{\tau_{\mathrm{dark}}(t=0)-\tau_{\mathrm{light}}(t)}{\tau_{\mathrm{light}}(t)}$,[31,42,54,56] where τ is the amplitude-weighted average lifetime from a biexponential fit. NPQ_τ also enables direct comparison of different mutants that have slightly different dark-state lifetimes.

Figure 4-2 shows the values of NPQ_τ for each strain over 10 light–dark cycles. During high light (HL, 700 µmol photons m^{-2} s^{-1}), the quenching rapidly increases as the NPQ components turn on. During subsequent exposure to darkness, the quenching drops but the fluorescence lifetime does not fully return to the original dark-acclimated value (Figure 4-1). After a few HL–dark cycles, the lifetimes saturate at the maximum quenching value, followed a few cycles later by the saturation of the maximum recovery values. By the end of the 10 cycles, the dynamics have reached a periodic steady state, with only small variations between periods. In electronic circuits and in signal processing, the smooth curves that describe the time-dependent extrema are called "envelopes" and we will use this term.

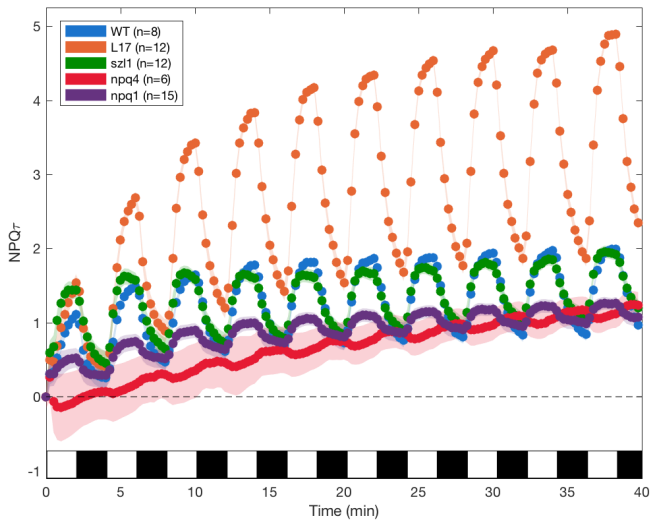

Figure 4-2. Comparison of NPQ_τ traces for each strain: WT (blue), *L17* (orange), *szl1* (green), *npq4* (red), and *npq1* (purple). The PsbS-containing lines (WT, *L17*, *szl1*, and *npq1*) show oscillatory quenching induction and relaxation within each period. The PsbS-deficient mutant *npq4* does not show the strong oscillatory behavior and the Zea-deficient mutant *npq1* shows a dampened oscillatory behavior. Data are presented as the mean NPQ_τ value and the shaded regions represent the standard error. The number of independent leaf samples measured for each genotype is indicated in the legend.

All of the PsbS-containing lines (WT, *szl1*, *L17*, and *npq1*) show significant intraperiod responses, in agreement with previous conclusions about the role of PsbS in rapidly reversible quenching.[3,11,59,60,35–37,41,42,52,57,58] Compared to WT (blue trace in Figure 4-2), *L17* (PsbS overexpressor, orange trace) has an increased amplitude of rapidly reversible quenching and recovery, while *npq4* (inactive PsbS, red trace) almost entirely lacks rapidly reversible NPQ, both of which agree with previous observations.[35,37,52,57] Under HL, VDE is active and Zea reaches near maximal accumulation in the first few periods, unable to return to antheraxanthin or violaxanthin in the short (2 min) dark relaxation time as revealed by previous high-performance liquid chromatography measurements.[42,53] Therefore, in later periods the interperiod dynamics should be attributable to slowly reversible or irreversible quenching processes rather than changes in the carotenoid (i.e., Zea) pool or the presence/activity of PsbS.

The *npq1* mutant (lacks Zea, purple trace) still shows oscillations in NPQ, but the magnitude is greatly dampened relative to WT. Interestingly, *szl1* (excess Lut, green trace) displays quenching behavior qualitatively very similar to WT, despite its inability to accumulate detectable levels of Zea. These findings are consistent with previous suggestions that Lut is capable of quenching Chl excited states in the absence of Zea,[44,45,61] though with a lower efficiency on a per-molecule basis.[53]

4.4.2 Interperiod and Intraperiod Dynamics

Analysis of inter- and intraperiod dynamics allows for the separation of fast and slow quenching processes that depend on common biochemical regulators, such as the PsbS protein and various carotenoids. The quenching dynamics during the first few HL–dark cycles depend on the simultaneous action of fast- and slow-timescale processes, making it difficult to interpret them separately. However, during the later HL–dark cycles, the observed intraperiod oscillations in NPQτ arise entirely from the magnitude and timescales of the rapidly reversible response because the moderate-to-long timescale responses have reached a steady state in terms of activation and relaxation. Thus, periodic illumination experiments allow for the rapid response that appears within single periods (intraperiod) to be distinguished from the moderate-timescale response that appears in period-to-period (interperiod) comparisons without requiring a direct comparison of different mutant lines. We note that the rapidly reversible response can be considered as analogous to the traditional quenching component qE, while the moderate-timescale response can be considered as analogous to slower quenching components (e.g., qZ and qI). Framing the processes as temporal "responses" instead of biochemically regulated "components" allows us to separate the temporal overlap of the effects usually attributed to traditional components (qE, qZ, qI, etc.).

Figure 4-3 shows interperiod envelope traces of the maximum quenching NPQ_τ values and maximum recovery NPQ_τ values. To estimate the timescale and extent of the slowly varying interperiod behavior, both the upper and lower envelopes were fit to simple exponential decays. Although multiple biochemical processes occur with different timescales, such as the accumulation of Zea and longer-timescale protein and membrane structural reorganizations, only a single time constant was resolvable in the envelopes. Fit values are provided in Table 4-2.

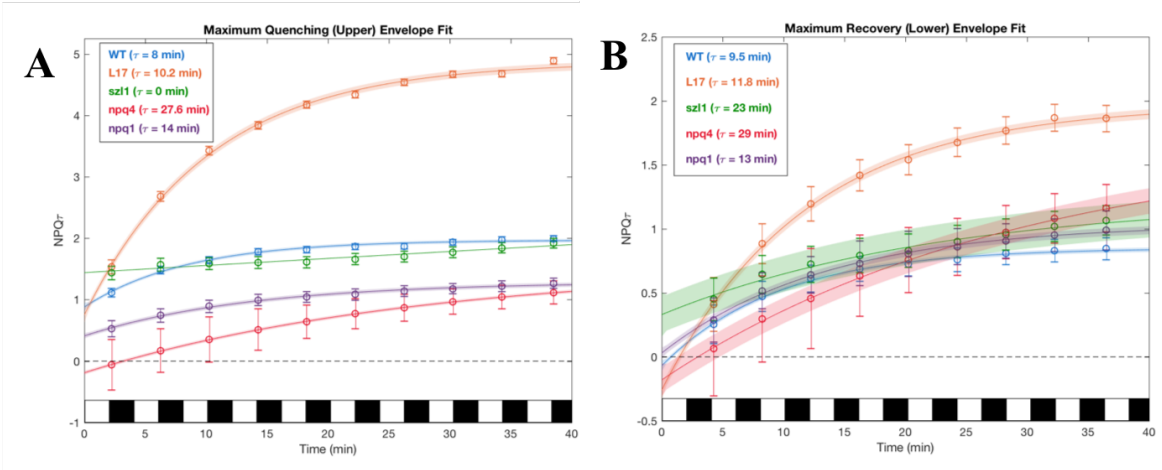

Figure 4-3. Slow interperiod dynamics of (A) maximum quenching envelope and (B) maximum recovery envelope. Open circles represent NPQ_τ trace values from Figure 4-2 selected at (A) the light-to-dark transition and (B) the dark-to-light transition and the error bars represent the standard error in NPQ_τ. The solid line represents the best fit to a single exponential decay and the shaded regions represent the standard error in the fit. The shaded error region is omitted for the *szl1* maximum quenching envelope due to the poor quality of the exponential fit (time constant significantly longer than the timescale of the experiment). The lifetimes (τ) obtained from fitting are listed in the legend and all fit values with errors are presented in Table 4-2.

Table 4-2. Fit Values for Maximum Quenching and Recovery Envelopes:

(A) Maximum Quenching Fit Values: $NPQ_\tau^{max}(t) = a\, e^{-t/\tau} + c$

Max Quenching Fits	*a*	τ (min)	*c*
WT	-1.09 ± 0.06	8 ± 1	1.97 ± 0.03
L17	-4.1 ± 0.1	10.2 ± 0.7	4.87 ± 0.06
szl1	---	---	---
npq4	-1.73 ± 0.02	27.6 ± 0.8	1.54 ± 0.03
npq1	-0.88 ± 0.03	14 ± 2	1.29 ± 0.03

(B) Maximum Recovery Envelope Fit Values: $NPQ_\tau^{min}(t) = a\, e^{-t/\tau} + c$

Max Recovery Fits	*a*	τ (min)	*c*
WT	-0.92 ± 0.04	9.5 ± 0.9	0.85 ± 0.02
L17	-2.23 ± 0.06	11.8 ± 0.8	1.97 ± 0.04
szl1	-0.9 ± 0.1	23 ± 8	1.2 ± 0.1
npq4	-1.88 ± 0.08	29 ± 3	1.7 ± 0.1
npq1	-1.01 ± 0.03	13 ± 1	1.04 ± 0.03

Values for exponential fits of the moderate-to-long timescale envelope dynamics for (A) the maximum quenching (upper) envelope fit obtained from selection of trace values at the light-to-dark transition and (B) the maximum recovery (lower) envelope fit obtained from selection of trace values at the dark-to-light transition. Note that no maximum quenching exponential lifetime component was observed for *szl1* within the timescale of the experiment; instead the maximum quenching envelope increased constantly. Fit values reported are the mean and error is the standard error of the fit reported to one significant digit. Parameters *a* and *c* are unitless values of NPQ_τ and τ is reported in minutes.

The maximum induction timescale fit of zero for *szl1* suggests there are no interperiod quenching dynamics present at this temporal resolution; the level is constant or already at a "steady state". In contrast, WT shows an 8 min timescale to achieve maximum quenching, similar to the timescale for the accumulation of Zea in various plants.[42,53,56] There is excess Lut but no Zea accumulation in *szl1*, while WT possesses Lut and accumulates Zea in HL until a steady state is reached within

a few periods. The differences between WT and the *szl1* mutant therefore suggest that the maximum quenching induction depends on both Zea and Lut accumulation. This could explain the faster initial induction of quenching in *szl1* compared to WT, as was previously observed for measurements during one or two HL–dark cycles.[45,53] The even slower induction behavior for *npq1* (slower timescale of 14 min) further reinforces this dependence of NPQ on de-epoxidized carotenoids given that *npq1* entirely lacks Zea, but possesses Lut.[45,48,49]

As mentioned above, the *npq4* mutant (deficient in PsbS) displays very little rapidly reversible quenching. However, it still shows a slow increase (timescale of 27.6 min) in the maximum quenching over successive periods. This moderate-timescale quenching that occurs in the absence of PsbS appears to be distinct from the role that PsbS plays in photoinhibitory quenching (qI) under prolonged (>hour) HL illumination.[27,37,57,62]

Beyond *szl1* and *npq4*, all other mutants exhibit similar timescales of maximum interperiod quenching and recovery as WT, although *npq1* is slightly slower with a 14 min induction timescale (Figure 4-3 and Table 4-2).

The rapid steady-state intraperiod dynamics are presented in Figure 4-4 with fit parameters listed in Table 4-3. These data come from fits of the penultimate HL–dark cycle in Figure 4-2 and represent a quasi-periodic steady-state as the intraperiod timescales (time constants) were observed to remain unchanged after the third or fourth HL–dark cycle (Figure 4-5). Once the steady state has been reached, intraperiod HL quenching induction is consistently faster than the dark recovery with timescales of 30–50 and 60–90 s (Table 4-3), which may reflect the kinetics of ΔpH buildup and relaxation, respectively. Additionally, the intraperiod timescales are more or less the same for the different genotypes, suggesting that differences in the carotenoid composition or PsbS activity modulate the amplitude of rapidly reversible quenching but not the inherent timescales or kinetics. An exception is the intraperiod recovery in *npq1*, which is significantly faster at 34 s.

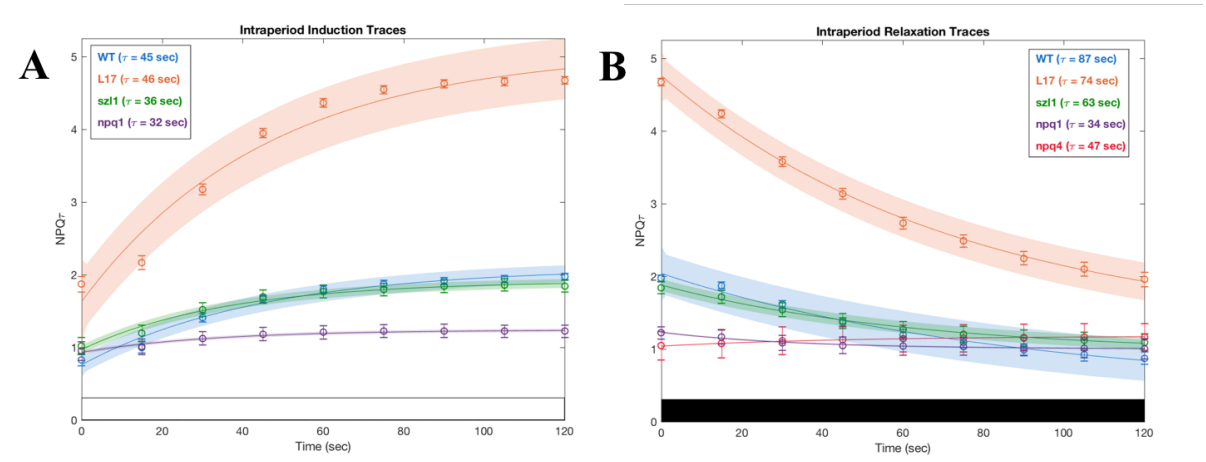

Figure 4-4. Rapidly reversible intraperiod dynamics of (A) high-light quenching induction and (B) dark relaxation. Data are presented as the NPQ_τ values (open circles) and error bars represent the standard error from the penultimate light and dark cycles presented in Figure 4-2 to ensure that a steady state has been reached. Solid lines represent the best fit to a single exponential decay and shaded regions indicate the standard error in the fit. The lifetimes (τ) obtained from fitting are listed in the legend and all fit values with errors are presented in Table 4-3.

Table 4-3. Rapidly Reversible Quenching Fit Values:

(A) Induction Fit Values: $NPQ_\tau(t) = a\, e^{-t/\tau} + c$

Induction Fits	*a*	τ (sec)	*c*
WT	-1.3 ± 0.1	45 ± 11	2.1 ± 0.1
L17	-3.5 ± 0.4	46 ± 15	5.1 ± 0.4
szl1	-0.94 ± 0.07	36 ± 8	1.91 ± 0.06
npq1	-0.31 ± 0.03	32 ± 8	1.24 ± 0.02

(B) Relaxation Fit Values: $NPQ_\tau(t) = a\, e^{-t/\tau} + c$

Relaxation Fits	*a*	τ (sec)	*c*
WT	1.6 ± 0.3	87 ± 28	0.4 ± 0.3
L17	3.5 ± 0.2	74 ± 11	1.2 ± 0.3
szl1	0.94 ± 0.07	63 ± 12	0.94 ± 0.08
npq1	0.23 ± 0.02	34 ± 7	1.00 ± 0.01
Npq4	-0.14 ± 0.01	47 ± 6	1.18 ± 0.01

Exponential fit values for quasi-periodic steady-state rapidly reversible (A) high-light induction and (B) dark recovery. Fit values reported are the mean and error is the standard error of the fit reported to one significant digit. Parameters *a* and *c* are unitless values of NPQ_τ and τ is reported in seconds.

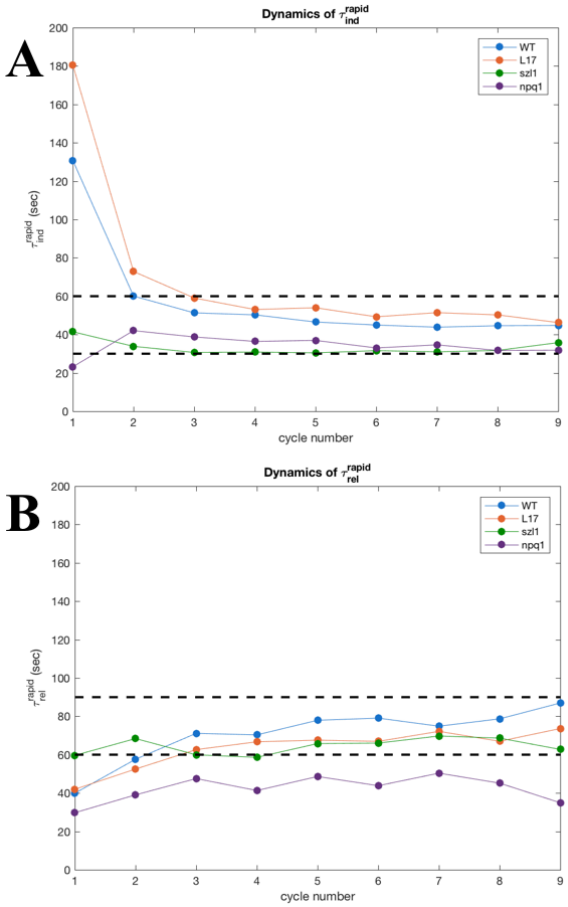

Figure 4-5. Comparison of the intra-period time constant as a function of HL-dark cycle number for (A) quenching induction during HL and (B) quenching relaxation during dark. The timescale of both the rapidly-reversible quenching and recovery reaches steady-state by the third cycle (indicated by dashed black lines) and exhibits minimal differences between different mutants. Note that the mathematical model makes use of the intra-period time constant from the penultimate period (cycle #9).

4.4.3 Mathematical Model of Multi-timescale Regulatory Processes

To draw additional conclusions regarding the various known molecular actors in NPQ and their timescales of quenching induction and recovery, we constructed a mathematical model that includes the simultaneous actions of rapidly reversible and more slowly varying regulatory processes. Before describing the detailed mathematical structure of the model, we will highlight some general characteristics that the model must satisfy to capture the experimentally observed oscillatory quenching behavior of intact leaves. The model should:

1. Capture amplitude changes within periods without altering the empirically determined timescales.
2. Retain memory of previous cycles to describe slow envelopes of the maximum quenching and recovery.
3. Allow NPQ to turn on and off with rates that vary as a function of the illumination history.
4. Be agnostic about specific quenching mechanisms with all of the input parameters for the model determined directly from the experiment.
5. Be flexible enough to describe WT and all PsbS-containing mutants studied in this work.

The quenching giving rise to NPQ is thought to occur mainly within the light-harvesting complex proteins associated with PSII (LHCII),[11,59,63–65] though LHCII is not necessarily the only site.[64,66,67] Additionally, the quenching is likely the combined result of processes occurring on varying timescales, such as the relatively slow accumulation of Zea/Lut[14,38,68,69] and/or membrane reorganization events[70–72] as well as more rapid conformational changes within individual pigment–protein complexes.[73–75] Therefore, our model treats slower regulatory processes as constraints on the result of the rapidly reversible regulation of quenching to incorporate the combined effects of the multiple timescales. Including interactions between the various regulatory responses is a key difference from a model where the traditional quenching components (e.g., qE, qZ, and qI) arise from separate photochemical mechanisms and independent regulatory schemes.[58,76] Our model is thus able to relate the multiple experimentally observed timescale responses to an overall extent of quenching (as opposed to biochemical observables) to draw conclusions about how the multiple regulatory responses combine to result in the overall quenching regulation on the seconds-to-minutes timescales.

A diagram of the regulatory model along with a table of the eight specific input parameters is shown in Figure 4-6, and the detailed equations for the model are presented in an Appendix (Section 4.7). The model is based on the following differential equation

$$\frac{dq^{active}}{dt} = -[k_1(t) + k_2(t)]q^{active} + k_2(t)$$

which has a biexponential solution within each time period. q^{active} is the modeled variable that represents the trajectory of NPQ_τ and $k_1(t)$ and $k_2(t)$ are rate terms that describe the kinetics of turning NPQ off and on, respectively. These rates are piecewise defined to track whether the light is on or off at any given time during the experiment. Additionally, the rate terms are influenced by both the constant rates of induction or relaxation of the rapidly reversible quenching within a single period as well as the time-dependent state of the maximum quenching and maximum recovery

envelopes. Therefore $k_1(t)$ and $k_2(t)$ (Equations 2 to 3 in the Appendix) incorporate multi-timescale regulatory behavior through contributions from both rapid intraperiod processes ($k^{rapid}(t)$ terms as defined in Equations 4 to 5 in the Appendix) and gradual interperiod processes ($k^{envelope}$ terms as defined in Equations 6–9 in the Appendix).

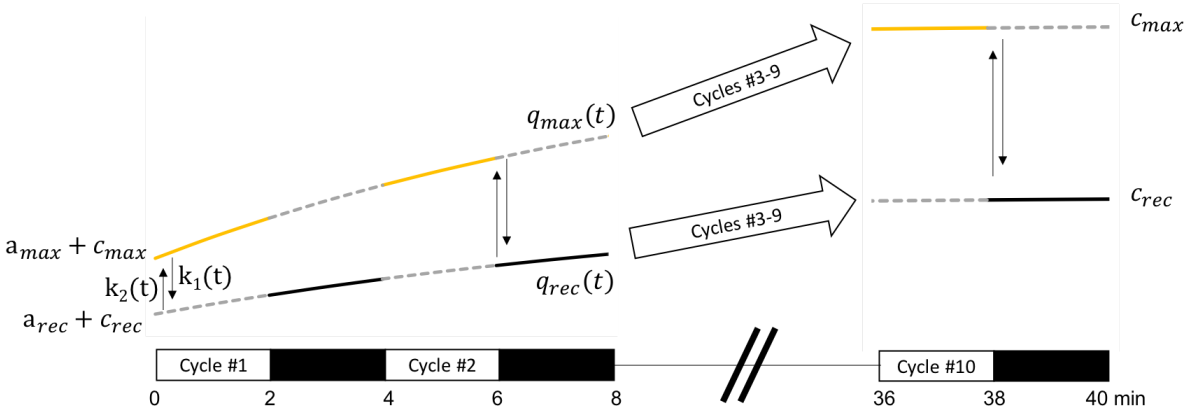

Input parameters for the model:

	Inter-period HL	Inter-period Dark	Intra-period HL	Intra-period Dark
Amplitude	a_{max}	a_{rec}	-	-
Kinetics	τ_{max}^{env}	τ_{rec}^{env}	τ_{ind}^{rapid}	τ_{rel}^{rapid}
Steady State	c_{max}	c_{rec}	-	-

Figure 4-6. Diagrammatic Representation of the Mathematical Model Describing the Regulation of Quenching. Quenching is modeled by q^{active} whose trajectory is governed by two piecewise time-dependent rate constants, $k_1(t)$ and $k_2(t)$. The observed macroscopic quenching moves within the region between the maximum quenching ($q_{max}(t)$, yellow) and maximum recovery states ($q_{rec}(t)$, black), whose values are determined from empirical interperiod fit parameters (bottom table). The values for each of these eight parameters are determined from direct exponential fits to the experimental data for each genotype. The interperiod and intraperiod dynamics are fit to the same mathematical construction (a single exponential of the form $q = a\,e^{-t/\tau} + c$). Interperiod HL and dark values for a, τ^{env}, and c in addition to intraperiod HL and dark kinetics (τ^{rapid}) are the only inputs to the model.

As described in Figure 4-6, there are 8 input parameters for each genotype, all of which come from fits to the experimental data. Of the 8 parameters, 4 describe the induction of quenching during HL and 4 describe the relaxation of quenching during the dark. Within the slowly-varying quenching and recovery envelope systems, a_{max} and a_{rec} represent the amplitudes, τ_{max}^{env} and τ_{rec}^{env} represent the exponential time constants describing the kinetics, and c_{max} and c_{rec} represent the steady-state values for the envelope. The remaining 2 parameters, τ_{ind}^{rapid} and τ_{rel}^{rapid}, describe the kinetics of the intra-period response at steady state (cycle 9).

Specifically, $k^{rapid}(t)$ contains the rapid intraperiod kinetics through τ_{ind}^{rapid} or τ_{rel}^{rapid} and the time-dependence arises from the slowly varying value of $q_{max}(t)$ or $q_{rec}(t)$ (Equations 4 and 5 in the Appendix). Here, τ_{ind}^{rapid} and τ_{rel}^{rapid} are the constant best fit values of the time constants for the induction and relaxation of rapidly reversible quenching upon the envelopes reaching steady state in the final periods of the experimental data, as shown in Figure 4-4A,B and Table 4-3. $q_{max}(t)$

and $q_{rec}(t)$ represent the time-dependent values of the maximum quenching and recovery envelope systems, respectively.

For both quenching and recovery, $k^{envelope}$ is parametrized entirely based on τ_{max}^{env} or τ_{rec}^{env}, and c_{max} or c_{rec} (Equations 6–9 in the Appendix). τ_{max}^{env} and τ_{rec}^{env} are the best fit time constants from exponential fits of the maximum quenching and recovery envelopes, respectively, obtained as previously described and shown in Figure 4-3A,B and Table 4-2. Similarly, c_{max} and c_{rec} are the best fit additive constants, representing steady-state values of NPQ, obtained from the corresponding exponential fits of the envelopes. In our model construction, $k^{envelope}$ is assumed to be constant on the timescale of the experiment, which is reasonable given that the state of the maximum quenching and maximum recovery envelopes varies slowly relative to the rapid induction or relaxation within periods.

It is important to note that both of the rate values $k_1(t)$ and $k_2(t)$ must change as a function of the HL–dark cycle number throughout the overall experimental time, instead of a simpler formulation where only a single rate value is modulated by the light or darkness. This is necessary to achieve a simultaneous agreement between the experimental data and the model (Figure 4-7). This is because the ratio of the rate constants (i.e., k_1/k_2) in the differential equation system determines the steady-state value (the maximum quenching or maximum recovery within a period). For a fixed recovery rate constant, either the induction rate or the resulting steady-state values can be accurately reproduced, but not both simultaneously.

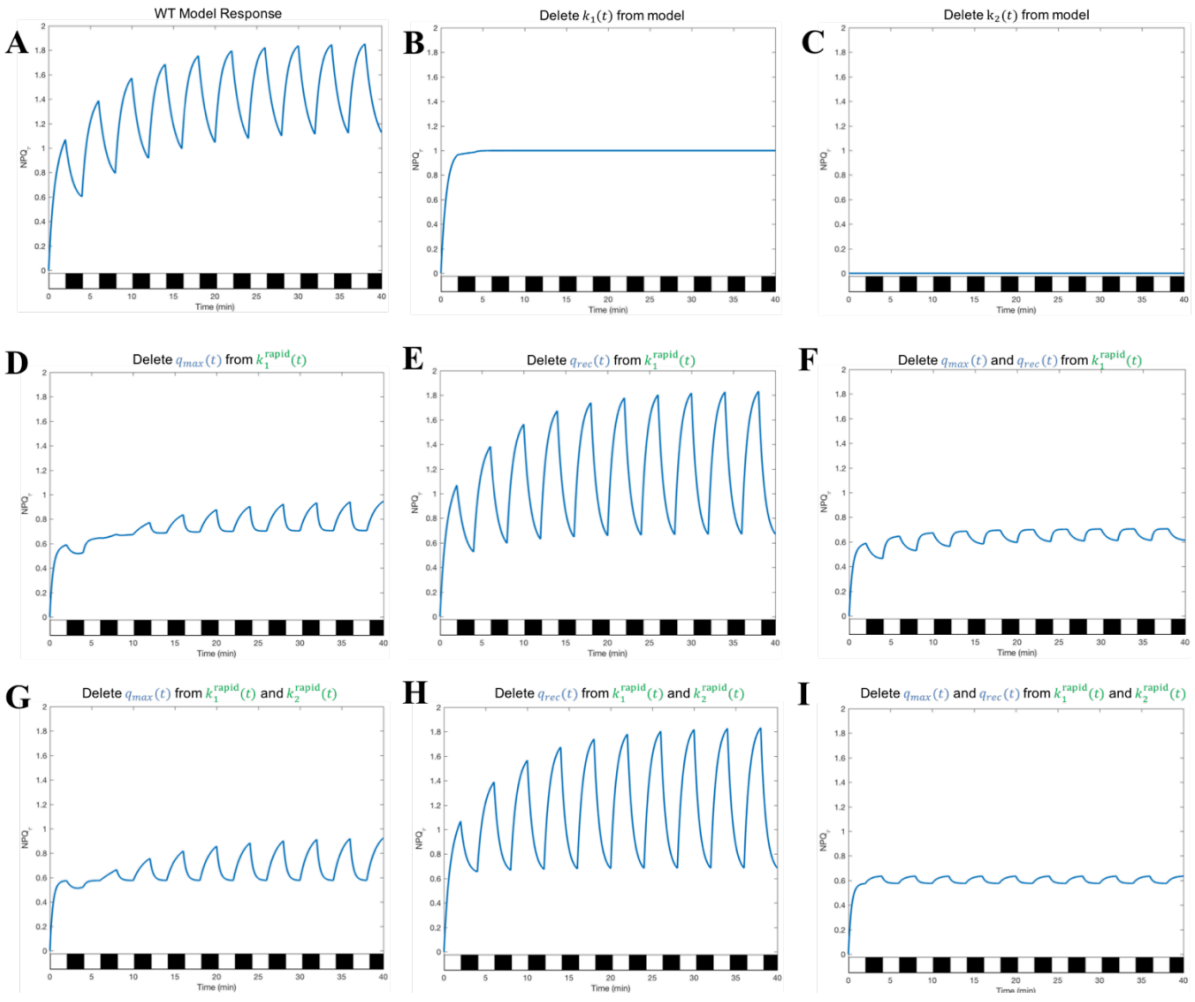

Figure 4-7. Effect of removing the time-dependent slowly-varying envelope components from the rapidly-reversible rate constants in model equations 4 and 5. For comparison, (A) shows the normal WT response. (B) Omitting $k_1(t)$ results in quenching turning on, but not turning off. (C) Omitting $k_2(t)$ results in no quenching. Removing (D,G) q_{max}, (E,H) q_{rec}, or (F,I) both q_{max} and q_{rec} significantly changes the modeled NPQ_τ dynamics, resulting in noticeable discrepancies compared to the WT experimental results, especially in terms of the evolution of the recovery envelope as the measurement sequence progresses.

With all the model parameters predetermined from direct fits of the data, the differential equation (Equation 1 in the Appendix) is solved numerically without subsequent fitting to obtain the model traces presented in Figure 4-8 for each mutant. The model satisfies the requirements previously mentioned, allowing it to describe the observed behavior of oscillatory quenching and recovery during HL and dark periods constrained by multiperiod envelopes with reasonable (but not perfect) accuracy. For example, while the model and experiment agree well for *szl1* (Figure 4-8B) and *npq1* (Figure 4-8C), the model's predicted NPQ dynamics deviate from the experimental values for WT (Figure 4-8A) and *L17* (Figure 4-8D), especially during early HL–dark cycles. Specifically, while the model successfully captures the induction of quenching during all HL periods (Table 4-4), the modeled traces for WT and *L17* do not capture the full relaxation of quenching during the early dark periods (Table 4-5). Yet the difference between the model and experiment, which is largest for the *L17* mutant at ~0.5 a unit of NPQ_τ (Figure 4-8D), still only corresponds to a relative error of 27% by the end of the ninth cycle, while most other strains have

relative errors of 5% or less (Table 4-5). The difficulty of describing the *L17* trajectory using the model is not surprising given this mutant's larger dynamical range of oscillations in NPQ as a result of excess PsbS.

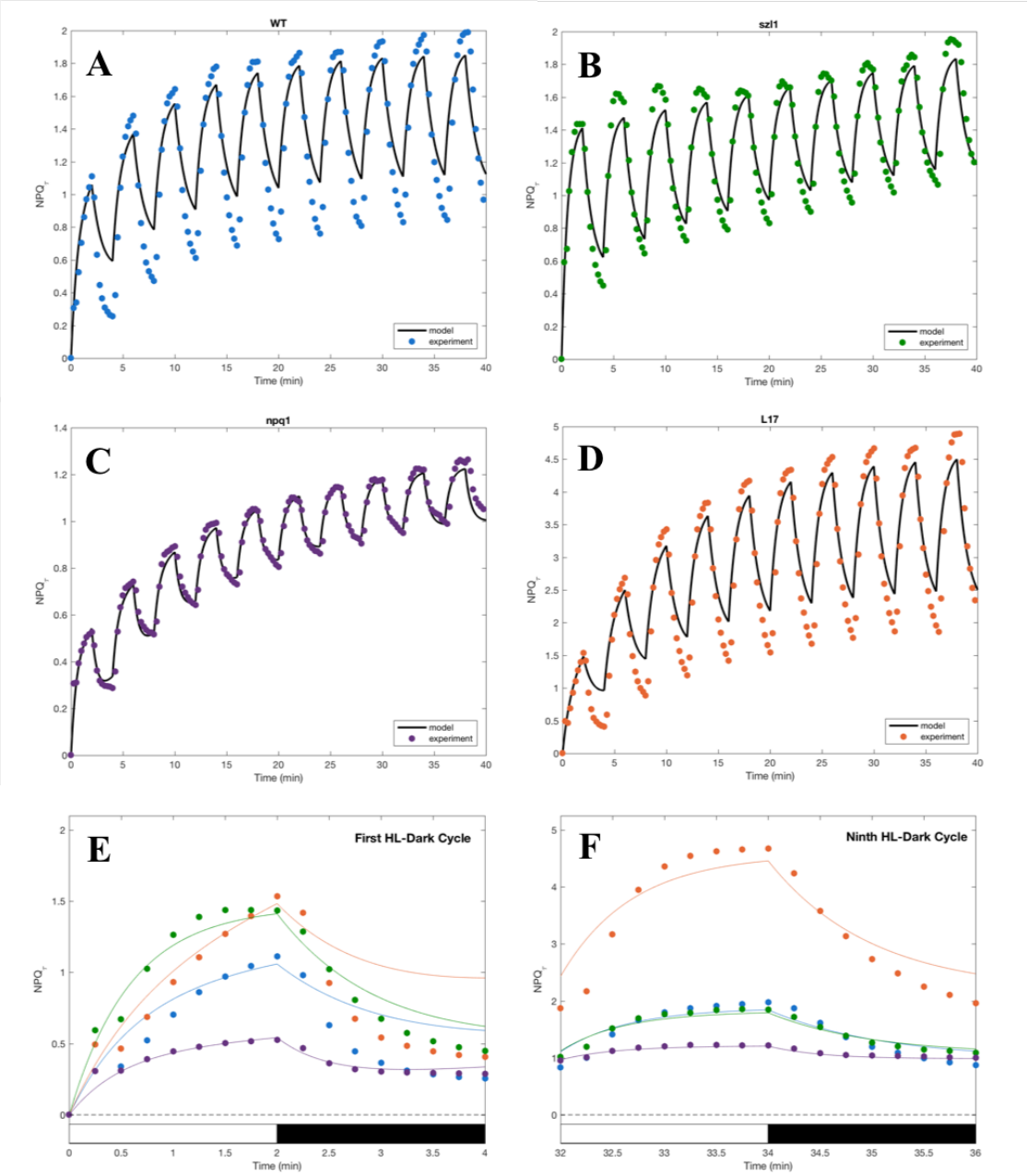

Figure 4-8. Comparison of modeled (solid lines) and experimental NPQτ values (closed circles) for all PsbS-containing lines: (A) WT (blue), (B) *szl1* (green), (C) *npq1* (purple), and (D) *L17* (orange). The first (E) and penultimate HL–dark cycles (F) are also shown for all strains. At the beginning of illumination (first HL–dark cycle), the model accurately captures the induction of quenching but does not fully capture the relaxation. The agreement is better for *npq1* that shows low magnitude oscillations as well as *szl1*, both of which lack Zea. By the end of the experiment (ninth HL–dark cycle), agreement between the model and experiment is improved, successfully capturing the induction and recovery dynamics. All model parameters are determined from best fit values of exponential decay fits of the maximum quenching and maximum recovery interperiod envelopes and the induction and relaxation of rapidly reversible intraperiod quenching reaching the quasi-periodic steady state. The simple model accurately depicts the nature of rapidly reversible quenching induction and relaxation occurring simultaneously with, and intertwined to, slower timescale quenching processes.

Table 4-4. Comparison of model and experiment after the first and penultimate high light periods. The error for each period represents the absolute value of the difference between model and experimental trajectories at the given time. All values are in units of NPQ_τ except relative error (unitless) which is calculated as (Error/Experiment)*100.

Strain	End of Light Period 1 (t = 2 min)				End of Light Period 9 (t = 34 min)			
	Model Output	Experiment Value	Error	Relative Error	Model Output	Experiment Value	Error	Relative Error
WT	1.06	1.11	0.05	5%	1.84	1.94	0.10	5%
L17	1.48	1.54	0.06	4%	4.46	4.66	0.20	4%
szl1	1.42	1.44	0.02	1%	1.79	1.86	0.07	4%
npq1	0.54	0.53	0.01	2%	1.21	1.22	0.01	1%

Table 4-5. Comparison of model and experiment after the first and penultimate dark periods. The error for each period represents the absolute value of the difference between model and experimental trajectories at the given time. All values are in units of NPQ_τ except relative error (unitless) which is calculated as (Error/Experiment)*100.

Strain	End of Dark Period 1 (t = 4 min)				End of Dark Period 9 (t = 36 min)			
	Model Output	Experiment Value	Error	Relative Error	Model Output	Experiment Value	Error	Relative Error
WT	0.59	0.26	0.33	127%	1.12	0.92	0.20	22%
L17	0.96	0.41	0.55	134%	2.48	1.96	0.52	27%
szl1	0.62	0.45	0.17	38%	1.16	1.12	0.04	4%
npq1	0.34	0.29	0.05	17%	0.99	1.01	0.02	2%

As alluded to earlier, perfect correspondence between the calculated and experimental values for NPQ_τ is not expected from a model that incorporates only minimal empirical kinetic data. As shown in Figure 4-6, only eight empirical parameters are built into the structure of the model; six of these describe the interperiod maximum quenching and recovery envelopes and the remaining two represent the rates for intraperiod induction and relaxation. Therefore, the fidelity of the model in describing the experiment relies on our ability to accurately extract these parameters from the exponential fits to the experimental data. In fact, by simply varying a single parameter, such as the intraperiod dark relaxation time constant τ_{rel}^{rapid}, acceptable agreement between the model and experiment can be easily obtained for both WT and *L17* (Figure 4-9).

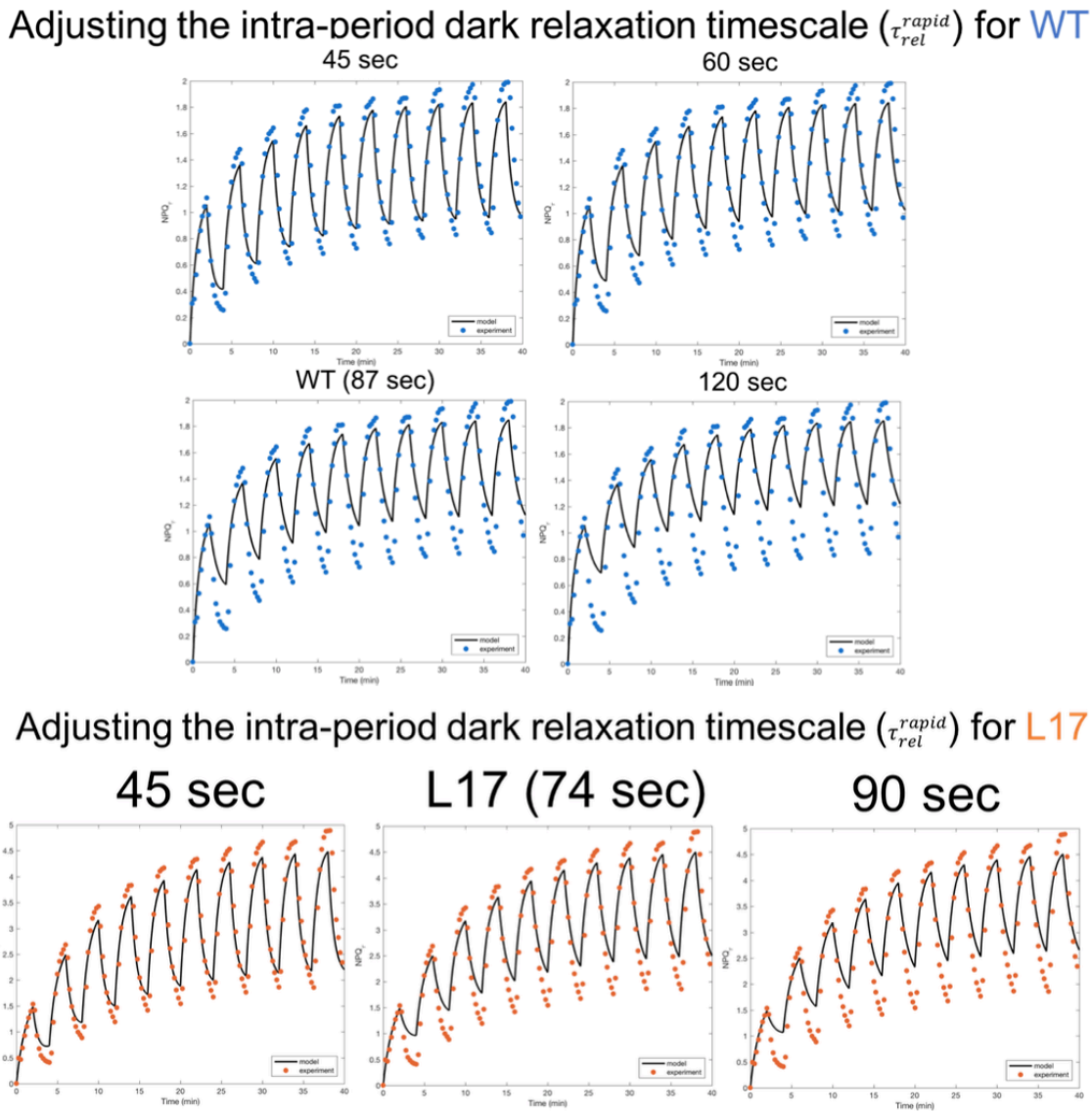

Figure 4-9. Adjusting the intra-period dark relaxation time constant (τ_{rel}^{rapid}) largely removes the discrepancy between model and experiment observed for WT (top panels, *blue*) and *L17* (bottom panels, *orange*). For each panel, the numbers above indicates the value of τ_{rel}^{rapid} used for each computation. As indicated, the experimental values for WT and *L17* were 87 sec and 74 sec, respectively.

In general, the intraperiod induction of quenching is well reproduced during the early periods, while the intraperiod relaxation is not (Figure 4-8E; Tables 4-4 and 4-5). In contrast, during the later periods, both the induction and recovery are well described by our model (Figure 4-8F; Tables 4-4 and 4-5). We postpone for the discussion an analysis of these differences between the early and late periods of HL and darkness because we can draw important insights from them.

Despite the discrepancies between the model and experiment, the mathematical description allows the connection between the rapidly reversible regulation and the slower regulation to be highlighted: the model demonstrates how the initial induction of NPQ depends on both the

induction timescale of rapidly reversible quenching and the slower timescale dynamics of the maximum quenching envelope. In other words, by accurately reproducing the changing magnitude of rapidly reversible quenching over successive HL–dark cycles, the model shows that the rapidly reversible regulation of quenching (qE) is likely intertwined with the status of the slower quenching processes (such as the qZ and qI components).

4.5 Discussion

4.5.1 General Comments

Isolating quenching responses using periodic actinic light exposure reveals the complex, overlapping, and interdependent nature of the various regulatory processes contributing to observed nonphotochemical quenching in *A. thaliana*. For all strains, our data and analysis suggest that the traditional designation of the rapidly reversible component of NPQ, qE, cannot be described independently of the slower NPQ components, such as qZ or qI. The interdependence of fast and slow processes is in contrast to models in which each "timescale" component operates independently. This suggests that the components of quenching likely operate to regulate one or more common photochemical mechanism(s) in different ways, either through modification of the intrinsic quenching rate via rapidly inducible conformational changes within individual pigment–protein complexes or more slowly modulating the effective density of quenchers via chemical substitutions. Large-scale membrane organization changes are likely to further influence the connectivity of quenching sites to other areas of the photosynthetic antenna.

As stated in the methods, the plants are dark-adapted for 30 min before exposure to the periodic light sequence. Thus, during the first HL period both the fast and slow NPQ responses are initiated, which combine to generate the τ^{rapid} observed during the first several cycles. Interestingly, by the third cycle, the observed rapid intraperiod induction and relaxation kinetics have reached a steady state (Figure 4-5), while the slow processes continue to gradually approach full activation. Therefore, after the third cycle, the fast pathway becomes the dominant contributor to the intraperiod kinetics and consequently the observed values for τ^{rapid} appear unaffected by the illumination history.

The timescales of induction and relaxation within a single HL or dark period (Figure 4-4 and Figure 4-5) and over the duration of the 10 HL–dark cycles of our measurement (Figure 4-3) are quite similar for all of the mutants. An interesting exception is the *szl1* mutant that contains large quantities of Lut in the dark[45,53] for which no exponential rise component is detectable for the maximum quenching envelope within the 15 s time resolution of these measurements. Instead, the maximum quenching envelope in *szl1* increased linearly, unlike all the other lines where the maximum NPQ_τ envelope is well described by an exponential rise. This suggests that a relatively rapid conformational change in an individual pigment–protein complex is an initiator of quenching in *szl1*, rather than the slower or more complex membrane reorganization that may be necessary for the other strains. In contrast to the quenching envelope, the recovery envelope for *szl1* follows a similar mathematical form to the other lines, suggesting that *szl1* has a different "turn on" mechanism but a similar "turn off" mechanism compared to the other strains.

The plants reach steady state in quenching and recovery kinetics by cycle 3 (Figure 4-5). At steady state, the rapid intraperiod induction timescales are all similar at 30–50 s (Figure 4-4A and Table 4-3A). The recovery timescales are also similar to each other at 60–90 s (Figure 4-4B and Table 4-3B), though notably slower than induction. An exception is *npq1* which has a faster recovery time of ∼30 s, in agreement with reports in the literature.[61,77]

Although our model was chosen to be agnostic to the underlying biochemical or photophysical mechanisms, by exploring the sensitivity of the modeled quenching magnitude and dynamics to

the input model parameters, we are able to make a number of conclusions from combining the data with the model. By fixing all the other parameters at their wild-type values (see Table 4-6), we explored how changes in a single parameter influence the overall response (Figure 4-10 and Figure 4-11). For example, a_{max} and a_{rec}, representing the amplitudes of the slowly evolving intraperiod envelopes $q_{max}(t)$ and $q_{rec}(t)$, respectively, significantly influence the intraperiod behavior during the first few periods (see Figure 4-11A,B). This suggests that gradual quenching processes may have a direct impact on rapid quenching during the initial exposure to high light. In other words, the initial quenching response and the more gradual changes over multiple minutes should not be simply viewed as independent processes; the amplitude of the rapidly reversible component is intertwined with the state of the slower processes. For a model to reproduce this behavior it must retain this memory between periods since the biochemical systems do not fully relax to the dark-adapted state during the short, 2 min periods of darkness.

We also investigated the effects of modifying the remaining model parameters. Altering τ_{max}^{env} and τ_{rec}^{env}, which represent the slow envelope kinetics, results in changes to both the overall envelope and intra-period dynamics (Figure 4-11C,D). Changing the magnitude of c_{max} and c_{rec} can also influence both envelope and intra-period dynamics (Figure 4-11E,F). Unsurprisingly, oscillations in NPQ can only arise c_{max} does not equal c_{rec}. Finally, modifying τ_{ind}^{rapid} or τ_{rel}^{rapid} results in changes to the intra-period dynamics (Figure 4-11G,H). However, unlike a_{max} which alters only the early intra-period behavior, manipulating τ^{rapid} influences intra-period dynamics during every period.

Next, we briefly discuss the insights on the roles of PsbS, the xanthophylls Zea and Lut, and ΔpH suggested by our data and model before making some final comments regarding potential uses of the model for improving biomass yields.

Table 4-6. Model Parameters and the Approximate Values for the Wild Type

Parameter	HL Max Quenching Value	Dark Recovery Value
a	-1	-1
$\tau = 1/b$	10 min	10 min
c	2	1
k^{-1}	46 sec	85 sec
$q_{max}(t) = a_{max}e^{-t/\tau_{max}} + c_{max}$ $q_{recovery}(t) = a_{rec}e^{-t/\tau_{rec}} + c_{rec}$ $k_{\text{fit}}^{\text{induction}}$ or $k_{\text{fit}}^{\text{relaxation}}$		

For all of the exploratory calculations (presented in Figure 4-10 and Figure 4-11), only one individual parameter is varied and the other seven are fixed to the experimental value for the wild type *A. thaliana*.

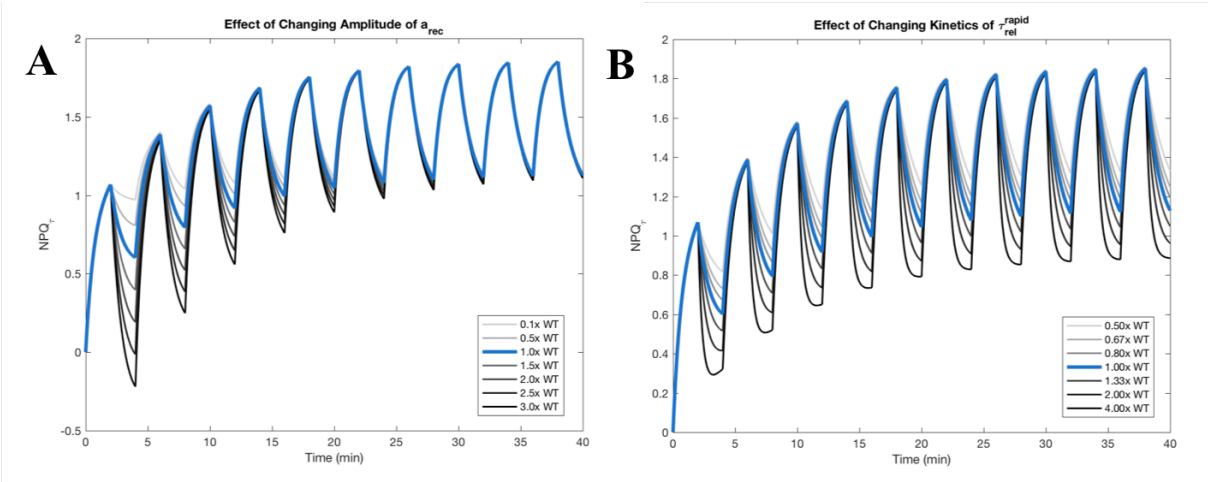

Figure 4-10. Predicted NPQ_t dynamics resulting from varying a single model parameter, while keeping the others fixed to the value of WT (listed in Table 4-6). (A) Influence of a_{max} where the legend specifies the scaled amplitude relative to the wild type. For example, "2.0× WT" means $a_{max} = 2 \times -1 = -2$. (B) Influence of τ_{rel}^{rapid} where the legend specifies the fractional improvement. For example, here, 2.00× WT signifies an acceleration of the kinetics by a factor of 2 relative to the wild type, or $\tau_{rel}^{rapid} = \frac{85}{2} = 43.5\ s$. For comparison, the model result when all eight parameters are set to the experimental value of WT is depicted by the thick blue line. For visual clarity, the white and black bars for the actinic light sequence have been omitted.

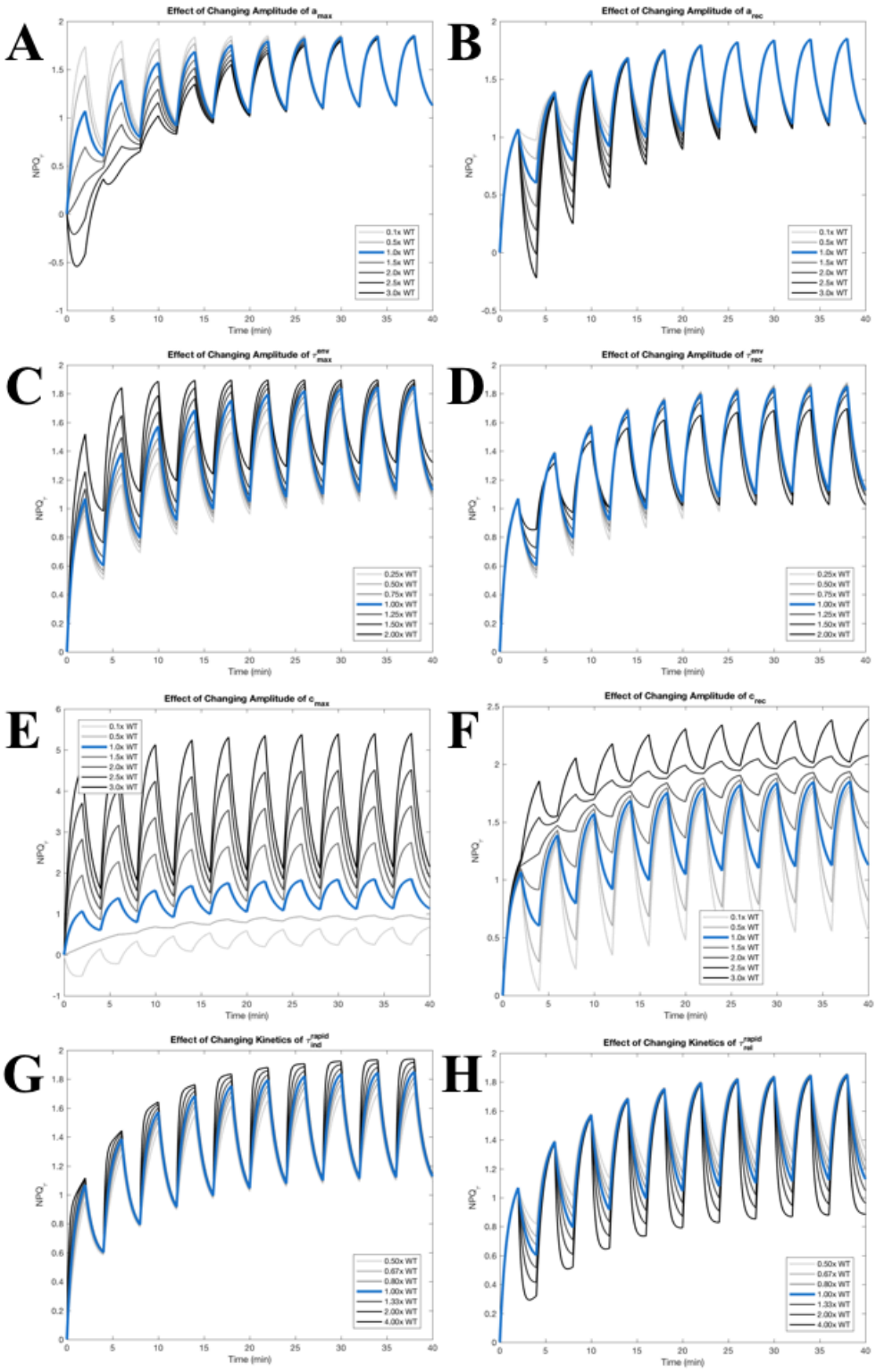

Figure 4-11. Effect of varying each individual model parameter (while keeping the other 7 fixed at the approximate value of WT) on predicted NPQ_τ dynamics under the periodic actinic light sequence. For comparison, the model result when all 8 parameters are set to the experimental value of WT is depicted by the thick blue line. For visual clarity, the white and black bars for the actinic light sequence have been omitted. Note that panels B and H are repeated from Figure 4-10.

4.5.2 Role of PsbS

The role of PsbS in enabling the plant to respond to rapid changes in the light intensity is evident in *npq4* (lacks PsbS), which shows almost no modulation of quenching when cycling between HL and dark conditions (Figure 4-2). Surprisingly, the quenching response of *npq4* was observed to be "out-of-phase" with respect to the HL–dark periods (i.e., NPQ_τ decreased during HL and increased during the dark). This finding, which will be discussed later in the context of the model, bolsters the idea that the pH-sensing protein PsbS is necessary for the normal WT response to both HL and dark conditions.

When considering how PsbS interactions with LHCII might induce quenching, the simplest conceivable mechanism assumes that LHCII naturally favors an unquenched state, and when an interaction with protonated PsbS activated by ΔpH occurs, LHCII is forced into a quenched state.[38,57,59,60,70,73,74,78] When ΔpH relaxes during the dark, the simplest assumption is that the interaction between PsbS and LHCII ceases, and LHCII can relax back to an unquenched state. This corresponds to a model description where only the induction rate (k_2) and not the relaxation rate (k_1) is modulated by the light and dark illumination sequence, but this is unable to reproduce the experimental results (Figure 4-7D-F). Therefore, the model suggests that not only do interactions between protonated PsbS and LHCII induce quenching, but that interactions between PsbS and LHCII might also actively induce recovery of LHCII from quenching, or at the very least that the protein interactions involved are not well described by such a simple kinetic scheme.

The role of PsbS in the relaxation of quenching is further supported by the exponential fits to the *L17* data, which give a larger value for a_{rec} (−2.33) than the wild type (a_{rec} = −0.92). All other mutants (disregarding *npq4*, which largely lacks an oscillatory quenching behavior) have a_{rec} values similar to the wild type. This comparison of *L17* and WT again raises the idea that PsbS may play a significant role in the rapid intraperiod relaxation of quenching during the dark. Assuming a WT structural and biochemical background, our model predicts that a value of a_{rec} = −2.33 would result in almost complete relaxation of NPQ during the first dark period (see the first dark period in Figure 4-10A), with decreasing percentages of full recovery as the steady-state response is reached.

In summary, a reasonable assumption may be that PsbS is involved in generating quenching sites leading to greater overall maximum NPQ values and less recovery (larger NPQ_τ values in the dark). However, we do not rule out that PsbS may also have more subtle or long-term effects, such as changing the membrane morphology or organization.[57,59,60,71]

4.5.3 Roles of Zeaxanthin and Lutein

npq1, lacking Zea, shows substantially reduced modulation of quenching over HL–dark cycles compared to WT or *szl1* (though still greater than *npq4*) despite containing similar levels of PsbS. Unless there is excess Lut (as is the case for *szl1*), Zea is clearly required to obtain maximum quenching, though whether this implies a PsbS–Zea cooperativity or is simply additive is not clear. In the initial transition from the dark-adapted to HL conditions, very little Vio to Zea conversion will occur.[38,69,79] It therefore appears that at least the initial increase in NPQ_τ (the first few data points in each HL period) likely does not require Zea. However, Zea is clearly involved in slower quenching processes as the comparison of maximum quenching envelopes for WT and *szl1* shows, with WT beginning at smaller NPQ_τ max values and then reaching and slightly exceeding the value for *szl1* after three cycles (see Figure 4-3A). This gradual increase of NPQ_τ observed in WT could reflect the replacement of violaxanthin with Zea in LHCII in VDE enzyme-containing plants. *szl1* on the other hand, as noted above, lacks the exponential rise component in the maximum quenching envelope, suggesting that no pigment interchange and only a small conformational change is necessary to switch Lut into a quenching configuration in LHCII.

The picture of common photophysical mechanisms of energy dissipation controlled in different ways and with differing timescales of activation/deactivation could explain how Zea impacts multiple quenching processes: the substitution of Zea may influence an intrinsic rate of quenching or the density of quenching sites for which Zea plays a direct role, as well as influence structural properties of pigment–protein complexes that regulate conformational fluctuations and membrane organization that gradually activate additional or alternate quenching mechanisms.

In order to gain insight into the kinetics of the VAZ cycle carotenoids during fluctuating light, we performed preliminary HPLC analysis for pigments extracted from WT and *npq1* leaves that had been exposed to the periodic actinic light sequence. The *npq1* mutant showed no changes in the concentrations of Vio, Ant, or Zea, as expected based on the lack of violaxanthin de-epoxidase (VDE) activity. As shown in Figure 4-12, dark-adapted leaves of WT showed high levels of Vio and low levels of Zea prior to illumination. Upon exposure to the fluctuating light sequence, Ant rapidly reached a steady state (~2 min), while net conversion from Vio to Zea continued throughout the 40 minute experiment. Interestingly, the timescales associated with Vio consumption and Zea formation, 10 ± 1.4 min and 16.5 ± 6.4 min respectively (Table 4-7), are similar to the 8 ± 2 min timescale of the maximum quenching envelope measured by TCSPC (Table 4-2). This suggests that the de-epoxidation state of the VAZ cycle pool may be related to the maximum capacity for NPQ during fluctuating illumination.

We also investigated the VAZ cycle dynamics at a higher illumination intensity of 1500 μE (Figure 4-12). The timescales associated with Vio and Zea were significantly faster at this higher light intensity (Table 4-7) indicating that the dynamics of the VAZ cycle are extremely sensitive to the illumination intensity. Future experimental and modeling work is needed to ascertain the mechanistic links between the concentrations of the VAZ cycle pigments and the resulting kinetics of NPQ under a range of illumination intensities.

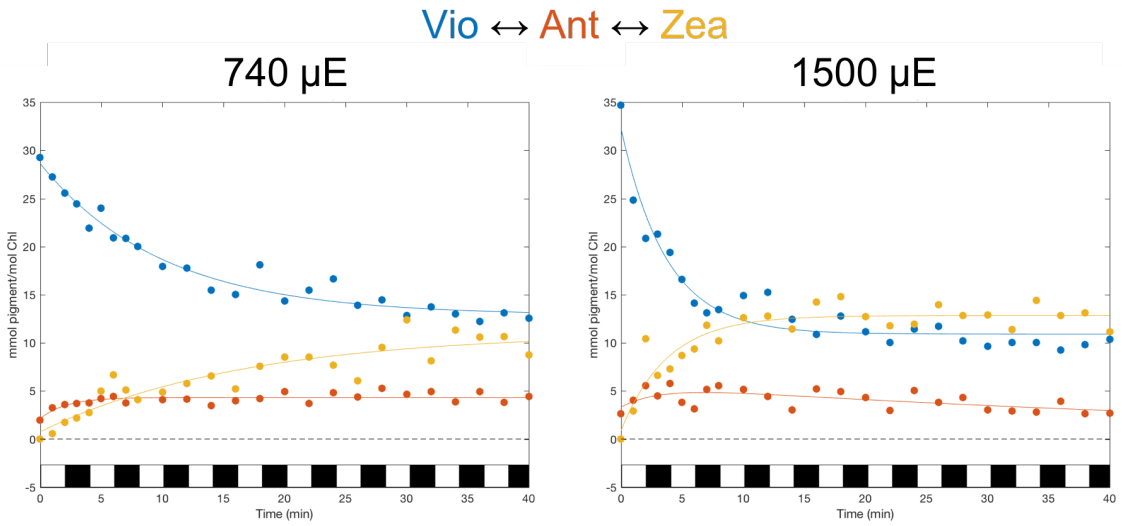

Figure 4-12. HPLC analysis of the kinetics of violaxanthin (Vio, *blue*), antheraxanthin (Ant, *red*), and zeaxanthin (Zea, *yellow*) in leaves of *A. thaliana* exposed to 40 minutes of fluctuating high light-dark with 2 minute periods. The high light intensity was either 740 µE or 1500 µE. Circles represent the average of n = 3-5 replicate measurements at each time point. Solid lines represent exponential fits to the data (time constants are presented in Table 4-7).

Table 4-7. Dynamics of Vio-Ant-Zea cycle obtained from single exponential fits to the HPLC data in Figure 4-12.

	740 µE	1500 µE
Vio	10.0 ± 1.4 min	3.7 ± 1.4 min
Ant	2.2 ± 0.8 min	--
Zea	16.5 ± 6.4 min	3.8 ± 0.8 min

The timescale for Ant is omitted for the 1500 µE sequence because the data fit best to a bi-exponential function including a rapid rise followed by a much slower decay.

4.5.4 Comparisons of Experimental and Modeled NPQ Trajectories

As mentioned above, by comparing the modeled NPQ_τ trajectory with the experimental data points, we are able to gain further insight into how the plant's most immediate response on exposure to HL or darkness depends on the illumination history. This analysis is centered around the fact that the model input for the intraperiod rapid responses comes only from the penultimate (ninth) periods; our model does not include any intraperiod input from the early illumination periods. Nonetheless, our empirically based kinetic model successfully captures the induction of quenching during all 10 HL–dark cycles (Figure 4-8 and Table 4-4). Thus, the steady-state intraperiod induction time constant (τ_{ind}^{rapid}) seems sufficient to describe the plant's immediate response to HL and is independent of the illumination history. Since ΔpH is one of the fastest responses to HL exposure,[13–15,58] this suggests that the kinetics of ΔpH formation may be unaffected by the illumination history.

On the other hand, our model is unable to reproduce the experimental dark relaxation dynamics during the early HL–dark cycles (Figure 4-8E and Table 4-5), but successfully captures the relaxation during the later dark periods (Figure 4-8F and Table 4-5). In other words, the rapid response associated with periodic exposure to darkness evolves (or changes) from cycle to cycle. Consequently, the steady-state relaxation time constant (τ_{rel}^{rapid}) is a poor descriptor for the kinetics associated with quenching relaxation in the dark, especially during the early HL–dark cycles. Additionally, given that the agreement between the model and experiment during the early dark periods is better for the Zea-deficient *npq1* and *szl1* mutants, the cumulative rapid dark response seems to be dependent on Zea. In the future, time-resolved HPLC measurements[55] may provide additional insight into the roles of specific xanthophyll pigments during periodic illumination sequences. *In vivo* optical measurements of Zea formation[61,80] and ΔpH[81] may provide additional clarity by allowing us to directly test the molecular basis for some of our observations.

4.5.5 Insights into NPQ Regulatory Processes

Returning to the structure of the model, we assume that τ_{ind}^{rapid} and τ_{rel}^{rapid} are constants modified by $q_{max}(t)$ or $q_{rec}(t)$ to give $k_1^{rapid}(t)$ and $k_2^{rapid}(t)$, respectively. This time independence of the rapid intraperiod dynamics is consistent with all of the mutant data after the first few cycles (Figure 4-5), i.e., when steady-state quenching and recovery are reached. At first glance, this might suggest that the rapid behavior does not depend on Zea or PsbS. However, the Zea concentration should be nearly constant by period 3 or 4 leading to similar rates of rapid NPQ relaxation. The *npq1* mutant shows a faster recovery, which is consistent with its lack of Zea. As we noted above, the interaction of PsbS with the antenna is likely more complex than a simple induction of quenching. If there are both short- and long-term influences of PsbS and, again, the long-term process(es) have reached a steady state by period 4, this could explain the similarity of the quenching induction and recovery traces at the steady state (period 9; see Table 4-3 for timescales) when comparing the mutants (except for *npq4* that lacks both induction and recovery character).

Using our model we systematically explored the effects of omitting the slowly varying time-dependent state of the envelopes from the rapidly reversible rate constants (Figure 4-7). When $q_{max}(t)$ is not included in $k^{rapid}(t)$, the model is unable to produce the expected response during HL or dark periods and, in fact, the response becomes out-of-phase (increasing NPQ_τ in the dark and decreasing NPQ_τ in HL) (Figure 4-7D,G). This out-of-phase behavior resembles the aforementioned experimental response for the *npq4* mutant under periodically fluctuating light (see red trace in Figure 4-2), further hinting that PsbS may play a role in both the HL and the dark response. Similar discrepancies between the model and experiment were also observed upon omitting $q_{rec}(t)$ from $k^{rapid}(t)$ (Figure 4-7E,H). Importantly, these findings reinforce the idea that the fast and slow processes involved in NPQ are inherently intertwined.

After fixing all of the model parameters at their wild-type values (see Table 4-6 and also the description in the Supplemental), we also explored how changes in a single parameter influence the overall quenching response. Our exploration of the dependence of the eight parameters highlights the significance of two parameters — a_{rec} (the amplitude of the maximum recovery envelope) and τ_{rel}^{rapid} (the rate of intraperiod relaxation) (Figure 4-10; the effects of varying all eight parameters are shown individually in Figure 4-11). Both quantities modulate the magnitude of NPQ relaxation without changing the extent of quenching. Therefore, optimizing these parameters could be an appropriate target for optimizing crop/biomass yields by accelerating the recovery from photoprotection while not compromising the plant's ability to protect itself under excess light. In future studies, periodic illumination will be a useful way to characterize new mutants with enhanced recovery amplitudes for improved biomass yields.

4.6 Concluding Remarks

A summary of the combined experimental and modeling approach employed in the present study is depicted in Figure 4-13. Before discussing the implication of our analysis for efforts to optimize the NPQ response to enhance biomass yields, we briefly summarize the major findings from this work which, in some cases, differ significantly from conclusions based on single HL–dark measurement sequences.

1. The quenching response within individual periods as well as of the overall envelopes between periods lead to the conclusion that many timescales are very similar between the different mutants. The major effect of removing Zea or enhancing PsbS concentration is on the amplitudes of the slower (interperiod) induction and relaxation envelopes and not on their timescales. This is in contrast to conclusions from single HL–dark periods, which suggest that the qE component has the largest impact on quenching.

2. By comparing the model and experiment, it appears that the plant's immediate response to HL—aside from the initial transient response during the first two cycles—is independent of the illumination history, while the plant's immediate response to the dark evolves throughout repeated HL–dark cycles and seems to be dependent on Zea.

3. Both PsbS and Zea/Lut have distinct roles in the NPQ response. For example, not only is PsbS required for the rapidly reversible quenching, but also longer timescale components likely involving changes in the membrane organization or morphology. In the absence of Zea, Lut can serve as an effective quencher, especially when present in increased amounts as is the case for the *szl1* mutant. Zea itself appears to be necessary for WT-levels of NPQ and is specifically involved in slower quenching processes.

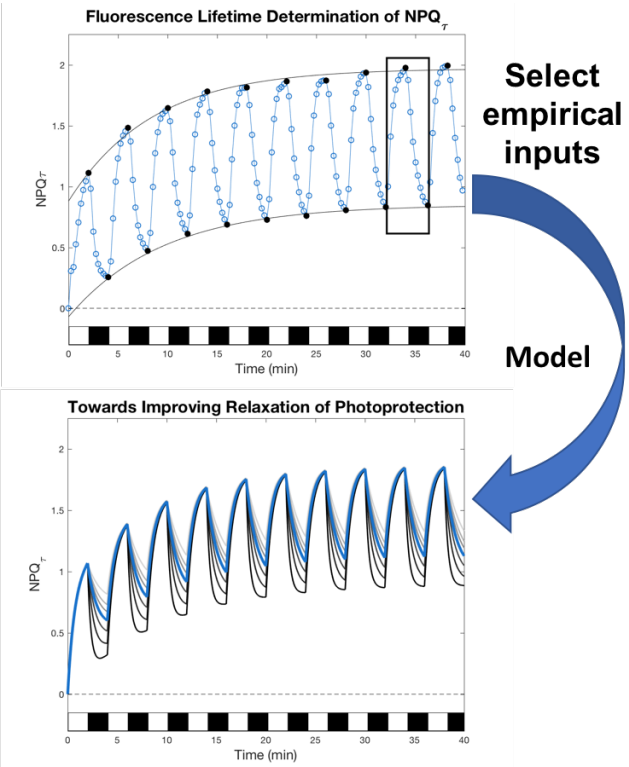

Figure 4-13. Summary of the approach employed in this study. Following the collection of fluorescence lifetime snapshot measurements on intact leaves under exposure to repeating cycles of 2 min HL and 2 min darkness, simple exponential fits were used to capture information about the interperiod (black data points and curves) and intraperiod dynamics (black box around cycle 9) for each mutant. Next, these empirical fit values were used as the sole inputs into the kinetic model, which is then able to describe the plant's overall response to repetitive HL and dark exposure with reasonable accuracy. Our model therefore provides a valuable framework to screen the ability of mutants to rapidly adjust NPQ to an illumination sequence that more closely resembles the fluctuating light conditions found in nature.

As we have discussed previously, monitoring the quenching response throughout multiple light–dark cycles has the potential to reveal new insights into the complicated and overlapping nature of the various responses associated with NPQ induction and relaxation and the complex roles of the various molecular actors. The use of periodic illumination and the description of the data for five strains of *A. thaliana* clearly demonstrate that the rapidly reversible and slower responses to excess light cannot be viewed independently. This interdependence of responses has important implications for efforts to optimize the NPQ response to increase yields in field growth conditions where plants are routinely subjected to fluctuating light.[4,27]

Our analysis suggests that modifying the kinetics of the slow process does not appear to be a viable approach for increasing crop yields. Instead, by systematically varying the input parameters, our model suggests that attention should be focused on altering the amplitude of the slow recovery process (a_{rec}) as well as the kinetics of the rapidly reversible quenching process (τ_{rel}^{rapid}; refer to the Appendix and Figure 4-6 for definitions of each parameter). Determining these parameters in the lab could provide a rapid method for selecting new mutants and overexpressors with enhanced recovery amplitudes for field trials aimed at increasing biomass yields.

Despite the potential for predictive power, kinetic models derived from fluorescence measurements alone cannot directly connect the understanding of dissipative mechanisms and structural processes from steady-state measurements to the observed regulation of fluorescence quenching dynamics. Snapshot transient absorption measurements have been developed that relate observables of quenching mechanisms to regulatory timescales.[82] Further development of similar "snapshot" versions of techniques that can relate changes in protein conformation dynamics or membrane organization to these regulatory timescales will be necessary to integrate the understanding of physical phenomena with kinetic regulatory models. In addition, improved analysis methods for multiperiod data sets such as those presented here should lead to more refined insights about the complicated and overlapping response of NPQ in the presence of dynamically changing light environments.

4.7 Appendix: Equations for the Multi-Timescale Model of NPQ

Terms in green come from fits to rapid intra-period dynamics (penultimate period number 9), while terms in blue come from fits to slowly-varying inter-period envelopes.

$$\frac{dq^{active}}{dt} = -[k_1(t) + k_2(t)]q^{active} + k_2(t) \quad (1)$$

$$k_1(t) = k_1^{\text{rapid}}(t) + k_1^{\text{quenching envelope}} + k_1^{\text{recovery envelope}} \quad (2)$$

$$k_2(t) = k_2^{\text{rapid}}(t) + k_2^{\text{quenching envelope}} + k_2^{\text{recovery envelope}} \quad (3)$$

$$k_1^{\text{rapid}}(t) = \begin{cases} k_{\text{fit}}^{\text{induction}}(1 - q_{\text{max}}(t)), \text{ light} \\ k_{\text{fit}}^{\text{relaxation}}(1 - q_{\text{rec}}(t)), \text{ dark} \end{cases} \quad (4)$$

$$k_2^{\text{rapid}}(t) = \begin{cases} k_{\text{fit}}^{\text{induction}} q_{\text{max}}(t), \text{ light} \\ k_{\text{fit}}^{\text{relaxation}} q_{\text{rec}}(t), \text{ dark} \end{cases} \quad (5)$$

(Where $q_{\text{max}}(t) = a_{\text{max}} e^{-t/\tau_{\text{max}}} + c_{\text{max}}$ and $q_{\text{rec}}(t) = a_{\text{rec}} e^{-t/\tau_{\text{rec}}} + c_{\text{rec}}$)

$$k_1^{\text{quenching envelope}} = k_{\text{fit}}^{\text{quenching}} \left(1 - q_{\text{ss}}^{\text{quenching}}\right) \quad (6)$$

$$k_2^{\text{quenching envelope}} = k_{\text{fit}}^{\text{quenching}} q_{\text{ss}}^{\text{quenching}} \quad (7)$$

$$k_1^{\text{recovery envelope}} = k_{\text{fit}}^{\text{recovery}} \left(1 - q_{\text{ss}}^{\text{recovery}}\right) \quad (8)$$

$$k_2^{\text{recovery envelope}} = k_{\text{fit}}^{\text{recovery}} q_{\text{ss}}^{\text{recovery}} \quad (9)$$

4.8 References

(1) Blankenship, R. E. *Molecular Mechanisms of Photosynthesis*, 2nd ed.; Blackwell Science, 2014.

(2) Demmig-Adams, B.; Garab, G.; Adams Iii, W. *Non-Photochemical Quenching and Energy Dissipation in Plants, Algae and Cyanobacteria*; 2014.

(3) Kromdijk, J.; Głowacka, K.; Leonelli, L.; Gabilly, S. T.; Iwai, M.; Niyogi, K. K.; Long, S. P. Improving photosynthesis and crop productivity by accelerating recovery from photoprotection. *Science* **2016**, *354* (6314), 857–861.

(4) Zhu, X.-G.; Ort, D. R.; Whitmarsh, J.; Long, S. P. The slow reversibility of photosystem II thermal energy dissipation on transfer from high to low light may cause large losses in carbon gain by crop canopies: a theoretical analysis. *J. Exp. Bot.* **2004**, *55* (400), 1167–1175.

(5) Farooq, S.; Chmeliov, J.; Wientjes, E.; Koehorst, R.; Bader, A.; Valkunas, L.; Trinkunas, G.; van Amerongen, H. Dynamic feedback of the photosystem II reaction centre on photoprotection in plants. *Nat. Plants* **2018**, *4* (4), 225–231.

(6) Melis, A. Photosystem-II damage and repair cycle in chloroplasts: what modulates the rate of photodamage in vivo? *Trends Plant Sci.* **1999**, *4* (4), 130–135.

(7) Tyystjärvi, E.; Aro, E. M. The rate constant of photoinhibition, measured in lincomycin-treated leaves, is directly proportional to light intensity. *Proc. Natl. Acad. Sci. U. S. A.* **1996**, *93* (5), 2213–2218.

(8) Keren, N.; Berg, A.; van Kan PJ, P. J. M.; Levanon, H.; Ohad, I. Mechanism of photosystem II photoinactivation and D1 protein degradation at low light: the role of back electron flow. *Proc. Natl. Acad. Sci. U. S. A.* **1997**, *94* (4), 1579–1584.

(9) Niyogi, K. K. Photoprotection Revisited: Genetic and Molecular Approaches. *Annu. Rev. Plant Physiol. Plant Mol. Biol.* **1999**, *50* (1), 333–359.

(10) Demmig-Adams, B.; Adams, W. W. Photoprotection and Other Responses of Plants to High Light Stress. *Annu. Rev. Plant Physiol. Plant Mol. Biol.* **1992**, *43* (1), 599–626.

(11) Ruban, A. V. Nonphotochemical Chlorophyll Fluorescence Quenching: Mechanism and Effectiveness in Protecting Plants from Photodamage. *Plant Physiol.* **2016**, *170* (4), 1903–1916.

(12) Wraight, C. A.; Crofts, A. R. Energy-Dependent Quenching of Chlorophyll a Fluorescence in Isolated Chloroplasts. *Eur. J. Biochem.* **1970**, *17* (2), 319–327.

(13) Briantais, J.-M.; Vernotte, C.; Picaud, M.; Krause, G. H. A quantitative study of the slow decline of chlorophyll a fluorescence in isolated chloroplasts. *Biochim. Biophys. Acta - Bioenerg.* **1979**, *548* (1), 128–138.

(14) Noctor, G.; Rees, D.; Young, A.; Horton, P. The relationship between zeaxanthin, energy-dependent quenching of chlorophyll fluorescence, and trans-thylakoid pH gradient in isolated chloroplasts. *Biochim. Biophys. Acta - Bioenerg.* **1991**, *1057* (3), 320–330.

(15) Goss, R.; Richter, M.; Wild, A. Role of ΔpH in the mechanism of zeaxanthin-dependent amplification of qE. *J. Photochem. Photobiol. B Biol.* **1995**, *27* (2), 147–152.

(16) Müller, P.; Li, X.-P.; Niyogi, K. K. Non-photochemical quenching. A response to excess light energy. *Plant Physiol.* **2001**, *125* (4), 1558–1566.

(17) de Bianchi, S.; Ballottari, M.; Dall'osto, L.; Bassi, R. Regulation of plant light harvesting by thermal dissipation of excess energy. *Biochem. Soc. Trans.* **2010**, *38* (2), 651–660.

(18) Dall'Osto, L.; Caffarri, S.; Bassi, R. A Mechanism of Nonphotochemical Energy

Dissipation, Independent from PsbS, Revealed by a Conformational Change in the Antenna Protein CP26. *Plant Cell* **2005**, *17* (4), 1217–1232.
(19) Nilkens, M.; Kress, E.; Lambrev, P.; Miloslavina, Y.; Müller, M.; Holzwarth, A. R.; Jahns, P. Identification of a slowly inducible zeaxanthin-dependent component of non-photochemical quenching of chlorophyll fluorescence generated under steady-state conditions in Arabidopsis. *Biochim. Biophys. Acta - Bioenerg.* **2010**, *1797* (4), 466–475.
(20) Xu, P.; Tian, L.; Kloz, M.; Croce, R. Molecular insights into Zeaxanthin-dependent quenching in higher plants. *Sci. Rep.* **2015**, *5* (1), 13679.
(21) Tian, L.; Xu, P.; Chukhutsina, V. U.; Holzwarth, A. R.; Croce, R. Zeaxanthin-dependent nonphotochemical quenching does not occur in photosystem I in the higher plant Arabidopsis thaliana. *Proc. Natl. Acad. Sci. U. S. A.* **2017**, *114* (18), 4828–4832.
(22) Krause, G. H. Photoinhibition of photosynthesis. An evaluation of damaging and protective mechanisms. *Physiol. Plant.* **1988**, *74* (3), 566–574.
(23) Ruban, A. V.; Horton, P. An investigation of the sustained component of nonphotochemical quenching of chlorophyll fluorescence in isolated chloroplasts and leaves of spinach. *Plant Physiol.* **1995**, *108* (2), 721–726.
(24) Verhoeven, A. Sustained energy dissipation in winter evergreens. *New Phytol.* **2014**, *201* (1), 57–65.
(25) Tian, Y.; Sacharz, J.; Ware, M. A.; Zhang, H.; Ruban, A. V. Effects of periodic photoinhibitory light exposure on physiology and productivity of Arabidopsis plants grown under low light. *J. Exp. Bot.* **2017**, *68* (15), 4249–4262.
(26) Malnoë, A. Photoinhibition or photoprotection of photosynthesis? Update on the (newly termed) sustained quenching component qH. *Environ. Exp. Bot.* **2018**, *154* (1), 123–133.
(27) Külheim, C.; Agren, J.; Jansson, S. Rapid regulation of light harvesting and plant fitness in the field. *Science* **2002**, *297* (5578), 91–93.
(28) Reinhardt, K.; Smith, W. K.; Carter, G. A. Clouds and cloud immersion alter photosynthetic light quality in a temperate mountain cloud forest. *Botany* **2010**, *88* (5), 462–470.
(29) Slattery, R. A.; Walker, B. J.; Weber, A. P. M.; Ort, D. R. The Impacts of Fluctuating Light on Crop Performance. *Plant Physiol.* **2018**, *176* (2), 990–1003.
(30) Kaiser, E.; Morales, A.; Harbinson, J. Fluctuating Light Takes Crop Photosynthesis on a Rollercoaster Ride. *Plant Physiol.* **2018**, *176* (2), 977–989.
(31) Sylak-Glassman, E. J.; Zaks, J.; Amarnath, K.; Leuenberger, M.; Fleming, G. R. Characterizing non-photochemical quenching in leaves through fluorescence lifetime snapshots. *Photosynth. Res.* **2016**, *127* (1), 69–76.
(32) Baker, N. R. Chlorophyll Fluorescence: A Probe of Photosynthesis In Vivo. *Annu. Rev. Plant Biol.* **2008**, *59* (1), 89–113.
(33) Kalaji, H. M.; Schansker, G.; Ladle, R. J.; Goltsev, V.; Bosa, K.; Allakhverdiev, S. I.; Brestic, M.; Bussotti, F.; Calatayud, A.; Dąbrowski, P.; Elsheery, N. I.; Ferroni, L.; Guidi, L.; Hogewoning, S. W.; Jajoo, A.; Misra, A. N.; Nebauer, S. G.; Pancaldi, S.; Penella, C.; Poli, D.; Pollastrini, M.; Romanowska-Duda, Z. B.; Rutkowska, B.; Serôdio, J.; Suresh, K.; Szulc, W.; Tambussi, E.; Yanniccari, M.; Zivcak, M. Frequently asked questions about in vivo chlorophyll fluorescence: practical issues. *Photosynth. Res.* **2014**, *122* (2), 121–158.
(34) Brugnoli, E.; Björkman, O. Chloroplast movements in leaves: Influence on chlorophyll fluorescence and measurements of light-induced absorbance changes related to ΔpH and zeaxanthin formation. *Photosynth. Res.* **1992**, *32* (1), 23–35.
(35) Li, X.-P.; Björkman, O.; Shih, C.; Grossman, A. R.; Rosenquist, M.; Jansson, S.; Niyogi,

K. K. A pigment-binding protein essential for regulation of photosynthetic light harvesting. *Nature* **2000**, *403* (6768), 391–395.
(36) Li, X.-P.; Gilmore, A. M.; Caffarri, S.; Bassi, R.; Golan, T.; Kramer, D. M.; Niyogi, K. K. Regulation of photosynthetic light harvesting involves intrathylakoid lumen pH sensing by the PsbS protein. *J. Biol. Chem.* **2004**, *279* (22), 22866–22874.
(37) Li, X.-P.; Muller-Moule, P.; Gilmore, A. M.; Niyogi, K. K. PsbS-dependent enhancement of feedback de-excitation protects photosystem II from photoinhibition. *Proc. Natl. Acad. Sci. U. S. A.* **2002**, *99* (23), 15222–15227.
(38) Jahns, P.; Latowski, D.; Strzalka, K. Mechanism and regulation of the violaxanthin cycle: The role of antenna proteins and membrane lipids. *Biochim. Biophys. Acta - Bioenerg.* **2009**, *1787* (1), 3–14.
(39) Ma, Y.-Z.; Holt, N. E.; Li, X.-P.; Niyogi, K. K.; Fleming, G. R. Evidence for direct carotenoid involvement in the regulation of photosynthetic light harvesting. *Proc. Natl. Acad. Sci.* **2003**, *100* (3), 4377–4382.
(40) Holt, N. E.; Zigmantas, D.; Valkūnas, L.; Li, X.-P.; Niyogi, K. K.; Fleming, G. R. Carotenoid cation formation and the regulation of photosynthetic light harvesting. *Science* **2005**, *307* (5708), 433–436.
(41) Bode, S.; Quentmeier, C. C.; Liao, P.-N.; Hafi, N.; Barros, T.; Wilk, L.; Bittner, F.; Walla, P. J. On the regulation of photosynthesis by excitonic interactions between carotenoids and chlorophylls. *Proc. Natl. Acad. Sci. U. S. A.* **2009**, *106* (30), 12311–12316.
(42) Park, S.; Fischer, A. L.; Steen, C. J.; Iwai, M.; Morris, J. M.; Walla, P. J.; Niyogi, K. K.; Fleming, G. R. Chlorophyll-Carotenoid Excitation Energy Transfer in High-Light-Exposed Thylakoid Membranes Investigated by Snapshot Transient Absorption Spectroscopy. *J. Am. Chem. Soc.* **2018**, *140* (38), 11965–11973.
(43) Park, S.; Steen, C. J.; Lyska, D.; Fischer, A. L.; Endelman, B.; Iwai, M.; Niyogi, K. K.; Fleming, G. R. Chlorophyll–carotenoid excitation energy transfer and charge transfer in Nannochloropsis oceanica for the regulation of photosynthesis. *Proc. Natl. Acad. Sci.* **2019**, *116* (9), 3385–3390.
(44) Ruban, A. V.; Berera, R.; Ilioaia, C.; van Stokkum, I. H. M.; Kennis, J. T. M.; Pascal, A. A.; van Amerongen, H.; Robert, B.; Horton, P.; van Grondelle, R. Identification of a mechanism of photoprotective energy dissipation in higher plants. *Nature* **2007**, *450* (7169), 575–578.
(45) Li, Z.; Ahn, T. K.; Avenson, T. J.; Ballottari, M.; Cruz, J. A.; Kramer, D. M.; Bassi, R.; Fleming, G. R.; Keasling, J. D.; Niyogi, K. K. Lutein accumulation in the absence of zeaxanthin restores nonphotochemical quenching in the Arabidopsis thaliana npq1 mutant. *Plant Cell* **2009**, *21* (6), 1798–1812.
(46) Mascoli, V.; Liguori, N.; Xu, P.; Roy, L. M.; van Stokkum, I. H. M.; Croce, R. Capturing the Quenching Mechanism of Light-Harvesting Complexes of Plants by Zooming in on the Ensemble. *Chem* **2019**, *5* (11), 2900–2912.
(47) Cupellini, L.; Calvani, D.; Jacquemin, D.; Mennucci, B. Charge transfer from the carotenoid can quench chlorophyll excitation in antenna complexes of plants. *Nat. Commun.* **2020**, *11* (1), 662.
(48) Niyogi, K. K.; Grossman, A. R.; Björkman, O. Arabidopsis mutants define a central role for the xanthophyll cycle in the regulation of photosynthetic energy conversion. *Plant Cell* **1998**, *10* (7), 1121–1134.
(49) Havaux, M.; Niyogi, K. K. The violaxanthin cycle protects plants from photooxidative

damage by more than one mechanism. *Proc. Natl. Acad. Sci.* **1999**, *96* (15), 8762–8767.
(50) Cazzaniga, S.; Li, Z.; Niyogi, K. K.; Bassi, R.; Dall'Osto, L. The Arabidopsis szl1 mutant reveals a critical role of β-carotene in photosystem I photoprotection. *Plant Physiol.* **2012**, *159* (4), 1745–1758.
(51) Schansker, G.; Tóth, S. Z.; Strasser, R. J. Dark recovery of the Chl a fluorescence transient (OJIP) after light adaptation: The qT-component of non-photochemical quenching is related to an activated photosystem I acceptor side. *Biochim. Biophys. Acta - Bioenerg.* **2006**, *1757* (7), 787–797.
(52) Sylak-Glassman, E. J.; Malnoë, A.; De Re, E.; Brooks, M. D.; Fischer, A. L.; Niyogi, K. K.; Fleming, G. R. Distinct roles of the photosystem II protein PsbS and zeaxanthin in the regulation of light harvesting in plants revealed by fluorescence lifetime snapshots. *Proc. Natl. Acad. Sci. U. S. A.* **2014**, *111* (49), 17498–17503.
(53) Leuenberger, M.; Morris, J. M.; Chan, A. M.; Leonelli, L.; Niyogi, K. K.; Fleming, G. R. Dissecting and modeling zeaxanthin- and lutein-dependent nonphotochemical quenching in Arabidopsis thaliana. *Proc. Natl. Acad. Sci. U. S. A.* **2017**, *114* (33), E7009–E7017.
(54) Bennett, D. I. G.; Amarnath, K.; Park, S.; Steen, C. J.; Morris, J. M.; Fleming, G. R. Models and mechanisms of the rapidly reversible regulation of photosynthetic light harvesting. *Open Biol.* **2019**, *9* (4), 190043.
(55) Müller-Moulé, P.; Conklin, P. L.; Niyogi, K. K. Ascorbate deficiency can limit violaxanthin de-epoxidase activity in vivo. *Plant Physiol.* **2002**, *128* (3), 970–977.
(56) Park, S.; Fischer, A. L.; Li, Z.; Bassi, R.; Niyogi, K. K.; Fleming, G. R. Snapshot Transient Absorption Spectroscopy of Carotenoid Radical Cations in High-Light-Acclimating Thylakoid Membranes. *J. Phys. Chem. Lett.* **2017**, *8* (22), 5548–5554.
(57) Johnson, M. P.; Ruban, A. V. Arabidopsis plants lacking PsbS protein possess photoprotective energy dissipation. *Plant J.* **2010**, *61* (2), 283–289.
(58) Zaks, J.; Amarnath, K.; Kramer, D. M.; Niyogi, K. K.; Fleming, G. R. A kinetic model of rapidly reversible nonphotochemical quenching. *Proc. Natl. Acad. Sci. U. S. A.* **2012**, *109* (39), 15757–15762.
(59) Correa-Galvis, V.; Poschmann, G.; Melzer, M.; Stühler, K.; Jahns, P. PsbS interactions involved in the activation of energy dissipation in Arabidopsis. *Nat. Plants* **2016**, *2* (2), 15225.
(60) Sacharz, J.; Giovagnetti, V.; Ungerer, P.; Mastroianni, G.; Ruban, A. V. The xanthophyll cycle affects reversible interactions between PsbS and light-harvesting complex II to control non-photochemical quenching. *Nat. Plants* **2017**, *3* (2), 16225.
(61) Johnson, M. P.; Pérez-Bueno, M. L.; Zia, A.; Horton, P.; Ruban, A. V. The zeaxanthin-independent and zeaxanthin-dependent qE components of nonphotochemical quenching involve common conformational changes within the photosystem II antenna in Arabidopsis. *Plant Physiol.* **2009**, *149* (2), 1061–1075.
(62) Roach, T.; Krieger-Liszkay, A. The role of the PsbS protein in the protection of photosystems I and II against high light in Arabidopsis thaliana. *Biochim. Biophys. Acta - Bioenerg.* **2012**, *1817* (12), 2158–2165.
(63) Townsend, A. J.; Saccon, F.; Giovagnetti, V.; Wilson, S.; Ungerer, P.; Ruban, A. V. The causes of altered chlorophyll fluorescence quenching induction in the Arabidopsis mutant lacking all minor antenna complexes. *Biochim. Biophys. Acta - Bioenerg.* **2018**, *1859* (9), 666–675.
(64) Nicol, L.; Nawrocki, W. J.; Croce, R. Disentangling the sites of non-photochemical

quenching in vascular plants. *Nat. Plants* **2019**, *5*, 1177–1183.
(65) Saccon, F.; Giovagnetti, V.; Shukla, M. K.; Ruban, A. V. Rapid regulation of photosynthetic light harvesting in the absence of minor antenna and reaction centre complexes. *J. Exp. Bot.* **2020**, *71* (12), 3626–3637.
(66) Dall'Osto, L.; Cazzaniga, S.; Bressan, M.; Paleček, D.; Židek, K.; Niyogi, K. K.; Fleming, G. R.; Zigmantas, D.; Bassi, R. Two mechanisms for dissipation of excess light in monomeric and trimeric light-harvesting complexes. *Nat. Plants* **2017**, *3* (5), 17033.
(67) Ruban, A. V.; Johnson, M. P.; Duffy, C. D. P. The photoprotective molecular switch in the photosystem II antenna. *Biochim. Biophys. Acta - Bioenerg.* **2012**, *1817* (1), 167–181.
(68) Demmig, B.; Winter, K.; Krüger, A.; Czygan, F. C. Photoinhibition and zeaxanthin formation in intact leaves : a possible role of the xanthophyll cycle in the dissipation of excess light energy. *Plant Physiol.* **1987**, *84* (2), 218–224.
(69) Gilmore, A. M.; Mohanty, N.; Yamamoto, H. Y. Epoxidation of zeaxanthin and antheraxanthin reverses non-photochemical quenching of photosystem II chlorophyll a fluorescence in the presence of trans-thylakoid ΔpH. *FEBS Lett.* **1994**, *350* (2–3), 271–274.
(70) Goral, T. K.; Johnson, M. P.; Duffy, C. D. P.; Brain, A. P. R.; Ruban, A. V.; Mullineaux, C. W. Light-harvesting antenna composition controls the macrostructure and dynamics of thylakoid membranes in Arabidopsis. *Plant J.* **2012**, *69* (2), 289–301.
(71) Albanese, P.; Tamara, S.; Saracco, G.; Scheltema, R. A.; Pagliano, C. How paired PSII–LHCII supercomplexes mediate the stacking of plant thylakoid membranes unveiled by structural mass-spectrometry. *Nat. Commun.* **2020**, *11* (1), 1361.
(72) Anderson, J. M.; Horton, P.; Kim, E.-H.; Chow, W. S. Towards elucidation of dynamic structural changes of plant thylakoid architecture. *Philos. Trans. R. Soc. Lond. B. Biol. Sci.* **2012**, *367* (1608), 3515–3524.
(73) Johnson, M. P.; Goral, T. K.; Duffy, C. D. P.; Brain, A. P. R.; Mullineaux, C. W.; Ruban, A. V. Photoprotective energy dissipation involves the reorganization of photosystem II light-harvesting complexes in the grana membranes of spinach chloroplasts. *Plant Cell* **2011**, *23* (4), 1468–1479.
(74) Kiss, A. Z.; Ruban, A. V; Horton, P. The PsbS protein controls the organization of the photosystem II antenna in higher plant thylakoid membranes. *J. Biol. Chem.* **2008**, *283* (7), 3972–3978.
(75) Betterle, N.; Ballottari, M.; Zorzan, S.; de Bianchi, S.; Cazzaniga, S.; Dall'osto, L.; Morosinotto, T.; Bassi, R. Light-induced dissociation of an antenna hetero-oligomer is needed for non-photochemical quenching induction. *J. Biol. Chem.* **2009**, *284* (22), 15255–15266.
(76) Morris, J. M.; Fleming, G. R. Quantitative modeling of energy dissipation in Arabidopsis thaliana. *Environ. Exp. Bot.* **2018**, *154*, 99–109.
(77) Zia, A.; Johnson, M. P.; Ruban, A. V. Acclimation- and mutation-induced enhancement of PsbS levels affects the kinetics of non-photochemical quenching in Arabidopsis thaliana. *Planta* **2011**, *233* (6), 1253–1264.
(78) Ware, M. A.; Giovagnetti, V.; Belgio, E.; Ruban, A. V. PsbS protein modulates non-photochemical chlorophyll fluorescence quenching in membranes depleted of photosystems. *J. Photochem. Photobiol. B Biol.* **2015**, *152*, 301–307.
(79) Matuszyńska, A.; Heidari, S.; Jahns, P.; Ebenhöh, O. A mathematical model of non-photochemical quenching to study short-term light memory in plants. *Biochim. Biophys. Acta - Bioenerg.* **2016**, *1857* (12), 1860–1869.

(80) Zhang, R.; Kramer, D. M.; Cruz, J. A.; Struck, K. R.; Sharkey, T. D. The effects of moderately high temperature on zeaxanthin accumulation and decay. *Photosynth. Res.* **2011**, *108* (2–3), 171–181.
(81) Takizawa, K.; Cruz, J. A.; Kanazawa, A.; Kramer, D. M. The thylakoid proton motive force in vivo. Quantitative, non-invasive probes, energetics, and regulatory consequences of light-induced pmf. *Biochim. Biophys. Acta - Bioenerg.* **2007**, *1767* (10), 1233–1244.
(82) Park, S.; Steen, C. J.; Fischer, A. L.; Fleming, G. R. Snapshot transient absorption spectroscopy: toward in vivo investigations of nonphotochemical quenching mechanisms. *Photosynth. Res.* **2019**, *141* (3), 367–376.

Chapter 5

Photoprotection in *C. reinhardtii* under Fluctuating Light

This chapter is reproduced with permission from

C.J. Steen, A. Burlacot, A.H. Short, K.N. Niyogi, G.R. Fleming
"Interplay between LHCSR proteins and state transitions governs the NPQ response in intact cells of *Chlamydomonas* during light fluctuations"
bioRxiv (2022)
DOI: 10.1101/2021.12.31.474662.

5.1 Abstract

Photosynthetic organisms use sunlight as the primary energy source to fix CO_2. However, in the environment, light energy fluctuates rapidly and often exceeds saturating levels for periods ranging from seconds to hours, which can lead to detrimental effects for cells. Safe dissipation of excess light energy occurs primarily by non-photochemical quenching (NPQ) processes. In the model green microalga *Chlamydomonas reinhardtii*, photoprotective NPQ is mostly mediated by pH-sensing light-harvesting complex stress-related (LHCSR) proteins and the redistribution of light-harvesting antenna proteins between the photosystems (state transition). Although each component underlying NPQ has been documented, their relative contributions to the dynamic functioning of NPQ under fluctuating light conditions remains unknown. Here, by monitoring NPQ throughout multiple high light-dark cycles with HL/dark periods ranging from 1 to 10 minutes, we show that the dynamics of NPQ depend on the frequency of light fluctuations. Mutants impaired in the accumulation of LHCSRs (*npq4*, *lhcsr1*, and *npq4lhcsr1*) showed significantly less quenching during illumination, demonstrating that LHCSR proteins are responsible for the majority of NPQ during repetitive exposure to HL/dark fluctuations. Activation of NPQ was also observed during the dark phases of light fluctuations, and this was exacerbated in mutants lacking LHCSRs. By analyzing 77K chlorophyll fluorescence spectra and chlorophyll fluorescence lifetimes and yields in a mutant impaired in state transition, we show that this phenomenon arises from state transition. Finally, we quantified the contributions of LHCSRs and state transitions to the overall NPQ amplitude and dynamics for all light fluctuating frequencies tested and show that both processes interact to facilitate NPQ during light fluctuations. We further assess the role of LHCSRs in cell growth under various frequencies of fluctuating light. These results highlight the dynamic functioning of photoprotection under light fluctuations and open a new way to systematically characterize the photosynthetic response to an ever-changing light environment.

5.2 Introduction

Most life on Earth is sustained by photosynthetic organisms that capture sunlight energy to convert CO_2 and water into chemical energy. Light is captured by light-harvesting antenna complexes that contain a network of pigments absorbing photons and funneling the energy towards photosystems II and I that use it to perform photochemical reactions. Under light-limiting conditions, efficient light harvesting is crucial for maximizing the rate of CO_2 fixation.[1] However, high light (HL) intensities can saturate reaction centers and lead to the build-up of excess excitation energy, which, if unchecked, can lead to the production of reactive oxygen species and damage to both reaction centers[2]. In nature, light exposure rapidly fluctuates in intensity with periods of HL ranging from milliseconds to hours[3], requiring photosynthesis to acclimate to different frequencies of HL fluctuations. For each period of HL acclimation, photosynthetic organisms exhibit photoprotective mechanisms that regulate light harvesting and safely remove excess[4–6].

As elaborated in earlier chapters, upon light absorption, the energy can be dissipated as heat in the process of NPQ. NPQ involves five components, each of which has been distinguished by its time of induction and relaxation during transition between dark and HL[4]. The fastest component, called energy-dependent quenching (qE), is triggered by luminal acidification[7] and is induced and relaxed within seconds. State transition (qT) occurs within minutes and involves the phosphorylation of light-harvesting complexes (LHCs)[8] resulting in their detachment from Photosystem (PS) II and subsequent aggregation in a quenched state and/or association to PSI[9–11]. Zeaxanthin-dependent quenching (qZ) requires the accumulation of zeaxanthin and probably involves quenching in the minor LHCs of PSII[12–14]. On longer time scales, two more sustained forms of NPQ occur: qH that takes places it the antennae of PSII[15] directly in the LHCII trimers[16] and photoinhibition (qI) that occurs when degradation of the PSII core protein D1 exceeds its capacity for repair due to excess excitation energy[17].

In the green microalga *Chlamydomonas reinhardtii*, qE is mediated by pigment-binding LHC stress-related (LHCSR) proteins[18,19]. LHCSRs contain protonatable residues, which sense the decreasing luminal pH generated under HL conditions[20,21]; the protonation of LHCSRs triggers NPQ within the protein[22–24], allowing fast activation of qE. While there are two types of LHCSR proteins (LHCSR1 and LHCSR3), both of which bind pigments[25,26], LHCSR3 (for which two homologs are present in *Chlamydomonas*) is thought to be the main actor in qE[18,27]. On the other hand, qT is activated by the buildup of reducing equivalents in the thylakoid membrane, which activates a serine/threonine-protein kinase (STT7)[28,29] that phosphorylates LHCII, enabling it to detach from PSII and ultimately reattach to PSI[30,31]. While qZ has been described in *Chlamydomonas*[32], it does not seem to play a significant role in overall NPQ[21,33], and its potential mechanism of action remains to be determined. Finally, while qH has not been described in *Chlamydomonas*, qI occurs upon continued excess illumination[4,17] at the level of the PSII center, where oxygen-mediated sensitization creates the irreversible formation of a quenching site[34].

The photophysical and biochemical bases for NPQ have been studied for decades[4], however the *in vivo* operation has mostly been assessed under a single dark-to-HL transition[35] leaving our understanding of photoprotection under more complex light patterns limited. While LHCSR and STT7 activity are both known to be important for steady-state NPQ based on measurements performed under non-repeating HL/dark periods[36], their relative contributions to NPQ have not

been quantified, and their response to faster-timescale fluctuating light remains unstudied. Recent work has started looking at the response of NPQ to some specific light fluctuations in *Chlamydomonas*[6] and in the moss *Physcomitrella*[37]. However, the physiological role and the functioning of the NPQ components under the wide diversity of light patterns that are present in the natural environment is unexplored.

Here we utilized two distinct methods to monitor chlorophyll fluorescence in intact cells of *Chlamydomonas* that were exposed to varying frequencies of fluctuating light with HL/dark periods ranging from 1 to 10 min (Figure 5-1). The roles of qE and qT were investigated using single or double mutants of LHCSRs and STT7. Our analysis of LHCSR mutants (*npq4*[18], *lhcsr1*[27], and *npq4lhcsr1*[27]) revealed that LHCSR3 is the main contributor to the NPQ response during the HL phase of light fluctuations. Using mutants impaired in state transition (*stt7-9*[28] and *stt7npq4*[36]), we showed that qT quenching occurs primarily during the dark portion of the fluctuating light sequence and represents a significant part of NPQ during repeated light fluctuations. Our results showed that while qE and qT sustain most of the NPQ throughout light fluctuations, their relative importance varies during different phases of the fluctuating light response, with qT playing a larger role during dark periods and after repeated HL-dark fluctuations. Surprisingly, the light fluctuation frequency did not seem to have a major impact on the respective contributions of qE and qT, although the contribution of qE during the dark phase was frequency dependent. Nonetheless, the various components of NPQ are not completely independent, and we reveal an interplay between LHCSR- and STT7-mediated NPQ that enables the wild-type photoprotective response. We further show that while *stt7* mutants are not impaired in growth under light fluctuations, short time scale light fluctuations highly impair LHCSR mutants. These findings represent an important first step in investigating the photosynthetic response to the diversity of HL periods that occur in nature.

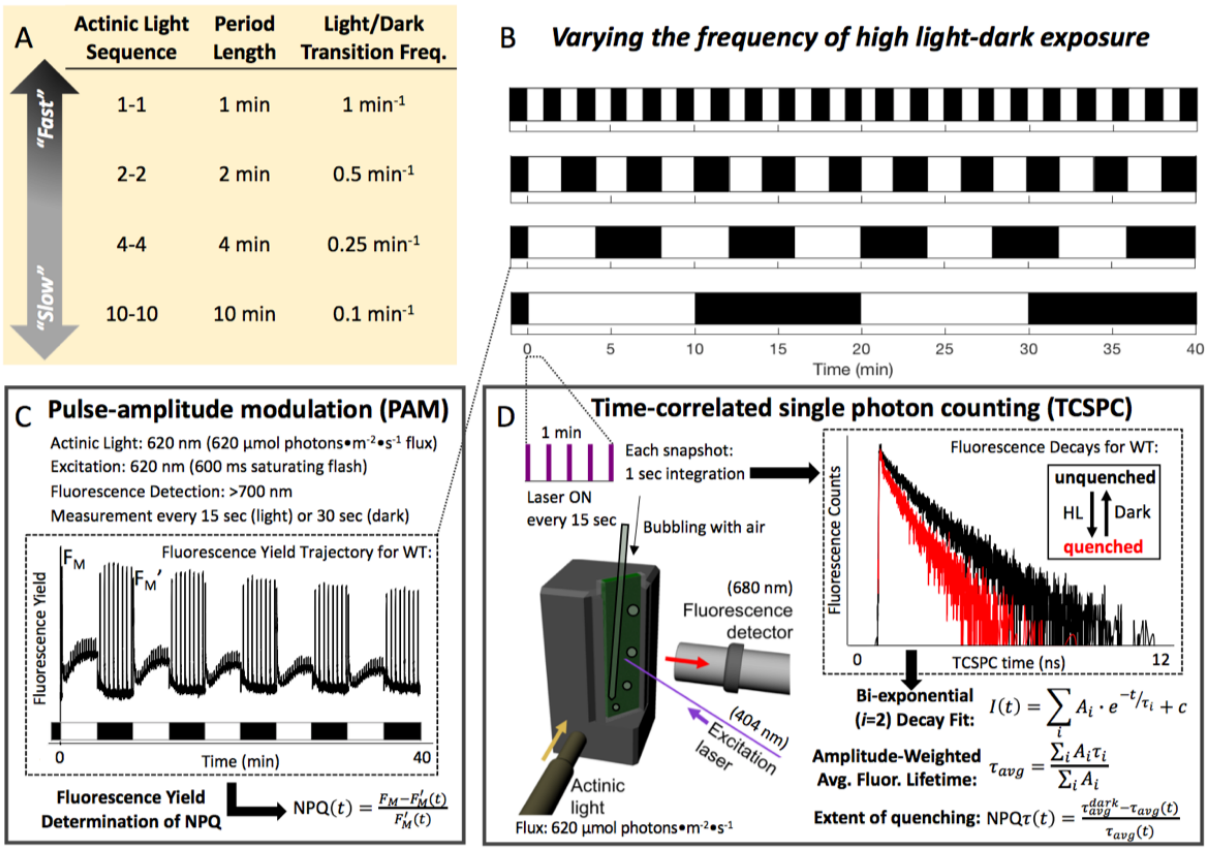

Figure 5-1. Experimental design for Chl *a* fluorescence measurements throughout exposure of *Chlamydomonas* cells to fluctuating light with various periods of HL-dark exposure. (A, B) Representation of the HL-dark cycles used for the 40 minutes of light fluctuation and their corresponding period, frequency, and name used throughout this chapter. NPQ was measured using Pulsed Amplitude Modulation (PAM, C) and Time-Correlated Single Photon Counting (TCSPC, D). (C) Characteristics of the PAM measurement and representative data of fluorescence yield in WT cells. (D) Characteristics of the TCSPC apparatus. Shown are two decays representative of two snapshots taken in a quenched and unquenched state.

5.3 Materials and Methods

5.3.1 Strains and culture conditions

Chlamydomonas mutants and their respective wild-type 4A- were previously described (*npq4*[18], *lhcsr1*[27], *npq4lhcsr1*[27], *stt7-9*[38], *stt7npq4*[36]). All strains were grown photoautotrophically under moderate light (50 µmol photons m^{-2} s^{-1}) in minimal HS medium under air level of CO_2 (20°C). Except for the growth test, cell cultures (5-8 µg Chl mL^{-1}) were incubated overnight at high light (400 µmol photons m^{-2} s^{-1}), for maximizing expression of LHCSR proteins[39]. Prior to each measurement, cells were illuminated for at least 15 min with low intensity far-red light (3in1LED panel with far-red LED; 3LH series, NK system, Japan) to ensure a complete state 1 configuration[40]. All replicates shown are biological replicates from independent cultures.

5.3.2 Chlorophyll Fluorescence Measurements

In this work, we employ two techniques to monitor the activation and deactivation of NPQ throughout 40 minutes of exposure to repeated periods of high light and dark on the basis of changes in Chl fluorescence emission (see Figure 5-1 for an illustration of the experimental design). Time-resolved Chl fluorescence was measured via time-correlated single photon counting (TCSPC) while Chl fluorescence yield was measured in parallel experiments using pulse-amplitude modulation (PAM) fluorimetry. Although both methods can monitor NPQ, the fluorescence lifetime is not susceptible to a range of non-quenching processes that can impact the fluorescence yield (such as chromophore bleaching, changes in chlorophyll concentration, chloroplast movement, or enhanced light scattering[41,42]. Therefore, fluorescence lifetime measurements provide insight into processes that directly quench chlorophyll fluorescence.

TCSPC measurement and fitting

The average chlorophyll fluorescence lifetime was measured by time-correlated single photon counting (TCSPC), as previously described[42,43]. A diode laser (Coherent Verdi G10, 532 nm) pumped a Ti:Sapphire oscillator (Coherent Mira 900f, 808 nm, 76 MHz) and the output was subsequently frequency doubled using a β-barium borate crystal to obtain 404 nm light. These pulses were used for excitation of the sample with a power of 1.7 mW (20 pJ/pulse) and Chl fluorescence emission at 680 nm was detected via an MCP-PMT (Hamamatsu R3809U). A custom-built LABVIEW software was used to synchronize three shutters located in the laser path, actinic light path, and the path between the sample and detector. Every 15 sec, a fluorescence lifetime snapshot measurement was acquired by exposing the cells to the saturating laser (404 nm) for 1 second and detecting the emission. Fluorescence lifetime snapshots were measured by TCSPC using a Becker-Hickl SPC-850 data acquisition card and SPCM software. In between the snapshot measurements, high-light illumination of the cells was achieved by exposing the cuvette to white light set to an intensity of 620 µmol photons m^{-2} s^{-1} (Leica KL1500 LCD, peak 648 nm, FWHM 220 nm), chosen as the minimal light level necessary to saturate photosynthetic reactions and induce qE activity at the onset of illumination. It was also chosen such that PAM and TCSPC would use identical high light intensities. The sample concentration was adjusted to ~80 µg Chl mL^{-1} for TCSPC measurements. To control the gas composition of the culture and prevent cells from settling to the bottom of the cuvette, the sample was bubbled with air (ambient CO_2

concentrations) at a rate of 2-7 mL min^{-1} throughout the entire 40 min experiment duration, although note that such bubbling increased the noise of the measurements.

For each fluorescence decay measurement, to ensure that PSII reaction centers were closed, we selected the 0.2 s step with the longest lifetime from the overall 1 s snapshot measurement duration[42]. This longest step was then fit to a bi-exponential decay (Picoquant, Fluofit Pro-4.6) and the average amplitude-weighted fluorescence lifetime (τ_{avg}) was calculated for each snapshot measurement. The NPQτ parameter is derived from the fluorescence lifetime snapshot measurements and is defined analogously to NPQ[42,44]:

$$NPQ_{\tau}(t) = \frac{\tau_{\mathrm{avg}}(0) - \tau_{\mathrm{avg}}(t)}{\tau_{\mathrm{avg}}(t)}$$

The value of NPQτ represents the magnitude of the quenching response based on the change in the average fluorescence lifetimes between time t = 0 (after far-red acclimation but before HL exposure) and any other time t during the 40 min snapshot trajectory. Therefore, using NPQτ removes confounding effects arising from any differences in the average chlorophyll excited state lifetime of the different strains following far-red acclimation. For all TCSPC measurements, each biological replicate represents the average of three technical replicates measured on the same day.

PAM measurements

Chlorophyll fluorescence yield was measured using a pulsed-amplitude modulation (PAM) fluorimeter (Dual-PAM 100, Walz GmbH, Effeltrich, Germany) with the red measuring head. Red saturating flashes (8,000 μmol photons m^{-2} s^{-1}, 600 ms, 620 nm) were delivered to measure FM (maximal fluorescence yield in dark-acclimated samples) and then every 15 s or 30 s to measure FM′ under actinic light exposure or dark phase respectively. Actinic light illumination (620 nm) was set to 620 μmol photons m^{-2} s^{-1}. Fluorescence emission was detected using a long-pass filter (>700 nm). NPQ was calculated as $(F_M - F_M')/F_M'$ where F_M and F_M' represent the maximal fluorescence prior to and during the actinic light sequence, respectively. The Chl concentration was ~5-8 μg Chl mL^{-1} and as for TCSPC, all PAM measurements and the sample was bubbled with air at a flux of 2-7 mL min^{-1} for proper control of the gas concentrations of the sample throughout the entire 40 min experiment duration, note that such bubbling increased the noise of the measurements (but to a lesser extent than for TCSPC).

Quantifying the contributions of LHCSRs and STT7 to NPQ

To assess the relative contributions of LHCSR1, LHCSR3, and STT7 to overall NPQ, we analyzed the NPQ (PAM) and NPQτ (TCSPC) trajectories for WT and each mutant. The relative contribution of each protein was determined as the percent change in the integrated snapshot trajectory of NPQ or NPQτ for each mutant relative to the control WT strain. As the contribution of each actor was found to be overall independent of HL-dark fluctuation frequencies in the range of 1 min^{-1} to 0.1 min^{-1}, the average contribution of each protein under the four light fluctuating sequences for both PAM and TCSPC was considered. Additionally, to characterize the involvement in activation or deactivation of NPQ, the quenching trajectories were integrated solely under HL or dark periods, respectively. The contributions of each protein to the early vs. late

responses were further assessed by integrating from 0-20 min and 20-40 min, respectively. Since it has been suggested that the *stt7-9* mutant may be "leaky"[45], our estimates for the STT7 contribution are lower-bound estimates. The potential leakiness of the *stt7-9* mutant does not affect any of the conclusions presented in this chapter. In addition to quantifying the relative contribution to NPQ of each protein relative to the WT strain, we also assessed the contribution of STT7 in the absence of LHCSR3 by integrating the PAM NPQ trajectory of *npq4stt7* relative to that of *npq4*. Likewise, the contribution of LHCSR3 was assessed independently of STT7 by integrating the PAM NPQ trajectory of *npq4stt7* relative to that of *stt7*.

5.3.3 77K Chlorophyll fluorescence emission

Chlorophyll fluorescence emission spectra of *Chlamydomonas* cells at 77 K were obtained by freezing whole cells (~5-8 µg Chl mL^{-1} final concentration) in liquid nitrogen. The emission spectrum was then measured between 600 and 800 nm (435 nm excitation wavelength, RF-5300PC spectrophotometer, Shimadzu).

5.3.4 Growth tests

The different *Chlamydomonas* strains were cultivated photoautotrophically under moderate light (50 µmol photons m^{-2} s^{-1}) in minimal medium under air level of CO_2 (20°C). Cells were harvested during exponential growth and resuspended in fresh minimal medium to 0.1, 0.5, or 2 µg Chl mL^{-1}. Eight-microliter drops were spotted on minimal medium plates at pH=7.2 and exposed to the various light conditions. Homogeneous light was supplied by LED panels. Temperature was maintained at 25°C at the level of plates.

5.4 Results

5.4.1 Varying light fluctuation periods affect the dynamic NPQ response.

While the photosynthetic response of *Chlamydomonas* to some light fluctuations has been reported[6,46], an analysis of NPQ for various periods of light fluctuations is lacking. We therefore measured chlorophyll fluorescence during light-dark cycles of 40 min with individual fluctuation periods ranging from 1 min to 10 min (Figure 5-1). Chlorophyll fluorescence yield was measured using PAM fluorometry and used to calculate NPQ[47]. In tandem experiments, TCSPC was used to measure the chlorophyll fluorescence lifetime[48], which was used to calculate NPQτ[44]. For all periods of light fluctuations in the wild-type strain, NPQ quickly turned on upon illumination but turned off more slowly (Figure 5-2). The same trend was observed in NPQτ (Figure 5-2). The 1 min period light fluctuation led to a nearly square-like response of NPQ and NPQτ (Figure 5-2).

For the longer fluctuation periods ranging from 2 minutes to 10 minutes, after an initial burst of NPQ in HL, the level of NPQ decreased with continued illumination, eventually reaching a steady state for the 10 min fluctuating period (Figure 5-2). A similar trend was also seen in NPQτ (Figure 5-2). Therefore, these kinetics are directly related to chlorophyll fluorescence quenching, rather than other non-quenching processes that affect chlorophyll fluorescence. This phenomenon of decreasing NPQ during the light has been previously attributed to the consumption of the proton gradient by the activity of the CO_2 concentration mechanism (CCM)[49]. In addition to the effect arising from CCM, state transition via the induction of state 1 could also play some role in the NPQ decrease observed during HL periods, though this would not contribute during the first HL period in which cells are already in state 1 (following far-red acclimation). For fluctuating light periods longer than 4 minutes, upon a transition from HL to dark, the NPQ turned off rapidly but was then followed by a gradual rise in NPQ during further darkness, a trend that was also observed in NPQτ (Figure 5-2). However, compared to NPQ, NPQτ showed a larger magnitude of increase during the long dark periods (Figure 5-2C,D). Differences between the NPQ and NPQτ traces are considered in the discussion.

We conclude from these experiments that, when exposed to light fluctuations with HL/dark periods ranging from 1 to 10 min, at least three components of NPQ are present: (i) a rapidly responding component, (ii) a slowly inducible component induced throughout the light fluctuations, and (iii) a component induced in the dark phases of light fluctuations.

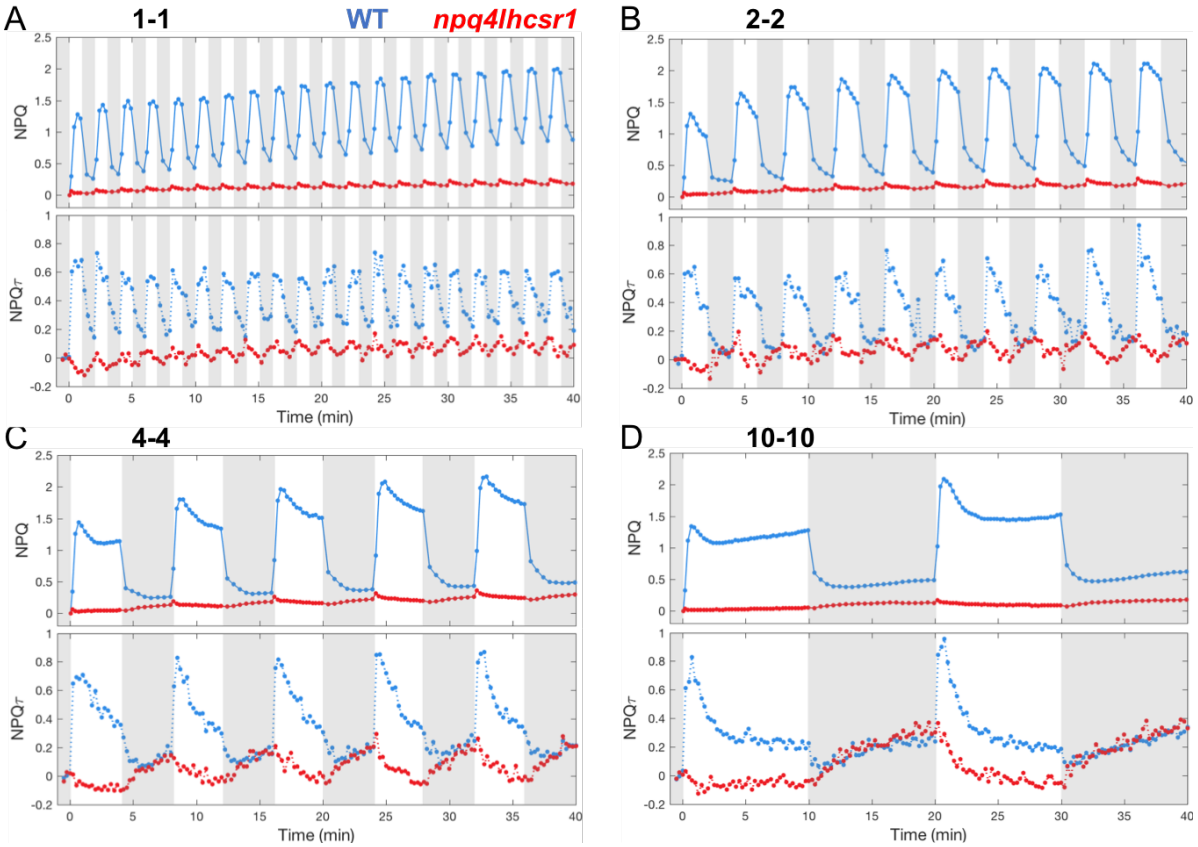

Figure 5-2. Quenching trajectories during light fluctuations in *npq4lhcsr1* and its control strain. The response of NPQ and NPQτ (upper and lower panel respectively) were measured in *npq4lhcsr1* mutant and its control strain (red and blue curves respectively) during 40 minutes of light fluctuations with HL/dark periods of 1, 2, 4 and 10 minutes (A, B, C and D respectively) as described in Figure 5-1. Shown are average of three biological replicates. For TCSPC data, each biological replicate was averaged from three technical replicates. The fluorescence lifetime values used to calculate NPQτ are shown in Figure S1.

5.4.2 The majority of NPQ during light fluctuations is mediated by LHCSR proteins.

It has been well established that LHCSR proteins are crucial for NPQ in *Chlamydomonas* during a single dark-to-light transition[18,27,50]. To examine the relative importance of each LHCSR protein for the functioning of NPQ during light fluctuations, we measured the chlorophyll fluorescence yield and lifetime during the same light-dark cycles on mutants impaired in the accumulation of LHCSR1 (*lhcsr1*)[27], LHCSR3-1 and LHCSR3-2 (*npq4*)[18], or all three LHCSRs (*npq4lhscr1*)[20,27]. While the *npq4lhcsr1* mutant was highly impaired in its NPQ capacity for all light fluctuations (Figure 5-2), single *npq4* and *lhcsr1* mutants showed some NPQ in response to light fluctuation (Figure 5-3). Noticeably, for fluctuating periods longer than 4 minutes, the increasing NPQ observed during dark phases was more pronounced in the *npq4lhcsr1* mutant (Figure 5-2). We conclude from these experiments that although LHCSRs are responsible for most of the NPQ during the light phase of all light fluctuations, a substantial portion of the NPQ in WT is nonetheless mediated by other biochemical processes, part of which is induced during the dark periods of light fluctuations.

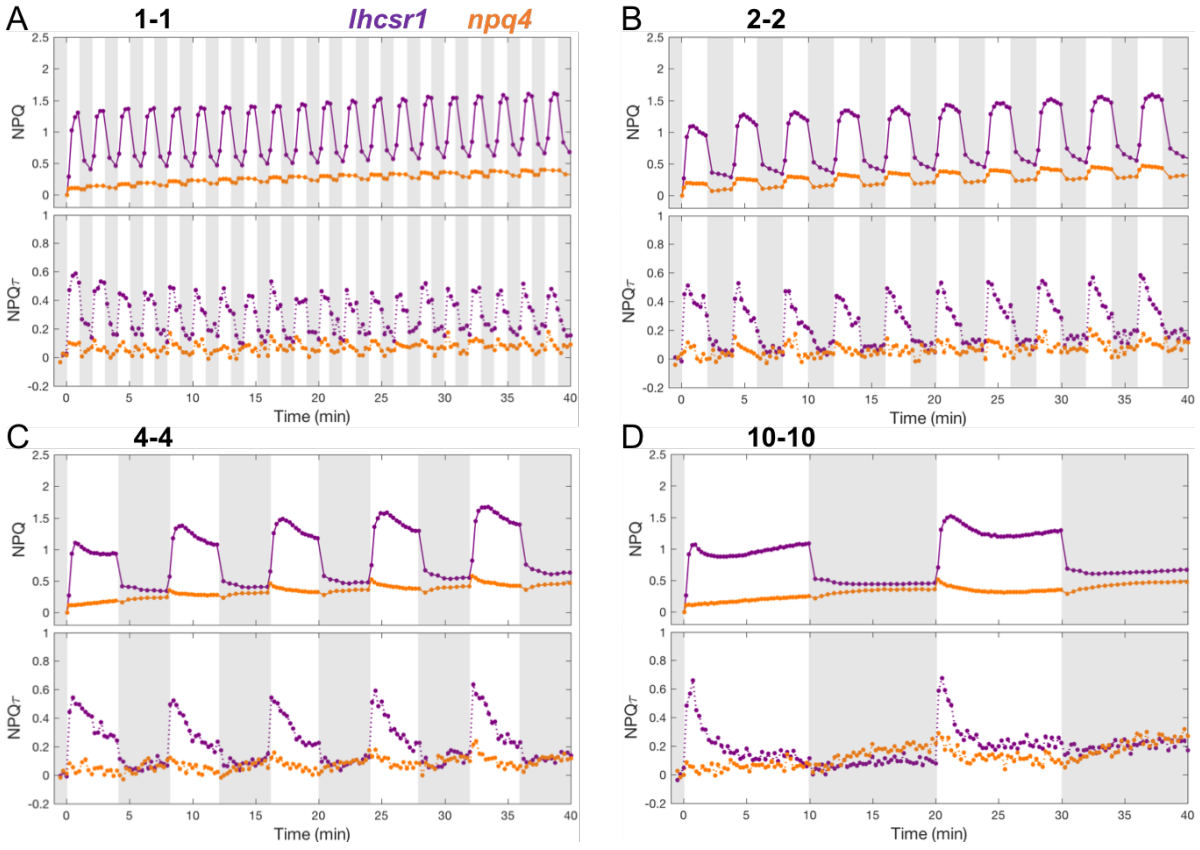

Figure 5-3. Quenching trajectories during light fluctuations in *lhcsr1* and *npq4*. The response of NPQ and NPQτ (upper and lower panel respectively) were measured in *lhcsr1* and *npq4* (purple and orange curves respectively) during 40 minutes of light fluctuations with HL/dark periods of 1, 2, 4 and 10 minutes (A, B, C and D respectively) as described in Figure 5-1. Shown are average of three biological replicates. For TCSPC data, each biological replicate was averaged from three technical replicates. The fluorescence lifetime values used to calculate NPQτ are shown in Figure S2.

5.4.3 The increasing quenching in the dark periods arises from state transition.

Induction of NPQ during darkness has been previously reported in chlorophytes[36,51], and qT has been proposed to be involved[36]. Re-organization of light-harvesting antennae between PSII and PSI was thus followed throughout a light fluctuation by measuring 77K fluorescence emission spectra. The spectra for cells were compared at three time points: after acclimation to far-red light (cells in state 1[52]), after 10 min HL, and after 10 additional min dark (see vertical lines in Figure 5-4A). In WT and *npq4lhcsr1*, an increase in the emission at 710 nm specific to PSI-bound LHCII was observed between the 10 min (after HL) and 20 min (after dark) time points, suggesting that some re-association of LHCII from PSII to PSI occurs during the dark portion of our measurements (Figure 5-4, see Figure 5-5 for replicates). In contrast, mutants lacking the STT7 kinase responsible for qT (*stt7* and *stt7npq4*) showed negligible changes in the 77K fluorescence emission spectra (Figure 5-6) and only showed a minimal increase in NPQ or NPQτ during the dark periods of light fluctuations (Figure 5-7) and with increasing duration of exposure to light fluctuations (Figure 5-8).

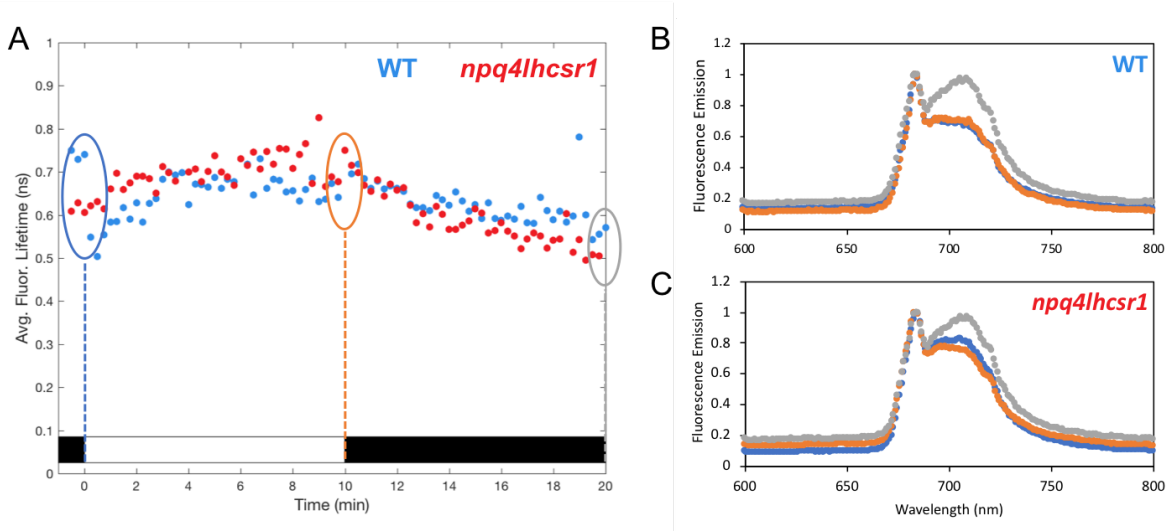

Figure 5-4. 77K chlorophyll fluorescence emission spectra during the first high light-dark cycle of light fluctuations. Cells were placed in a TCSPC cuvette as described in Figure 5-1 and both fluorescence lifetime snapshots and 77K chlorophyll fluorescence emission spectra were taken through 10 minutes of high light and 10 minutes darkness. (A) Fluorescence lifetime trajectory of *npq4lhcsr1* mutant (red dots) and its control strain (WT, blue dots). On the graph, dashed vertical lines depict the timepoints at which samples were taken for 77K fluorescence spectra measurement. (B, C) 77K fluorescence emission spectra of samples taken in A on the control strain (WT, B) and *npq4lhcsr1* mutant (C). Spectra were taken at 0, 10, and 20 min timepoints (blue, orange and grey spectra respectively). Shown are representative spectra. Three independent biological replicate spectra for WT and npq4lhcsr1 are shown in Figure 5-5. 77K spectra for the stt7 and stt7npq4 strains are shown in Figure 5-6.

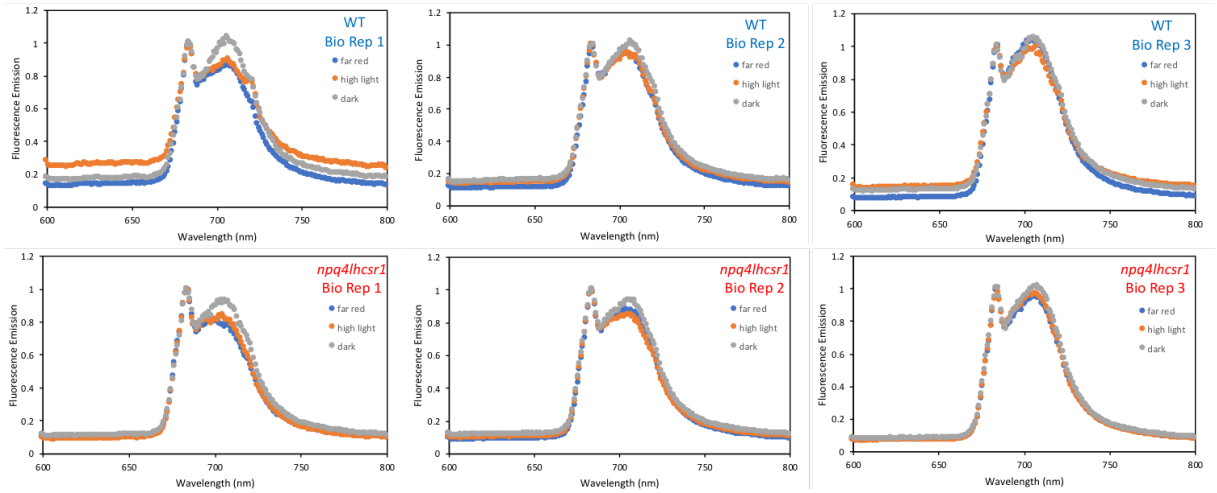

Figure 5-5. Independent biological replicates of 77K fluorescence emission spectra for WT and *npq4lhcsr1*. Within each graph, the spectra colored in blue, orange, and gray represent those taken at 0 min (far-red acclimated), 10 min (HL-exposed cells), and 20 min (dark-exposed cells) timepoints, respectively. Samples were taken under PAM conditions.

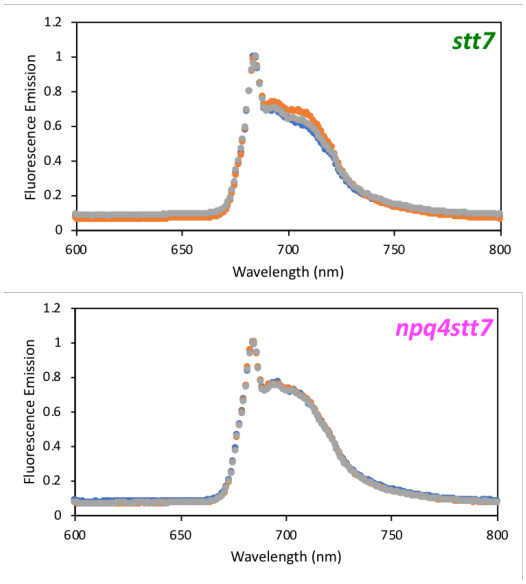

Figure 5-6. Representative 77K fluorescence emission spectra for *stt7* and *npq4stt7* strains. For each strain, the spectra colored in blue, orange, and gray represent those taken at 0 min (far-red acclimated), 10 min (HL-exposed cells), and 20 min (dark-exposed cells) timepoints, respectively. Samples were taken under TCSPC conditions.

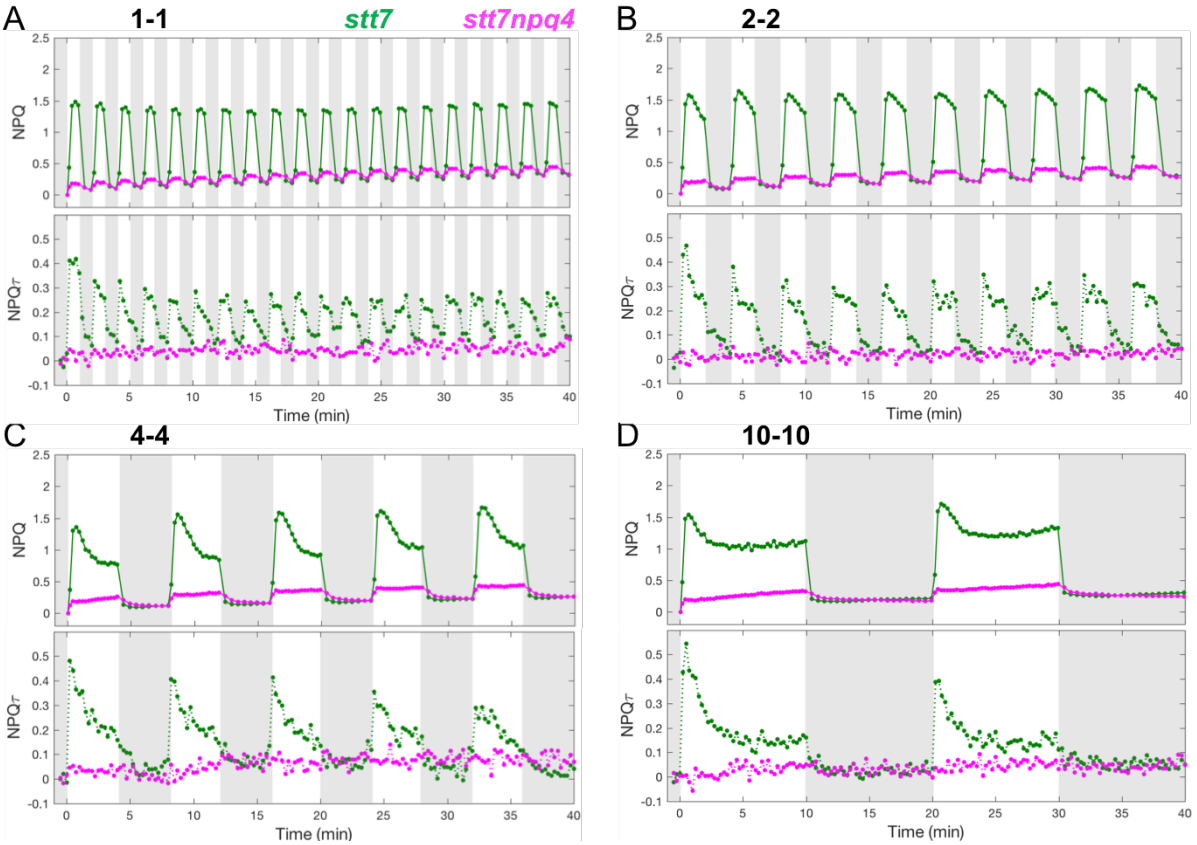

Figure 5-7. Quenching trajectories during light fluctuations in *stt7* and *stt7npq4*. The response of NPQ and NPQτ (upper and lower panel respectively) were measured in *stt7* and *stt7npq4* (green and magenta curves respectively) during 40 minutes of light fluctuations with HL/dark periods of 1, 2, 4 and 10 minutes (A, B, C and D respectively) as described in Figure 5-1. Shown are average of three biological replicates. For TCSPC data, each biological replicate was averaged from three technical replicates. The fluorescence lifetime values used to calculate NPQτ are shown in the Figure S3.

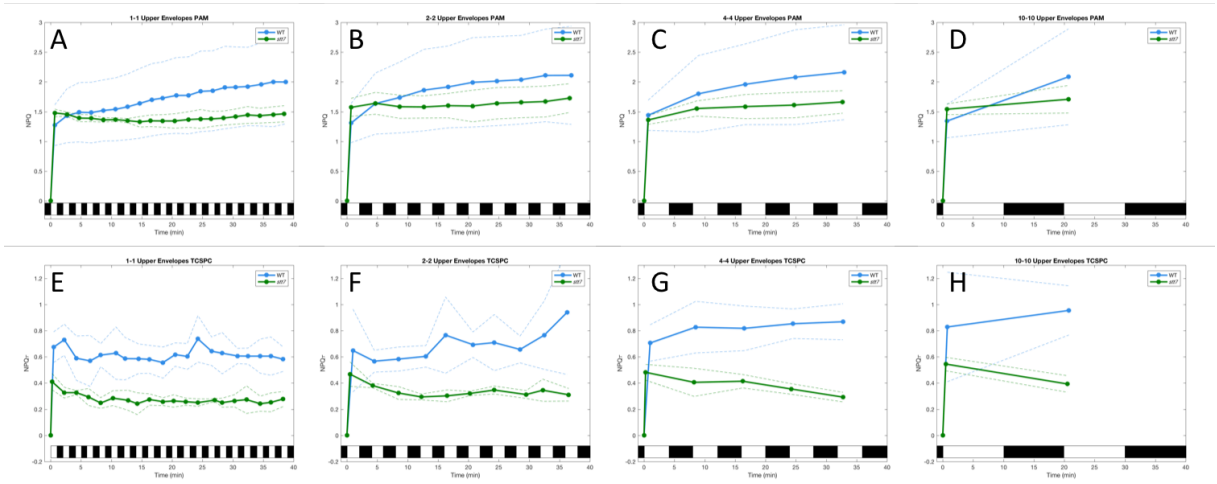

Figure 5-8. Maximum quenching envelopes defined by the maximum values of NPQ (measured by PAM, A-D) or NPQτ (measured by TCSPC, E-H) during every high light period for WT (blue) and *stt7* (green). Solid lines denote the experimental data points, while dashed lines above and below the curves show the addition and subtraction of the experimental standard deviation. Note that when comparing the envelopes between the two measurement techniques, there are qualitative differences in the envelope structure. In the case of the PAM measurements, WT shows a maximum NPQ value that gradually increases as light fluctuations progress (due to activation of qT as the experiment progresses), while *stt7* shows no such increase (due to the absence of qT). For TCSPC measurements, WT shows a maximum NPQτ value that is relatively flat as light fluctuations progress (includes the effects of qT), while *stt7* shows a slightly decreasing quenching envelope (due to the absence of qT).

To characterize the kinetics of qT occurring during the light-to-dark transition, we analyzed the response of the chlorophyll fluorescence lifetime for WT and *npq4lhcsr1* mutant cells that were exposed to 10 min of HL followed by 30 min of dark. Interestingly, upon light-to-dark transition, both strains showed steadily decreasing lifetimes for the first 10 min of darkness, after which, the fluorescence lifetimes began to reverse, eventually reaching the starting lifetime after 30 minutes of darkness (Figure 5-9). In contrast, *stt7* showed no such quenching of fluorescence lifetime during the 10 min dark period. Therefore, we conclude that the quenching observed during the dark phases of light fluctuations in *Chlamydomonas* arises from qT, which has an induction timescale of about 10 min and is reversible upon continued exposure to darkness.

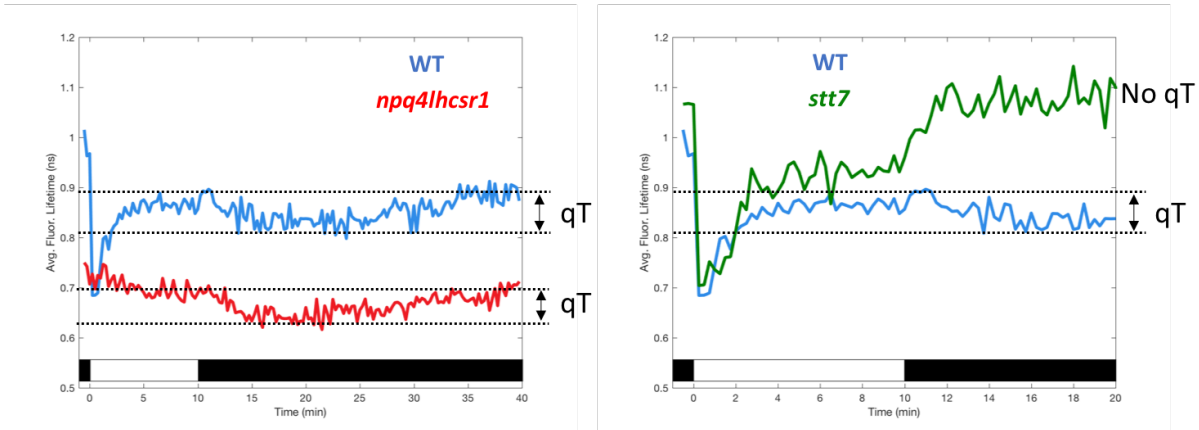

Figure 5-9. Kinetics of qT measured by TCSPC. Following 15 min of far-red acclimation, cells were exposed to 10 min of HL followed by 30 min of darkness (left panel) or 10 min HL followed by 10 min of darkness (right panel). WT is shown in blue, *npq4lhcsr1* in red, and *stt7* in green. Each lifetime trajectory is the average of 3 biological replicates where each biological replicate is average of 3 technical replicates. Dashed horizontal lines highlight the extent of the decreasing lifetime observed upon HL-to-dark transition in STT7-containing lines. Note that after 10 to 15 min of quenching (evidenced by the decreasing average fluorescence lifetimes in each strain), the quenching then begins to turn off and eventually returns to the starting lifetime. The *stt7* mutant shows no such decrease in lifetime during a 10-minute dark period.

5.4.4 Contributions of qE and qT to NPQ and growth under fluctuating light.

It has been previously proposed that, while LHCSRs play an important role during short periods of illumination, state transitions are important for longer periods of high light acclimation[4]. To test this hypothesis and assess the scenario under fluctuating light conditions, we quantified the amount of NPQ that was mediated by each protein by comparing the remaining NPQ (or NPQτ) in each mutant relative to the NPQ (or NPQτ) in the WT reference strain (Figure 5-10A, Table 5-1). Surprisingly, the contribution of each protein to overall NPQ did not seem to depend on the period of the light fluctuation (Figure 5-11). Therefore, as a first estimate for the contribution of LHCSRs and STT7, we calculated the average contribution under all four light fluctuation sequences. The donut charts in Figure 5-10B,C,D depict the contribution of each protein as a percentage of the total NPQ observed in the WT strain (represented as the complete donut). While LHCSR3 is responsible for the majority of overall NPQ (72%, Figure 5-10B), STT7 had a substantial contribution mediating 42% of the NPQ, with LHCSR1 having a smaller contribution at 22% of NPQ. LHCSRs were found to have a substantially larger contribution during light phases, where they are responsible for 94% of WT NPQ, while in the dark phases, their contribution declined to 57% (Figure 5-10C, Figure 5-12). On the other hand, STT7 played a significantly larger role in the NPQ during darkness (60%) than it does during illumination (36%) this latter result being likely due to inhibition of STT7 by high light[36,53,54]. Interestingly, the amount of NPQ mediated by LHCSRs was more important during the beginning of light fluctuations while state transitions contributed more after 20 minutes of light fluctuation (Figure 5-10D, Figure 5-13), revealing increased relative contribution of qT and decreasing contribution of qE with increasing time of exposure to light fluctuations.

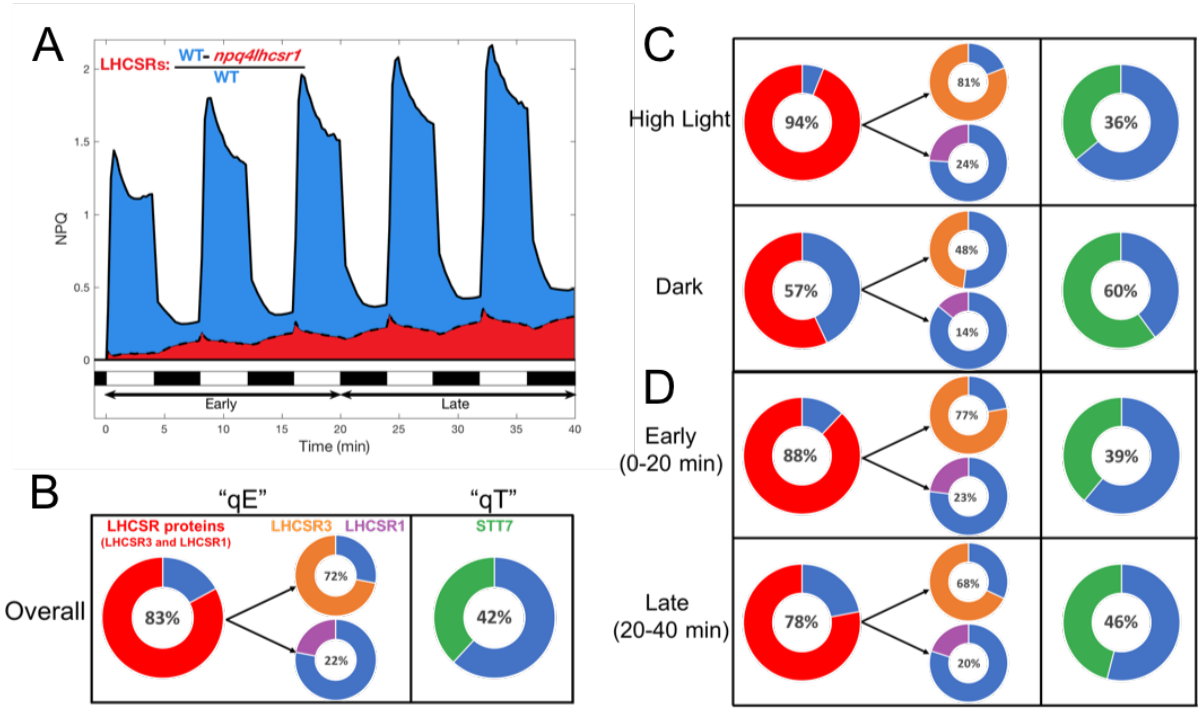

Figure 5-10. Quantification of the contribution of LHCSRs and STT7 to wild-type NPQ under fluctuating light. (A) Example of quantification of the relative NPQ mediated by LHCSRs. The area under the NPQ curve of *npq4lhcsr1* mutant (red) was subtracted from that of the control strain (blue) and expressed relative to the area of NPQ of the control strain. (B, C) Overall contribution of LHCSRs (red), LHCSR3 (orange), LHCSR1 (purple) and STT7 (green) averaged over all 40 minutes (B) or specific periods of the light fluctuations (C). For each protein, the part of the donut shown in red, orange, purple or green is the percentage of wild type NPQ lost in each mutant impaired in the accumulation of LHCSRs, LHCSR3, LHCSR1 and STT7 respectively. Given that the contribution of each protein was largely independent of HL/dark period (Figure 5-12), shown are the average of all 4 light fluctuation sequences. Distribution of individual replicates and estimates of error (i) overall, (ii) during HL or dark, and (iii) during early and late portion of light fluctuations are presented in Figures 5-11, 5-12, and 5-13, respectively.

Table 5-1. Average contribution of each protein to overall wild-type NPQ for each light fluctuation sequence. Shown is the average value (n=6, evaluated from 3 TCSPC and 3 PAM replicates) and standard deviation of all individual replicates. The contributions of LHCSR3 (orange) and LHCSR1 (purple) were determined from the single mutants *npq4* and *lhcsr1*. The contribution of LHCSRs overall (red) was evaluated from the *npq4lhcsr1* mutant. The contribution of qT was assessed from the *stt7* mutant. Each error in the right column represents the standard deviation of each protein's contribution across the 4 light fluctuation sequences. For simplicity, only the average values (shown in the right column) were used to generate Figure 5-10. Full distributions of the individual TCSPC and PAM data points are shown in Figure 5-11.

Overall Contributions	1-1	2-2	4-4	10-10	AVERAGE
LHCSRs	89 ± 7%	84 ± 7%	83 ± 13%	77 ± 24%	83 ± 5%
LHCSR1	22 ± 12%	22 ± 10%	24 ± 16%	19 ± 30%	22 ± 2%
LHCSR3	81 ± 5%	78 ± 5%	73 ± 8%	58 ± 15%	72 ± 10%
STT7	46 ± 12%	38 ± 16%	46 ± 13%	39 ± 22%	42 ± 4%

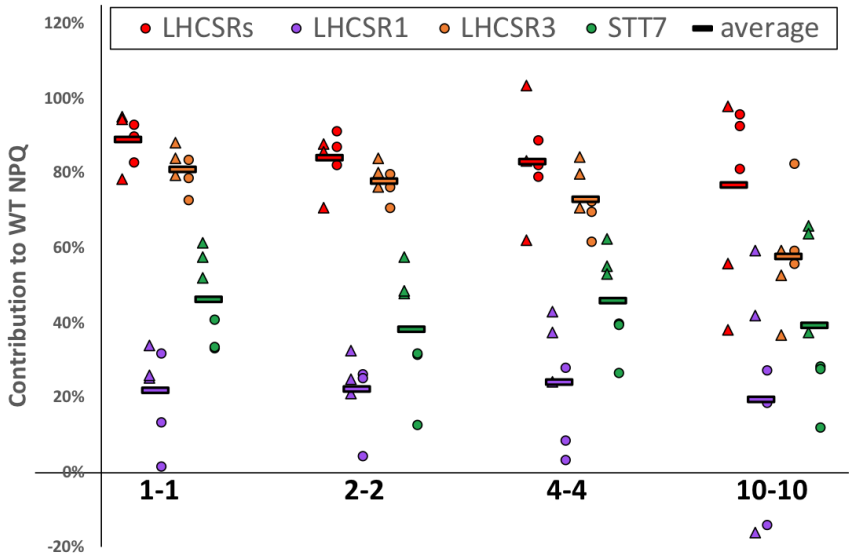

Figure 5-11. Distribution of replicate measurements for the contribution of each protein to overall WT NPQ as a function of fluctuating light sequence. Each data point represents the percentage of the WT NPQ that is lost in each mutant following integration of the trajectories of NPQ (measured by PAM, *circles*) or NPQτ (measured by TCSPC, *triangles*). The contribution of each protein is colored according to the respective mutant that was used for quantification relative to WT (*red,* LHCSRs from *npq4lhcsr1*; *purple*, LHCSR1 from *lhcsr1*; *orange*, LHCSR3 from *npq4*; *green*, STT7 from *stt7*). Within each colored cluster, the triangles represent the 3 biological replicates measured by TCSPC (each biological replicate is the average of 3 technical replicates) and the circles represent the 3 biological replicates measured by PAM. The colored horizontal lines represent the average of all TCSPC and PAM data points for each protein.

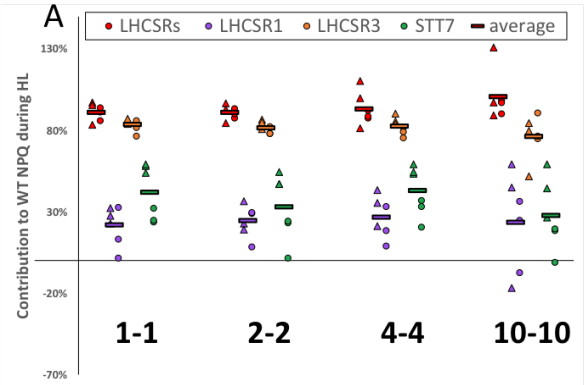

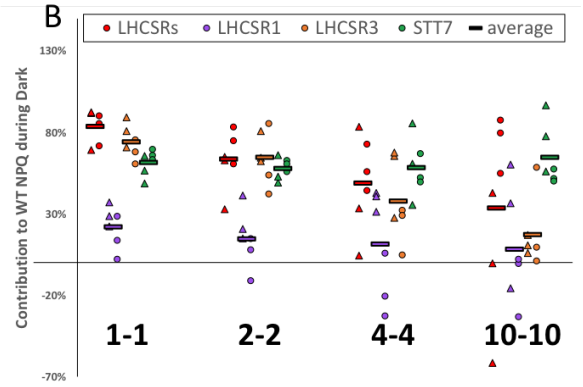

HL Contributions	1-1	2-2	4-4	10-10	AVERAGE
LHCSRs	91 ± 5%	91 ± 4%	93 ± 10%	100 ± 15%	94%
LHCSR1	22 ± 12%	24 ± 10%	27 ± 13%	23 ± 30%	24%
LHCSR3	83 ± 4%	82 ± 4%	82 ± 5%	74 ± 13%	81%
STT7	42 ± 17%	33 ± 20%	43 ± 15%	28 ± 21%	36%

Dark Contributions	1-1	2-2	4-4	10-10	AVERAGE
LHCSRs	83 ± 10%	62 ± 17%	49 ± 28%	34 ± 56%	57%
LHCSR1	22 ± 13%	15 ± 17%	11 ± 33%	8 ± 35%	14%
LHCSR3	74 ± 10%	65 ± 16%	38 ± 25%	17 ± 21%	48%
STT7	61 ± 7%	58 ± 6%	58 ± 17%	65 ± 19%	60%

Ratio HL/Dark	1-1	2-2	4-4	10-10	AVERAGE
LHCSRs	1.09	1.43	1.91	2.99	1.86
LHCSR1	0.99	1.66	2.41	2.87	1.98
LHCSR3	1.13	1.26	2.19	4.48	2.27
STT7	0.68	0.57	0.73	0.43	0.60

Ratio >1: larger role in HL
Ratio <1: larger role in Dark

Difference HL -Dark	1-1	2-2	4-4	10-10	AVERAGE
LHCSRs	7.8%	27.5%	44.3%	66.8%	37%
LHCSR1	-0.3%	9.6%	15.6%	15.3%	10%
LHCSR3	9.3%	16.9%	44.9%	59.2%	33%
STT7	-19.5%	-24.9%	-15.4%	-37.0%	-24%

Positive: larger role in HL
Negative: larger role in Dark

Figure 5-12. Distribution of replicate measurements for the contribution of each protein to WT NPQ during HL (A) or dark (B) as a function of fluctuating light sequence. The tables below show the ratio of the contribution of each protein during HL to dark (obtained by dividing the two values) or the difference in contribution in HL and dark (obtained by subtracting the two values). All other details are as described in Figure 5-11.

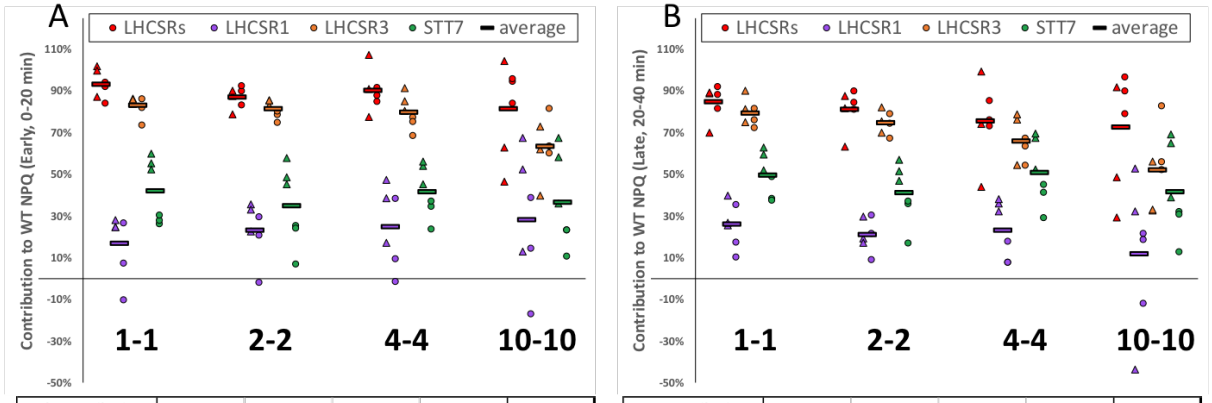

Early Contributions	1-1	2-2	4-4	10-10	AVERAGE
LHCSRs	93 ± 7%	87 ± 5%	90 ± 10%	81 ± 22%	88%
LHCSR1	17 ± 15%	23 ± 14%	25 ± 19%	28 ± 31%	23%
LHCSR3	83 ± 5%	81 ± 4%	80 ± 8%	63 ± 14%	77%
STT7	42 ± 16%	35 ± 19%	42 ± 12%	36 ± 22%	39%

Late Contributions	1-1	2-2	4-4	10-10	AVERAGE
LHCSRs	85 ± 8%	81 ± 9%	75 ± 18%	72 ± 27%	78%
LHCSR1	26 ± 11%	21 ± 8%	23 ± 14%	12 ± 34%	20%
LHCSR3	79 ± 6%	75 ± 6%	66 ± 10%	52 ± 18%	68%
STT7	50 ± 11%	41 ± 14%	51 ± 16%	41 ± 22%	46%

Ratio Early/Late	1-1	2-2	4-4	10-10	AVERAGE
LHCSRs	1.10	1.07	1.20	1.12	1.12
LHCSR1	0.65	1.10	1.07	2.43	1.31
LHCSR3	1.04	1.09	1.21	1.21	1.14
STT7	0.85	0.85	0.82	0.88	0.85

Ratio >1: larger role early
Ratio <1: larger role later

Difference Early-Late	1-1	2-2	4-4	10-10	AVERAGE
LHCSRs	8.2%	5.8%	14.7%	8.7%	9%
LHCSR1	-9.1%	2.1%	1.6%	16.5%	3%
LHCSR3	3.6%	6.5%	13.8%	11.1%	9%
STT7	-7.7%	-6.3%	-9.0%	-5.0%	-7%

Positive: larger role early
Negative: larger role late

Figure 5-13. Distribution of replicate measurements for the contribution of each protein to WT NPQ during the early portion (0-20 min, A) or during the later portion of the experiment (20-40 min, B) as a function of fluctuating light sequence. The tables below show the ratio of the contribution of each protein during HL to dark (obtained by dividing the two values) or the difference in contribution in HL and dark (obtained by subtracting the two values). All other details are as described in Figure 5-11.

Since LHCSR3 is part of the mobile fraction of photosynthetic antenna and has been proposed to be affected by STT7 activity[36], giving a potential mechanistic connection between qE and qT[55], we aimed to interrogate the involvement of qT both together and separately from qE under fluctuating light. We compared the integrated PAM NPQ trajectories of *npq4stt7* relative to that of *npq4*, both of which lack LHCSR3, or *npq4stt7* relative to that of *stt7*, both of which lack STT7. The relative contribution of STT7 to NPQ was found to be different in the presence vs absence of LHCSR3, with STT7 playing a larger role when LHCSR3 is present (Figure 5-14, Table 5-2). Likewise, the contribution of LHCSR3 was larger when STT7 was present. These data suggest that STT7 and LHCSR3 are cooperating to induce quenching during dark periods of light fluctuations. We propose that the activity of STT7 resulting in LHCSR phosphorylation and antenna mobility is responsible for this crosstalk between qE and qT during light fluctuations.

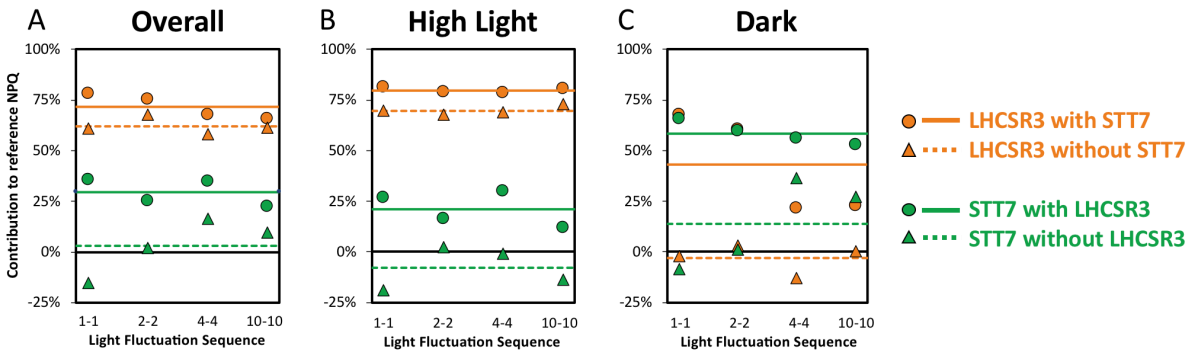

Figure 5-14. Untangling qE and qT: the quantification of the contributions of LHCSR3 (orange) and STT7 (green) to the NPQ response both in the presence (solid lines, circle markers) and absence (dashed lines, triangle markers) of the other protein is plotted as a function of the light fluctuation frequency. Horizonal lines, show the average contribution for each protein, considering all light fluctuation frequencies. For reference, the black lines represent zero contribution. The contribution of each protein was evaluated (A) over all 40 minutes of the experiment, (B) only during HL periods, or (**C**) only during dark periods. All of these were evaluated from PAM trajectories using various combinations of WT along with the *npq4*, *stt7*, and *stt7npq4* mutants as discussed in the Materials and Methods section.

Table 5-2. Average contribution of LHCSR3 and STT7 in the presence and absence of the other protein for each light fluctuation sequence. Shown is the average value (evaluated from 3 PAM replicates) and standard deviation of individual replicates. Each error in the right column represents the standard deviation of the 4 light fluctuation sequences.

Overall Contributions	1-1	2-2	4-4	10-10	AVERAGE
LHCSR3 w/ STT7	78 ± 5%	75 ± 5%	67 ± 6%	66 ± 14%	72 ± 6%
LHCSR3 w/out STT7	61 ± 5%	67 ± 4%	58 ± 3%	61 ± 3%	62 ± 4%
STT7 w/ LHCSR3	36 ± 4%	25 ± 11%	35 ± 8%	22 ± 9%	29 ± 7%
STT7 w/o LHCSR3	-16 ± 15%	2 ± 12%	16 ± 5%	9 ± 6%	2 ± 14%

Although mutants impaired in the accumulation of LHCSRs and STT7 have strongly impaired NPQ capacities, this does not seem to impair the growth of those strains under continuous high light conditions[18,28,46]. Recent data have shown that the growth of npq4 and npq4lhcsr1 mutants is impaired under certain light fluctuation conditions[6,46]. We therefore investigated whether the growth impairment of those strains could be dependent on the period of light fluctuation. While all the mutants grew as well as the control strain under continuous illumination (Figure 5-15), *npq4*, *lhcsr1*, *npq4lhcsr1* and *stt7npq4* mutants exhibited impaired growth under fast light fluctuations with a 1-minute period (Figure 5-16). In contrast, only *npq4lhcsr1* and *stt7npq4* mutants showed an impaired growth under slower light fluctuations with a period of 10 minutes, and the growth of all mutants was similar when the period was increased to 30 minutes (Figure 5-16). We conclude from this experiment that qE mediated by LHCSR proteins is critical for growth under light fluctuations and that this role is more important for rapid light fluctuations.

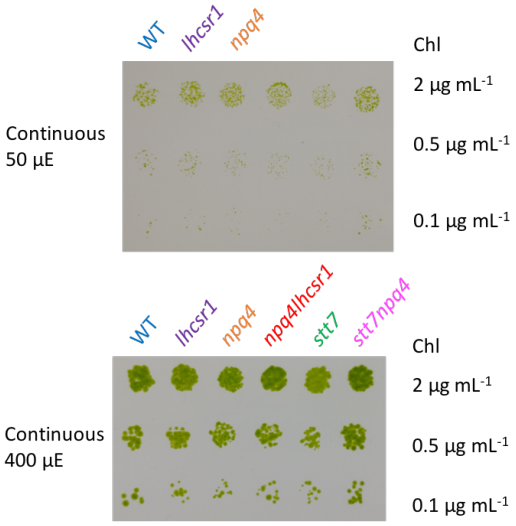

Figure 5-15. Growth of cells under continuous low light (50 µE) or high light (400 µE) conditions. All other details are as described in Figure 5-16 and in the Methods.

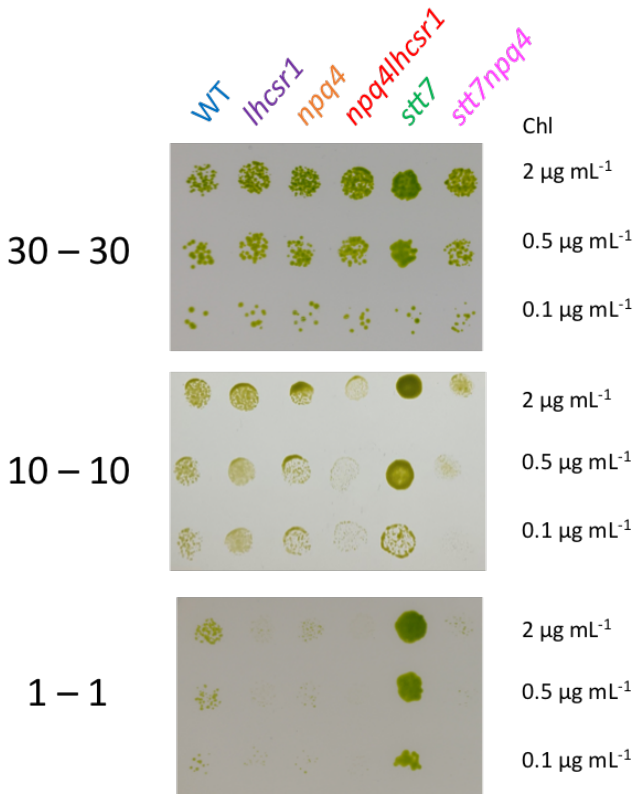

Figure 5-16. Growth of mutants impaired in qE and/or qT under various periods of dark/light cycles. *lhcsr1*, *npq4*, *npq4lhcsr1*, *stt7* and *stt7npq4* mutants and their control strain (WT) were diluted and spotted at different chlorophyll concentration and grown on plates under dark/light cycles with a period of 30 (30-30, upper panel), 10 (10-10, middle panel) or 1 minute (1-1, lower panel). Each row represents a different chlorophyll concentration. Shown are representative spots of three biological replicates. Growth under constant low light or high light are shown in Figure 5-15.

5.5 Discussion

The involvement of pH-sensing LHCSR proteins and state transitions in the photoprotective response of *Chlamydomonas* has been previously described[18,36]. While mutants impaired in accumulation of LHCSRs were shown to have limited growth when light is provided in a day/night cycle[46] or fluctuating with a 10-minute period[6], our understanding of the contribution of LHCSRs and state transitions to photoprotection during fluctuating light remains limited. Here, by measuring the NPQ levels during light fluctuations in a range of mutants impaired in the accumulation of LHCSR3, LHCSR1, and/or STT7 we have unraveled their relative contributions to NPQ. Varying the length of fluctuating periods from 1 to 10 min allowed us to assess the dynamics of rapid qE- and slower qT-type processes. Interestingly, we observe that qT builds up during the dark periods of the light fluctuations and continues to play a role in the NPQ response during subsequent light phases. It occurs even in the absence of LHCSR3 (see *npq4* and *npq4lhcsr1* mutant in Figure 5-2 and Figure 5-4), has a timescale of 10 min, and is reversible (Figure 5-9), which is consistent with recent literature[36,52]. During a transition between low-light and high-light stress, qE proteins take a few hours to be fully induced[18], and it was hypothesized that qT may substitute for qE during this delay[36]. Our results show that even when LHCSRs are fully activated (i.e., in high light-acclimated cells), the occurrence of qT remains substantial during light fluctuations (Figure 5-2). State transition or qE mutants were previously shown to have high reactive oxygen species (ROS) production[36,56]. Thus, the substantial amount of qT induced during the dark periods of light fluctuations may enhance photoprotection and limit ROS production by "anticipating" the next exposure to high light. The combination of fast qE (turns on rapidly upon HL exposure due to ΔpH) and residual qT (from previous dark periods) could therefore provide effective photoprotection in an unpredictable fluctuating-light environment.

Since qE has long been ascribed as the fastest component of NPQ, directly responding to the thylakoid lumen proton concentration[7], and qT as a slower component[36], the contribution of qE to NPQ was proposed to be stronger for short periods of HL, with the contribution of qT becoming increasingly important during longer periods of high-light stress[4]. Our approach of systematically assessing the response of photosynthesis to various frequencies of light fluctuations has revealed nuances in this interpretation. Surprisingly, we found that the overall contributions of qE and qT are different in the presence vs absence of the other component (Figure 5-14) revealing that interactions between qE and qT contribute to the NPQ response during light fluctuations. Additionally, the *npq4* mutant showed significantly reduced NPQ capacity compared to WT in the dark periods (by 74%) under fast light fluctuations (1-1 sequence), but only a 17% impairment under slower fluctuations (10-10) (see Figure 5-12B), showing that relaxation of qE (around 1 min) is mediated by LHCSR3 and contributes substantially to the response of NPQ to rapid light fluctuations. Such relaxation kinetics may contribute to a faster response of NPQ to the next illumination if the time scale of light fluctuations is shorter than 2 minutes. It is also worth noting that the relative importance of qE in NPQ decreased after 20 minutes of light fluctuations, while the opposite occurred for qT (Figure 5-10), reflecting a build-up in qT throughout the 40 minutes of light fluctuations. Modeling the response of photosynthesis to complex light fluctuations has been done[35,41,43,57,58] and would allow targeting specific mechanisms for increasing plant yields in the field. Our results show that such efforts should consider both the period of light and dark as well as the total time exposed to fluctuating light. The light intensities used during light fluctuations may also affect the relative contributions of each mechanism. In green microalgae it

is tempting to speculate that in nature, where exposure to HL and dark occur repeatedly, qE may play a more important role in the beginning of light fluctuations while qT may provide a photoprotective response on a longer time scale.

Although qI is known to contribute to NPQ during prolonged illumination, it is likely negligible in our experimental conditions since both *npq4lhcsr1* and *npq4stt7* mutants did not show a strong buildup of NPQ or NPQτ during the 20 min of HL exposure during the light fluctuations (Figure 5-3 and Figure 5-7). Additionally, Fv/Fm were not significantly different between strains prior to light fluctuations, with the exception of *npq4lhcsr1* which showed a lower Fv/Fm, reflecting some constitutive qI following overnight HL acclimation in the complete absence of LHCSRs (Figure 5-17).

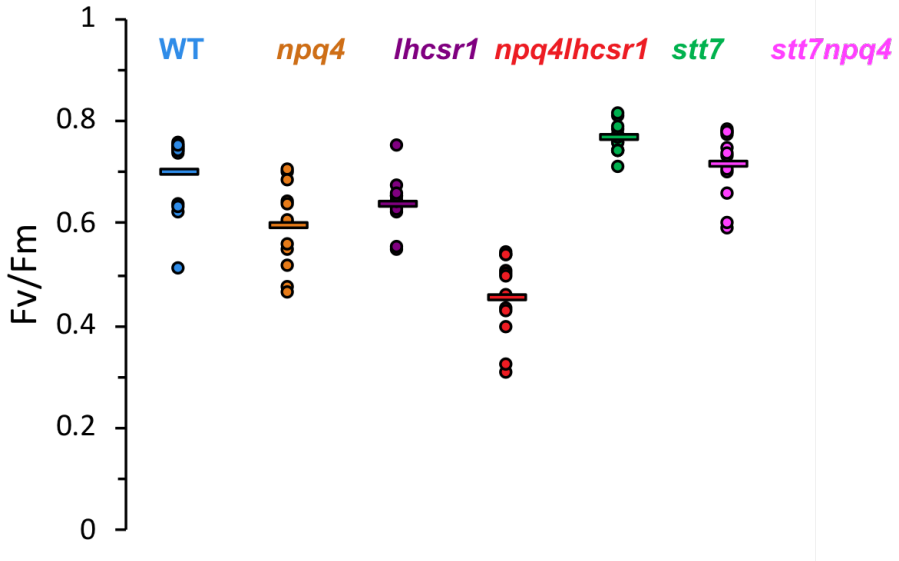

Figure 5-17. Fv/Fm values for each strain measured prior to exposure to fluctuating light sequences. Circles represent independent biological replicates. Horizontal lines show the average of 12 replicate measurements.

Interestingly, when comparing NPQ and NPQτ, the magnitude of the quenching decrease during HL was larger for NPQτ than NPQ (Figure 5-2). The energetic requirement (and thus its proton gradient consumption) of the CCM depends on the inorganic carbon (C_i) availability[59]. Since the high cell concentration in the TCSPC sample leads to strong C_i consumption, this could deplete the C_i concentration even in the presence of bubbling, leading to a C_i level sensed by cells in the TCSPC sample being lower than what is experienced by cells in the PAM sample. This would lead to higher activity of CCM, and hence a larger decrease in quenching, under TCSPC sample conditions compared to PAM sample conditions. The decrease in both NPQ and NPQτ was also stronger for longer HL periods as well as later in the sequence (Figure 5-2). The slope of the initial decrease in NPQτ or NPQ during HL was similar for all four sequences (Figure 5-18) and is likely dictated by C_i availability and its influence on the CCM kinetics. The magnitude of the decrease in NPQ and NPQτ was larger for longer light periods (Figure 5-18D,H), likely due to simultaneous activation of the CCM that dissipates the proton gradient and the onset of slower forms of NPQ such as state transitions. Conversely, the differences in the magnitude of the increase in NPQ and

NPQτ during the dark periods could be due to differences in O_2 concentrations sensed by the cells in both conditions, which is known to affect the extent and rate of state transition[60].

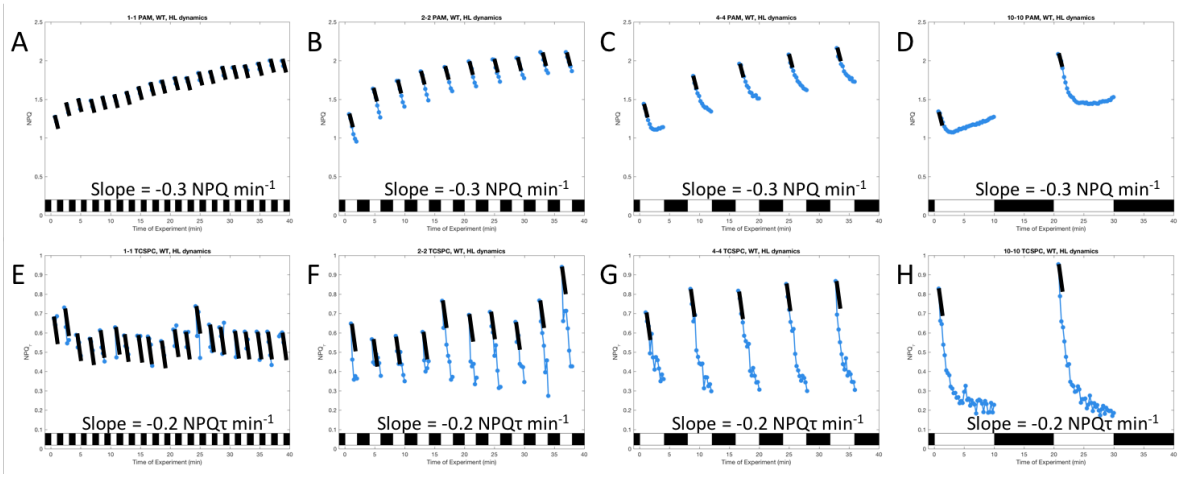

Figure 5-18. Analysis of the kinetics associated with the decrease in NPQ (measured by PAM, A-D) or NPQτ (measured by TCSPC, E-H) during every high light (HL) period for the WT strain. Within each HL period, the maximum value of NPQ (or NPQτ) and all subsequent data points after the maximum are shown (blue circles). Superimposed are solid black line segments. These lines segments have identical length and slope for panels A-D (PAM) and E-H (TCSPC). The line segments adequately capture the decrease of NPQ or NPQτ in each HL period, corresponding to approximate rates of 0.3 units of NPQ per minute (A-D, PAM) and 0.2 units of NPQτ per minute (E-H, TCSPC). As the fluctuating light period increases, a larger extent of the decrease in both NPQ and NPQτ is observed.

Although LHCSR3 plays the dominant role in photoprotection under constant and fluctuating light conditions, we also observe a role for LHCSR1 in our measurements. While the chlorophyll fluorescence dynamics of *lhcsr1* are similar to those of WT (Figure 5-3), we observe a ~20% reduction in overall NPQ in this mutant under fluctuating light conditions (Figure 5-10). This small amount of photoprotection afforded by LHCSR1 *in vivo* is consistent with previous *in vitro* investigations[61,62] in which LHCSR1 has been suggested to mediate energy transfer between LHCII and PSI[63] and to compensate for the absence of LHCSR3[33]. Interestingly, our results suggest that different from the case for LHCSR3, the qE that is mediated by LHCSR1 is largely frequency independent (Figure 5-11). Both LHCSR1 and LHCSR3 are thought to generate NPQ in response to (i) the proton gradient and (ii) carotenoid composition,[23,24] thus the frequency-dependent LHCSR3 and frequency-independent LHCSR1 could differ in their pH or carotenoid dependency.

The relationship between NPQ capacities and growth have remained puzzling in *Chlamydomonas*, because only some light fluctuation regimes have consistently been shown to impair growth[6,18,27,46]. Here we show that all mutants lacking LHCSRs showed impaired growth under rapid light fluctuations (1-1 sequence), and that this impairment was lower under slower fluctuations (10-10 sequence) and absent under an even slower 30-30 sequence or constant illumination (Figures 5-15 and 5-16). There seems to be a good relationship between defect of NPQ and growth deficiency under short time-scale fluctuations when considering *npq4lhcsr1* and *stt7npq4* mutants (Figure 5-16), clearly showing that LHCSR-dependent qE is critical for growth when light fluctuates rapidly over a short period of time. However, surprisingly, the growth defect of *lhcsr1* seemed larger than *npq4* under the 1-1 sequence. This suggests that the growth capacity

of LHCSR mutants under light fluctuations may not depend only on the level of NPQ. The growth defects observed for qE mutants under short time-scale light fluctuations may be affected by deactivation of the Calvin-Benson-Basham (CBB) cycle during the dark phases, as previously proposed by Roach[6]. Such a frequency dependence for the growth may thus additionally reveal the specific time scales of CBB cycle activation and deactivation during extended periods of fluctuating light. Other factors may include activation of compensatory mechanisms that enable photoprotection at the expense of growth or the increased production of reactive oxygen species in *npq4* mutants[6,56], which could be greater in the *lhscr1* mutant. Note here that in our conditions, due to slightly different genetic background between *stt7* and the WT control, we cannot make a conclusion on the mechanism by which *stt7* grew better under short timescale fluctuations (Figure 5-16). The WT background may be particularly sensitive to fast 1-1 and 10-10 fluctuations; another possibility could be that qT is detrimental for growth under medium to short time scale fluctuations.

Through 77K fluorescence emission spectra analysis, we have shown that the increasing dissipation observed in the dark requires the STT7 kinase responsible for state transition (Figure 5-4 and Figure 5-6). This effect, already described in *Chlamydomonas*[36] and *Dunaliella salina*[51], greatly contributes to NPQ during light fluctuations. In plants, the occurrence of state transitions and its involvement in NPQ is thought to be minor[8,31] even if mutants of *Arabidopsis thaliana* impaired in state transition (*stn7*) exhibit impaired growth under light fluctuations[64]. Interestingly, an increase of NPQ during the dark periods of fluctuating light was recently reported in *npq4* leaves of *A. thaliana*[43] for which about 53% of the WT NPQτ remained in the mutant after 40 minutes of exposure to light fluctuations despite the absence of the pH-sensing protein PsbS (Figure 5-19). However, it remains unclear as to how much of the dark quenching in plants originates from qT as opposed to effects related to de-epoxidized xanthophyll pigments[43] or LHC protein conformation and/or aggregation[65]. In the future, periodic illumination experiments performed on A. thaliana mutants impaired in qE and/or qT could clarify the relative importance of each mechanism and allow a comparison of the *in vivo* functioning of NPQ in higher plants and green algae under light fluctuations.

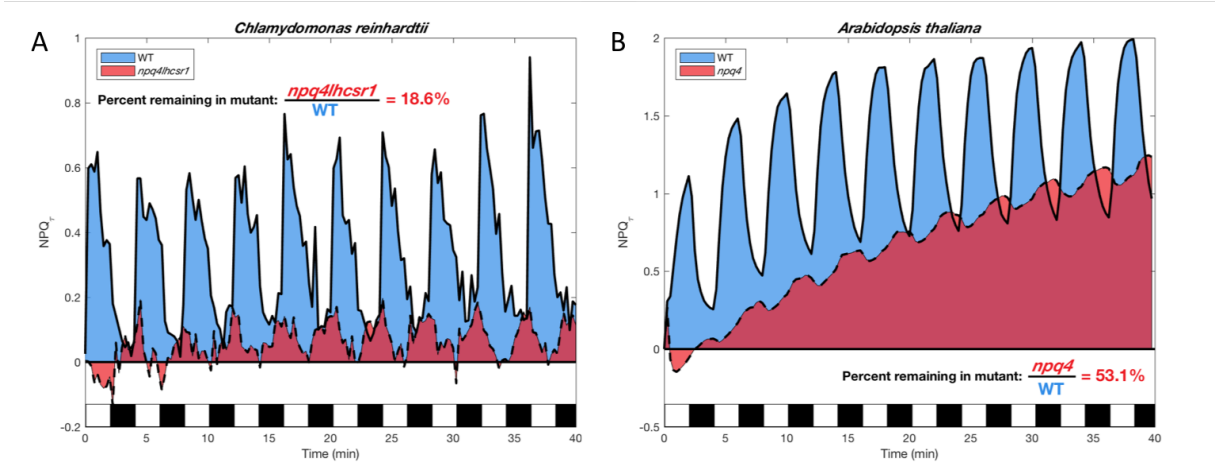

Figure 5-19. Comparison of integration results for *C. reinhardtii* cells (left) or *A. thaliana* leaves (right) exposed to 2 min HL – 2 min dark fluctuating actinic light sequence. The quantification of the amount of NPQτ remaining in each mutant lacking pH-sensing protein (*C. reinhardtii* LHCSR1 and LHCSR3; *A. thaliana* PsbS) is shown. Both were measured by TCSPC. The *C. reinhardtii* data is taken from Figure 5-2. The *A. thaliana* data was derived from a previous study published by our groups (ref [43]).

Tuning the relaxation kinetics of NPQ in higher plants has been shown to improve crop plant productivity[66], and recent modelling of the response of plant canopies to natural light fluctuations has shown that there remains ample room for improving photosynthetic efficiency under non-steady state conditions[67]. Similar opportunities for improvement also exist for increasing biofuel production from microalgae[68–70]. In both cases, such optimization will require detailed understanding of the dynamic activity of NPQ mechanisms. The sum of the NPQ contributions of each protein is greater than 100% (Figure 5-10) which cannot be explained by a difference in the amount of LHCSR3 between WT and *stt7* (Figure 5-20). Additionally, our quantifications of qE and qT reveal that each of them depends on the presence of the other process (Figure 5-14), showing that there is an interaction between qE and qT in *Chlamydomonas* under fluctuating light.

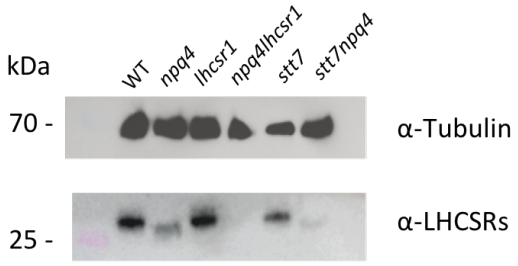

Figure 5-20. Immunodetection of LHCSRs in mutants and their control strain. Cells were harvested before the measurements described in Figure 5-1. Immunoanalysis of LHCSRs proteins was carried out using a previously described LHCSRs antibody (ref [71]). A tubilin antibody (Agrisera XXX) was used as a loading control.

The possibility of an interaction between qE and qT has been previously suggested on the basis of a kinetic analysis of qT in the presence and absence of LHCSR3 protein (*npq4* mutant)[55]. Our findings are consistent with a partial overlap of the functions of LHCSR3 and STT7 in both qE and qT. This partial overlap highlights the need for further investigations of the interactions occurring between proteins that underlie the *in vivo* NPQ response, not only in HL but also in dark, and more generally during light fluctuations. For example, in microalgae, the quenching mediated by LHCSR3 both at PSII and PSI level[33] could be tuned by the movement of LHCSR3 from PSI to PSII during state transitions[36]. Thus, the described LHCSR3 phosphorylation by STT7[45] could explain the crosstalk between qE and qT. LHCSR3 is also known to associate with LHCII trimers in the PSII supercomplex[72]; therefore, a similar LHCSR3-LHCII interaction may also generate quenching in the trimers following the detachment of LHCII from PSII. It should be noted that in the thylakoid membrane, LHCII can exist in a range of different conformations and/or quenching states[73,74]. At this point it is not possible to distinguish the relative contributions of different forms of LHCII in individual snapshot measurements. The ensemble fluorescence lifetime likely originates from some combination of at least three LHCII subpopulations: unphosphorylated and bound to PSII (state 1)[10] with an intermediate fluorescence decay component, phosphorylated and unbound (free LHCII)[75] which has been previously assigned to a long fluorescence decay component[10], and phosphorylated and bound to PSI (state 2)[76] with a short fluorescence decay component. In intact algal cells, the relative abundance of each form of LHCII likely dynamically evolves throughout exposure to the fluctuating HL-dark sequences. Further development of *in vivo* spectroscopic tools will be required to disentangle the dynamics of LHCII conformations and correlate them with photoprotection. Overall, a deeper understanding of the protein interactions underlying NPQ dynamics will be highly valuable in finding new ways to improve plant and microalgal productivity.

5.6 Conclusions

LHCSR- and STT7-mediated nonphotochemical quenching processes (qE and qT) are known to underly the photoprotective response of the microalgae *Chlamydomonas*. Here, we have applied a new method to disentangle the involvement of qE and qT in real time by exposing intact algal cells to repetitive cycles of high light and darkness alternating at different frequencies. While both qE- and qT-type responses are present during all light fluctuations, LHCSR-dependent qE plays a larger role in the beginning of light fluctuations and during the HL periods. The contribution of STT7-dependent qT became more pronounced upon longer exposure to fluctuating light and especially during the dark periods of light fluctuations. Over the long term, rapid light fluctuations reduced the growth of mutants impaired in LHCSRs, demonstrating the importance of LHCSR proteins during abrupt changes in light intensity. Overall, our work shows that a cooperativity between LHCSR proteins and STT7 constitutes an important regulatory feature of the photoprotective response in *Chlamydomonas*, likely mediated by phosphorylation of LHCSR3 by STT7. These findings provide a foundation for disentangling and modelling how the diverse molecular mechanisms involved in plant and microalgal acclimation to light fluctuations interact and enable robust photosynthesis in nature. We envision that further knowledge on the response of photosynthetic mechanisms to various frequencies of light fluctuations will open new avenues for building a strong understanding of how photosynthetic organisms respond to complex light fluctuations.

5.7 Supporting Information

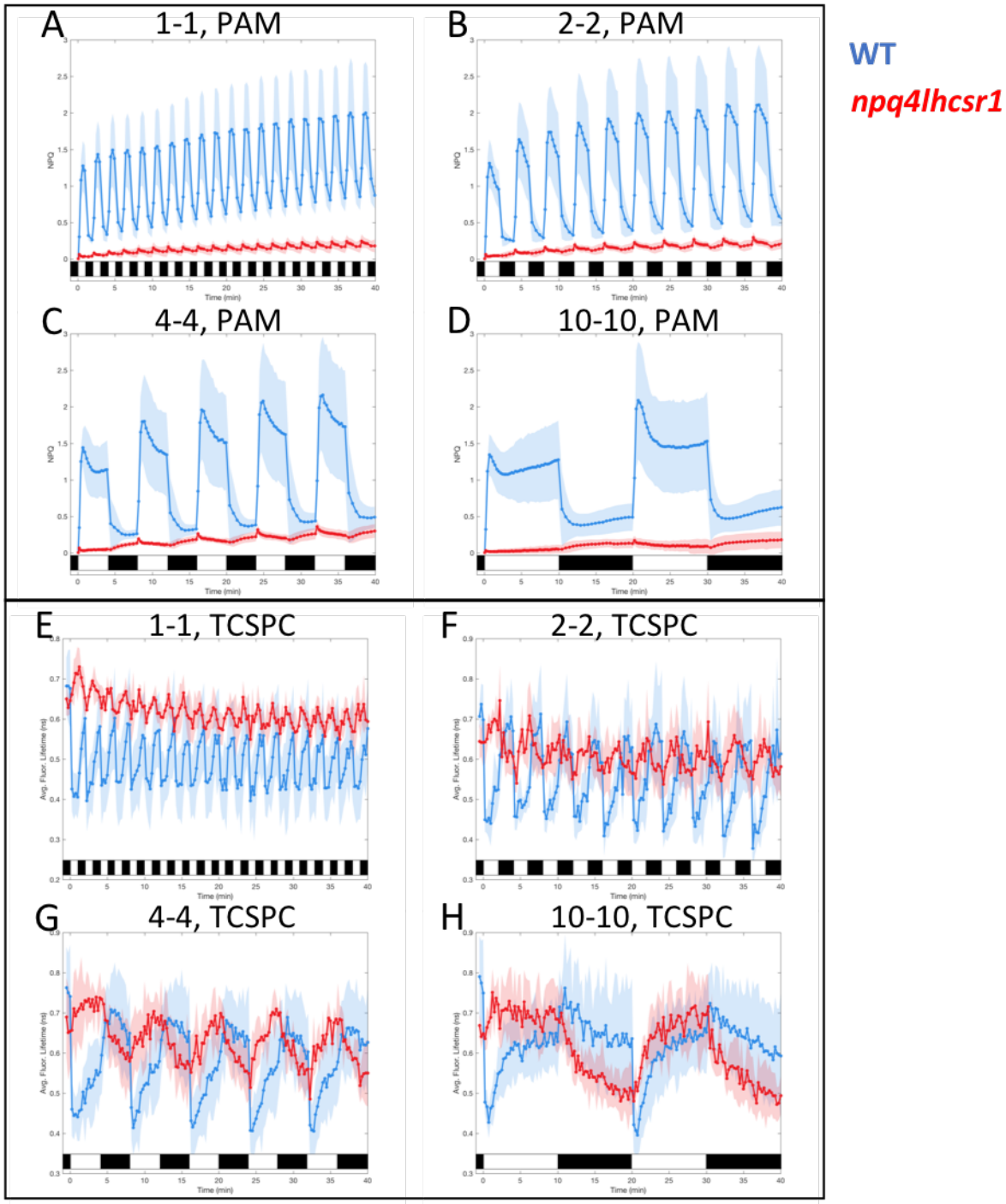

Figure S1. Quenching trajectories during light fluctuations in WT and *npq4lhcsr1*. The response of NPQ (A-D, measured by PAM) and average Chl fluorescence lifetime (E-F, measured by TCSPC) were monitored in *npq4lhcsr1* mutant and its control strain (red and blue curves respectively) during 40 minutes of light fluctuations with HL/dark periods of 1, 2, 4 and 10 minutes (A/E, B/F, C/G and D/H respectively) as described in Fig. 5-1. The solid lines represent the average of three biological replicates. Shaded regions represent standard deviation. For TCSPC data, each biological replicate was averaged from three technical replicates.

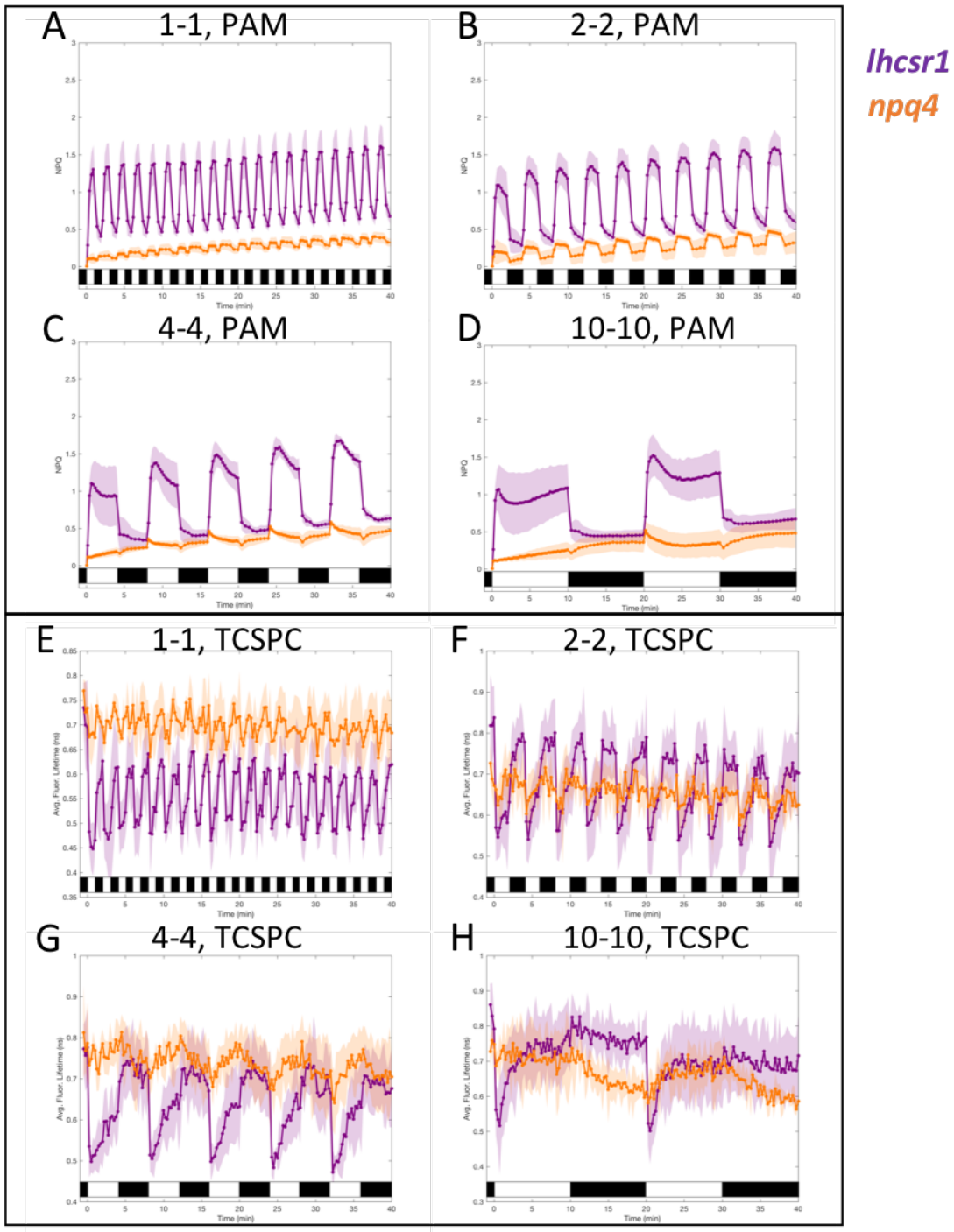

Figure S2. Quenching trajectories during light fluctuations in *lhcsr1* and *npq4*. The response of NPQ (A-D, measured by PAM) and average Chl fluorescence lifetime (E-F, measured by TCSPC) were monitored in *lhcsr1* and *npq4* (purple and orange curves respectively) during 40 minutes of light fluctuations with HL/dark periods of 1, 2, 4 and 10 minutes (A/E, B/F, C/G and D/H respectively) as described in Fig. 5-1. The solid lines represent the average of three biological replicates. Shaded regions represent standard deviation. For TCSPC data, each biological replicate was averaged from three technical replicates.

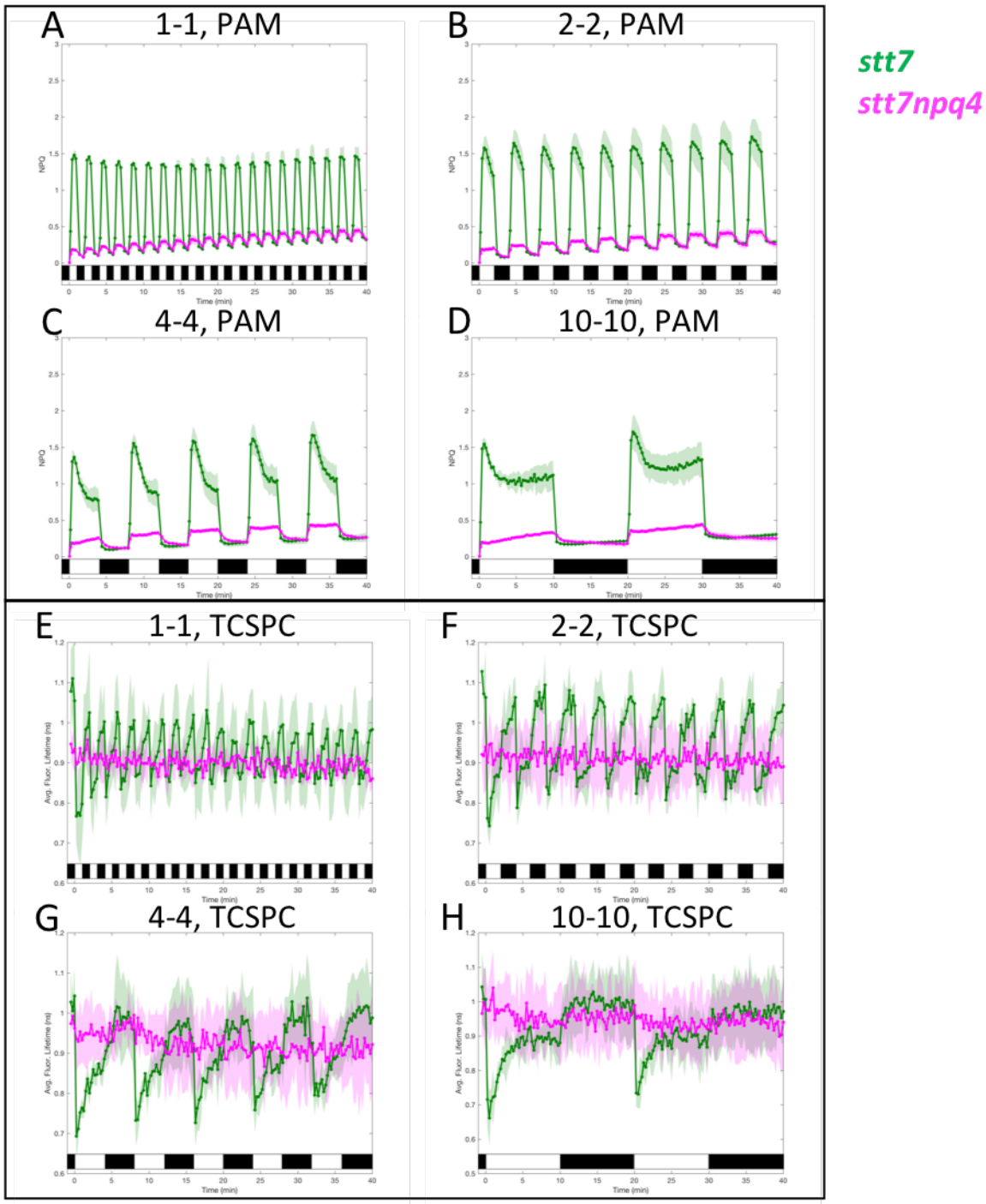

Figure S3. Quenching trajectories during light fluctuations in *stt7* and *stt7npq4*. The response of NPQ (A-D, measured by PAM) and average Chl fluorescence lifetime (E-F, measured by TCSPC) were monitored in *stt7* and *stt7npq4* (green and magenta curves respectively) during 40 minutes of light fluctuations with HL/dark periods of 1, 2, 4 and 10 minutes (A/E, B/F, C/G and D/H respectively) as described in Fig. 5-1. The solid lines represent the average of three biological replicates. Shaded regions represent standard deviation. For TCSPC data, each biological replicate was averaged from three technical replicates.

5.8 References

(1) Björkman, O.; Demmig, B. Photon yield of O2 evolution and chlorophyll fluorescence characteristics at 77 K among vascular plants of diverse origins. *Planta* **1987**, *170* (4), 489–504.

(2) Khorobrykh, S.; Havurinne, V.; Mattila, H.; Tyystjärvi, E. Oxygen and ROS in Photosynthesis. *Plants* **2020**, *9* (1), 91.

(3) Graham, P. J.; Nguyen, B.; Burdyny, T.; Sinton, D. A penalty on photosynthetic growth in fluctuating light. *Sci. Rep.* **2017**, *7* (1), 1–11.

(4) Erickson, E.; Wakao, S.; Niyogi, K. K. Light stress and photoprotection in Chlamydomonas reinhardtii. *Plant J.* **2015**, *82* (3), 449–465.

(5) Son, M.; Pinnola, A.; Gordon, S. C.; Bassi, R.; Schlau-Cohen, G. S. Observation of dissipative chlorophyll-to-carotenoid energy transfer in light-harvesting complex II in membrane nanodiscs. *Nat. Commun.* **2020**, *11* (1), 1295.

(6) Roach, T. LHCSR3-Type NPQ Prevents Photoinhibition and Slowed Growth under Fluctuating Light in Chlamydomonas reinhardtii. *Plants* **2020**, *9* (11), 1604.

(7) Briantais, J.-M.; Vernotte, C.; Picaud, M.; Krause, G. H. A quantitative study of the slow decline of chlorophyll a fluorescence in isolated chloroplasts. *Biochim. Biophys. Acta - Bioenerg.* **1979**, *548* (1), 128–138.

(8) Allen, J. F. Protein phosphorylation in regulation of photosynthesis. *Biochim. Biophys. Acta - Bioenerg.* **1992**, *1098* (3), 275–335.

(9) Nagy, G.; Ünnep, R.; Zsiros, O.; Tokutsu, R.; Takizawa, K.; Porcar, L.; Moyet, L.; Petroutsos, D.; Garab, G.; Finazzi, G.; Minagawa, J. Chloroplast remodeling during state transitions in Chlamydomonas reinhardtii as revealed by noninvasive techniques in vivo. *Proc. Natl. Acad. Sci.* **2014**, *111* (13), 5042–5047.

(10) Ünlü, C.; Drop, B.; Croce, R.; van Amerongen, H. State transitions in Chlamydomonas reinhardtii strongly modulate the functional size of photosystem II but not of photosystem I. *Proc. Natl. Acad. Sci. U. S. A.* **2014**, *111* (9), 3460–3465.

(11) Nawrocki, W. J.; Santabarbara, S.; Mosebach, L.; Wollman, F. A.; Rappaport, F. State transitions redistribute rather than dissipate energy between the two photosystems in Chlamydomonas. *Nat. Plants* **2016**, *2* (4), 1–7.

(12) Dall'Osto, L.; Caffarri, S.; Bassi, R. A Mechanism of Nonphotochemical Energy Dissipation, Independent from PsbS, Revealed by a Conformational Change in the Antenna Protein CP26. *Plant Cell* **2005**, *17* (4), 1217–1232.

(13) Wehner, A.; Grasses, T.; Jahns, P. De-epoxidation of Violaxanthin in the Minor Antenna Proteins of Photosystem II, LHCB4, LHCB5, and LHCB6. *J. Biol. Chem.* **2006**, *281* (31), 21924–21933.

(14) Nilkens, M.; Kress, E.; Lambrev, P.; Miloslavina, Y.; Müller, M.; Holzwarth, A. R.; Jahns, P. Identification of a slowly inducible zeaxanthin-dependent component of non-photochemical quenching of chlorophyll fluorescence generated under steady-state conditions in Arabidopsis. *Biochim. Biophys. Acta - Bioenerg.* **2010**, *1797* (4), 466–475.

(15) Malnoë, A.; Schultink, A.; Shahrasbi, S.; Rumeau, D.; Havaux, M.; Niyogi, K. K. The Plastid Lipocalin LCNP Is Required for Sustained Photoprotective Energy Dissipation in Arabidopsis. *Plant Cell* **2018**, *30* (1), 196–208.

(16) Bru, P.; Steen, C. J.; Park, S.; Amstutz, C. L.; Sylak-Glassman, E. J.; Lam, L.; Fekete, A.; Mueller, M. J.; Longoni, F.; Fleming, G. R.; Niyogi, K. K.; Malnoë, A. An energy-

dissipative state of the major antenna complex of plants. *bioRxiv* **2022**, 2021.07.09.450705.
(17) Aro, E.-M.; Virgin, I.; Andersson, B. Photoinhibition of Photosystem II. Inactivation, protein damage and turnover. *Biochim. Biophys. Acta - Bioenerg.* **1993**, *1143* (2), 113–134.
(18) Peers, G.; Truong, T. B.; Ostendorf, E.; Busch, A.; Elrad, D.; Grossman, A. R.; Hippler, M.; Niyogi, K. K. An ancient light-harvesting protein is critical for the regulation of algal photosynthesis. *Nature* **2009**, *462* (7272), 518–521.
(19) Rochaix, J.-D.; Bassi, R. LHC-like proteins involved in stress responses and biogenesis/repair of the photosynthetic apparatus. *Biochem. J.* **2019**, *476* (3), 581–593.
(20) Ballottari, M.; Truong, T. B.; De Re, E.; Erickson, E.; Stella, G. R.; Fleming, G. R.; Bassi, R.; Niyogi, K. K. Identification of pH-sensing Sites in the Light Harvesting Complex Stress-related 3 Protein Essential for Triggering Non-photochemical Quenching in Chlamydomonas reinhardtii. *J. Biol. Chem.* **2016**, *291* (14), 7334–7346.
(21) Tian, L.; Nawrocki, W. J.; Liu, X.; Polukhina, I.; van Stokkum, I. H. M.; Croce, R. pH dependence, kinetics and light-harvesting regulation of nonphotochemical quenching in Chlamydomonas. *Proc. Natl. Acad. Sci. U. S. A.* **2019**, *116* (17), 8320–8325.
(22) Liguori, N.; Roy, L. M.; Opacic, M.; Durand, G.; Croce, R. Regulation of Light Harvesting in the Green Alga Chlamydomonas reinhardtii : The C-Terminus of LHCSR Is the Knob of a Dimmer Switch. *J. Am. Chem. Soc.* **2013**, *135* (49), 18339–18342.
(23) Kondo, T.; Pinnola, A.; Chen, W. J.; Dall'Osto, L.; Bassi, R.; Schlau-Cohen, G. S. Single-molecule spectroscopy of LHCSR1 protein dynamics identifies two distinct states responsible for multi-timescale photosynthetic photoprotection. *Nat. Chem.* **2017**, *9* (8), 772–778.
(24) Troiano, J. M.; Perozeni, F.; Moya, R.; Zuliani, L.; Baek, K.; Jin, E.; Cazzaniga, S.; Ballottari, M.; Schlau-Cohen, G. S. Identification of distinct pH- and zeaxanthin-dependent quenching in LHCSR3 from chlamydomonas reinhardtii. *eLife* **2021**, *10*, 1–59.
(25) Bonente, G.; Ballottari, M.; Truong, T. B.; Morosinotto, T.; Ahn, T. K.; Fleming, G. R.; Niyogi, K. K.; Bassi, R. Analysis of LhcSR3, a Protein Essential for Feedback De-Excitation in the Green Alga Chlamydomonas reinhardtii. *PLoS Biol.* **2011**, *9* (1), e1000577.
(26) Perozeni, F.; Beghini, G.; Cazzaniga, S.; Ballottari, M. Chlamydomonas reinhardtii LHCSR1 and LHCSR3 proteins involved in photoprotective non-photochemical quenching have different quenching efficiency and different carotenoid affinity. *Sci. Rep.* **2020**, *10* (1).
(27) Truong, T. B. Investigating the Role(s) of LHCSRs in Chlamydomonas reinhardtii, 2011.
(28) Depège, N.; Bellafiore, S.; Rochaix, J. D. Role of chloroplast protein kinase Stt7 in LHCII phosphorylation and state transition in Chlamydomonas. *Science* **2003**, *299* (5612), 1572–1575.
(29) Lemeille, S.; Willig, A.; Depège-Fargeix, N.; Delessert, C.; Bassi, R.; Rochaix, J.-D. Analysis of the Chloroplast Protein Kinase Stt7 during State Transitions. *PLOS Biol.* **2009**, *7* (3), e1000045.
(30) Iwai, M.; Takizawa, K.; Tokutsu, R.; Okamuro, A.; Takahashi, Y.; Minagawa, J. Isolation of the elusive supercomplex that drives cyclic electron flow in photosynthesis. *Nature* **2010**, *464* (7292), 1210–1213.
(31) Minagawa, J. State transitions—The molecular remodeling of photosynthetic supercomplexes that controls energy flow in the chloroplast. *Biochim. Biophys. Acta - Bioenerg.* **2011**, *1807* (8), 897–905.
(32) Niyogi, K. K.; Bjorkman, O.; Grossman, A. R. Chlamydomonas Xanthophyll Cycle

Mutants Identified by Video Imaging of Chlorophyll Fluorescence Quenching. *Plant Cell* **1997**, *9* (8), 1369–1380.
(33) Girolomoni, L.; Cazzaniga, S.; Pinnola, A.; Perozeni, F.; Ballottari, M.; Bassi, R. LHCSR3 is a nonphotochemical quencher of both photosystems in Chlamydomonas reinhardtii. *Proc. Natl. Acad. Sci. U. S. A.* **2019**, *116* (10), 4212–4217.
(34) Nawrocki, W. J.; Liu, X.; Raber, B.; Hu, C.; Vitry, C. de; Bennett, D. I. G.; Croce, R. Molecular origins of induction and loss of photoinhibition-related energy dissipation qI. *Sci. Adv.* **2021**, *7* (52), 55.
(35) Nedbal, L.; Lazár, D. Photosynthesis dynamics and regulation sensed in the frequency domain. *Plant Physiol.* **2021**, *187* (2), 646–661.
(36) Allorent, G.; Tokutsu, R.; Roach, T.; Peers, G.; Cardol, P.; Girard-Bascou, J.; Seigneurin-Berny, D.; Petroutsos, D.; Kuntz, M.; Breyton, C.; Franck, F.; Wollman, F.-A.; Niyogi, K. K.; Krieger-Liszkay, A.; Minagawa, J.; Finazzi, G. A dual strategy to cope with high light in Chlamydomonas reinhardtii. *Plant Cell* **2013**, *25* (2), 545–557.
(37) Gao, S.; Pinnola, A.; Zhou, L.; Zheng, Z.; Li, Z.; Bassi, R.; Wang, G. Light-harvesting complex stress-related proteins play crucial roles in the acclimation of Physcomitrella patens under fluctuating light conditions. *Photosynth. Res.* **2021**, *1*, 1–10.
(38) Cardol, P.; Alric, J.; Girard-Bascou, J.; Franck, F.; Wollman, F.-A.; Finazzi, G. Impaired respiration discloses the physiological significance of state transitions in Chlamydomonas. *Proc. Natl. Acad. Sci.* **2009**, *106* (37), 15979–15984.
(39) Tibiletti, T.; Auroy, P.; Peltier, G.; Caffarri, S. Chlamydomonas reinhardtii PsbS Protein Is Functional and Accumulates Rapidly and Transiently under High Light. *Plant Physiol.* **2016**, *171* (4), 2717–2730.
(40) Bonaventura, C.; Myers, J. Fluorescence and oxygen evolution from Chlorella pyrenoidosa. *Biochim. Biophys. Acta - Bioenerg.* **1969**, *189* (3), 366–383.
(41) Zaks, J.; Amarnath, K.; Sylak-Glassman, E. J.; Fleming, G. R. Models and measurements of energy-dependent quenching. *Photosynth. Res.* **2013**, *116* (2–3), 389–409.
(42) Sylak-Glassman, E. J.; Zaks, J.; Amarnath, K.; Leuenberger, M.; Fleming, G. R. Characterizing non-photochemical quenching in leaves through fluorescence lifetime snapshots. *Photosynth. Res.* **2016**, *127* (1), 69–76.
(43) Steen, C. J.; Morris, J. M.; Short, A. H.; Niyogi, K. K.; Fleming, G. R. Complex Roles of PsbS and Xanthophylls in the Regulation of Nonphotochemical Quenching in Arabidopsis thaliana under Fluctuating Light. *J. Phys. Chem. B* **2020**, *124* (46), 10311–10325.
(44) Sylak-Glassman, E. J.; Malnoë, A.; De Re, E.; Brooks, M. D.; Fischer, A. L.; Niyogi, K. K.; Fleming, G. R. Distinct roles of the photosystem II protein PsbS and zeaxanthin in the regulation of light harvesting in plants revealed by fluorescence lifetime snapshots. *Proc. Natl. Acad. Sci. U. S. A.* **2014**, *111* (49), 17498–17503.
(45) Bergner, S. V.; Scholz, M.; Trompelt, K.; Barth, J.; Gäbelein, P.; Steinbeck, J.; Xue, H.; Clowez, S.; Fucile, G.; Goldschmidt-Clermont, M.; Fufezan, C.; Hippler, M. STATE TRANSITION7-Dependent Phosphorylation Is Modulated by Changing Environmental Conditions, and Its Absence Triggers Remodeling of Photosynthetic Protein Complexes. *Plant Physiol.* **2015**, *168* (2), 615–634.
(46) Cantrell, M.; Peers, G. A mutant of Chlamydomonas without LHCSR maintains high rates of photosynthesis, but has reduced cell division rates in sinusoidal light conditions. *PLoS One* **2017**, *12* (6), e0179395.
(47) Klughammer, C.; Schreiber, U.; Walz, H. Complementary PS II quantum yields calculated

from simple fluorescence parameters measured by PAM fluorometry and the Saturation Pulse method. *PAM Appl. Notes, Heinz Walz GmbH* **2008**, *1*, 27–35.
(48) Amarnath, K.; Zaks, J.; Park, S. D.; Niyogi, K. K.; Fleming, G. R. Fluorescence lifetime snapshots reveal two rapidly reversible mechanisms of photoprotection in live cells of Chlamydomonas reinhardtii. *Proc. Natl. Acad. Sci. U. S. A.* **2012**, *109* (22), 8405–8410.
(49) Burlacot, A.; Dao, O.; Auroy, P.; Cuiné, S.; Li-Beisson, Y.; Peltier, G. Alternative photosynthesis pathways drive the algal CO2-concentrating mechanism. *Nature* **2022**, 1–6.
(50) Correa-Galvis, V.; Redekop, P.; Guan, K.; Griess, A.; Truong, T. B.; Wakao, S.; Niyogi, K. K.; Jahns, P. Photosystem II Subunit PsbS Is Involved in the Induction of LHCSR Protein-dependent Energy Dissipation in Chlamydomonas reinhardtii. *J. Biol. Chem.* **2016**, *291* (33), 17478–17487.
(51) Casper-Lindley, C.; Björkman, O. Nigericin insensitive post-illumination reduction in fluorescence yield in Dunaliella tertiolecta (chlorophyte). *Photosynth. Res.* **1996**, *50* (3), 209–222.
(52) Zhang, X. J.; Fujita, Y.; Tokutsu, R.; Minagawa, J.; Ye, S.; Shibata, Y. High-Speed Excitation-Spectral Microscopy Uncovers In Situ Rearrangement of Light-Harvesting Apparatus in Chlamydomonas during State Transitions at Submicron Precision. *Plant Cell Physiol.* **2021**, *62* (5), 872–882.
(53) Rintamäki, E.; Martinsuo, P.; Pursiheimo, S.; Aro, E. M. Cooperative regulation of light-harvesting complex II phosphorylation via the plastoquinol and ferredoxin-thioredoxin system in chloroplasts. *Proc. Natl. Acad. Sci. U. S. A.* **2000**, *97* (21), 11644–11649.
(54) Vink, M.; Zer, H.; Alumot, N.; Gaathon, A.; Niyogi, K.; Herrmann, R. G.; Andersson, B.; Ohad, I. Light-modulated exposure of the light-harvesting complex II (LHCII) to protein kinase(s) and state transition in Chlamydomonas reinhardtii xanthophyll mutants. *Biochemistry* **2004**, *43* (24), 7824–7833.
(55) Roach, T.; Na, C. S. LHCSR3 affects de-coupling and re-coupling of LHCII to PSII during state transitions in Chlamydomonas reinhardtii. *Sci. Rep.* **2017**, *7* (1), 1–9.
(56) Barera, S.; Dall'Osto, L.; Bassi, R. Effect of lhcsr gene dosage on oxidative stress and light use efficiency by Chlamydomonas reinhardtii cultures. *J. Biotechnol.* **2021**, *328*, 12–22.
(57) Zaks, J.; Amarnath, K.; Kramer, D. M.; Niyogi, K. K.; Fleming, G. R. A kinetic model of rapidly reversible nonphotochemical quenching. *Proc. Natl. Acad. Sci. U. S. A.* **2012**, *109* (39), 15757–15762.
(58) Tanaka, Y.; Adachi, S.; Yamori, W. Natural genetic variation of the photosynthetic induction response to fluctuating light environment. *Curr. Opin. Plant Biol.* **2019**, *49*, 52–59.
(59) Fei, C.; Wilson, A. T.; Mangan, N. M.; Wingreen, N. S.; Jonikas, M. C. Diffusion barriers and adaptive carbon uptake strategies enhance the modeled performance of the algal CO2-concentrating mechanism. *bioRxiv* **2021**, 2021.03.04.433933.
(60) Forti, G.; Caldiroli, G. State Transitions in Chlamydomonas reinhardtii. The Role of the Mehler Reaction in State 2-to-State 1 Transition. *Plant Physiol.* **2005**, *137* (2), 492–499.
(61) Dinc, E.; Tian, L.; Roy, L. M.; Roth, R.; Goodenough, U.; Croce, R. LHCSR1 induces a fast and reversible pH-dependent fluorescence quenching in LHCII in Chlamydomonas reinhardtii cells. *Proc. Natl. Acad. Sci. U. S. A.* **2016**, *113* (27), 7673–7678.
(62) Nawrocki, W. J.; Liu, X.; Croce, R. Chlamydomonas reinhardtii exhibits de facto constitutive NPQ capacity in physiologically relevant conditions. *Plant Physiol.* **2020**, *182* (1), 472–479.

(63) Kosuge, K.; Tokutsu, R.; Kim, E.; Akimoto, S.; Yokono, M.; Ueno, Y.; Minagawa, J. LHCSR1-dependent fluorescence quenching is mediated by excitation energy transfer from LHCII to photosystem I in Chlamydomonas reinhardtii. *Proc. Natl. Acad. Sci. U. S. A.* **2018**, *115* (14), 3722–3727.
(64) Bellafiore, S.; Barneche, F.; Peltier, G.; Rochaix, J.-D. State transitions and light adaptation require chloroplast thylakoid protein kinase STN7. *Nature* **2005**, *433* (7028), 892–895.
(65) Goral, T. K.; Johnson, M. P.; Duffy, C. D. P.; Brain, A. P. R.; Ruban, A. V.; Mullineaux, C. W. Light-harvesting antenna composition controls the macrostructure and dynamics of thylakoid membranes in Arabidopsis. *Plant J.* **2012**, *69* (2), 289–301.
(66) Kromdijk, J.; Głowacka, K.; Leonelli, L.; Gabilly, S. T.; Iwai, M.; Niyogi, K. K.; Long, S. P. Improving photosynthesis and crop productivity by accelerating recovery from photoprotection. *Science* **2016**, *354* (6314), 857–861.
(67) Wang, Y.; Burgess, S. J.; Becker, E. M.; Long, S. P. Photosynthesis in the fleeting shadows: an overlooked opportunity for increasing crop productivity? *Plant J.* **2020**, *101* (4), 874–884.
(68) Benedetti, M.; Vecchi, V.; Barera, S.; Dall'Osto, L. Biomass from microalgae: the potential of domestication towards sustainable biofactories. *Microb. Cell Fact.* **2018**, *17* (1), 173.
(69) Perin, G.; Jones, P. R. Economic feasibility and long-term sustainability criteria on the path to enable a transition from fossil fuels to biofuels. *Curr. Opin. Biotechnol.* **2019**, *57*, 175–182.
(70) Vecchi, V.; Barera, S.; Bassi, R.; Dall'Osto, L. Potential and Challenges of Improving Photosynthesis in Algae. *Plants* **2020**, *9* (1), 67.
(71) Semchonok, D. A.; Sathish Yadav, K. N.; Xu, P.; Drop, B.; Croce, R.; Boekema, E. J. Interaction between the photoprotective protein LHCSR3 and C2S2 Photosystem II supercomplex in Chlamydomonas reinhardtii. *Biochim. Biophys. Acta - Bioenerg.* **2017**, *1858* (5), 379–385.
(72) Tian, L.; Dinc, E.; Croce, R. LHCII Populations in Different Quenching States Are Present in the Thylakoid Membranes in a Ratio that Depends on the Light Conditions. *J. Phys. Chem. Lett.* **2015**, *6* (12), 2339–2344.
(73) Kawakami, K.; Tokutsu, R.; Kim, E.; Minagawa, J. Four distinct trimeric forms of light-harvesting complex II isolated from the green alga Chlamydomonas reinhardtii. *Photosynth. Res.* **2019**, 1–7.
(74) Iwai, M.; Yokono, M.; Inada, N.; Minagawa, J. Live-cell imaging of photosystem II antenna dissociation during state transitions. *Proc. Natl. Acad. Sci. U. S. A.* **2010**, *107* (5), 2337–2342.
(75) Huang, Z.; Shen, L.; Wang, W.; Mao, Z.; Yi, X.; Kuang, T.; Shen, J. R.; Zhang, X.; Han, G. Structure of photosystem I-LHCI-LHCII from the green alga Chlamydomonas reinhardtii in State 2. *Nat. Commun.* **2021**, *12* (1), 1–14.
(76) Richard, C.; Ouellet, H.; Guertin, M. Characterization of the LI818 polypeptide from the green unicellular alga Chlamydomonas reinhardtii. *Plant Mol. Biol.* **2000**, *42* (2), 303–316.

Chapter 6

Spin-trapping EPR spectroscopy for monitoring the real-time dynamics of singlet oxygen during photoprotection

This chapter is based on work performed by C.J. Steen at Argonne National Laboratory in collaboration with L.M. Utschig, O.G. Poluektov, and J. Niklas as part of a Department of Energy Office of Science Graduate Student Research (SCGSR) award to C.J.S.

6.1 Introduction

6.1.1 Source of Reactive Oxygen Species in Photosynthesis

As sessile organisms, plants must acclimate to fluctuating environmental conditions. One highly dynamic variable in nature is the incident light intensity reaching the photosynthetic apparatus inside chloroplasts. This photosynthetic membrane is composed of an array of pigment-protein complexes capable of highly efficient light absorption via elaborate networks of light-absorbing pigments.[1,2] In fact, photosynthetic light harvesting operates with near unity quantum efficiency under optimal conditions, such as the low light levels that regularly occur in nature.[3] However, in the environment, saturating light intensities are also regularly encountered, resulting in build-up of excitation energy in the thylakoid membrane. As the photosynthetic photon flux density (PPFD, units of $\mu mol\ m^{-2}\ s^{-1}$) increases, there is a growing mismatch in the rate of light absorption relative to the rate of photosynthesis.[4] While light absorption continues to rise linearly with increasing PPFD, the rate of photosynthesis saturates at relatively low light intensities. Specifically, this rate is dictated by the flux of electrons through the photosynthetic electron transport chain from photosystem (PS) II to PSI, which is modulated by the cytochrome b_6f complex[5] as well as subsequent constraints involved with fixing carbon dioxide during the Calvin-Benson cycle.[6]

A consequence of the mismatch between light absorption and electron transfer under high PPFDs is the saturation of reaction centers due to the depletion of oxidized plastoquinone molecules involved in accepting electrons from PSII. When the reaction centers of PSII close, there is accumulation of excited states of chlorophyll (Chl), the primary light-harvesting pigment, throughout the light-harvesting antenna of PSII. Importantly, as the average Chl excited state lifetime becomes longer, the probability for intersystem crossing (ISC) from the singlet excited state (^{1}Chl*) to the triplet excited state (^{3}Chl*) also increases.

One important photophysical reaction in photosynthetic systems is the photosensitized production of the electronically excited state of molecular oxygen, $^1\Delta_g$,[7] referred to hereafter as singlet oxygen ($^1O_2$*). While the energetic requirement for producing $^1O_2$* from the triplet ground-state ($^3O_2$) is only 94 kJ mol^{-1},[8] corresponding to absorption of near-infrared light, direct optical excitation of isolated oxygen molecules is quantum-mechanically forbidden due to the change in spin state. In liquids, the transition can be observed due to interactions with solvent molecules, though the

spectroscopic signal is extremely weak.[9] Thus, the absorption of IR photons does not represent a significant source of singlet oxygen generation in photosynthesis.

More commonly, $^1O_2$* can be efficiently produced via photosensitization, a process in which a light-absorbing molecule transfers excitation energy to $^3O_2$.[10,11] This is a common occurrence in natural photosynthetic systems due to an abundance of photosensitizer (Chl) and oxygen molecules, the latter being created from the light-driven splitting of water by the oxygen-evolving complex (OEC; also referred to as WOC, water-oxidizing complex) of PSII.[12] The triplet excited state of Chl (^{3}Chl*) is well known to react with molecular oxygen, yielding $^1O_2$*. Molecular oxygen can also be reduced leading to the formation of various other reactive oxygen species (ROS) including superoxide (O_2^-), hydrogen peroxide (H_2O_2), and hydroxyl radical ($OH^•$),[13] all of which are produced in photosynthetic systems under stress conditions.[14,15] Therefore, the presence of ROS is an unavoidable consequence of oxygenic photosynthesis (Figure 6-1). For more information on $^1O_2$* and ROS in photosynthesis, see References 16–22.

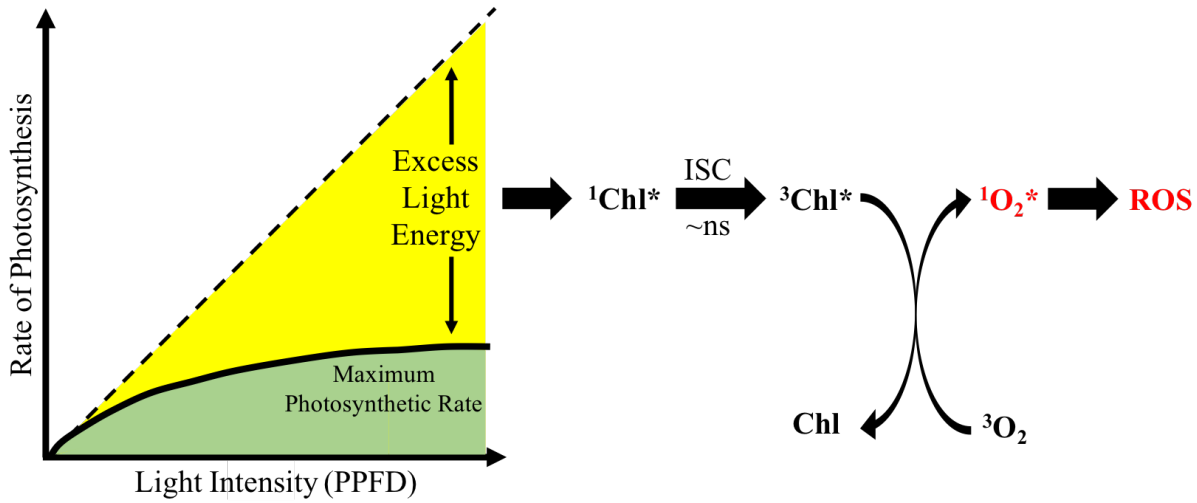

Figure 6-1. The rate of photosynthesis does not match the rate of light absorption especially at high light intensities (photosynthetic photon flux densities, PPFD), where singlet oxygen photosensitization can occur via triplet-triplet energy transfer from triplet chlorophyll generated by intersystem crossing (ISC). The production of singlet oxygen and other reactive oxygen species (ROS) can pose a danger to the organism. Figure adapted from Erickson et al. *Plant Journal.* 2015, *82*, 449-465.

6.1.2 Reactivity and Regulation of Singlet Oxygen in Photosynthesis

Given its relatively short lifetime and small intracellular diffusion distance,[23] $^1O_2$* is thought to react with nearby targets in the photosynthetic apparatus. Nonetheless, it is an electrophilic species that is highly reactive for a wide array of biomolecules. One such vulnerable target is the D1 protein of PSII, which is in close proximity to the OEC, the main source of molecular oxygen in the photosynthetic membrane. In fact, $^1O_2$* is thought to be directly involved in damage and inactivation of D1,[24–27] leading to decreased photosynthetic efficiency. $^1O_2$* has also been implicated in the degradation of LHCII or other photosynthetic antenna proteins.[28,29] More broadly, it is capable of oxidizing amino acid residues of proteins, including Trp, Tyr, His, Met, and Cys side chains.[30] $^1O_2$* can also react with the abundant double bonds found in DNA[31] or in

lipids, the latter of which leads to lipid peroxidation, an event that has often been linked to cell death.[32,33] The presence of $^1O_2$* has also been reported to be involved in chloroplast degradation processes.[34,35]

Photosynthetic cells house a wide array of molecules that participate in detoxification of ROS. Carotenoid pigments are efficient scavengers of $^1O_2$* and other ROS.[36–38] They can also receive energy from ^{3}Chl* and non-radiatively dissipate it.[39] One such carotenoid, β-carotene, is found at the PSII reaction center[40] where it has been documented to quench $^1O_2$*,[41] likely protecting against photoinhibition and damage.[42–44] Tocopherol,[37,45,46] plastoquinol,[47,48] and ascorbate[49,50] are also well-known quenchers of $^1O_2$*. Despite its widespread reactivity, $^1O_2$*, and ROS more generally, represent crucial cellular stress signals, inducing cellular and genetic acclimation responses to existing environmental conditions.[51–57] Nonetheless, photosynthetic organism survival requires a multi-pronged approach to preventing and mitigating photo-oxidative stress, including real-time regulation of ROS concentrations inside cells.

One important regulatory process is nonphotochemical quenching (NPQ)[58,59] which harmlessly dissipates excess excitation energy in the light-harvesting antenna, thereby protecting PSII against damage. Despite the known importance of NPQ to plant fitness and survival,[60] many of its underlying molecular mechanisms remain controversial. Additionally, while the necessity of NPQ is frequently framed in terms of preventing the buildup of ROS, such as $^1O_2$*, this has not been explicitly demonstrated, and more recent thinking posits that ROS may play essential roles in plant signaling and stress responses.[61] Despite the centrality of $^1O_2$* to the operation of photosynthesis, and possibly photoprotection, there remains much to be learned in terms of its production, reactivity, or regulation inside intact photosynthetic systems, such as thylakoids, chloroplasts, and plant cells.[62]

6.1.3 Detection of Reactive Oxygen Species in Photosynthesis

Direct detection of $^1O_2$* is possible by measuring the near-IR phosphorescence ($^1\Delta_g \rightarrow {}^3\sum_g^-$) at 1270 nm. The lifetime of this emission has a pronounced solvent dependence.[8] Whereas $^1\Delta_g$ has a ms lifetime in the gas phase, it is dramatically shortened in condensed phases. The lifetime in aqueous solution is ~2-5 μs, but this is slightly prolonged in deuterated solvent (i.e. approximately 10-times longer in D_2O than H_2O).[63–65] Time-resolved luminescence measurements have been used to detect $^1O_2$* in isolated PSII reaction centers in buffer,[25,66–70] or in intact mammalian cells.[71–74] Of note, $^1O_2$* was found to be surprisingly long-lived in a single neuron or HeLa cell (with lifetimes ranging from ~600 ns to ~3 μs), suggesting that $^1O_2$* may be able to diffuse across distances on the order of ~100 nm.[23,75] Yet, the apparent lifetime of $^1O_2$* strongly depends on the local environment, being largely dictated by the intracellular domain in which it was produced.[76,77] Unsurprisingly, the lifetime of $^1O_2$* is strongly affected by interaction with biomolecules, resulting in its quenching in congested biological environments.[77]

While successful detection of $^1O_2$* phosphorescence in intact photosynthetic systems has been demonstrated, the method has rarely been extended to samples more complex than isolated PSII in buffer. In fact, Li et al. remarked that "experimental determination of the kinetic rate constants of the singlet oxygen emission endogenously produced by PSII in chloroplasts would be a tall order."[70] It is possible that improved detection capabilities, such as newly-available

superconducting nanowire single-photon detectors,[78] could enable direct measurements of $^1O_2$* in intact photosynthetic systems.

For the time being, most studies of $^1O_2$* in photosynthesis instead rely on indirect detection schemes, generally based on introducing an exogenous probe molecule to the sample. Currently available indirect detection approaches for $^1O_2$* face several challenges. Ideally the probe molecule should react selectively with $^1O_2$*, not other ROS, although this is not always the case. Additionally, it can be difficult to localize the probe molecule at the sites of $^1O_2$* in the thylakoid membrane inside plant or algal cells without disturbing the cell wall or overall health of the cell. Finally, the probe must be able to withstand continued white light illumination at similar PPFDs as those regularly encountered in the natural environment.

The molecular structures for two common commercially available molecular probes for $^1O_2$* detection are shown in Figure 6-2. The first, the fluorophore singlet oxygen sensor green (SOSG), is converted to an endoperoxide product (SOSG-EP) upon reaction with $^1O_2$*, which then emits in the green region of the spectrum (Fig. 6-2A).[79] While fluorescence-based detection is convenient, there are many obstacles associated with reliable detection of $^1O_2$* in intact photosynthetic systems by SOSG. For example, the photochemical properties of SOSG are highly dependent on the irradiation wavelength; exposure of SOSG to light with wavelengths of 355 nm or 532 nm can photosensitize $^1O_2$*,[80,81] limiting the reliability of SOSG for tracking $^1O_2$* during illumination with white light of high PPFD. Even more challenging are issues related to the permeability of the bulky SOSG molecule across cellular barriers. While SOSG has been successfully used in some photosynthetic organisms, it is not readily able to diffuse across the cell walls and membranes of many species of algae and cyanobacteria.[82]

Therefore, given the obstacles associated with optical detection of $^1O_2$* using SOSG, an alternative detection scheme is necessary, ideally using a less bulky molecular probe. Like SOSG, the sterically hindered amine, 2,2,6,6-tetramethylpiperidine (TEMP), is thought to react selectively with $^1O_2$*. The reaction product is the stable nitroxide radical species 2,2,6,6-tetramethyl-1-piperidinyloxyl, referred to as TEMPO, which is detectible by EPR methods (Fig. 6-2B).[83] Importantly, unlike SOSG, which has a molar mass of 601.1 g/mol, TEMP is significantly smaller at 141.3 g/mol and thereby TEMP may be more easily able to pass through cellular barriers.

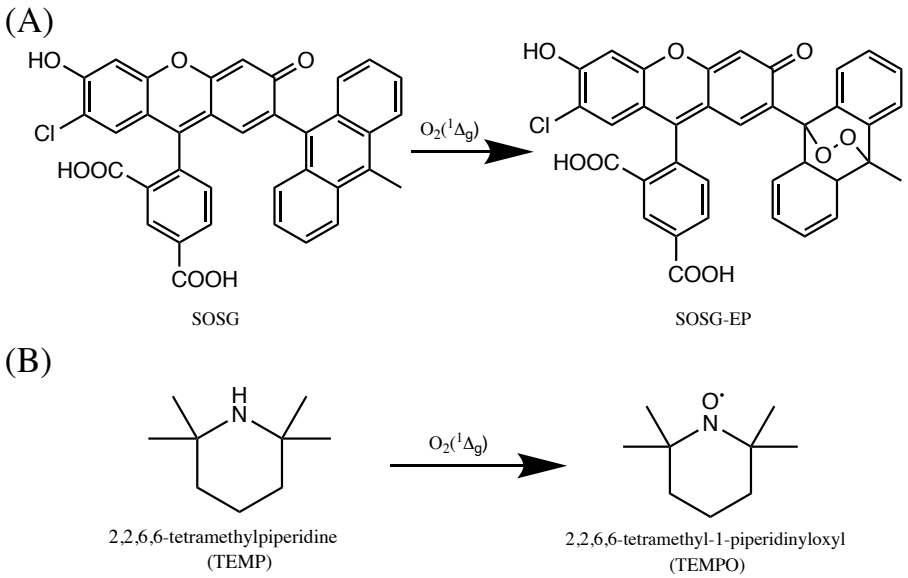

Figure 6-2. Common singlet oxygen reaction detection schemes. (A) Fluorescence-based detection of the SOSG-EP product (excitation 504 nm; emission 525 nm). (B) EPR-based detection of TEMPO, the nitroxide radical product.

There have been numerous studies using TEMP, or similar spin traps, for EPR-based detection of $^1O_2$* in photosynthetic systems of various complexity. The approaches have varied widely in terms of experimental parameters, including the type of sample preparation (ranging from isolated LHCII to PSII-enriched BBY or thylakoid membranes isolated from various species), spin trap (TEMP or TEMPD), spin trap concentration (typically ranging from 10 to 100 mM), buffer pH (from 6.3 to 8.0), and high-light illumination conditions (PPFD, color and duration). A selection of such papers is shown in Figure 6-3 and the relevant experimental details for each study are listed in Table 6-1. Generally, previous uses of TEMP for detection of $^1O_2$* have been limited to isolated photosynthetic systems that are no more complicated than the thylakoid membrane. However, recently TEMP-based detection of $^1O_2$* has been employed in chloroplasts from *A. thaliana* during short-term (i.e. 2 min) illumination[84] as well as intact cells of *C. reinhardtii* under heat stress in the dark.[85] Yet, the method has not been used to systematically explore the temporal connections between $^1O_2$* and NPQ dissipation mechanisms while a photosynthetic sample is exposed to various high light intensities.

In this chapter, I employ spin-trapping EPR spectroscopy for detection of $^1O_2$* produced by photosensitization in dye-based chemical systems and extend it to monitoring the dynamics of $^1O_2$* production in natural Chl-based photosynthetic systems. By combining EPR measurements alongside time-resolved fluorescence measurements of NPQ in spinach thylakoid membranes, we observe an intriguing correlation between the amount of $^1O_2$* (as detected by EPR) and the average lifetime of the Chl excited state (as detected by TCSPC). These results support the conventional model of NPQ in regulating the amount of $^1O_2$* produced during short term photo-oxidative stress (i.e. <15 min of high light).

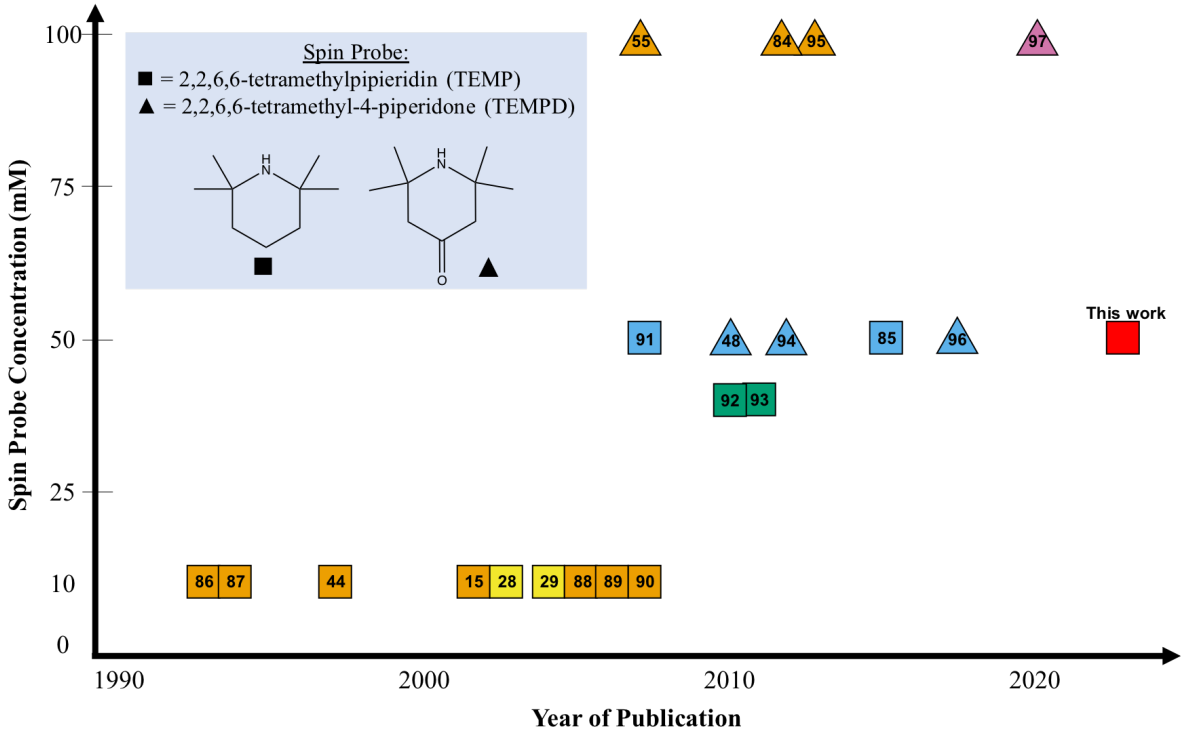

Figure 6-3. A selected history of literature articles that utilize spin-trapping EPR for detection of $^1O_2$* in photosynthetic samples. Shown are journal articles employing TEMP (square markers) or TEMPD (triangle markers) and the concentration of spin probe used. The figure inset shows the chemical structures of the relevant spin probes. Literature papers are color-coded according to the following groupings of shared senior researchers: Hideg and/or Krieger-Liszkay (orange), Rinalducci and Zolla (yellow), Pospíšil (blue), Sang (green), and Lambrev (pink). For reference, the concentration of TEMP used in the current work is shown in red. Experimental details for each literature article are documented in Table 6-1 – including the type of photosynthetic sample, buffer pH, and illumination intensity, color, and duration – along with the author and year of publication.

Table 6-1. Experimental parameters used in previous EPR-based studies of $^1O_2$* in the photosynthesis literature. Abbreviations used are as follows. For photosynthetic species, A.t. = *Arabidopsis thaliana*, B.c. = *Bryopsis corticulans,* C.r. = *Chlamydomonas reinhardtii*, T.e. = *Thermosynechococcus elongatus*. Other abbreviations include BBY for Berthold–Babcock–Yocum PSII-enriched thylakoid membranes, n/a for "non-applicable", and n/s for "not specified by authors". PPFD (photosynthetic photon flux density) is listed in units of µE = µmol m^{-2} s^{-1}.

Reference	Author (Year)	Sample	Spin Label	pH	Illumination (PPFD)	Illumination (Color)	Illumination (Time)
86	Hideg (1994)	spinach thylakoids	TEMP	7.5	1000 µE	white	0-180 min
87	Hideg (1994)	spinach thylakoids	TEMP	7.5	1000 µE	white	0-180 min
44	Krieger (1998)	spinach BBY	TEMP	6.5	1100 µE	white	25 min
15	Fufezan (2002)	spinach BBY	TEMP	6.5	1800 µE	red	15 min
28	Zolla (2002)	LHCII	TEMP	6.3	1000 µE	white	0-120 min
29	Rinalducci (2004)	LHCII	TEMP	6.3	100 µE	white	60 min
88	Fischer (2005)	spinach thylakoids	TEMP	n/s	150 or 250 µE	white	10 min
89	Fischer (2006)	spinach BBY	TEMP	6.5	120 or 3000 µE	white	0-40 min
55	Fischer (2007)	C.r. thylakoids	TEMPD	6.7	1600 µE	white	10 min
90	Fufezan (2007)	T.e. BBY	TEMP	6.5	1500 µE	red	0-90 min
91	Pospíšil (2007)	spinach BBY	TEMP	6.5	0 µE @47 °C	n/a	n/a
48	Yadav (2010)	spinach BBY	TEMPD	6.5	1000 µE	white	10 min
92	Sang (2010)	B.c. cyt b_6f	TEMP	8.0	1500 µE	white	0-15 min
93	Sang (2011)	spinach cyt b_6f	TEMP	8.0	3000 µE	white	9 min
94	Yadav (2012)	spinach BBY	TEMPD	6.5	1000 µE	white	0-30 min
84	Roach (2012)	A.t. chloroplast	TEMPD	7.6	500 µE	red	2 min
95	Ramel (2013)	A.t. thylakoid	TEMPD	7.5	1500 µE	red	3 min
85	Prasad (2016)	C.r. cells	TEMP	7.0	0 µE @40 °C	n/a	n/a
96	Ksas (2018)	A.t. thylakoid	TEMPD	6.5	1000 µE	white	30 min
97	Lingvay (2020)	pea LHCII	TEMPD	n/s	2400 µE	white	30 min

6.2 Materials and Methods

6.2.1 Thylakoid membrane preparation

Preparation of thylakoid membranes was performed in a dark room with a green headlamp as the only light source. All glassware and centrifuge tubes were chilled prior to use. Baby spinach leaves (10-16 oz, store bought) were washed with cold water, placed into a paper towel-lined bin, and dark-adapted overnight at 4 °C. Destemmed leaves were placed in a blender (Sunbeam, 1.5 L) with 300-500 mL of ice-cold Grinding Buffer. The leaves were ground using 3-5 short pulses of 1 sec duration. Immediately after grinding, the leaf suspension was filtered through a Hamilton Beach Big Mouth juice extractor to remove large particulates. The spinach solution was then transferred to centrifuge bottles and spun in a Beckman Coulter Avanti J-26 XP set to 4 °C, according to the two different protocols specified below.

Isolation of crude thylakoid membranes was based on the protocol reported by Gilmore et al.[98] and modified according to Park et al. for transient absorption spectroscopy (see Chapter 2 of this dissertation).[99,100] The Grinding Buffer (pH 8.2) contained 0.33 M sorbitol, 50 mM Na_2HPO_4, 50 mM KH_2PO_4, 25 mM KCl, 5 mM $MgCl_2$, and 10 mM EDTA, with 12 mM L-ascorbic acid added immediately prior to use. The spinach solution was centrifuged for 5 min at 2000 g. The supernatant was discarded, and the pellet was gently resuspended in ~10 mL Resuspension Buffer using a paint brush and stored on ice until use. The Resuspension Buffer (pH 7.6) contained 0.33 M sorbitol, 5 mM $MgCl_2$, 4 mM EDTA, 2 mM $MnCl_2$, 100 mM HEPES, and 0.2% (w/v) fatty acids-free BSA. Protease inhibitors consisted of 0.2 mM PMSF, 2 mM benzamidine, and 1 mM ε-aminocaproic acid. The Measuring Buffer (pH 8.0) contained 0.1 M sucrose, 5 mM $MgCl_2$, 10 mM NaCl, 10 mM KCl, 1 mM KH_2PO_4, 10 mM tricine, and 0.2% (w/v) fatty acids-free BSA, with 30 mM L-ascorbic acid used immediately prior to use.

Isolation of purified thylakoid membranes was performed following the protocol of Utschig et al.[101] The Grinding Buffer (pH 7.5) contained 0.4 M NaCl, 20 mM HEPES, 4 mM $MgCl_2$, 5 mM EDTA, and 1 mg/mL fatty acids-free BSA. The spinach solution was centrifuged for 6 min at 6466 g. Supernatant was discarded and pellet was gently resuspended in Wash Buffer using a paint brush. The Wash Buffer (pH 6.5) contained 0.15 M NaCl, 20 mM HEPES, 4 mM $MgCl_2$, 1 mM EDTA, and 1 mg/mL fatty acids-free BSA. Resuspended thylakoids were centrifuged for 1 min at 483 g. The supernatant was collected and centrifuged for 6 min at 5915 g. Pellets were resuspended using ~30 mL Suspension Buffer and centrifuged for 8 min at 12070 g. The Suspension Buffer (pH 6.0) contained 15 mM NaCl, 20 mM HEPES, 5 mM $MgCl_2$, 1 mM EDTA, 1 mg/mL fatty acids-free BSA, and 20% glycerol. Pellets were then resuspended in another 30 mL portion of Suspension Buffer and centrifuged for 8 min at 15960 g. Finally, pellets were resuspended in 6-8 mL Suspension Buffer and stored on ice until use.

The approximate chlorophyll concentration of each thylakoid preparation was measured in cold 80% acetone using a Beckman DU 800 spectrophotometer and quantified using the Arnon equations.[102,103] Thylakoid samples were either used fresh by diluting the stock directly into buffer, or frozen at -80 °C until use.

6.2.2 EPR Spin-Trapping Measurements

Continuous-wave (cw) X-band (9.5 GHz) EPR spectra and time traces were measured using a Bruker ELEXYS II E500 EPR spectrometer (Bruker Biospin Corp, Ettlingen, Germany) equipped with a TE_{102} rectangular EPR resonator (Bruker ER 4102ST). Samples were measured at room temperature in glass EPR capillary tubes with 1 mm inner diameter. All EPR spectra were acquired using field modulation (100 kHz) with an amplitude of 2 G and phase-sensitive detection, leading to first-derivative type spectra. Unless otherwise specified, spectra were acquired at 12 dB microwave attenuation (12.6 mW).

To illuminate samples for photosensitization of singlet oxygen, a daylight white LED (SOLIS-3C, Thorlabs) was focused into the EPR cavity. PPFD for illumination was changed by altering the brightness of the LED. The spin probes were purchased commercially and used as received. They included 2,2,6,6-tetramethylpiperidine (TEMP), 2,2,6,6-tetramethyl-4-piperidone (TEMPD), and 4-hydroxy-2,2,6,6-tetramethylpiperidine (TEMP-OH).

6.2.3 EPR Snapshot Measurements of Singlet Oxygen in Thylakoid Membranes

Purified thylakoid membranes (~2.8 mg Chl mL^{-1}) were diluted to a final concentration of ~250 µg Chl mL^{-1} in glycerol resuspension buffer (15 mM NaCl, 20 mM MES, and 20% glycerol in milli-Q water at pH 6) in the presence of 0.5 mM ATP. Where specified, 2 µL nigericin (50 mM stock prepared in ethanol) was also added at a final concentration of 100 µM. The thylakoid suspension was stirred and pre-illuminated with 1000 µmol m^{-2} s^{-1} of white light for a set amount of time using an LED (SOLIS-3C, Thorlabs). After the pre-illumination period was finished, 50 µL of TEMP (1 M stock prepared in acetonitrile) was added to the cuvette to reach a final concentration of 50 mM and allowed to incubate while stirring in the presence of continued illumination. Alternatively, in place of TEMP, 50 µL of the TEMPO nitroxide radical (600 µM stock prepared in acetonitrile) was added to the cuvette to reach a final concentration of 30 µM. All sample handling was performed under ambient conditions.

To avoid the light-induced decrease in the TEMPO nitroxide radical signal that was observed during extended illumination of thylakoid membranes in the EPR cavity, the incubation time for TEMP was limited to 1 minute, corresponding to the approximate timing for maximal TEMPO signal. Following exactly 1 min of incubation, aliquots were transferred to a microcentrifuge tube and immediately flash frozen with liquid nitrogen, a process that took 15-30 sec in total. Frozen samples were stored in the dark at -80 °C until measurement. All EPR spectra were measured within 10 days of freezing the thylakoid sample.

Prior to EPR measurement, each sample was annealed until thawed and promptly transferred to an EPR capillary tube (1 mm diameter), a process that took 1-2 minutes in total. Care was taken to minimize illumination of the sample during this process. A cw X-band EPR spectrum was recorded for each sample at room temperature with 2 G modulation amplitude and 12 dB microwave attenuation. Double integral fitting of each X-band EPR spectrum using a model spin representative of the nitroxide radical (XEPR Spin Count function) was used to quantify the concentration of TEMPO contained in each sample. As a secondary quantification, the relative intensities of the mid-field EPR peak at 3375 G were compared to estimate the changes in TEMPO signal.

6.2.4 Fluorescence Lifetime Measurements

All fluorescence lifetime measurements reported in this chapter were performed at the Center for Nanoscale Materials, a user facility at Argonne National Laboratory. Thylakoid membrane samples (in the presence of 50 μM methyl viologen and 0.5 mM ATP) were placed in a glass cuvette with a micro stir bar. In order to induce NPQ in the membranes, thylakoids were illuminated with 1000 μmol m^{-2} s^{-1} of white light provided by an LED (SOLIS-3C, Thorlabs). At specified time points, a 300 μL aliquot of the sample was transferred to a 1 mm cuvette (21-Q-1, Starna Cells) and then measured by time-correlated single-photon counting (TCSPC), where the combined transfer and measurement process took ~30 sec. Excitation was provided by a 405 nm laser diode (PC-405B, Picoquant) with a power of 91 μW at the sample. The repetition rate of the laser was set to 5 MHz for 1 second snapshot measurements or 20 MHz for 4 second snapshot measurements. Chl *a* fluorescence emission was collected using a 40 mm focal length collection lens, a monochromator (SP2300, Acton) set to 680 nm with slit width of 25 microns, and detected using an avalanche photodiode (PDM, OptoElectronics Corp). The bin size for collecting the fluorescence decay was 25 ps. Fluorescence decays were fit to an exponential decay function. The extent of quenching was calculated as $NPQ_\tau(t) = \frac{\tau_{\mathrm{dark}} - \tau(t)}{\tau(t)}$, where τ_{dark} is the original fluorescence lifetime prior to illumination and $\tau(t)$ is the fluorescence lifetime at time point *t* during the 30-min high-light illumination or subsequent 30-min dark relaxation period.

6.2.5 Oxygen Evolution Measurements

The functionality of thylakoid membrane preparations was characterized by measurements of oxygen evolution. 2,6-dichloro-1,4-benzoquinone (DCBQ), ferricyanide ($Fe(CN)_6$), and/or methyl viologen (MV) were added to thylakoid suspensions at concentrations of 250 μM, 1 mM, and 500 μM, respectively. DCBQ is a quinone capable of accepting electrons from PSII and ferricyanide oxidizes any reduced Q_A, thereby keeping PSII reaction centers open.[104] Methyl viologen was also used as an electron acceptor. 2-(3,4-dichlorophenyl)-1,1-dimethylurea (DCMU) was added as an inhibitor of PSII.[104]

Thylakoid samples were diluted into de-oxygenated buffer and placed into a septa-sealed cuvette with a micro stir bar. Care was taken to minimize light exposure prior to high light illumination. Thylakoids were illuminated with either 1000 or 3000 μmol m^{-2} s^{-1} of white light provided by an LED (SOLIS-3C, Thorlabs) during stirring at 500-700 rpm. A needle-piercing Clark-electrode (Oxy-NP, Unisense) was used for measurement of oxygen concentration. Prior to each experiment, a two-point O_2 concentration calibration was performed using zero-O_2 (containing 0.1 M sodium ascorbate and 0.1 M sodium hydroxide) and O_2-saturated solutions.

6.3 Results and Discussion

6.3.1 EPR spin-trapping method for detection of singlet oxygen photosensitization

The molecule 2,2,6,6,-tetramethylpiperidine (TEMP) is a commonly employed spin trap for EPR spectroscopy of biophysical systems.[105,106] TEMP does not have any unpaired electrons and hence it is EPR silent. However, in the presence of singlet oxygen ($^1O_2$*), TEMP is converted to the stable nitroxide radical TEMPO. TEMPO is an electronic doublet with nuclear spin I=1, leading to splitting of the EPR transition into a triplet (2I+1 = 3). Therefore, the TEMPO product is detectable as a triplet in the X-band EPR spectral region (Figure 6-4).

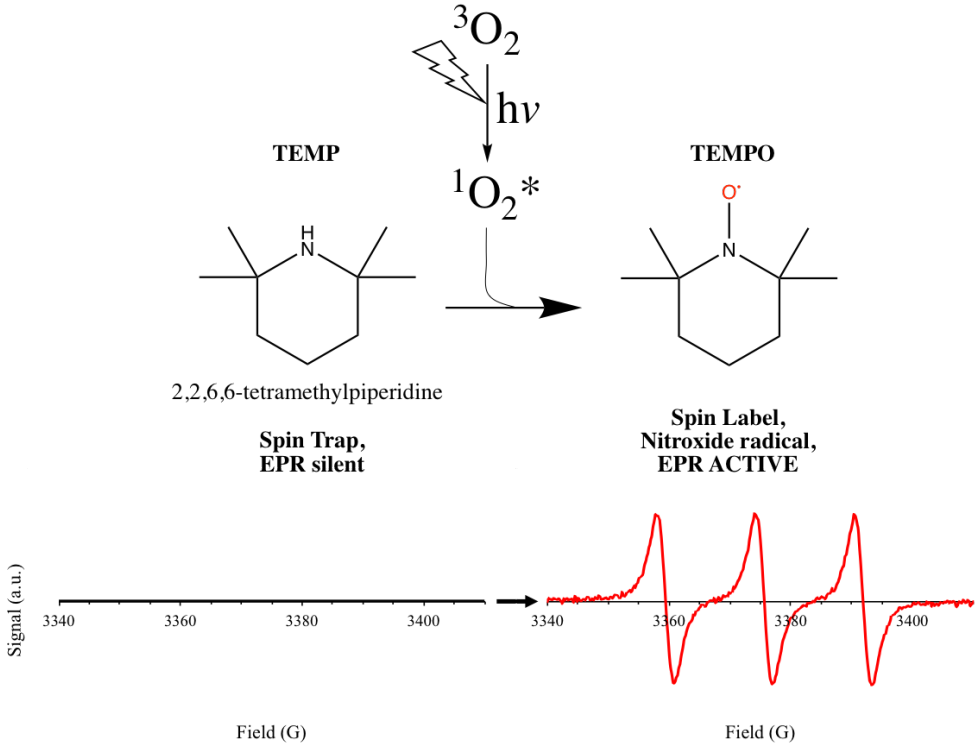

Figure 6-4. Principle of EPR-based spin trapping method for detection of singlet oxygen. The electronically excited state of molecular oxygen reacts with the spin trap, TEMP (2,2,6,6-tetramethypiperidine), producing the stable nitroxide radical TEMPO which is detectable as an EPR triplet at X-band (*spectrum*: 15 µM TEMPO in acetonitrile, measured at 2 G modulation amplitude and 12 dB attenuation).

In order to investigate a system significantly less complicated than that of the thylakoid membrane, we first selected two commercially available dyes that are commonly used for photosensitization of $^1O_2$*, toluidine blue (TB)[83,86,107] and rose bengal (RB)[108–110] (see Figure 6-5 for UV-visible absorption spectra of TB and RB). A daylight white LED covering the entire visible spectral region from 400-800 nm was used to illuminate the sample directly in the EPR cavity, exciting the dyes to the S_1 singlet excited states. Subsequent ns-timescale intersystem crossing to the longer-lived triplet state ($S_1 \rightarrow T_1$) enables triplet-triplet energy transfer (TTET) in which the T_1 state of the chromophore can be quenched by the ground state of molecular oxygen. The ultimate product of this photosensitization process, $^1O_2$*, can then be trapped by the spin trap TEMP, yielding the TEMPO nitroxide radical.

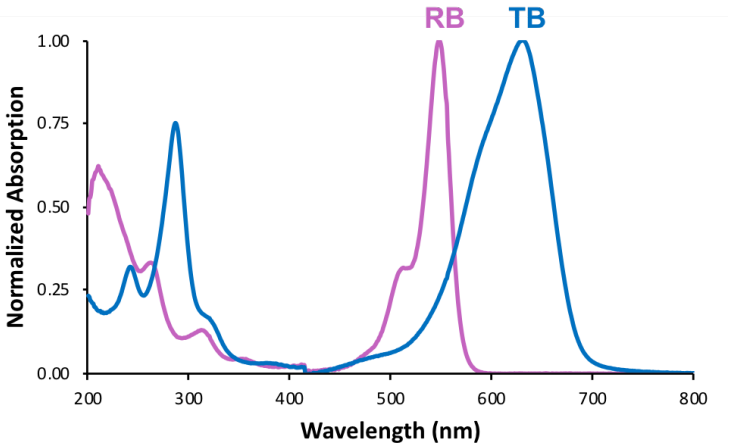

Figure 6-5. Absorption spectra for toluidine blue (TB, blue curve) and rose bengal (RB, pink curve) photosensitizers dissolved in milliQ water. Each spectrum is normalized at its maximum, 547 nm and 631 nm, respectively.

Upon illumination of an aqueous solution of TB and TEMP-OH in the EPR cavity with white light with PPFD of 1000 µmol m^{-2} s^{-1}, we observed an increase in the EPR signal confirming the real-time conversion of the EPR-silent form to the EPR-active TEMPO nitroxide radical. The rate of the signal increase was highly dependent on the light intensity used for illumination: at low PPFD (e.g. 2% LED brightness), the signal increased for at least 10 minutes, while under higher PPFD (e.g. 20% LED brightness) the maximal signal was reached much more quickly (Figure 6-6) even though the overall amount of signal was identical. Surprisingly, continued illumination after the maximum resulted in decreasing EPR signal, where the rate of decrease was again dependent on the illumination intensity.

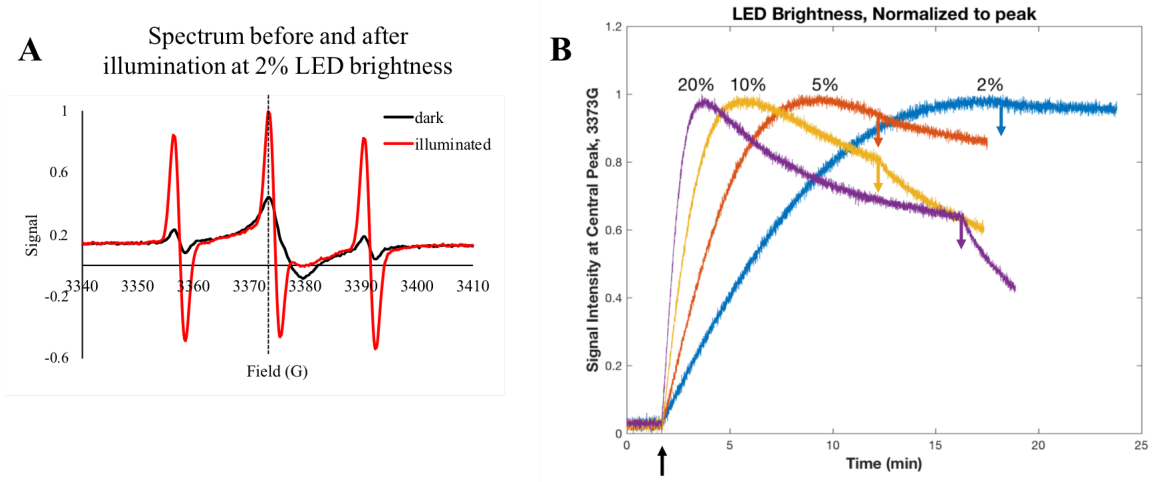

Figure 6-6. Toluidine blue (TB) as a photosensitizer for production of singlet oxygen. $^1O_2$* produced by illuminating 1 mM TB was detected using 50 mM 4-hydroxy-2,2,6,6-tetramethypiperidine (TEMP-OH) in water. (A) Spectra measured before and after illumination at 2% LED brightness (corresponding to ~1000 µmol m^{-2} s^{-1}). Vertical dashed line indicates the peak at 3373 G. (B) Time traces show the signal intensity for the central peak (3373 G) for different illumination intensities. The LED was turned ON at 2 min (see upright arrow), and turned OFF at 12, 16, or 18 min, respectively (see colored downright arrows). All EPR spectra and traces were measured at room temperature with 2 G modulation amplitude and 12 dB attenuation.

Compared to TB, illumination of an aqueous solution of RB and TEMP resulted in formation of a much larger TEMPO signal (Figure 6-7). This difference is due to a higher quantum yield of intersystem crossing (Φ_{ISC}) for RB relative to TB, likely enabled by the presence of multiple heavy atoms (halogen substituents) in RB.[110,111] It is also consistent with a reported ~75% singlet oxygen quantum yield (Φ_{Δ}) for RB compared to a Φ_{Δ} of ~50% for TB at neutral pH.[107,112,113] Therefore, given its high Φ_{ISC} and Φ_{Δ} leading to a significant TEMPO signal, RB was selected as an ideal dye for further systematic investigation of the effects of both light intensity and dissolved O_2 on $^1O_2$* photosensitization.

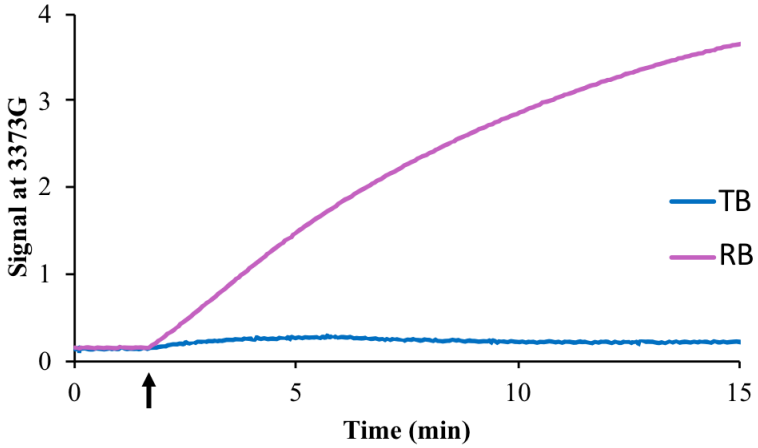

Figure 6-7. Comparison of toluidine blue (TB) and rose bengal (RB) as photosensitizers for production of singlet oxygen. $^1O_2$* produced by illuminating 0.2 mM TB or RB was detected using 10 mM 4-hydroxy-2,2,6,6-tetramethypiperidine (TEMP-OH) in water. Traces show the signal intensity at the central peak (3373 G) as a function of time. The LED was turned ON at 2 min (see upright arrow) with an LED brightness of 10%. Both traces were measured at room temperature with 2 G modulation amplitude and 12 dB attenuation.

We next illuminated an aqueous solution of 0.2 mM RB and 10 mM TEMP-OH directly in the EPR cavity. Upon exposure to low PPFD (220 µmol m^{-2} s^{-1}) we observed an increase in EPR signal at 3358 G corresponding to the TEMPO product (Figure 6-8). Upon increasing the PPFD to 1780 µmol m^{-2} s^{-1}, the rate of the signal increased, and subsequent increase of the PPFD to greater than 8000 µmol m^{-2} s^{-1} lead to an even larger increase in signal. Compared to an ambient solution, the oxygen-saturated solution of RB and TEMP-OH showed much larger rates of signal increase at all three PPFDs, likely due to the availability of more O_2 to react with the triplet excited state of RB. Conversely, an oxygen-depleted solution of RB and TEMP-OH showed no increase in signal, due to absence of O_2 and therefore lack of TTET between RB and molecular O_2.

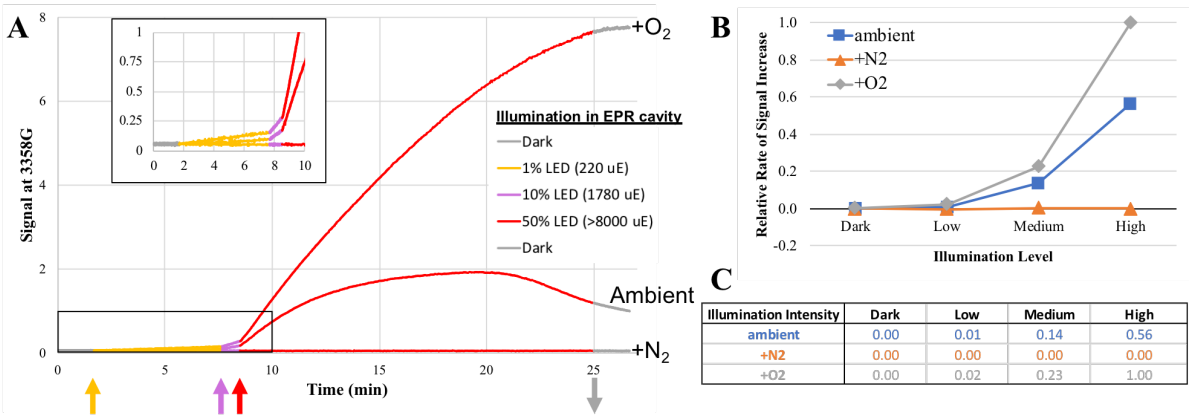

Illumination Intensity	Dark	Low	Medium	High
ambient	0.00	0.01	0.14	0.56
+N2	0.00	0.00	0.00	0.00
+O2	0.00	0.02	0.23	1.00

Figure 6-8. Kinetics of singlet oxygen photosensitization by rose bengal (0.2 mM), detected by TEMP-OH (10 mM) in water. (A) Time traces for the EPR signal monitored at 3358 G for ambient, O_2-saturated (+O_2), and O_2-depleted (+N_2) samples as a function of time during direct illumination in the EPR cavity. The legend shows approximate illumination intensities. The LED intensity was increased at the time points denoted by the yellow, pink, and red arrows. The LED was switched off at 25 min (grey arrow). *Inset*: enlargement of the first 10 min showing increasing signal for the low and medium light intensities. (B, C) The relative rates of singlet oxygen photosensitization for each LED illumination intensity, taken as the initial slope of the EPR signal increase at 3358 G during the first 100 sec of each illumination condition. Dark, low, medium and high correspond to 0%, 1%, 10%, and 50% LED brightness, respectively.

We conclude that rose bengal is an excellent photosensitizer for production of $^1O_2$* in aqueous solution, resulting in roughly ~17-fold higher EPR signal than toluidine blue under similar conditions (Figure 6-7). Nonetheless, both dyes enable photosensitization of $^1O_2$*, displaying rates of TEMPO production that scale with increasing PPFD. Furthermore, the rate of the increase in signal depends on the dissolved O_2 content in the solution, with larger TEMPO signals being observed for O_2-saturated solution. Surprisingly, continued illumination eventually results in destruction of the nitroxide radical TEMPO signal, a process that is also dependent on the PPFD.

6.3.2 Characterization of thylakoid membrane functionality: O_2 evolution

As demonstrated in the previous section, the yield of the TEMPO EPR signal is highly dependent on the amount of O_2 dissolved in solution. Therefore, various thylakoid membrane preparations (described in detail in the Materials and Methods section) were evaluated for their capability to evolve O_2 during illumination in the presence of various electron acceptor molecules and in different buffers at pH 6 or 8 (Figure 6-9). As expected, O_2 evolution was observed from thylakoid membranes only in the presence of external electron acceptors (Figure 6-9A). The amount of O_2 evolved from the thylakoids was significantly larger for a purified thylakoid membrane sample that had been freshly prepared compared to a crude thylakoid membrane preparation that had remained frozen for ~2 months prior to measurement. Using the fresh thylakoids, no O_2 evolution was observed in the presence of only MV, but significant O_2 was produced when the external quinone DCBQ was present (Figure 6-9B), regardless of the presence of either ferricyanide or methyl viologen.

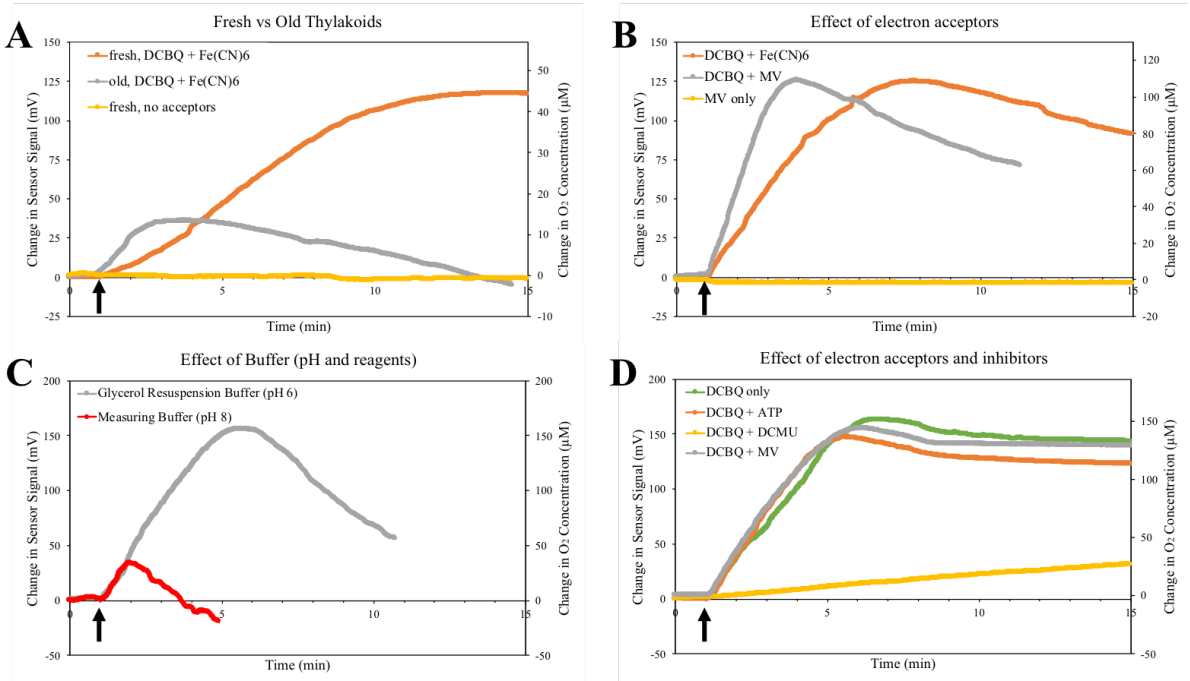

Figure 6-9. Functionality of thylakoid membrane samples: characterization of oxygen evolution activity. (A) Comparison of fresh 1-day-old purified and 2-month-old frozen crude thylakoids in the presence and absence of electron accepting molecules. (B) Comparison of different electron acceptor molecules, DCBQ, ferricyanide, and methyl viologen. (C) Comparison of glycerol resuspension buffer (pH 6) and sucrose measuring buffer (pH 8), where both samples used the same thylakoid stock in the presence of DCBQ and MV. (D) Comparison of electron acceptor molecules, DCBQ, ATP, MV, and PSII inhibitor DCMU. All O_2 evolution curves were measured using a Unisense Oxy-NP probe. Each panel represents an independent experiment with a unique 2-point O_2 concentration calibration, ranging from 0 to 278 µM. Prior to measurement, buffers were bubbled with N_2 for at least 30 min to minimize the concentration of O_2. Immediately prior to measurement, thylakoid stock was diluted into buffer in a septa-capped cuvette equipped with a stir bar and stored in the dark. For each experiment, the LED was turned ON at 1 min, as indicated by arrows.

The O_2 evolution capabilities were further evaluated using the purified membrane preparation diluted to identical Chl concentrations but using different buffers (Figure 6-9C). O_2 evolution was found to be significantly enhanced in a minimal glycerol Resuspension Buffer at pH 6 relative to a sucrose Measuring Buffer at pH 8. Finally, the minimal electron acceptor requirements for O_2 evolution from thylakoids were determined (Figure 6-9D). The amount of O_2 evolved was similar for DCBQ alone, DCBQ with ATP, or DCBQ with MV. However, O_2 evolution was significantly impaired upon addition of DCMU, consistent with DCMU's known function of blocking electron flow from Q_A to Q_B, resulting in closed PSII reaction centers.[104]

In sum, it is concluded that optimal O_2 evolution capabilities occur with freshly-prepared purified thylakoid membranes dissolved in a glycerol resuspension buffer at pH 6 and in the presence of the quinone DCBQ.

6.3.3 Characterization of thylakoid membrane functionality: NPQ

In order to monitor the nonphotochemical quenching (NPQ) capabilities in the two spinach thylakoid membrane preparations – purified vs crude thylakoids – we measured Chl fluorescence lifetimes throughout 30 min of illumination at 1000 µmol m^{-2} s^{-1} followed by 30 min of dark. During high light, the purified thylakoid membranes showed large changes in the average Chl

fluorescence lifetime, corresponding to an NPQ_τ value of approximately 2 (Figure 6-10, top panels). Surprisingly, the amount of quenching was lower in the presence of ascorbate, contrary to the expected role of ascorbate in the enzymatic conversion of violaxanthin to zeaxanthin by violaxanthin de-epoxidase.[114,115] Both the magnitude and kinetics of quenching in purified thylakoid membranes was largely unaffected by differences in the buffer composition and pH (i.e. glycerol resuspension buffer at pH 6 vs. sucrose measuring buffer at pH 8) or the addition of 50 µM methyl viologen, consistently reaching NPQ_τ values between 1.5 and 2 (Figure 6-10, bottom panels). However, addition of 250 µM DCBQ resulted in substantially quenched fluorescence lifetimes; even prior to illumination, the fluorescence lifetime was on the order of 0.5 ns when DCBQ was present compared to 1.8 ns when it was absent (Figure 6-10, green curves). Additionally, the sample with DCBQ exhibited very little change in fluorescence lifetime upon illumination. The addition of DCBQ, a supplementary quinone, to the thylakoid membranes may have enabled continuous turnover of PSII reaction centers, resulting in highly quenched fluorescence lifetimes due to enhanced trapping of excitation by P_{680} in the reaction center.

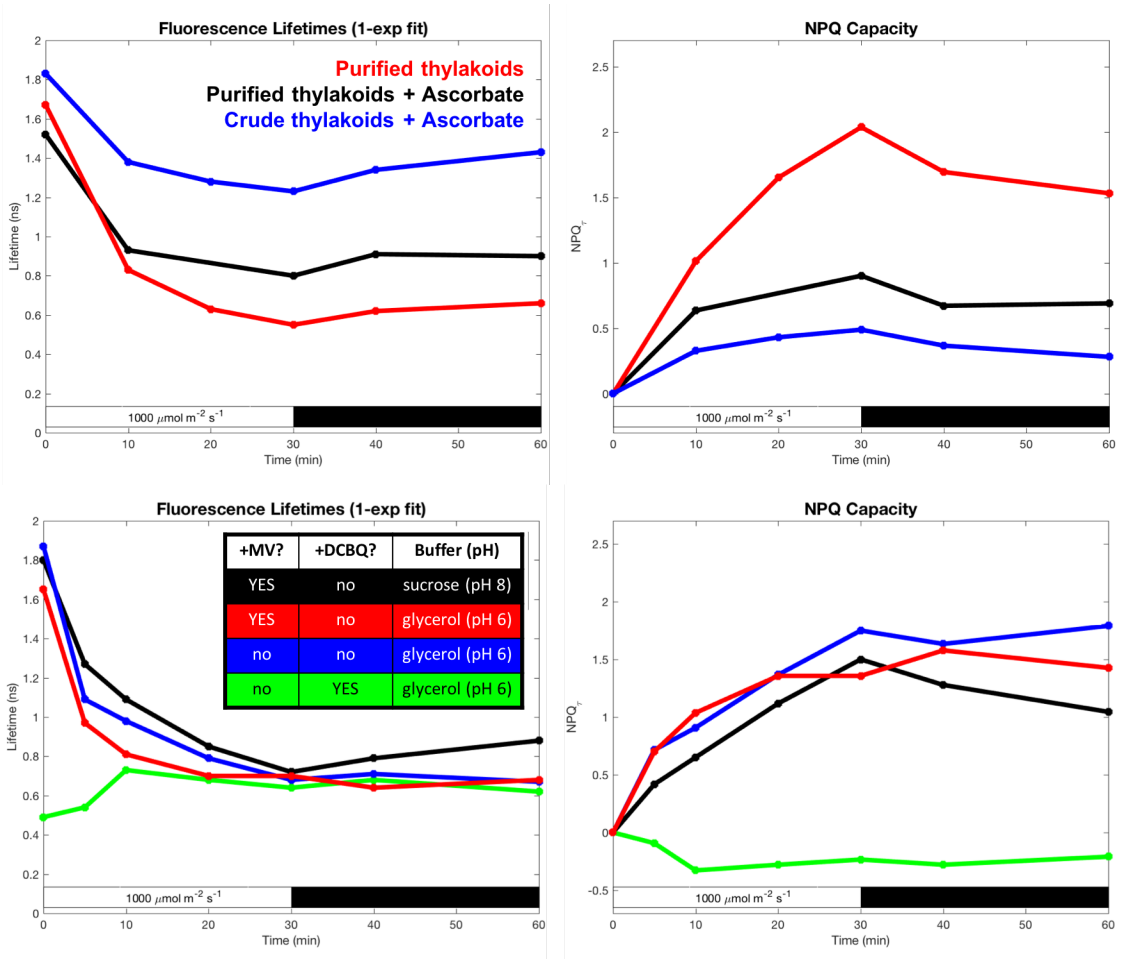

Figure 6-10. Functionality of thylakoid membranes in terms of quenching capabilities. Chl fluorescence lifetime snapshots were measured at various points during 30 min of high light (1000 µmol m^{-2} s^{-1}) followed by 30 min of dark. The top panels show the comparison of purified vs crude thylakoid preparations in the presence and absence of 30 mM ascorbate. The bottom panels show the influence of the electron acceptor methyl viologen, quinone DCBQ, buffer, and pH on observed quenching dynamics for purified thylakoid membranes.

6.3.4 EPR detection of singlet oxygen production in thylakoids during illumination

We next set out to determine which spin trap, TEMP[83] or TEMPD[94,116,117], is optimal for detection of photoinduced $^1O_2$* during illumination of intact thylakoid membrane samples. We compared the X-band EPR spectrum for thylakoids incubated with 50 mM TEMP or TEMPD in the dark and after illumination (Figure 6-11). While no signal representative of any nitroxide radical was observed for thylakoids with TEMPD (Fig. 6-11A), a characteristic triplet EPR signal appeared for the sample with TEMP (Fig. 6-11B). However, upon continued illumination of the membranes, the TEMPO signal gradually disappeared. Kinetic analysis of the low-field EPR peak at 3358 G suggested that the extent of the light-induced decrease in signal scaled with the PPFD (Fig. 6-11C and D). The differences observed in Fig. 6-11C and Fig. 6-11D may reflect some experimental variability.

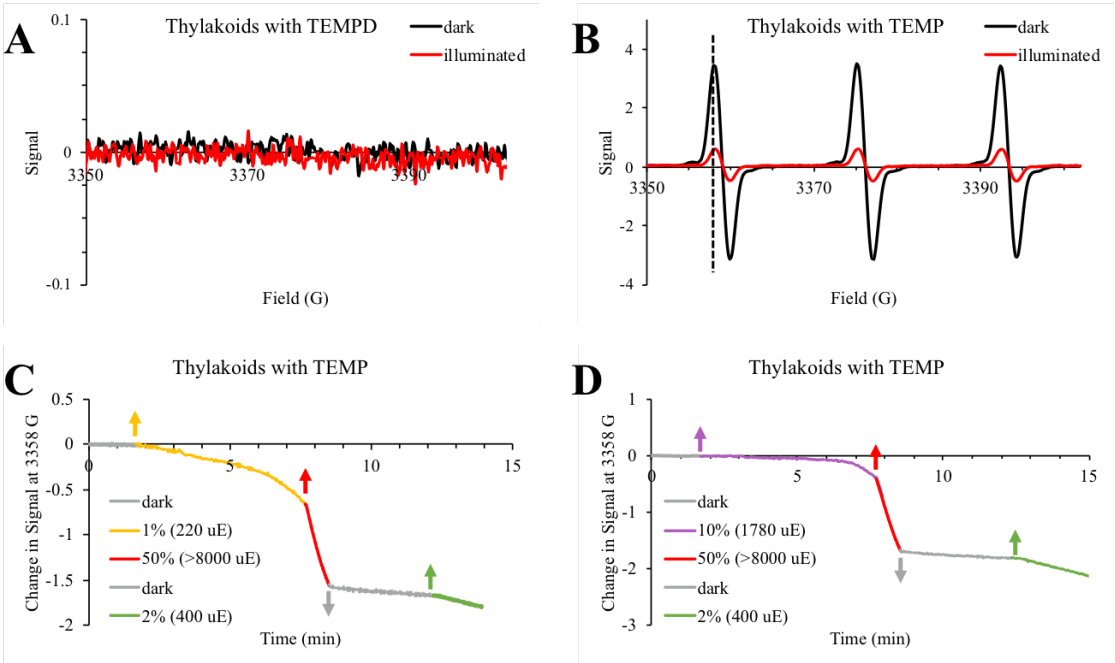

Figure 6-11. EPR spectral and kinetic analysis of purified thylakoid membranes in the presence of a spin trap, TEMPD (2,2,6,6-tetramethyl-4-piperidone hydrochloride, A) or TEMP (2,2,6,6-tetramethypiperidine, B-D). The spin trap concentration was 50 mM in glycerol resuspension buffer (pH 6) with 0.5 mM ATP. Thylakoid concentration was approximately 50 µg Chl/mL. Panels A and B: For each sample, a spectrum was recorded in the dark (black spectra) and following illumination (red spectra). The dashed vertical line in panel B corresponds to the low-field peak at 3358 G used for tracking illumination-induced kinetics. Panels C and D: Time traces showing the change in EPR signal monitored at 3358 G for two aliquots of sample exposed to sudden changes in illumination intensity inside the EPR cavity. Upward- and downward-facing arrows indicate the timing for light intensity increases and decreases, respectively. Legends specify LED brightness (and approximate light intensities in µE).

No increase in signal was observed for thylakoids at low Chl concentrations (~50 µg Chl/mL). Thylakoid samples at higher Chl concentrations (~500 µg Chl/mL) revealed a small increase in TEMPO signal during the initial illumination period. However, the signal eventually disappeared upon continued illumination even at relatively low PPFDs (Figure 6-12).

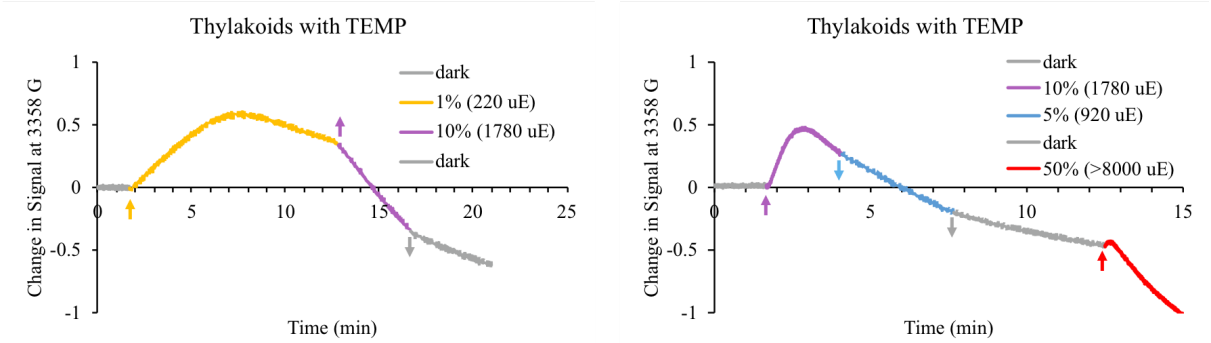

Figure 6-12. Light-intensity dependence of singlet oxygen production in purified thylakoid membranes in the presence of 50 mM TEMP (2,2,6,6-tetramethypiperidine) in glycerol resuspension buffer (pH 6) with 0.5 mM ATP. Thylakoid concentration was approximately 500 µg Chl/mL. The time traces show the change in EPR signal monitored at 3358 G for two representative samples exposed to sudden changes in illumination intensity inside the EPR cavity. Upward- and downward-facing arrows indicate the timing for light intensity increases and decreases, respectively. Legends specify LED brightness (and approximate light intensities in µE).

To investigate the origin of the decrease in TEMPO signal during illumination of thylakoid membranes, we illuminated various samples containing the nitroxide radical TEMPO and tracked the low-field peak at 3358 G (Figure 6-13). The sample consisting of 15 mM TEMPO dissolved in acetonitrile showed no change in TEMPO signal during illumination (Fig. 6-13A), while 15 mM TEMPO in the presence of 0.1 mM RB showed a sizable decrease in signal during illumination (Fig. 6-13B). Likewise, 300 mM TEMPO showed a very large decrease in signal during illumination of thylakoid membranes, with the signal entirely consumed within 15 min of illumination at PPFDs less than 2000 µmol m^{-2} s^{-1} (Fig. 6-13C).

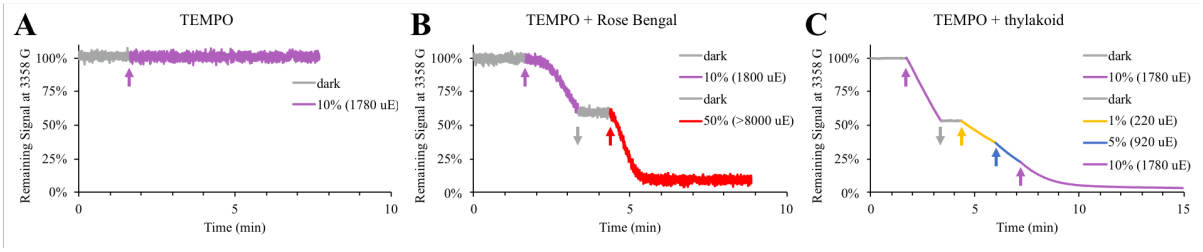

Figure 6-13. Light-intensity dependence of the nitroxide radical. Traces monitored for EPR signal at 3358 G of (A) 15 mM TEMPO in acetonitrile, (B) 15 mM TEMPO in the presence of photosensitizer (RB) in acetonitrile, and (C) 300 mM TEMPO in thylakoid membrane suspension with 0.5 mM ATP dissolved in glycerol resuspension buffer (pH 6). There was no TEMP is present, hence no increase in EPR signal is expected and each trace is instead plotted as the percent of the original signal remaining at each time point. The starting signal intensity at 3358 G was ~0.3 for 15 mM TEMPO in acetonitrile (A and B) and ~14.5 for 300 mM in thylakoid suspension (C). Upward- and downward-facing arrows indicate the timing for light intensity increases and decreases, respectively. Legends specify LED brightness (and approximate light intensities in µE).

Therefore, it was concluded that illumination of the TEMPO nitroxide radical is not directly responsible for the decrease in EPR signal. Such a decrease only occurs in the presence of a light-absorbing molecule, either dye or Chl, and the rate of the decrease is faster for higher PPFD, suggesting that an interaction between the excited states of the photosensitizer molecules and TEMPO may occur during continuous illumination. Additionally, chemical reactions leading to TEMPO degradation, such as those documented for TEMPO derivatives exposed to hydroxyl radicals,[118] might underlie the observed decrease in EPR signal during prolonged illumination.

The possibility of a secondary light-dependent reaction resulting in reduction of EPR-active TEMPO to an EPR-silent hydroxylamine implies that EPR detection of $^1O_2$* is likely an underestimate of the true $^1O_2$* concentration.[119] Such a reaction resulting in the disappearance of EPR signal during illumination has been observed in isolated LHCII proteins, with a rate that depended on the PPFD.[29] Therefore, this phenomenon is a major limitation associated with TEMPO-based detection in plant systems due to the high concentration of reducing equivalents generated during illumination of thylakoids. One possible solution is to attempt to re-oxidize the diamagnetic species back to the radical form via aeration in the presence of lead oxide, followed by extraction into ethylacetate.[29,86] Separately, a decrease in the TEMPO EPR signal has been previously observed in thylakoid membrane systems, which was interpreted as being caused by formation of a non-bilayer phase of the thylakoid membrane lipids.[120] It has also been suggested that a temporary burst of singlet oxygen produced by free and solubilized Chl may occur at the beginning of illumination,[28] though the mechanism remains undetermined.

6.3.5 Development of EPR "snapshot" spectroscopy for real-time detection of singlet oxygen in thylakoids

Due to the suspected interference of light-triggered thylakoid reducing equivalents with the TEMPO signal, we were unable to achieve tracking of $^1O_2$* in real time during extended periods of high-light illumination of thylakoid samples. Instead, we took advantage of the ~1-minute timing associated with maximal TEMPO signal from purified thylakoid membranes during high-light illumination. By incubating illuminated membranes with TEMP for exactly 1 minute, then rapidly stopping the illumination and terminating further chemical reactions, it may be possible to avoid the significant decreases in signal observed during prolonged illumination and monitor real changes in the $^1O_2$* chemistry of illuminated thylakoids.

We therefore explored whether we could reliably detect TEMPO signal after rapidly freezing and thawing an EPR capillary tube containing an illuminated thylakoid sample (Figure 6-14). For the thylakoid sample prior to illumination, quantification of spins yielded a concentration of 28 μM, likely representing impurities in the starting TEMP stock solution. However, following 1 min of illumination at 1000 μmol m^{-2} s^{-1}, the spin concentration increased by 46% to 41 μM due to production of $^1O_2$* and its subsequent trapping by TEMP. Importantly, the spin concentration remained identical when re-acquiring a spectrum for the same sample but after rapid freezing and thawing of the capillary. Following 5 additional minutes of dark in the EPR cavity, the spin concentration decreased by ~10% to 37 μM (not shown), although it should be noted that the magnitude of this decrease is not significantly different than the relative uncertainty in the quantification of the spin concentration. From this test experiment, we conclude that rapidly freezing and thawing the thylakoid membrane sample does not significantly alter the measurable concentration of TEMPO in pre-illuminated thylakoid membrane samples.

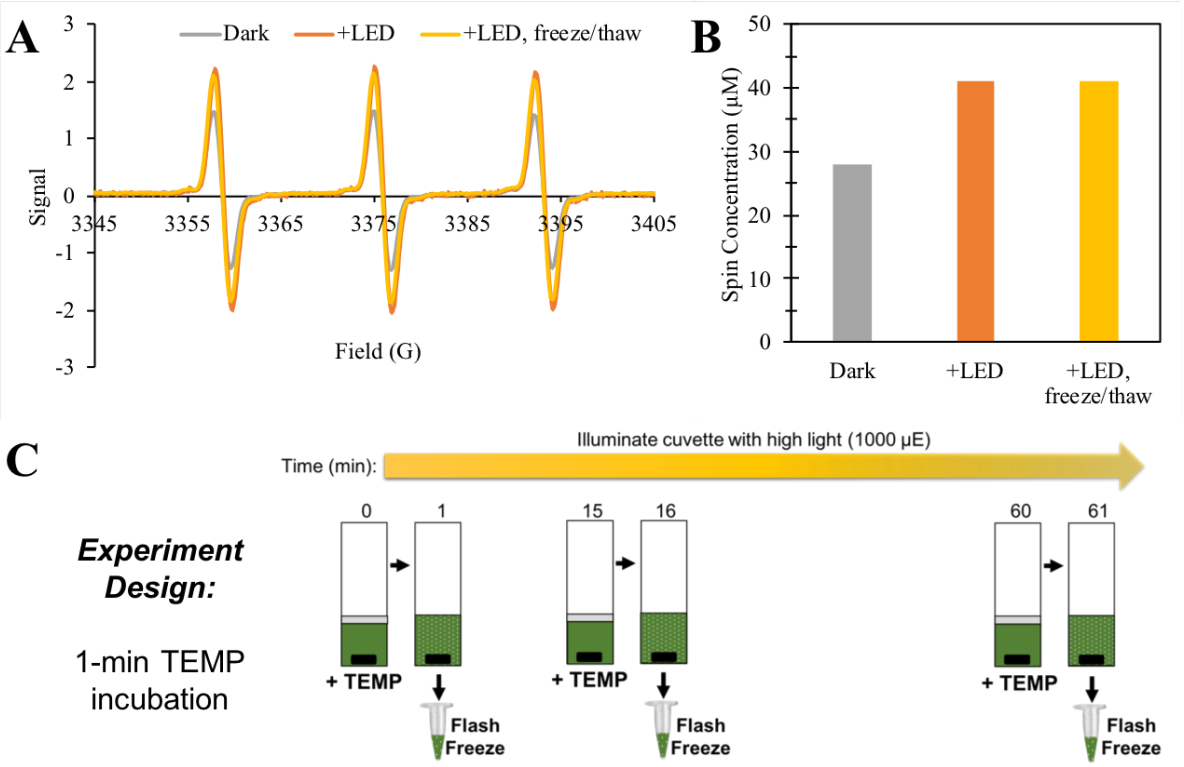

Figure 6-14. The "snapshot" EPR experiment design for thylakoid membrane samples. (A) EPR spectra for the same capillary with thylakoid membranes and TEMP in the dark (grey), following LED illumination in the EPR cavity (orange), and after freezing with LN2 and thawing (yellow). (B) Estimated concentration of TEMPO in µM obtained from double integration of each first-derivative EPR spectra shown in panel A. (C) Schematic of the experimental design for assessing light-induced changes in singlet oxygen concentration in intact thylakoid membranes. Thylakoid membrane samples were illuminated with white light at 1000 µmol m^{-2} s^{-1} in a cuvette with stirring for a specified amount of time, then TEMP was added to the cuvette and illuminated for 1 additional minute. After the 1-minute incubation, the sample was immediately flash frozen with LN_2, a process that took 15-30 seconds. Samples remained in the dark and frozen at -80 C for up to 1 week. For measurement, samples were thawed and immediately transferred to an EPR capillary tube (1 mm inner diameter).

With the knowledge that (1) we observe maximal TEMPO signal from thylakoids that are illuminated for only 1 min, and (2) freezing and thawing of the thylakoid sample does not change the apparent TEMPO concentration, we redesigned the experimental protocol for detection of $^1O_2$* during illumination of thylakoid membranes. We accordingly limited the incubation time for the TEMP spin probe to 1 minute in the light (see Figure 6-14C). By performing a 1-minute TEMP incubation for thylakoids that had been pre-illuminated for various amounts of time (ranging from 0 to 60 min of high light, 1000 µmol m^{-2} s^{-1}), we effectively sample the concentration of $^1O_2$* within the thylakoid sample. Following the 1-min incubation, rapid freezing of the sample and storage in the dark should effectively arrest most photophysical and photochemical processes, while preserving the TEMPO product. A similar experimental approach of storing pre-illuminated membrane samples in liquid nitrogen until measurement of the EPR spectrum at room temperature has been previously employed by Yadav et al.[48,94], though the range of time points investigated was much more limited.

Using this approach, we were able to detect changes in the apparent concentration of $^1O_2$* in thylakoid membrane samples during illumination (Figure 6-15). Interestingly, for samples incubated with TEMP, we observed a 20-25% decrease in the concentration of the TEMPO nitroxide radical during the first 5-15 min of illumination, with a minimum observed for thylakoids exposed to 5 min of pre-illumination (Fig. 6-15A, D). Following this initial decrease, the concentration of TEMPO increased, eventually returning to the initial value.

A similar trend was observed for samples treated with nigericin and subsequently incubated with TEMP for 1 minute (Fig. 6-15B, E). Nigericin is a well-known uncoupler that dissipates the transthylakoid pH gradient,[121] which subsequently prevents the conversion of violaxanthin to zeaxanthin, therefore hindering the activation of NPQ. Thylakoids in the presence of nigericin also showed a ~20% decrease in TEMPO. However, the decrease in signal was delayed by ~5 min relative to the untreated sample, with the minimum TEMPO signal in the presence of nigericin being observed following 10 min of pre-illumination.

Finally, as a control experiment to assess the effect of the duration of pre-illumination on the apparent spin concentration, thylakoids were incubated with TEMPO for exactly 1 minute at the 0, 15, and 60-minute timepoints of pre-illumination. The concentration of TEMPO measured for all of these time points was within ~10% of each other (Fig. 6-15C, F). While it is possible that this decrease represents small changes in the concentration or composition of reductants during illumination of membranes, it is more likely representative of the uncertainty (~10%) associated with the EPR measurements especially given that each thylakoid sample was measured using a different capillary. Therefore, it appears that the concentration of thylakoid reducing equivalents produced during a short 1-minute incubation is mostly independent of the duration of prior high-light illumination of the membranes.

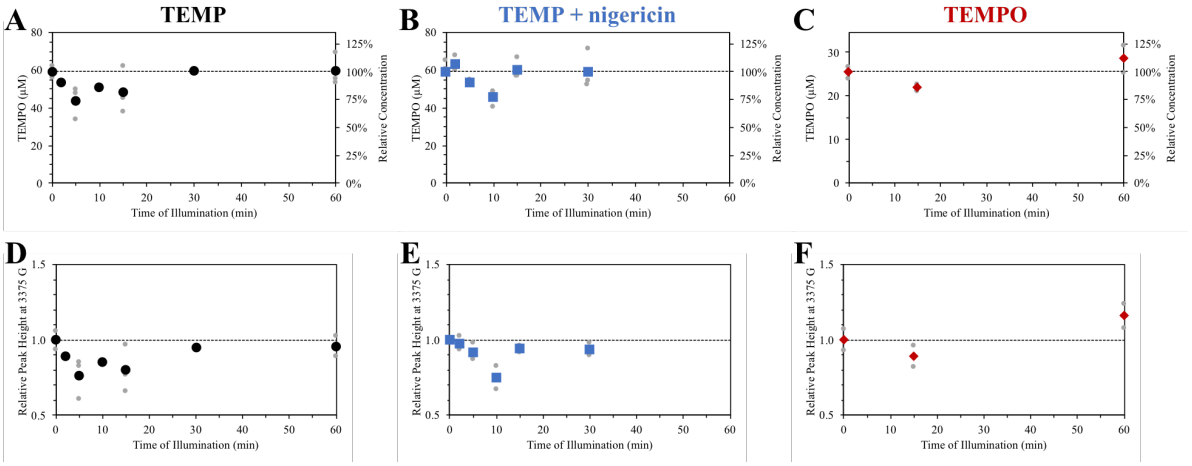

Figure 6-15. EPR snapshots for thylakoid membranes. Membrane samples were pre-illuminated with 1000 μmol m^{-2} s^{-1} in the presence or absence of 100 μM nigericin. Following pre-illumination, samples were incubated with either TEMP (50 mM) or TEMPO (30 μM) for 1 minute, then flash frozen. (A-C) Changes in measured TEMPO concentration (μM) as a function of time of high-light 1000 μE illumination treatment. TEMPO concentration was quantified by double integration after fitting of each EPR spectrum to a modelled nitroxide spin. (D-F) Relative change in TEMPO signal as indicated by the peak height at 3375 G. Individual replicate points are presented as small grey circles, average of replicates (n = 1-3) at each time point are shown by large colored markers. Dashed horizontal line shows the value corresponding to 0 min of pre-illumination.

6.3.6 Correlation of singlet oxygen production and chlorophyll fluorescence lifetimes in thylakoid membranes

To investigate the connection between $^1O_2$* production and NPQ under high light, we correlated our snapshot EPR measurements of TEMPO with snapshot Chl fluorescence lifetimes measured on thylakoid samples under similar conditions. Interestingly, the observed decrease in TEMPO correlated well with the dynamics of Chl fluorescence quenching upon illumination, both for the untreated thylakoids as well as those in the presence of the uncoupler nigericin (Figure 6-16). While both samples exhibited similar lifetimes prior to illumination (~1.8 ns), the untreated sample showed a larger quenching response, reaching a lifetime of ~1.1 ns within 5 min of illumination. In contrast, the uncoupler-treated (+nigericin) sample showed less overall quenching. It also exhibited a delayed onset of NPQ, requiring 10 min of illumination to reach the same 1.1-ns threshold, likely due to a slower formation of ΔpH in the light. Interestingly, this delay (approximately 5 min) also seems to be reflected in the TEMPO concentrations measured by EPR for the nigericin-treated sample, which had a minimal value at the 10-minute time point.

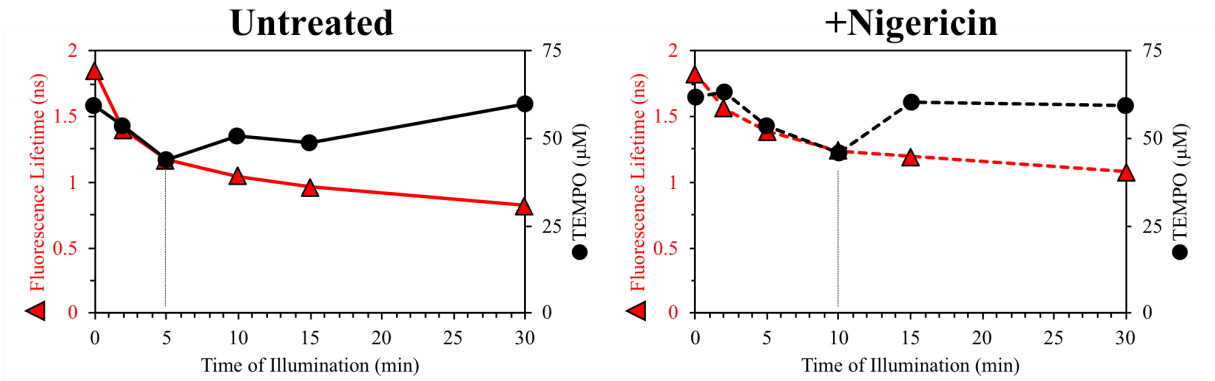

Figure 6-16. Comparison of fluorescence lifetime and TEMPO concentration at specified time points during illumination of thylakoid membranes with 1000 μmol m^{-2} s^{-1}. (A) Untreated thylakoids. (B) Thylakoids in presence of 100 μM nigericin. Vertical dashed lines indicate the time point corresponding to the minimum TEMPO concentration observed during the illumination sequence. Fluorescence lifetimes were measured in glycerol resuspension buffer (pH 6) in the presence of 50 μM methyl viologen and 0.5 mM ATP. TEMPO concentrations were measured as specified in Figure 6-14 and in the Materials and Methods section.

While the trends in the TEMPO concentrations and the average fluorescence lifetimes agree well during short periods of illumination, a large difference becomes apparent upon prolonged exposure to high light. Beyond the 15-minute time point, the thylakoid samples show only relatively small changes in fluorescence lifetime (Figure 6-16), likely due to nearly complete saturation of the quenching capacity of the membranes. At the same time, a marked increase in the TEMPO signal is observed, with the relative concentration of $^1O_2$* in the membranes eventually matching the starting concentration (i.e., prior to the induction of any NPQ) within 30 minutes of high light. Therefore, increased amounts of $^1O_2$* appear to be produced during illumination of thylakoid membranes upon saturation of all NPQ processes.

The combined EPR and TCSPC results suggest that there are at least two regimes involved in the activation of photoprotective NPQ in terms of protecting against ROS such as $^1O_2$* (see Figure 6-17 for a schematic showing expected changes in TEMPO signal as a function of duration of

exposure to high light). In the first regime, representing the short-term response to high-light exposure, the TEMPO signal is strongly correlated to the average Chl fluorescence lifetime. The activation of NPQ, resulting in the quenching of the ^{1}Chl* excited state lifetime, leads to less production of $^1O_2$*. Therefore, this first regime is "photoprotective" in terms of limiting $^1O_2$*. However, beyond the first 10-15 min of illumination, the photoprotective capacity of the thylakoid membranes becomes saturated. During this second regime, only relatively minor changes in the ^{1}Chl* excited state lifetime are observed. These modest changes in the fluorescence lifetime do not appear to provide much mitigation of $^1O_2$*. Consequently, the TEMPO signal rises, an apparent reflection of increased rates of $^1O_2$* production during this second "light-stressed" regime.

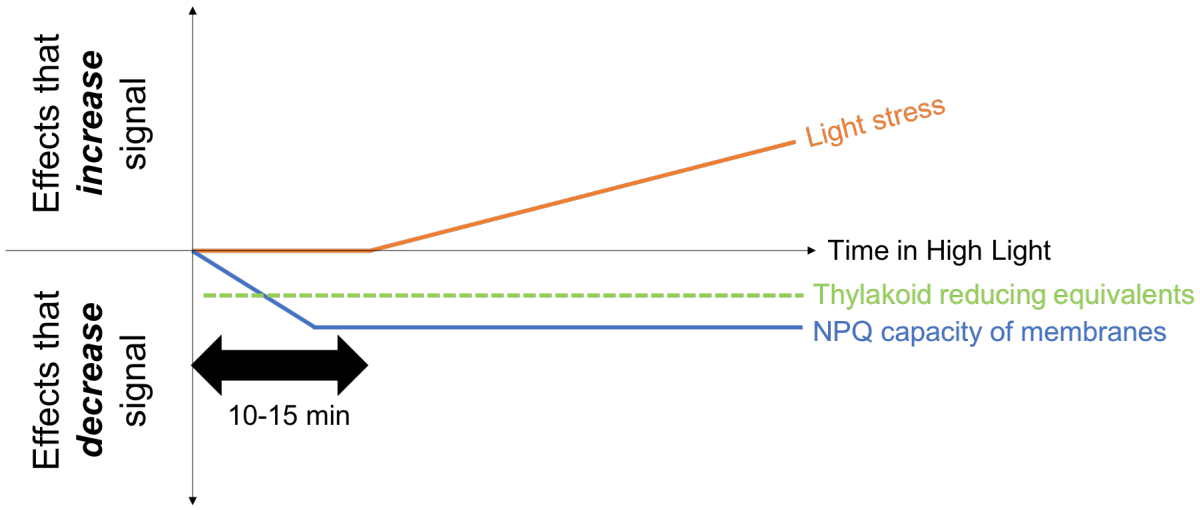

Figure 6-17. Schematic showing changes in nitroxide radical EPR signal during illumination of thylakoid membrane. In the first photoprotective regime, the activation of NPQ results in mitigation of photo-oxidative stress, leading to less production of $^1O_2$* and lower TEMPO signal. Eventually the NPQ capacity saturates, after which the thylakoids experience gradually increasing photo-oxidative stress, leading to more production of $^1O_2$* and higher TEMPO signal.

6.4 Conclusions and Future Directions

Singlet oxygen is an excited state of (triplet) molecular oxygen, an unavoidable byproduct of the process of photosynthetic light-harvesting. While it has crucial roles in both damage and signaling, the temporal evolution of $^1O_2$* during illumination is largely unknown. Here, by employing spin-trapping EPR spectroscopy, we reveal the complicated temporal dynamics of $^1O_2$* during 1 hour of high-light illumination of spinach thylakoid membranes. Surprisingly, we observe an interference effect on the nitroxide radical EPR signal that arises from direct illumination of chromophores, both in dye-based and natural Chl-based systems, that limits the ability of the spin trapping method to reliably track the real-time signal associated with $^1O_2$*. However, through careful modification of the experimental protocol, we demonstrate that the apparent $^1O_2$* concentration changes throughout different periods of illumination of thylakoid membranes. During the first regime, corresponding to the membrane's initial response to high light, the relative concentration of $^1O_2$* decreases concurrently with quenching of the Chl fluorescence lifetime. However, upon saturation of NPQ, the concentration of $^1O_2$* rises, presumably reflecting the utility of NPQ in mitigating photo-oxidative stress in the short term. These findings are consistent with previous speculations that the physiological role of photoprotective quenching is to reduce the amount of singlet oxygen produced in the photosynthetic apparatus.

On a more technical level, the findings highlight several of the limitations associated with utilizing spin traps for reliable detection of reactive oxygen species in photosynthesis. Purification of the spin trap is one possible improvement for the work and would likely remove the high baseline signal (impurity) observed in the dark. Measurement of additional sample replicates at each time point of illumination would be valuable. Extending the thylakoid illumination time beyond 1 hour, testing additional illumination intensities beyond 1000 μmol m^{-2} s^{-1}, and extending the spin-trapping method to monitor rapid changes in $^1O_2$* under fluctuating light conditions could be excellent ways to test the model developed in this study. More generally, the findings call for the continued development of new techniques for sensitive, specific, and accurate measurements of reactive oxygen species (ROS) and encourage caution when interpreting EPR data of ROS in complex biochemical systems.

6.5 References

(1) Scholes, G. D.; Fleming, G. R.; Olaya-Castro, A.; van Grondelle, R. Lessons from nature about solar light harvesting. *Nat. Chem.* **2011**, *3* (10), 763–774.

(2) Croce, R.; van Amerongen, H. Natural strategies for photosynthetic light harvesting. *Nat. Chem. Biol.* **2014**, *10* (7), 492–501.

(3) Blankenship, R. E.; Tiede, D. M.; Barber, J.; Brudvig, G. W.; Fleming, G. R.; Ghirardi, M.; Gunner, M. R.; Junge, W.; Kramer, D. M.; Melis, A.; Moore, T. A.; Moser, C. C.; Nocera, D. G.; Nozik, A. J.; Ort, D. R.; Parson, W. W.; Prince, R. C.; Sayre, R. T. Comparing photosynthetic and photovoltaic efficiencies and recognizing the potential for improvement. *Science* **2011**, *332* (6031), 805–809.

(4) Weis, E.; Berry, J. A. Quantum efficiency of Photosystem II in relation to 'energy'-dependent quenching of chlorophyll fluorescence. *Biochim. Biophys. Acta - Bioenerg.* **1987**, *894* (2), 198–208.

(5) Johnson, J. E.; Berry, J. A. The role of Cytochrome b6f in the control of steady-state photosynthesis: a conceptual and quantitative model. *Photosynth. Res.* **2021**, *1*, 3.

(6) Farquhar, G. D.; von Caemmerer, S.; Berry, J. A. A biochemical model of photosynthetic CO2 assimilation in leaves of C3 species. *Planta* **1980**, *149* (1), 78–90.

(7) Kasha, M.; Brabham, D. E. Singlet Oxygen Electronic Structure and Photosensitization. In *Singlet Oxygen*; 1979; pp 1–33.

(8) Wilkinson, F.; Helman, W. P.; Ross, A. B. Rate Constants for the Decay and Reactions of the Lowest Electronically Excited Singlet State of Molecular Oxygen in Solution. An Expanded and Revised Compilation. *J. Phys. Chem. Ref. Data* **1995**, *24* (2), 663–677.

(9) Bregnhøj, M.; Westberg, M.; Minaev, B. F.; Ogilby, P. R. Singlet Oxygen Photophysics in Liquid Solvents: Converging on a Unified Picture. *Acc. Chem. Res.* **2017**, *50* (8), 1920–1927.

(10) Foote, C. S. Mechanisms of photosensitized oxidation. *Science* **1968**, *162* (3857), 963–970.

(11) Ogilby, P. R. Singlet oxygen: there is indeed something new under the sun. *Chem. Soc. Rev.* **2010**, *39* (8), 3181.

(12) Lubitz, W.; Chrysina, M.; Cox, N. Water oxidation in photosystem II. *Photosynth. Res.* **2019**, *142* (1), 105–125.

(13) Cadenas, E. Biochemistry of Oxygen Toxicity. *Annu. Rev. Biochem.* **1989**, *58* (1), 79–110.

(14) Fryer, M. J.; Oxborough, K.; Mullineaux, P. M.; Baker, N. R. Imaging of photo-oxidative stress responses in leaves. *J. Exp. Bot.* **2002**, *53* (372), 1249–1254.

(15) Fufezan, C.; Rutherford, A. W.; Krieger-Liszkay, A. Singlet oxygen production in herbicide-treated photosystem II. *FEBS Lett.* **2002**, *532* (3), 407–410.

(16) Krieger-Liszkay, A. Singlet oxygen production in photosynthesis. *J. Exp. Bot.* **2004**, *56* (411), 337–346.

(17) Krieger-Liszkay, A.; Fufezan, C.; Trebst, A. Singlet oxygen production in photosystem II and related protection mechanism. *Photosynth. Res.* **2008**, *98* (1–3), 551–564.

(18) Pospíšil, P. Production of reactive oxygen species by photosystem II. *Biochim. Biophys. Acta - Bioenerg.* **2009**, *1787* (10), 1151–1160.

(19) Triantaphylidès, C.; Havaux, M. Singlet oxygen in plants: production, detoxification and signaling. *Trends Plant Sci.* **2009**, *14* (4), 219–228.

(20) Pospíšil, P. Production of Reactive Oxygen Species by Photosystem II as a Response to Light and Temperature Stress. *Front. Plant Sci.* **2016**, *7*, 1950.

(21) Foyer, C. H.; Ruban, A. V; Noctor, G. Viewing oxidative stress through the lens of oxidative signalling rather than damage. *Biochem. J.* **2017**, *474* (6), 877–883.
(22) Khorobrykh, S.; Havurinne, V.; Mattila, H.; Tyystjärvi, E. Oxygen and ROS in Photosynthesis. *Plants* **2020**, *9* (1), 91.
(23) Skovsen, E.; Snyder, J. W.; Lambert, J. D. C.; Ogilby, P. R. Lifetime and Diffusion of Singlet Oxygen in a Cell. *J. Phys. Chem. B* **2005**, *109* (18), 8570–8573.
(24) Barber, J.; Andersson, B. Too much of a good thing: light can be bad for photosynthesis. *Trends Biochem. Sci.* **1992**, *17* (2), 61–66.
(25) Telfer, A.; Bishop, S. M.; Phillips, D.; Barber, J. Isolated photosynthetic reaction center of photosystem II as a sensitizer for the formation of singlet oxygen. Detection and quantum yield determination using a chemical trapping technique. *J. Biol. Chem.* **1994**, *269* (18), 13244–13253.
(26) Weisz, D. A.; Gross, M. L.; Pakrasi, H. B. Reactive oxygen species leave a damage trail that reveals water channels in Photosystem II. *Sci. Adv.* **2017**, *3* (11).
(27) Kale, R.; Hebert, A. E.; Frankel, L. K.; Sallans, L.; Bricker, T. M.; Pospíšil, P. Amino acid oxidation of the D1 and D2 proteins by oxygen radicals during photoinhibition of Photosystem II. *Proc. Natl. Acad. Sci. U. S. A.* **2017**, *114* (11), 2988–2993.
(28) Zolla, L.; Rinalducci, S. Involvement of Active Oxygen Species in Degradation of Light-Harvesting Proteins under Light Stresses. *Biochemistry* **2002**, *41* (48), 14391–14402.
(29) Rinalducci, S.; Pedersen, J. Z.; Zolla, L. Formation of radicals from singlet oxygen produced during photoinhibition of isolated light-harvesting proteins of photosystem II. *Biochim. Biophys. Acta - Bioenerg.* **2004**, *1608* (1), 63–73.
(30) Davies, M. J. Reactive species formed on proteins exposed to singlet oxygen. *Photochem. Photobiol. Sci.* **2004**, *3* (1), 17.
(31) Martinez, G. R.; Loureiro, A. P. M.; Marques, S. A.; Miyamoto, S.; Yamaguchi, L. F.; Onuki, J.; Almeida, E. A.; Garcia, C. C. M.; Barbosa, L. F.; Medeiros, M. H. G.; Di Mascio, P. Oxidative and alkylating damage in DNA. *Mutat. Res. - Rev. Mutat. Res.* **2003**, *544* (2–3), 115–127.
(32) Triantaphylidès, C.; Krischke, M.; Hoeberichts, F. A.; Ksas, B.; Gresser, G.; Havaux, M.; Van Breusegem, F.; Mueller, M. J. Singlet oxygen is the major reactive oxygen species involved in photooxidative damage to plants. *Plant Physiol.* **2008**, *148* (2), 960–968.
(33) Johnson, M. P.; Havaux, M.; Triantaphylidès, C.; Ksas, B.; Pascal, A. A.; Robert, B.; Davison, P. A.; Ruban, A. V; Horton, P. Elevated zeaxanthin bound to oligomeric LHCII enhances the resistance of Arabidopsis to photooxidative stress by a lipid-protective, antioxidant mechanism. *J. Biol. Chem.* **2007**, *282* (31), 22605–22618.
(34) Fisher, K. E.; Krishnamoorthy, P.; Joens, M. S.; Chory, J.; Fitzpatrick, J. A. J.; Woodson, J. D. Singlet Oxygen Leads to Structural Changes to Chloroplasts during their Degradation in the Arabidopsis thaliana plastid ferrochelatase two Mutant. *Plant Cell Physiol.* **2022**, *63* (2), 248–264.
(35) Woodson, J. D.; Joens, M. S.; Sinson, A. B.; Gilkerson, J.; Salomé, P. A.; Weigel, D.; Fitzpatrick, J. A.; Chory, J. Ubiquitin facilitates a quality-control pathway that removes damaged chloroplasts. *Science* **2015**, *350* (6259), 450–454.
(36) Rodgers, M. A. J.; Bates, A. L. Kinetic and Spectroscopic Features of Some Carotenoid Triplet States: Sensitization by Singlet Oxygen. *Photochem. Photobiol.* **1980**, *31* (6), 533–537.
(37) Di Mascio, P.; Devasagayam, T. P.; Kaiser, S.; Sies, H. Carotenoids, tocopherols and thiols

as biological singlet molecular oxygen quenchers. *Biochem. Soc. Trans.* **1990**, *18* (6), 1054–1056.
(38) Hirayama, O.; Nakamura, K.; Hamada, S.; Kobayasi, Y. Singlet oxygen quenching ability of naturally occurring carotenoids. *Lipids* **1994**, *29* (2), 149–150.
(39) Schödel, R.; Irrgang, K.-D.; Voigt, J.; Renger, G. Rate of Carotenoid Triplet Formation in Solubilized Light-Harvesting Complex II (LHCII) from Spinach. *Biophys. J.* **1998**, *75* (6), 3143–3153.
(40) Telfer, A. What is β-carotene doing in the photosystem II reaction centre? *Philos. Trans. R. Soc. Lond. B. Biol. Sci.* **2002**, *357* (1426), 1431–1440.
(41) Telfer, A.; Dhami, S.; Bishop, S. M.; Phillips, D.; Barber, J. β-Carotene Quenches Singlet Oxygen Formed by Isolated Photosystem II Reaction Centers. *Biochemistry* **1994**, *33* (48), 14469–14474.
(42) De Las Rivas, J.; Telfer, A.; Barber, J. Two coupled β-carotene molecules protect P680 from photodamage in isolated Photosystem II reaction centres. *BBA - Bioenerg.* **1993**, *1142* (1–2), 155–164.
(43) Keren, N.; Berg, A.; van Kan PJ, P. J. M.; Levanon, H.; Ohad, I. Mechanism of photosystem II photoinactivation and D1 protein degradation at low light: the role of back electron flow. *Proc. Natl. Acad. Sci. U. S. A.* **1997**, *94* (4), 1579–1584.
(44) Krieger, A.; Rutherford, A. W.; Vass, I.; Hideg, É. Relationship between Activity, D1 Loss, and Mn Binding in Photoinhibition of Photosystem II. *Biochemistry* **1998**, *37* (46), 16262–16269.
(45) Kruk, J.; Holländer-Czytko, H.; Oettmeier, W.; Trebst, A. Tocopherol as singlet oxygen scavenger in photosystem II. *J. Plant Physiol.* **2005**, *162* (7), 749–757.
(46) Krieger-Liszkay, A.; Trebst, A. Tocopherol is the scavenger of singlet oxygen produced by the triplet states of chlorophyll in the PSII reaction centre. *J. Exp. Bot.* **2006**, *57* (8), 1677–1684.
(47) Kruk, J.; Trebst, A. Plastoquinol as a singlet oxygen scavenger in photosystem II. *Biochim. Biophys. Acta - Bioenerg.* **2008**, *1777* (2), 154–162.
(48) Yadav, D. K.; Kruk, J.; Sinha, R. K.; Pospíšil, P. Singlet oxygen scavenging activity of plastoquinol in photosystem II of higher plants: Electron paramagnetic resonance spin-trapping study. *Biochim. Biophys. Acta - Bioenerg.* **2010**, *1797* (11), 1807–1811.
(49) Roger H. Bisby; Morgan, C. G.; Ian Hamblett; Gorman, A. A. Quenching of Singlet Oxygen by Trolox C, Ascorbate, and Amino Acids: Effects of pH and Temperature. *J. Phys. Chem. A* **1999**, *103* (37), 7454–7459.
(50) Kramarenko, G. G.; Hummel, S. G.; Martin, S. M.; Buettner, G. R. Ascorbate Reacts with Singlet Oxygen to Produce Hydrogen Peroxide. *Photochem. Photobiol.* **2006**, *82* (6), 1634–1637.
(51) Apel, K.; Hirt, H. REACTIVE OXYGEN SPECIES: Metabolism, Oxidative Stress, and Signal Transduction. *Annu. Rev. Plant Biol.* **2004**, *55* (1), 373–399.
(52) Foyer, C. H.; Noctor, G. Stress-triggered redox signalling: what's in pROSpect? *Plant. Cell Environ.* **2016**, *39* (5), 951–964.
(53) Demmig-Adams, B.; Stewart, J. J.; Adams, W. W. Less photoprotection can be good in some genetic and environmental contexts. *Biochem. J.* **2019**, *476* (14), 2017–2029.
(54) Wagner, D.; Przybyla, D.; Op den Camp, R.; Kim, C.; Landgraf, F.; Lee, K. P.; Würsch, M.; Laloi, C.; Nater, M.; Hideg, E.; Apel, K. The genetic basis of singlet oxygen-induced stress responses of Arabidopsis thaliana. *Science* **2004**, *306* (5699), 1183–1185.

(55) Fischer, B. B.; Krieger-Liszkay, A.; Hideg, É.; Šnyrychová, I.; Wiesendanger, M.; Eggen, R. I. L. Role of singlet oxygen in chloroplast to nucleus retrograde signaling in *Chlamydomonas reinhardtii*. *FEBS Lett.* **2007**, *581* (29), 5555–5560.
(56) Reinbothe, C.; Pollmann, S.; Reinbothe, S. Singlet oxygen signaling links photosynthesis to translation and plant growth. *Trends Plant Sci.* **2010**, *15* (9), 499–506.
(57) Wakao, S.; Chin, B. L.; Ledford, H. K.; Dent, R. M.; Casero, D.; Pellegrini, M.; Merchant, S. S.; Niyogi, K. K. Phosphoprotein SAK1 is a regulator of acclimation to singlet oxygen in Chlamydomonas reinhardtii. *eLife* **2014**, *3*.
(58) Bennett, D. I. G.; Amarnath, K.; Park, S.; Steen, C. J.; Morris, J. M.; Fleming, G. R. Models and mechanisms of the rapidly reversible regulation of photosynthetic light harvesting. *Open Biol.* **2019**, *9* (4), 190043.
(59) Bassi, R.; Dall'Osto, L. Dissipation of Light Energy Absorbed in Excess: The Molecular Mechanisms. *Annu. Rev. Plant Biol.* **2021**, *72* (1), 47–76.
(60) Külheim, C.; Agren, J.; Jansson, S. Rapid regulation of light harvesting and plant fitness in the field. *Science* **2002**, *297* (5578), 91–93.
(61) Dogra, V.; Kim, C. Singlet Oxygen Metabolism: From Genesis to Signaling. *Front. Plant Sci.* **2020**, *10*, 1640.
(62) Krieger-Liszkay, A.; Shimakawa, G. Regulation of the generation of reactive oxygen species during photosynthetic electron transport. *Biochem. Soc. Trans.* **2022**.
(63) Merkel, P. B.; Nilsson, R.; Kearns, D. R. Deuterium effects on singlet oxygen lifetimes in solutions. New test of singlet oxygen reactions. *J. Am. Chem. Soc.* **1972**, *94* (3), 1030–1031.
(64) Kearns, D. Solvent and Solvent Isotope Effects on the Lifetime of Singlet Oxyegn. In *Singlet Oxygen*; 1979; pp 115–138.
(65) Chou, P.-T.; Frei, H. Sensitization of O2 $1\Sigma g+ \rightarrow 1\Delta g$ emission in solution, and observation of $O2 1\Delta g \rightarrow 3\Sigma g-$ chemiluminescence upon decomposition of 1,4-dimethylnaphthalene endoperoxide. *Chem. Phys. Lett.* **1985**, *122* (1–2), 87–92.
(66) Macpherson, A. N.; Telfer, A.; Barber, J.; Truscott, T. G. Direct detection of singlet oxygen from isolated Photosystem II reaction centres. *Biochim. Biophys. Acta - Bioenerg.* **1993**, *1143* (3), 301–309.
(67) Telfer, A.; Oldham, T. C.; Phillips, D.; Barber, J. Singlet oxygen formation detected by near-infrared emission from isolated photosystem II reaction centres: Direct correlation between P680 triplet decay and luminescence rise kinetics and its consequences for photoinhibition. *J. Photochem. Photobiol. B Biol.* **1999**, *48* (2–3), 89–96.
(68) Dědic, R.; Svoboda, A.; Psŕeněk, J.; Lupínková, L.; Komenda, J.; Hála, J. Time and spectral resolved phosphorescence of singlet oxygen and pigments in photosystem II particles. *J. Lumin.* **2003**, *102–103*, 313–317.
(69) Arellano, J. B.; Li, H.; González-Pérez, S.; Gutiérrez, J.; Melø, T. B.; Vacha, F.; Naqvi, K. R. Trolox, a Water-Soluble Analogue of α-Tocopherol, Photoprotects the Surface-Exposed Regions of the Photosystem II Reaction Center in Vitro. Is This Physiologically Relevant? *Biochemistry* **2011**, *50* (39), 8291–8301.
(70) Li, H.; Melø, T. B.; Arellano, J. B.; Razi Naqvi, K. Temporal profile of the singlet oxygen emission endogenously produced by photosystem II reaction centre in an aqueous buffer. *Photosynth. Res.* **2012**, *112* (1), 75–79.
(71) Zebger, I.; Snyder, J. W.; Andersen, L. K.; Poulsen, L.; Gao, Z.; Lambert, J. D. C.; Kristiansen, U.; Ogilby, P. R. Rapid Communication: Direct Optical Detection of Singlet Oxygen from a Single Cell. *Photochem. Photobiol.* **2004**, *79* (5), 319–322.

(72) Snyder, J. W.; Skovsen, E.; Lambert, J. D. C.; Ogilby, P. R. Subcellular, Time-Resolved Studies of Singlet Oxygen in Single Cells. *J. Am. Chem. Soc.* **2005**, *127* (42), 14558–14559.
(73) Snyder, J. W.; Skovsen, E.; Lambert, J. D. C.; Poulsen, L.; Ogilby, P. R. Optical detection of singlet oxygen from single cells. *Phys. Chem. Chem. Phys.* **2006**, *8* (37), 4280.
(74) Baier, J.; Maier, M.; Engl, R.; Landthaler, M.; Wolfgang Bäumler. Time-Resolved Investigations of Singlet Oxygen Luminescence in Water, in Phosphatidylcholine, and in Aqueous Suspensions of Phosphatidylcholine or HT29 Cells. *J. Phys. Chem. B* **2005**, *109* (7), 3041–3046.
(75) Hatz, S.; Lambert, J. D. C.; Ogilby, P. R. Measuring the lifetime of singlet oxygen in a single cell: Addressing the issue of cell viability. *Photochem. Photobiol. Sci.* **2007**, *6* (10), 1106–1116.
(76) Kuimova, M. K.; Yahioglu, G.; Ogilby, P. R. Singlet Oxygen in a Cell: Spatially Dependent Lifetimes and Quenching Rate Constants. *J. Am. Chem. Soc.* **2009**, *131* (1), 332–340.
(77) da Silva, E. F. F.; Pedersen, B. W.; Breitenbach, T.; Toftegaard, R.; Kuimova, M. K.; Arnaut, L. G.; Ogilby, P. R. Irradiation- and Sensitizer-Dependent Changes in the Lifetime of Intracellular Singlet Oxygen Produced in a Photosensitized Process. *J. Phys. Chem. B* **2012**, *116* (1), 445–461.
(78) Marsili, F.; Verma, V. B.; Stern, J. A.; Harrington, S.; Lita, A. E.; Gerrits, T.; Vayshenker, I.; Baek, B.; Shaw, M. D.; Mirin, R. P.; Nam, S. W. Detecting single infrared photons with 93% system efficiency. *Nat. Photonics* **2013**, *7* (3), 210–214.
(79) Flors, C.; Fryer, M. J.; Waring, J.; Reeder, B.; Bechtold, U.; Mullineaux, P. M.; Nonell, S.; Wilson, M. T.; Baker, N. R. Imaging the production of singlet oxygen in vivo using a new fluorescent sensor, Singlet Oxygen Sensor Green(R). *J. Exp. Bot.* **2006**, *57* (8), 1725–1734.
(80) Kim, S.; Fujitsuka, M.; Majima, T. Photochemistry of Singlet Oxygen Sensor Green. *J. Phys. Chem. B* **2013**, *117* (45), 13985–13992.
(81) Ragàs, X.; Jiménez-Banzo, A.; Sánchez-García, D.; Batllori, X.; Nonell, S. Singlet oxygen photosensitisation by the fluorescent probe Singlet Oxygen Sensor Green®. *Chem. Commun.* **2009**, No. 20, 2920.
(82) Prasad, A.; Sedlářová, M.; Pospíšil, P. Singlet oxygen imaging using fluorescent probe Singlet Oxygen Sensor Green in photosynthetic organisms. *Sci. Rep.* **2018**, *8* (1), 13685.
(83) Lion, Y.; Delmelle, M.; van de Vorst, A. New method of detecting singlet oxygen production. *Nature* **1976**, *263* (5576), 442–443.
(84) Roach, T.; Krieger-Liszkay, A. The role of the PsbS protein in the protection of photosystems I and II against high light in Arabidopsis thaliana. *Biochim. Biophys. Acta - Bioenerg.* **2012**, *1817* (12), 2158–2165.
(85) Prasad, A.; Ferretti, U.; Sedlářová, M.; Pospíšil, P. Singlet oxygen production in Chlamydomonas reinhardtii under heat stress. *Sci. Rep.* **2016**, *6* (1), 1–13.
(86) Hideg, E.; Spetea, C.; Vass, I. Singlet oxygen production in thylakoid membranes during photoinhibition as detected by EPR spectroscopy. *Photosynth. Res.* **1994**, *39* (2), 191–199.
(87) Hideg, É.; Spetea, C.; Vass, I. Singlet oxygen and free radical production during acceptor- and donor-side-induced photoinhibition: Studies with spin trapping EPR spectroscopy. *Biochim. Biophys. Acta - Bioenerg.* **1994**, *1186* (3), 143–152.
(88) Fischer, B. B.; Krieger-Liszkay, A.; Eggen, R. I. L. Oxidative stress induced by the photosensitizers neutral red (type I) or rose bengal (type II) in the light causes different molecular responses in Chlamydomonas reinhardtii. *Plant Sci.* **2005**, *168* (3), 747–759.
(89) Fischer, B. B.; Eggen, R. I. L.; Trebst, A.; Krieger-Liszkay, A. The glutathione peroxidase

homologous gene Gpxh in Chlamydomonas reinhardtii is upregulated by singlet oxygen produced in photosystem II. *Planta* **2006**, *223* (3), 583–590.
(90) Fufezan, C.; Gross, C. M.; Sjödin, M.; Rutherford, A. W.; Krieger-Liszkay, A.; Kirilovsky, D. Influence of the Redox Potential of the Primary Quinone Electron Acceptor on Photoinhibition in Photosystem II. *J. Biol. Chem.* **2007**, *282* (17), 12492–12502.
(91) Pospíšil, P.; Šnyrychová, I.; Nauš, J. Dark production of reactive oxygen species in photosystem II membrane particles at elevated temperature: EPR spin-trapping study. *Biochim. Biophys. Acta - Bioenerg.* **2007**, *1767* (6), 854–859.
(92) Sang, M.; Ma, F.; Xie, J.; Chen, X.-B.; Wang, K.-B.; Qin, X.-C.; Wang, W.-D.; Zhao, J.-Q.; Li, L.-B.; Zhang, J.-P.; Kuang, T.-Y. High-light induced singlet oxygen formation in cytochrome b6f complex from Bryopsis corticulans as detected by EPR spectroscopy. *Biophys. Chem.* **2010**, *146* (1), 7–12.
(93) Sang, M.; Qin, X. C.; Wang, W. D.; Xie, J.; Chen, X. B.; Wang, K. B.; Zhang, J. P.; Li, L. B.; Kuang, T. Y. High-light-induced superoxide anion radical formation in cytochrome b6f complex from spinach as detected by EPR spectroscopy. *Photosynthetica* **2011**, *49* (1), 48–54.
(94) Yadav, D. K.; Pospíšil, P. Evidence on the Formation of Singlet Oxygen in the Donor Side Photoinhibition of Photosystem II: EPR Spin-Trapping Study. *PLoS One* **2012**, *7* (9), e45883.
(95) Ramel, F.; Ksas, B.; Akkari, E.; Mialoundama, A. S.; Monnet, F.; Krieger-Liszkay, A.; Ravanat, J.-L.; Mueller, M. J.; Bouvier, F.; Havaux, M. Light-Induced Acclimation of the Arabidopsis chlorina1 Mutant to Singlet Oxygen. *Plant Cell* **2013**, *25* (4), 1445–1462.
(96) Ksas, B.; Légeret, B.; Ferretti, U.; Chevalier, A.; Pospíšil, P.; Alric, J.; Havaux, M. The plastoquinone pool outside the thylakoid membrane serves in plant photoprotection as a reservoir of singlet oxygen scavengers. *Plant. Cell Environ.* **2018**, *41* (10), 2277–2287.
(97) Lingvay, M.; Akhtar, P.; Sebők-Nagy, K.; Páli, T.; Lambrev, P. H. Photobleaching of Chlorophyll in Light-Harvesting Complex II Increases in Lipid Environment. *Front. Plant Sci.* **2020**, *0*, 849.
(98) Gilmore, A. M.; Shinkarev, V. P.; Hazlett, T. L.; Govindjee. Quantitative Analysis of the Effects of Intrathylakoid pH and Xanthophyll Cycle Pigments on Chlorophyll a Fluorescence Lifetime Distributions and Intensity in Thylakoids. *Biochemistry* **1998**, *37* (39), 13582–13593.
(99) Park, S.; Fischer, A. L.; Li, Z.; Bassi, R.; Niyogi, K. K.; Fleming, G. R. Snapshot Transient Absorption Spectroscopy of Carotenoid Radical Cations in High-Light-Acclimating Thylakoid Membranes. *J. Phys. Chem. Lett.* **2017**, *8* (22), 5548–5554.
(100) Park, S.; Fischer, A. L.; Steen, C. J.; Iwai, M.; Morris, J. M.; Walla, P. J.; Niyogi, K. K.; Fleming, G. R. Chlorophyll-Carotenoid Excitation Energy Transfer in High-Light-Exposed Thylakoid Membranes Investigated by Snapshot Transient Absorption Spectroscopy. *J. Am. Chem. Soc.* **2018**, *140* (38), 11965–11973.
(101) Utschig, L. M.; Soltau, S. R.; Mulfort, K. L.; Niklas, J.; Poluektov, O. G. Z-scheme solar water splitting: Via self-assembly of photosystem I-catalyst hybrids in thylakoid membranes. *Chem. Sci.* **2018**, *9* (45), 8504–8512.
(102) Porra, R. J.; Thompson, W. A.; Kriedemann, P. E. Determination of accurate extinction coefficients and simultaneous equations for assaying chlorophylls a and b extracted with four different solvents: verification of the concentration of chlorophyll standards by atomic absorption spectroscopy. *Biochim. Biophys. Acta - Bioenerg.* **1989**, *975* (3), 384–394.

(103) Arnon, D. I. Copper Enzymes in Isolated Chloroplasts. Polyphenoloxidase in Beta vulgaris. *Plant Physiol.* **1949**, *24* (1), 1–15.
(104) Keuper, H. J. K.; Sauer, K. Effect of photosystem II reaction center closure on nanosecond fluorescence relaxation kinetics. *Photosynth. Res.* **1989**, *20* (1), 85–103.
(105) Steffen-Heins, A.; Steffens, B. EPR spectroscopy and its use in planta - a promising technique to disentangle the origin of specific ROS. *Front. Environ. Sci.* **2015**, *3*, 1–6.
(106) Torricella, F.; Pierro, A.; Mileo, E.; Belle, V.; Bonucci, A. Nitroxide spin labels and EPR spectroscopy: A powerful association for protein dynamics studies. *Biochim. Biophys. Acta - Proteins Proteomics* **2021**, *1869* (7), 140653.
(107) Pottier, R.; Bonneau, R.; Joussot-Dubien, J. pH Dependence of Singlet Oxygen Production in Aqueous Solutions Using Toluidine Blue as a Photosensitzer. *Photochem. Photobiol.* **1975**, *22* (1–2), 59–61.
(108) Ledford, H. K.; Chin, B. L.; Niyogi, K. K. Acclimation to singlet oxygen stress in Chlamydomonas reinhardtii. *Eukaryot. Cell* **2007**, *6* (6), 919–930.
(109) Chou, P.-T.; Khan, S.; Frei, H. Time-resolved O2 1Δg→3Σg− chemiluminescence upon UV laser photolysis of an aromatic endoperoxide in aqueous solution. *Chem. Phys. Lett.* **1986**, *129* (5), 463–467.
(110) Stiel, H.; Teuchner, K.; Paul, A.; Leupold, D.; Kochevar, I. E. Quantitative comparison of excited state properties and intensity-dependent photosensitization by rose bengal. *J. Photochem. Photobiol. B Biol.* **1996**, *33* (3), 245–254.
(111) Murasecco-Suardi, P.; Gassmann, E.; Braun, A. M.; Oliveros, E. Determination of the Quantum Yield of Intersystem Crossing of Rose Bengal. *Helv. Chim. Acta* **1987**, *70* (7), 1760–1773.
(112) Redmond, R. W.; Gamlin, J. N. A Compilation of Singlet Oxygen Yields from Biologically Relevant Molecules. *Photochem. Photobiol.* **1999**, *70* (4), 391–475.
(113) Kochevar, I. E.; Redmond, R. W. Photosensitized production of singlet oxygen. In *Methods in Enzymology*; Academic Press, 2000; Vol. 319, pp 20–28.
(114) Müller-Moulé, P.; Conklin, P. L.; Niyogi, K. K. Ascorbate deficiency can limit violaxanthin de-epoxidase activity in vivo. *Plant Physiol.* **2002**, *128* (3), 970–977.
(115) Arnoux, P.; Morosinotto, T.; Saga, G.; Bassi, R.; Pignol, D. A structural basis for the pH-dependent xanthophyll cycle in Arabidopsis thaliana. *Plant Cell* **2009**, *21* (7), 2036–2044.
(116) Moan, J.; Wold, E. Detection of singlet oxygen production by ESR. *Nature* **1979**, *279* (5712), 450–451.
(117) Hideg, É.; Deák, Z.; Hakala-Yatkin, M.; Karonen, M.; Rutherford, A. W.; Tyystjärvi, E.; Vass, I.; Krieger-Liszkay, A. Pure forms of the singlet oxygen sensors TEMP and TEMPD do not inhibit Photosystem II. *Biochim. Biophys. Acta - Bioenerg.* **2011**, *1807* (12), 1658–1661.
(118) Marshall, D. L.; Christian, M. L.; Gryn'ova, G.; Coote, M. L.; Barker, P. J.; Blanksby, S. J. Oxidation of 4-substituted TEMPO derivatives reveals modifications at the 1- and 4-positions. *Org. Biomol. Chem.* **2011**, *9* (13), 4936–4947.
(119) Hideg, É.; Vass, I.; Kálai, T.; Hideg, K. Singlet oxygen detection with sterically hindered amine derivatives in plants under light stress. In *Methods in Enzymology*; Academic Press, 2000; Vol. 319, pp 77–85.
(120) Kóta, Z.; Horváth, L. I.; Droppa, M.; Horváth, G.; Farkas, T.; Páli, T. Protein assembly and heat stability in developing thylakoid membranes during greening. *Proc. Natl. Acad. Sci.* **2002**, *99* (19), 12149–12154.

(121) Rees, D.; Noctor, G.; Ruban, A. V.; Crofts, J.; Young, A.; Horton, P. pH dependent chlorophyll fluorescence quenching in spinach thylakoids from light treated or dark adapted leaves. *Photosynth. Res.* **1992**, *31* (1), 11–19.

Chapter 7

Conclusions and Future Directions

Snapshot spectroscopy provides a framework for monitoring the real-time operation of photosynthetic light harvesting in plants and algae. Throughout this dissertation, three different snapshot techniques have been employed to interrogate a range of photoprotective processes occurring on diverse timescales in the photosynthetic apparatus as well as how these processes are regulated during exposure to excess light. On the ultrafast timescale (ps-fs), snapshot TA spectroscopy probes the activation of molecular mechanisms underlying excess energy dissipation by NPQ. On the nanosecond timescale, snapshot Chl fluorescence lifetime spectroscopy tracks the kinetics associated with NPQ activation and deactivation in intact leaves and algal cells. Finally, spin-trapping EPR snapshot spectroscopy can provide information about the steady-state accumulation of singlet oxygen, a transient excited state of molecular oxygen with a sub-microsecond lifetime in photosynthetic systems. The combination of these three techniques is well-suited to address a range of open questions in the field of photoprotection. In this chapter, I briefly outline several of the overarching themes presented in this dissertation. I also provide recommendations for future experimental efforts designed to understand the operation of NPQ in complex physiologically relevant photosynthetic samples under conditions that mimic realistic environmental stress conditions.

Photoprotection by NPQ has traditionally been grouped into processes according to their activation timescale and/or molecular triggers. A common description of the initial NPQ response to excess light includes at least three distinct components: ΔpH-dependent qE, Zea-dependent qZ, and LHC antenna-dependent qT. However, as is discussed in other chapters, this categorization is complicated by overlapping timescales and it is not clear if the components operate independently or with shared molecular mechanisms. Additionally, relatively little is known about how each component functions under the irregular light conditions found in the natural environment. Open questions include the connection between observed NPQ components (i.e., qE, qZ, and qT) and the underlying photophysical mechanisms (i.e., EET and CT), the kinetics with which NPQ switches on and off upon transitions between dark and high light conditions, and the long-term changes in photoinduced oxidative chemistry occurring in the photosynthetic apparatus during light stress. As demonstrated throughout this dissertation, the application of snapshot spectroscopy to a range of intact photosynthetic samples provides valuable insights into each of these questions.

The combination of the snapshot TA and snapshot fluorescence lifetime methods has revealed new features of the complex *in vivo* operation of NPQ, including the coexistence of several photophysical dissipation mechanisms in the same intact photosynthetic sample. For example, in thylakoid membranes from spinach (Chapter 2) or living cells of the microalga *Nannochloropsis* (Chapter 3), the detection of spectroscopic features associated with both the Car S_1 and $Car^{\bullet+}$ excited states following excitation of Chl pigments suggests the involvement of two distinct photoprotective mechanisms operating on the ultrafast timescale. Studies based on chemical treatment and/or genetic mutants further suggest that both the EET and CT mechanisms require a putative pH-sensing protein (PsbS in plants or LHCX1 in *Nannochloropsis*) as well as de-

epoxidized xanthophyll pigments (likely Zea). Future efforts should focus on identifying the location of the quenching sites in the photosynthetic apparatus and developing an understanding of the *in vivo* regulatory control system(s) that activate and deactivate the NPQ mechanisms in response to changes in illumination conditions. Site-directed protonation mutants of the LHCX1 protein in *Nannochloropsis* should greatly help to dissect the molecular basis for CT and EET quenching *in vivo*.

Snapshot fluorescence lifetime spectroscopy provides the ability to monitor the magnitude and kinetics of the *in vivo* NPQ response based on changes in the average Chl fluorescence lifetime. The technique is therefore well suited to track photoprotection in real time during exposure of a photosynthetic organism to repeating cycles of high light and darkness, a situation designed to mimic the fluctuating light conditions found in nature. For example, in leaves of *Arabidopsis*, an interdependence between the rapidly-reversible (i.e., qE) and slower forms of NPQ (i.e., qZ, qT, qI) is observed (Chapter 4), suggesting that fast and slow quenching processes should not be viewed as independent. This finding raises the possibility that interactions between various biochemical actors are crucial for enabling the photoprotective response of the organism under changing light conditions. An important first step toward modeling the NPQ response of *Arabidopsis* is demonstrated using a "top-down" model parameterized solely using the timescales observed in the experimental fluorescence lifetime data. Future development of "bottom-up" models that are capable of accurately describing a plant's response to fluctuating light conditions will require integration of the various biochemical and structural changes occurring in the photosynthetic apparatus that give rise to photoprotection. Such advanced models may provide the ability to successfully predict the response of a photosynthetic organism to variations in the illumination intensity, which would be of great value for ongoing efforts to improve the biomass productivity of photosynthesis under field-like conditions.

Snapshot fluorescence lifetime measurements have also clarified the contributions of qE and qT in intact cells of the green alga *Chlamydomonas* exposed to fluctuating light conditions (Chapter 5). The LHCSR3 protein is necessary for much of the NPQ response, especially the qE-type quenching that occurs during periods of illumination. However, an increasing extent of dissipation is also observed during the dark periods of light fluctuations, which requires the activity of the STT7 kinase and therefore is related to qT. Quantification of the contributions of LHCSRs and STT7 to overall NPQ revealed that an interplay between the different molecular actors enables the wild-type photoprotective response under fluctuating light conditions. Characterizing the nature of the interaction between LHCSR proteins and the STT7 kinase is an important future step towards gaining a mechanistic understanding of photoprotection in *Chlamydomonas*. Additionally, extending the periodic high light/dark sequences to include more irregular switching frequencies along with variations in light intensity and light color may yield additional insights into the response of the photosynthetic apparatus to the complex light patterns regularly encountered by plants and algae in nature.

Finally, snapshot EPR measurements can provide insight into the accumulation and regulation of ROS during photoprotection. The involvement of one such ROS, singlet oxygen, in the steady-state operation of NPQ is currently unclear. As demonstrated in Chapter 6, the combination of snapshot EPR measurements and snapshot fluorescence lifetime measurements, both applied to spinach thylakoid membranes, suggests an interesting correlation between the dynamics of

photoprotective quenching and the concentration of singlet oxygen. Additional real-time measurements of singlet oxygen, perhaps using improved detection capabilities, alongside *in vivo* measurements of NPQ could help to uncover critical insights into the role of NPQ in modulating the concentration of reactive chemical species such as singlet oxygen during exposure to high-light stress.

As can be seen from this dissertation, there remains much to be discovered about how plants and algae protect against the damaging effects of excess illumination. Snapshot spectroscopy techniques have already revealed new insights regarding the molecular mechanisms, kinetics, and steady-state operation of NPQ in a range of photosynthetic organisms. The continued design and implementation of new snapshot techniques offers exciting possibilities to build on our understanding of the complex temporal, spatial, and molecular bases of NPQ. It is anticipated that a mechanistic understanding of natural photoprotection may inspire new strategies for improving the biomass and biofuel productivity of natural photosynthesis.